Ludwig Maximilian Universität - Munich
Fakultät für Physik

Université Joseph Fourier - Grenoble
UFR de Physique

Fundamental properties of very low mass star and brown dwarf binaries

THESIS

submitted on the 19 july 2004

for the degrees of

Doktor der Ludwig Maximilian Universität – Munich

(Naturwissenschaften)

Docteur de l'université Joseph Fourier – Grenoble 1

(Astrophysique et milieux dilués)

by

Hervé Bouy

Committee

Chairs :	Prof. Gregor Morfill (MPE, Munich, Germany) Prof. Jérôme Bouvier (UJF, Grenoble, France)
Referees :	Prof. Isabelle Baraffe (ENS, Lyon, France) Prof. Ralph Bender (LMU, Munich, Germany) Prof. Thomas Gehren (LMU, Munich, Germany)
Guests :	Dr. Wolfgang Brandner (MPIA, Heidelberg, Germany)

European Southern Observatory
Max Planck Institut für extraterrestrische Physik
Laboratoire d'AstrOphysique de Grenoble — UMR 5571

Erstgutgachter: Prof. Dr. Gregor Morfill

Zweitgutachter: Prof. Dr. Isabelle Baraffe

Date of the oral examination: 24/09/2004

Aknowledgments

Je veux tout d'abord remercier mes Parents, une fois pour leur patience, et une autre fois pour leurs encouragements constants.

I thank particularly Wolfgang Brandner and Ralph Neuhäuser for inviting me to work first at ESO and then at MPE. I am grateful to Jérôme Bouvier for co-supervising my work during these three years, and thus allowing me to make a cotutelle. I am grateful to Prof. Morfill for inviting me to stay at the MPE and supervising my work during the last year of my thesis. I am grateful to ESO and MPE for providing me fundings and fantastic working conditions. I aknowledge the L.A.O.G, the Ludwig Maximilian Universität, and the Université Joseph Fourier for allowing me to make a cotutelle. Without these persons and these institutions I would have never been able to do this work.

I thank all my collaborators, who generously helped me and shared their experiences and expertises, sometimes their friendships, and help me to grow on the way leading to an independent researcher.

I thank all my friends, in Germany, France and some other parts of the World, and in particular Ana Teresa.

I aknowledge the financial support of the Conseil Régional de la Région Rhône-Alpes.

Heureux qui, comme Ulysse, a fait un beau voyage,
Ou comme cestuy-là qui conquit la toison,
Et puis est retourné, plein d'usage et raison,
Vivre entre ses parents le reste de son âge !

Quand reverrai-je, hélas, de mon petit village
Fumer la cheminée, et en quelle saison
Reverrai-je le clos de ma pauvre maison,
Qui m'est une province, et beaucoup davantage ?

Plus me plaît le séjour qu'ont bâti mes aïeux,
Que des palais Romains le front audacieux,
Plus que le marbre dur me plaît l'ardoise fine

Plus mon Loir gaulois, que le Tibre latin,
Plus mon petit Liré, que le mont Palatin,
Et plus que l'air marin la doulceur angevine.

Joachim du Bellay, *Les Regrets.*

à mon frère Olivier.
à mes Grands-Parents.

Abstract

Keywords: Binaries, ultracool dwarfs, brown dwarfs, statistical and physical properties of ultracool dwarfs

This work presents the results of a detailed study of the statistical and physical properties of binary ultracool dwarfs and brown dwarfs (spectral type later than M7).

As for the statistical properties, we found that the frequency of binaries among ultracool objects is significantly lower than for earlier type objects, with a lower limit at 10–15% in the field, and <10% in the Pleiades Open cluster. While we were sensitive to systems with separations up to 100 A.U, we did not find any multiple system with separation greater than 20 A.U. At even larger separations, no wide binaries were reported by the all sky surveys such as 2MASS, DENIS or SDSS. The distribution of separations looks similar to that of F and G dwarfs (Gaussian), but with a peak at 4–8 A.U. Although we were sensitive to mass ratios down to 0.65, we found most of the objects to have mass ratios larger than 0.85. This latter result needs to be confirmed by further statistical studies on well defined statistical samples. Although the sample of known binaries in the Pleiades is too small for a similar analysis, we note that the binary frequency, the distributions of mass ratio and separations are similar, indicating that the properties of binary brown dwarfs might not depend on the age and environment after 125 Myr. Finally, although we did not have the opportunity to perform a similar statistical study in a star forming region, we report the first detection of a young binary brown dwarf with a disk in the R-CrA association.

These results provide strong constraints on the models of ultracool dwarf formation and evolution. The binary frequency is currently not reproduced by any of these models. The models of ejection could explain the lack of binaries wider than 20 A.U and the apparent preference for equal mass systems, but they predict a much lower binary frequency. The model assuming that brown dwarfs form in a smilar way than stars could reproduce the binary frequency we observe, but could not explain the distributions of separation and mass ratio. More efforts are required on the theoretical side in order to better explain the observed properties, and on the observational side to give new and improved constraints.

As for the physical properties, our observations lead to the discovery of a short period binary L dwarf. Observations at high angular resolution spread over 4 years allowed us to follow the companion on 60% of its orbit. For the first time, we were then able to compute the orbital parameters and total mass of such a very low mass object. In the near future, similar studies should enable us to calibrate brown dwarf mass and luminosity models. Using high angular resolution spectroscopy, we were able to disentangle the spectra of the individual components of 4 binary ultracool dwarfs and to compute their spectral types. Two binaries have companions with spectral types significantly later than their primary (by 3 to 4 spectral subclasses), allowing us to compare the evolution of their effective temperature and atmosphere. Finally, using our high angular resolution images, we were able to detect a possible third component in one of the binaries of our sample.

Résumé

Mots-clefs: Binaires, naines ultrafroides, naines brunes, propriétés physiques et statistiques des naines ultrafroides

Ce travail présente les résultats d'une étude détaillée des propriétés statistiques et physiques des binaires de naines brunes et ultra-froides (type spectral plus tardif que M7).

Concernant les propriétés statistiques, nous constatons que la fréquence de binaires parmi les objets ultra-froids est inférieure à celle des objets de types spectraux plus précoces, avec une limite inférieure à 10∼15% pour les objets du champ, et <10% dans l'amas ouvert des Pleïades. Alors que nous étions capables d'identifier les systèmes binaires jusqu'à des séparations de ∼100 U.A, nous n'avons trouvé aucun système mutliple aux séparations superieures à 20 U.A. À plus grande séparation encore, aucune binaire n'a été trouvée par les surveys 2MASS, DENIS ou SDSS. La distribution des séparations est semblable à celle des naines F et G (gaussienne), mais avec un maximum autour de 4∼8 U.A. Bien que nous étions sensibles aux binaires avec des rapports de masse allant jusqu'à 0,6, nous n'avons detecté aucune binaire avec un rapport de masse inférieur à ∼0,6; la plupart des objets ayant un rapport de masse plus grand que 0,85. Ce résultat devra être confirmé par d'autres études sur des échantillons mieux définis statistiquement. Bien que l'échantillon de binaires connues dans les Pleïades soit trop petit pour nous permettre de faire une analyse semblable, nous obervons que la fréquence de binaires, les distributions de rapport de masse et de séparations sont semblables, indiquant que les propriétés des naines brunes binaires ne dépendent probablement pas de l'âge et de l'environnement passé 125 millions d'années. Enfin, bien que nous n'ayons pas eu l'occasion de pouvoir mener une étude statistique similaire dans une région de formation stellaire, nous présentons la première détection d'une jeune naine brune binaire entourée d'un disque dans la région de la Couronne Australe (R-CrA).

Ces résultats apportent de fortes contraintes sur les modèles de formation et d'évolution. La fréquence de binaires n'est actuellement reproduite correctement par aucun des modèles. Les modèles d'éjection pourraient expliquer le manque de binaires aux séparations supérieures à 20 U.A ainsi que le manque apparent de systèmes de faibles rapports de masses, mais elle prévoit une fréquence de binaires beaucoup trop faible. Le modèle prévoyant que les naines brunes se forment d'une manière analogue aux étoiles pourrait quant à lui reproduire la fréquence de binaires que nous observons, mais ne pourrait pas expliquer les distributions de rapport de séparation et de masse. Plus d'efforts sont donc nécessaires à la fois du côté théorique afin de pouvoir expliquer les propriétés observées, et du côté observationnel pour apporter des contraintes nouvelles et plus precises.

Concernant les propriétés physiques des binaires de naines ultra-froides, nos observations ont mené à la découverte d'une binaire de naines L de courte période. Les observations à haute résolution angulaire réparties sur quatre ans nous ont permis de suivre le compagnon sur 60% de son orbite. Pour la première fois, nous avons pu calculer les paramètres orbitaux et la masse totale d'un objet de ce type. À moyen terme, ce genre de mesures devraient nous permettre de calibrer la très importante relation masse-luminosité. En utilisant la spectroscopie à haute résolution angulaire, nous avons été en mesure de séparer les spectres des composantes individuelles de quatres binaires de naines ultra-froides, et de calculer leurs types spectraux. Deux de ces binaries ont des compagnons de types spectraux relativement plus tardifs que leurs primaires (3 et 4 sous-classes spectrales de plus), nous permettant de comparer l'évolution de leurs températures effectives et leurs atmosphères. Enfin, utilisant nos images à haute résolution angulaire, nous avons détecté une possible troisième composante dans une des binaries de notre échantillon.

Kurzfassung

Stichworte: Doppelsterne, ultrakühle Zwerge, braune Zwerge, statistische und physikalische Eigenschaften brauner Zwerge

Diese Arbeit präsentiert die Ergebnisse einer detaillierten Untersuchung der statistischen und physikalischen Eigenschaften von ultrakühlen Zwergsternen und braunen Zwergen (Spektraltyp später als M7).

Hinsichtlich der statistischen Eigenschaften fanden wir, daß die Häufigkeit doppelter Systeme unter ultrakühlen Objekten mit 10–15% im Feld und <10% in dem offenen Sternhaufen Pleiaden signifikant niedriger ist als für Objekte mit früherem Spektraltyp. Obwohl wir Systeme mit Abständen bis zu 100 A.U. hätten nachweisen können, fanden wir keine Mehrfachsysteme mit Abständen größer als 20 A.U. Die Himmeldurchmusterungen 2MASS, DENIS oder SDSS entdeckten kein einziges weites Doppelsystem mit noch größeren Abständen. Die Verteilung der Abstände ähnelt der von F- und G-Zwergen (Gaussverteilung), allerdings mit einem Maximum bei 4–8 A.U. Die meisten Doppelsysteme weisen Massenverhältnisse größer als 0.85 auf, obwohl wir Doppelsysteme mit Massenverhältnissen bis hinunter zu 0.6 hätten nachweisen können. Dieses Ergebnis muß durch zukünftige Untersuchungen statistisch wohldefinierter Stichproben überprüft werden. Obwohl die Stichprobe der bekannten Doppelsysteme in den Pleiaden zu klein ist für eine den Feldobjekten vergleichbare Untersuchung, weisen wir darauf hin, daß die Häufigkeit der Doppelsysteme und die Verteilung der Massenverhältnisse und der Abstände ähnlich sind. Dies deutet an, daß sich die Eigenschaften doppelter brauner Zwerge ab einem Alter von etwa 125 Myr nicht mehr als Funktion des Alters oder der Umgebung ändern. Obwohl keine Gelegenheit bestand, eine ähnliche statistisch signifikante Untersuchtung in einem Sternentstehungsgebiete durchzuführen, führte diese Arbeit zur Entdeckung des ersten jungen, doppelten braunen Zwerges in der CrA-Assoziation.

Die Ergebnisse liefern starke Randbedingungen für Entstehungs- und Entwicklungsmodelle brauner Zwerge. Die Häufigkeit der Doppelsysteme wird momentan von keinem der Modelle richtig wiedergegeben. Dynamische Ausstoßmodelle können den Mangel an weiten Doppelsystemen mit Abständen größer als 20 A.U. und das bevorzugte Auftreten von Doppelsystemen mit Komponenten gleicher Masse erklären. Diese Modelle sagen allerdings eine noch geringere Häufigkeit von doppelten Systemen voraus. Der Sternentstehung analoge Fragmentations- und Kollapsmodelle können die beobachtete Häufigkeit der Doppelsysteme erklären, allerdings nicht die Verteilung der Abstände und Massenverhältnisse. Weiterreichende theoretische Modelle sind nun notwendig, um die beobachteten Eigenschaften zu erklären. Von Seiten der Beobachtung sollten die Randbedingungen weiter eingeschränkt werden.

Im Hinblick auf die physikalischen Eigenschaften der untersuchten Systeme, führten unsere Beobachtungen zur Entdeckung eines doppelten L-Zwerges mit kurzer Umlaufperiode. Über vier Jahre verteilte Beobachtungen mit hoher räumlichen Auflösung ermöglichten uns, 60% der Umlaufbahn des Doppelsystems zu vermessen. Zum ersten Mal waren wir hiermit in der Lage die Bahnparameter und die Gesamtmasse eines derartig massearmen Doppelsystems zu bestimmen. In naher Zukunft werden ähnliche Studien die Eichung der Masse- und Leuchtkraftmodelle von braunen Zwergen ermöglichen. Spektroskopische Beobachtungen mit hoher Winkelauflösung erlaubten uns die Spektraltypen der individuellen Komponenten in vier Doppelsystemen zu bestimmen. Zwei der Begleiter weisen deutlich spätere Spektraltypen auf als die Primärkomponenten (3 bis 4 spektrale Unterklassen), was vergleichende Untersuchungen des Abkühlverhaltens und der Atmosphäreneigenschaften ermöglicht. Darüber hinaus konnten wir in unseren hochauflösenden Bildern ein mögliches Dreifachsystem identifizieren.

Contents

List of Figures

List of Tables

Introduction

Very Low Mass stars and Brown Dwarfs

1 Definitions

Brown dwarfs are compact self-gravitating, self-luminous gaseous objects which are not sufficiently massive to ignite a in thermonuclear hydrogen fusion reactions in their core and cannot therefore be considered a star. The I.A.U defines brown dwarfs as "*substellar objects with true masses above the limiting mass for thermonuclear fusion of deuterium and below the limiting mass for thermonuclear fusion of hydrogen, no matter how they formed nor where they are located*". Recent calculations place the deuterium burning limit around $\sim$0.013 $M_{\odot}$, and the hydrogen burning limit around $\sim$0.075 $M_{\odot}$, both for solar metallicities. Although this definition of brown dwarfs is still a matter of intense debates (especially regarding the boundary between giants planets and brown dwarfs), most astronomers agree to use it, until a better one is proposed. Figure 1 shows that brown dwarfs are among the faintest objects.

2 History: hunting brown dwarfs

Although their existence was suspected since the early sixties (Kumar 1963), brown dwarfs have been identified for the first time in 1995, when Nakajima et al. (1995) observed the first unambiguous substellar object: Gl 229B. With increasing efficiency of infrared detectors and larger telescopes, the main problem to find brown dwarfs is not anymore to be sensitive enough, but to differentiate them from very low mass stars. The so-called "lithium test", proposed by Rebolo et al. (1995a), allowed astronomers to confirm unambiguously the nature of most of the before discovered brown dwarfs (see e.g Rebolo et al. 1995b, 1996; Zapatero Osorio et al. 1997; Stauffer et al. 1998). The lithium test takes advantage of the fact that objects below the hydrogen burning limit retain their initial lithium abundances forever, while the destruction of lithium via the nuclear reaction $Li^7(p,\alpha)He^4$ consumes the whole lithium of very low mass stars in only $\sim$50 Myr. The presence of lithium absorption lines in the spectrum of a candidate brown dwarf therefore allows to conclude unambiguously on its substellar nature. The non detection is nevertheless inconclusive, because this reaction also takes place in the core of the most massive brown dwarfs at the beginning of their lives. Brown dwarfs with masses between $\sim$0.065 and $\sim$0.080 $M_{\odot}$ are indeed able to fuse lithium into helium during their first $\sim$50 to 250 Myr. Although substellar, an older and more massive brown dwarf could have fused all its lithium during its youth and would not show any sign of it in its spectrum. The presence of lithium therefore gives not only a proof that the object is substellar, but also an indication on its age. It is thus ideally suited to identify brown dwarfs in star forming regions or young open clusters. Table 1 gives a summary of these properties.

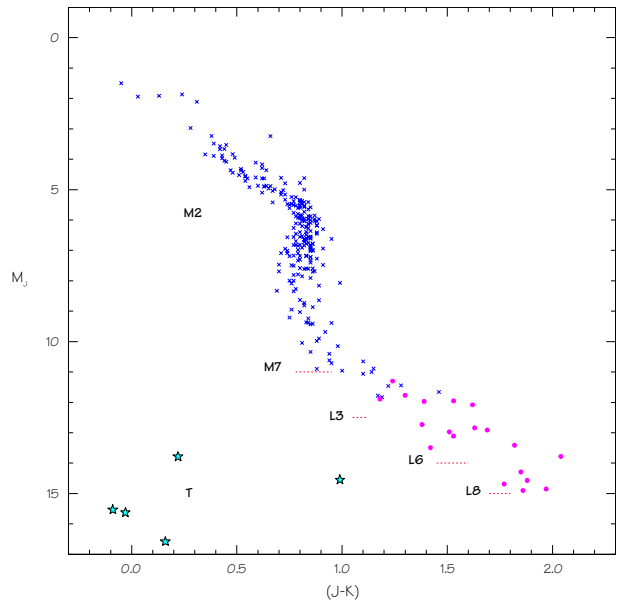

Figure 1 The position of brown dwarfs in the colour-magnitude diagram. Stars are represented with blue crosses; L dwarfs as solid magenta points; and T dwarfs as 5-point cyan stars. The boundaries between some spectral types are also indicated.

Effective strategies nowadays used to detect *ultracool dwarfs*[1] are proper motion surveys (e.g Ruiz et al. 1997), wide field CCD surveys in star forming regions and open clusters like the Pleiades (e.g Stauffer et al. 1994; Zapatero Osorio et al. 1997; Bouvier et al. 1998), or the new generation of optical and near-infrared all sky surveys. The Sloan Digital Sky Survey (York 2000), the DEep Near Infrared Survey (DENIS, Epchtein et al. 1997), and the 2 Micron All Sky Survey (2MASS, Cutri et al. 2003) have thus identified several hundreds of nearby free-floating brown dwarfs, and many more candidates are waiting for confirmation. So far, DENIS has produced a list of $\sim$ 300 nearby very low-mass objects (see e.g Delfosse et al. 1997, 2003; Martín et al. 1999a), and a similar number has been detected by 2MASS (see e.g

[1]for the purpose of this study, and although it is not officially defined by the I.A.U, we will refer to objects with spectral type later than M7 as "*ultracool dwarfs*". This definition therefore includes not only brown dwarfs but also very low mass stars.

Table 1. The lithium test

Object type	Mass range	Fusion of H	Fusion of D	Presence of Li
Stars	>0.075	yes	yes	no
Brown dwarfs	0.065–0.075	briefly	briefly	yes, but age dependent
Brown dwarfs	0.013–0.065	no	briefly	yes

Kirkpatrick et al. 1997, 1999, 2001; Kirkpatrick 2003; Burgasser et al. 1999; Gizis et al. 2000). This nearby sample is ideal for resolving ultracool and brown dwarfs binaries, and is large enough for statistical studies.

3 State of the art at the beginning of my thesis

3.1 Models of formation

The formation and evolution of brown dwarfs and very low mass stars is still poorly understood, and is one of the current fields of intense research. The currently most accepted scenarios of formation and evolution can be split in two categories: the "*star-like*" scenarios, and the "*planet-like*" scenarios.

Star-like formation

The Star-like formation scenario assumes that brown dwarfs form just like stars due to fragmentation and collapse of molecular cloud cores. The contraction could then result in a brown dwarf if: 1) the mass of the initial cloud is to small to form a star (we will refer to this scenario as the scaled "*Jeans*" model); or 2) if the accretion is stopped at an early stage because of external processes, preventing the object to accrete enough mass to start the fusion of hydrogen in its core. Two external processes are currently admitted as possible explanations for the formation of brown dwarfs and very low mass stars:

- the ejection of the lowest mass objects from forming multiple systems before they can reach the critical hydrogen-burning mass limit ("*embryo-ejection*" model),
- the loss of the accretion envelope due to photo-evaporation through a nearby massive star before the central object can reach the critical hydrogen-burning mass limit("*photo-evaporation*" model).

In the coming paragraphs we will give a short review of these three possible scenarios of formation, starting with the Jeans model.

Stellar models and the Jeans theory had suggested that a true star must have a mass greater than 0.08 $M_{\odot}$ to be able to sustain fusion of hydrogen in its core. In the early sixties Kumar (1963) showed that under specific conditions smaller dense molecular clouds would also be able to contract and form substellar objects. It took 32 years until astronomers discovered such an object, after considerable observational efforts (Nakajima et al. 1995). Supporting Kumar's theory and the Jeans model, recent results of high angular resolution observations of molecular clouds have showed that the clouds can have a clumpy small substructure (Alves et al. 2001), in which brown dwarfs and very low mass stars could later form. Figure 2 shows the visible (left) and near-infrared (right) images of the molecular cloud Barnard 68. The dust is completely opaque to the visible light of the background stars while the infrared light can pass through it. Using these images, Alves et al. (2001) were able to draw detailed extinction and cloud density maps, showing the small-scale substructures in which brown dwarfs are expected to be able to form. Finally, the recent discovery that a large fraction (up to 50%) of brown dwarfs in star forming regions have disks (see e.g Jayawardhana et al. 2003a; Liu et al. 2003) is also supporting the idea that brown dwarfs can form like stars from the collapse of cloud clumps followed by accretion.

The embryo-ejection model was first suggested by Reipurth & Clarke (2001). This scenario is motivated by the fact that many stars are known to form in clusters of two, three or even

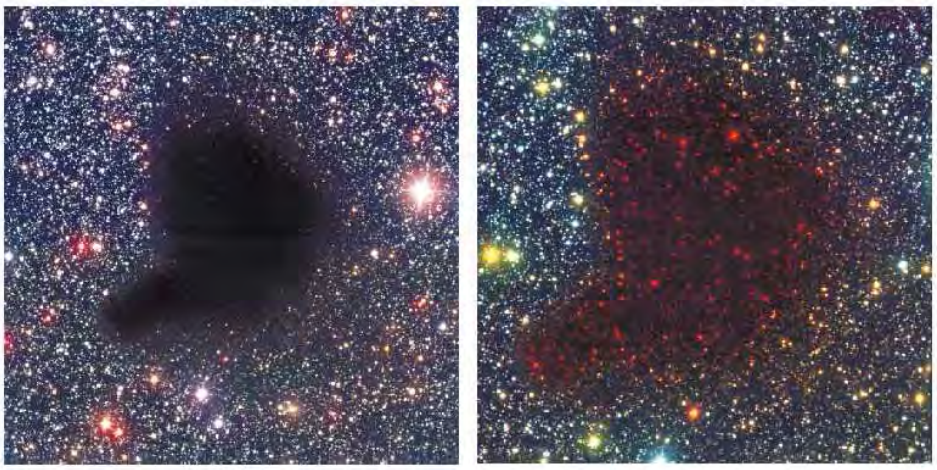

Figure 2 Visible and near-IR images of Barnard 68 (Alves et al. 2001).

more stars. Brown dwarfs start out as the runts among these newborn stars, suffering from the competition for accretion, and therefore growing slower. Due to gravitational interactions with the "fratricidal" neighbouring stars, the smallest stellar embryos are ultimately ejected out of the central feeding ground, preventing them to develop into large, hydrogen-burning grown-ups. The calculations performed by Reipurth & Clarke (2001) show indeed that the gravitational interactions between stellar embryos almost always end up with the lightest member being violently flung out of the little group. More recent and detailed numerical simulations of star formation performed by Bate et al. (2003) confirm these results. Figure 3 gives an overview of the results of these extremely heavy and impressive calculations[2], showing different stages in the collapse and fragmentation of an initial molecular clouds into a small cluster of ∼50 stars and brown dwarfs. These simulations show that, while forming, stars are so close that they interact with each other. The accretion of gas is always in favour of the more massive object, while the least massive are not able to grow fast enough to start the fusion of hydrogen in their core before they get ejected.

The photo-evaporation scenario is motivated by the observations in star forming regions of protoplanetary disks perturbed by the influence of neighbouring massive stars. Figure 4 shows the centre of the Orion Nebula where many so-called "proplyds" (star embryos with protoplanetary disks surrounded by ionization fronts) are visible. The intense ultra-violet radiation and subatomic particle wind from nearby hot stars blow back the material from the disk's surface, producing the characteristic elongated comet-like tail. One can imagine forming very low mass stars and brown dwarfs in a similar way, when such a disk is "evaporated" before the object can accrete enough material.

Planet-like formation

The currently prevailing theory of planet formation says that planets form when dust particles in a disk of material surrounding a young star begin to clump. Under the influence of the gravitational interactions, these clumps accumulate into larger rocky cores called planetesimals. If the planetesimal accumulates enough material to reach the critical mass (at 10∼15 $M_{\odot}$),

[2] the simulations of Bate et al. (2003) required about 100 000 CPU hours on a 128-processor supercomputer

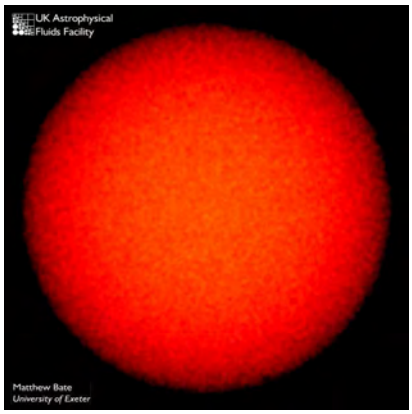

1) Clouds of interstellar gas are seen to be very turbulent with supersonic motions. We begin with such a gas cloud, 1.2 light-years across, and containing 50 times the mass of the Sun.

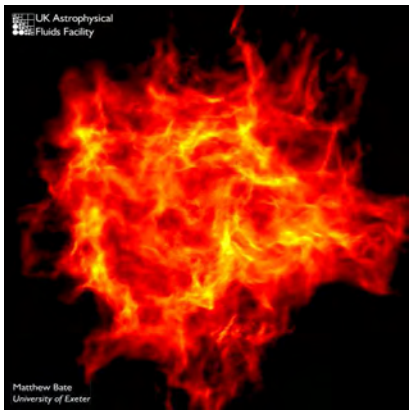

2) As the calculation proceeds, the turbulent motions in the cloud form shock waves that slowly damp the supersonic motions.

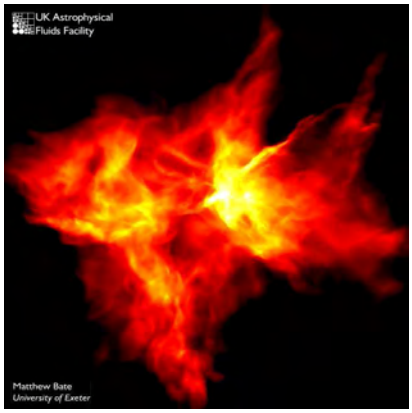

3) When enough energy has been lost in some regions of the simulation, gravity can pull the gas together to form a dense "core".

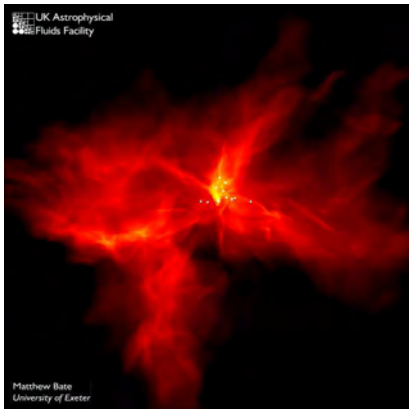

4) The formation of stars and brown dwarfs begins in this dense core.

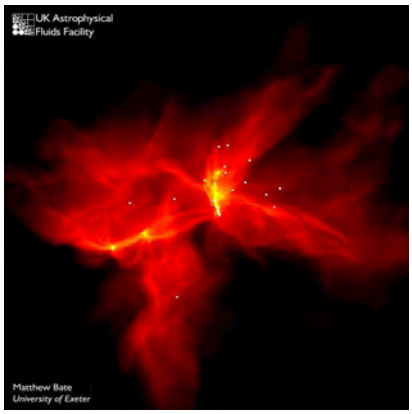

5) As the stars and brown dwarfs interact with each other, many are ejected from the cloud.

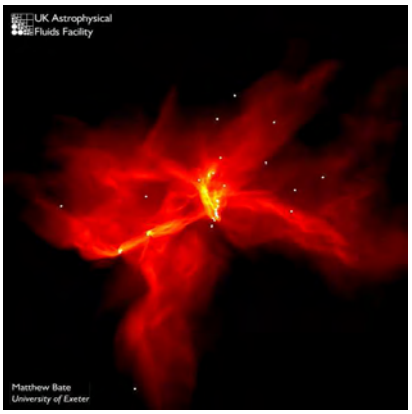

6) The cloud and star cluster at the end of simulation. Some stars and brown dwarfs have been ejected to large distances from the regions of dense gas in which the star formation occurs.

Credits: M. Bate , University of Exeter.

Figure 3 Star formation numerical simulations of Bate et al. (2003). This simulation followed the collapse of an interstellar gas cloud which was over one light year across and 50 times the mass of the Sun, eventually resulting in the formation of a cluster of 50 stars and brown dwarfs.

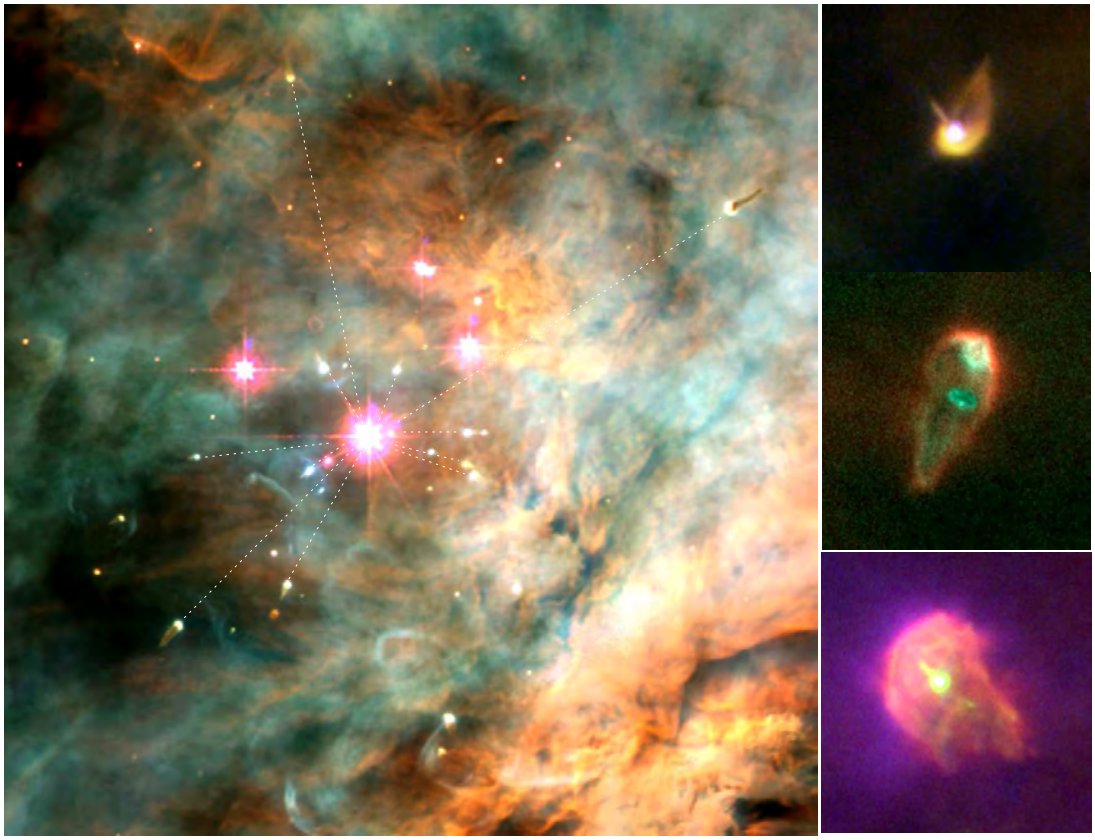

Figure 4 **Left image:** HST image of the Trapezium in the Orion Nebula. Many proplyds appear in the field, all oriented toward one of the bright central star (as indicated by the dotted lines), showing that the radiative pressure and the stellar wind from the hot star push the dust and gas away from the outside layers of the proplyds. (Credit: C.R. O'Dell and S.K. Wong (Rice University); NASA)
Right images: Zoom on individual proplyds. (Credit: C.R. O'Dell/Rice University; NASA)

it will start to attract gas and form a gaseous giant like Jupiter, until it eventually becomes massive enough (∼13 $M_{Jup.}$) to fuse deuterium and form a brown dwarf. This process, called core accretion, is thought to occur in between one million to eight million years.

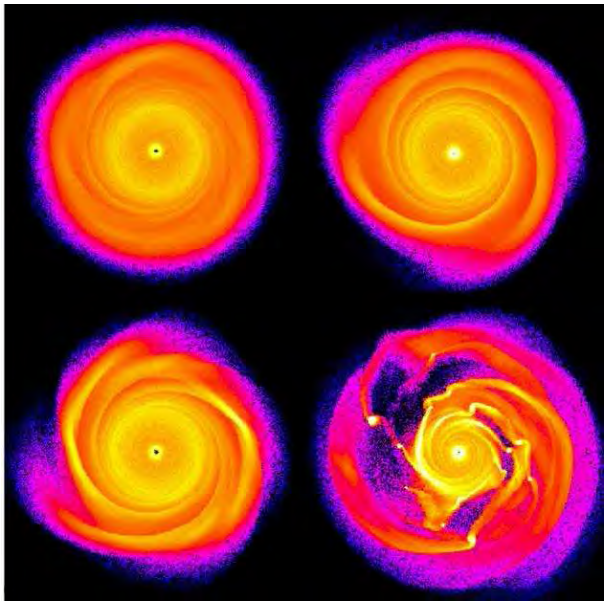

Figure 5 Snapshots of the numerical simulations of Mayer et al. (2002) showing a 200 000 particles disk of material around a young star. The disk is evolved until it starts to form spiral waves of density, which generate the tidal instabilities causing the fragmentation and speeding up the formation of planetary cores.

Another theory recently developed by Boss (2001) holds that tidally-induced instabilities - caused by waves that naturally emerge in the dust disk - speed up the nucleation process greatly, producing planetary objects in only a few thousand years. Studies of infinitesimal thin, self-gravitating disks have indeed shown that, under certain conditions, the disk becomes unstable and starts to develop long-wavelength, spiral shaped instabilities (Papaloizou & Lin 1989; Shu et al. 1990). In his numerical simulations, Boss (2001) was able to form clumps of material that began to spin and condense, but did not have enough computing power to follow the process until the creation of a stable planet. Mayer et al. (2002) recently refined and extended his study and were able to follow the formation of individual planets in the arms of the disk over a longer time-scale, showing that the clumps that form can persist long enough to become stable giant planets. Figure 5 shows the results of their simulation at different stages. The 200 000 particles disk starts to form spiral waves of density, which generate the tidal instabilities causing the fragmentation and speeding up the formation of planetary cores. Some of these cores might then form brown dwarfs before or after they eventually get ejected from the multiple system.

3.2 Models of evolution & physical properties

After their deuterium is exhausted, brown dwarfs continue to glow in red and infrared light, caused by their gravitational contraction and from the leftover heat generated by their formation and by the earlier deuterium and lithium fusion. The temperatures of known brown dwarfs range from about 2800 to 800 K. All brown dwarfs cool steadily over time; more massive objects cooling

more slowly than the less massive ones (see Fig. 6). For brown dwarf cooler than T_{eff} ∼1500 K, lithium starts to form molecules and it becomes more difficult to detect lithium absorption features in the spectra (Burrows & Sharp 1999). On the other hand, the temperature is so low that it allows the formation of CH_4, a molecule that luckily shows strong absorption features in the near-infrared (see Fig. 7). It becomes therefore possible to identify these brown dwarfs via the detection of methane in their spectra. These "cool" brown dwarfs are called "methane dwarfs", and form a new spectral class: the T dwarfs.

With spectral properties intermediate between those of giant planets and late-type stars, ultracool dwarfs have opened a new chapter in the study of atmospheric physics and chemistry. While theoretical models on the interplay of chemical and physical processes governing brown dwarf atmospheres have now reached a high level of sophistication, the observational side has fallen behind. In particular, precise calibrations of the basic physical properties of brown dwarfs, like mass, age, radius, luminosity, or surface gravity are still missing. Unfortunately, the degeneracy in the age-temperature relation for brown dwarfs makes it difficult to pin down their physical properties. Luminosities and effective temperatures of brown dwarfs are indeed function of both age and mass (Burrows et al. 1997; Chabrier et al. 2000) so that an older, slightly more massive brown dwarf can exhibit the same effective temperature as a younger, less massive one (see Fig. 6). Developments on both the observational and theoretical fronts are essential to obtain meaningful and important estimates of the physical properties of the very low mass stars.

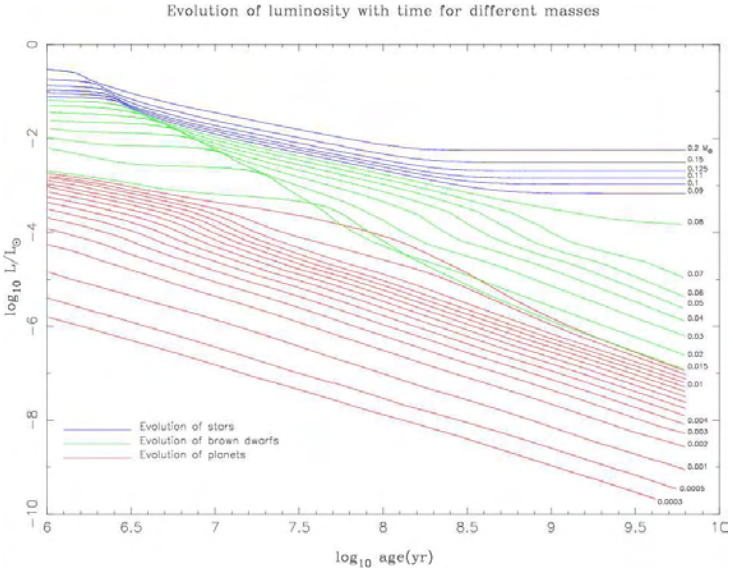

Figure 6 T_{eff} vs. Age for stars and brown dwarfs from the models of Burrows et al. (1997)

3.3 Models of atmospheres

As stated by Allard & Hauschildt (1995), the energy distribution of brown dwarfs is very peculiar. The molecular opacities, which globally define the continuum, cause the spectral energy distribution to peak around 1.1 μm for solar metallicities, almost independently of the effective temperature. While the initial atmospheric models were successful in reproducing the strong H_2O and H_2 absorption bands that depress the infrared flux in favor of near-infrared band-

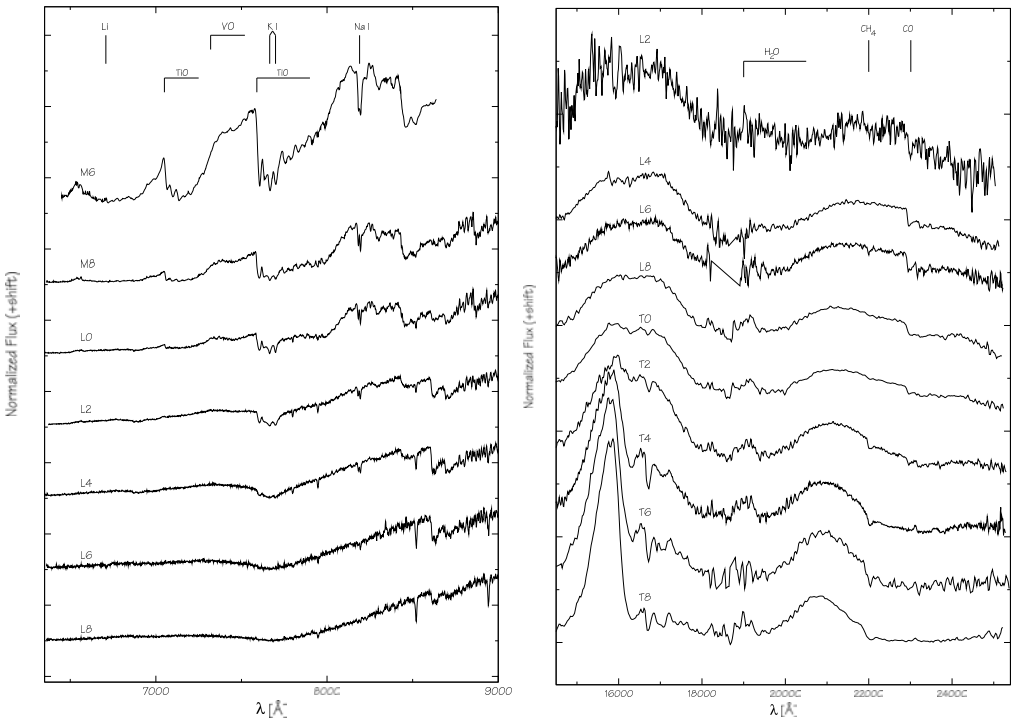

Figure 7 Spectral Sequence from M6 to T8 in the optical (left panel) and in the near infrared (right panel). Some molecular bands and atomic lines are indicated. The CH_4 absorption at 22 000 Å is characteristic for T-dwarfs. Data from Leggett et al. (2001).

passes, they at the same time failed to accurately reproduce the photometric properties for objects cooler than M6. All models predicted colours (V−K, I−K, J−K) to be bluer by as much as 1 mag than actually observed.

This discrepancy between observations and theory led to the suggestion that dust formation, in particular the condensation of corundum (Al_2O_3), is taking place in brown dwarf atmospheres (Tsuji et al. 1996). The new AMES-Dusty 1999 models of Allard et al. (2000) which employ the NASA AMES water lines list and a more detailed treatment of dust, appear to be more successful than previous models. In the extreme case of no dust settling, heating effects due to dust opacities hinder the formation of methane and ease the dissociation of H_2O. Surface gravity (and the depth/height of the convection zone) determines the efficiency of dust settling, and also affects the strength of hybrid bands (CaH at 624 and 639 nm). Surface gravity also influence the strength of atomic "gravity sensitive" lines (Ti I at 735.8 nm, Ca II at 854.2 nm, Na I doublet at 818.3 and 819.5 nm, and Hα).

Figures 7 shows two spectral sequences, in the optical for the M to L transition, and in the near infrared for the L to T transition.

3.4 Multiple systems among very low mass stars and brown dwarfs

While systematic surveys of the physical properties of ultracool dwarfs were just starting, we already had indications that binaries are not rare. PPL 15, the first brown dwarf in the Pleiades with confirmed lithium (Basri et al. 1996), turned out to be a spectroscopic binary (Basri & Martín 1999). Several direct imaging surveys in the field or in open clusters using the

high spatial resolution provided by both HST and/or adaptive optics led to the discovery of a dozen of visual binaries (Martín et al. 1997, 1999a, 2000a; Koerner et al. 1999; Reid et al. 2001). This sample of binaries was nevertheless too small for a systematic study of their properties, such as the binary frequency, the distribution of separations or of mass ratio. Using HST and adaptive optics, my main goal at the beginning of my thesis was to identify more binaries, in order to increase the sample, and start to derive statistical and physical properties.

Open questions and goals of my thesis work

1 How do ultracool dwarfs form ? Binaries as testimonies

To this key question brown dwarf binaries are an important piece of the puzzle. Where do free-floating brown dwarfs originate? Are they ejected stellar embryos (Reipurth & Clarke 2001; Bate et al. 2002; Delgado-Donate et al. 2003), or do they form more isolated like ordinary stars due to fragmentation of collapsing molecular cloud clumps (Bodenheimer 1998, 1999)?

These different scenarii, reviewed in the previous chapter, lead to different outcomes in the properties of the brown dwarf population, and in particular in the properties of multiple systems. In the first case, the dynamical interaction leading to ejections would disrupt most primordial binaries, and most brown dwarfs ought to be single objects. In the second scenario, the binary frequency among brown dwarfs can be expected to be similar to that of stars ($\sim$30% for the early M-dwarfs). In the embryo-ejection scenario, the few remaining multiple systems should have small separations, because of the gravitational interactions responsible for their ejection, while in the star-like scenario, one can reasonably expect that the distributions of separations of star and brown dwarf binaries should be similar. These properties hold important clues on the origin of (binary) ultracool dwarfs. Hence, measuring and comparing the occurrence of binary systems in substellar populations hold clues to their formation and evolution mechanisms. One can then ask how the binary properties of brown dwarfs, such as their frequency, distribution of separations, distribution of mass-ratios (is there a lower mass limit for companions to brown dwarfs and very low mass stars?), or the relation between orbital period and eccentricity, compare to the properties of stellar binaries. What role does duplicity play in stellar and substellar evolution? How does multiplicity change with time? How does it depend on the environment (is it different in star forming regions, open or globular clusters, than in the field)? How does multiplicity depend on the spectral classification (see Figure 1)? An agreement of ultracool dwarf and stellar binary properties would suggest the same formation mechanism for both types of objects.

2 Binaries as scales

The mass is the fundamental quantity which determines an astrophysical object's luminosity, size, lifetime, heavy element generation, and ultimate fate, so that one of the ultimate goals of a theory of very low mass and substellar objects is an accurate determination of the mass of an object based on spectroscopic characteristics and luminosity. Brown dwarf binaries provide a very valuable opportunity to measure substellar dynamical masses. The first such measurement has been reported by Lane et al. (2001) for the brown dwarf binary Gliese 569B, discovered

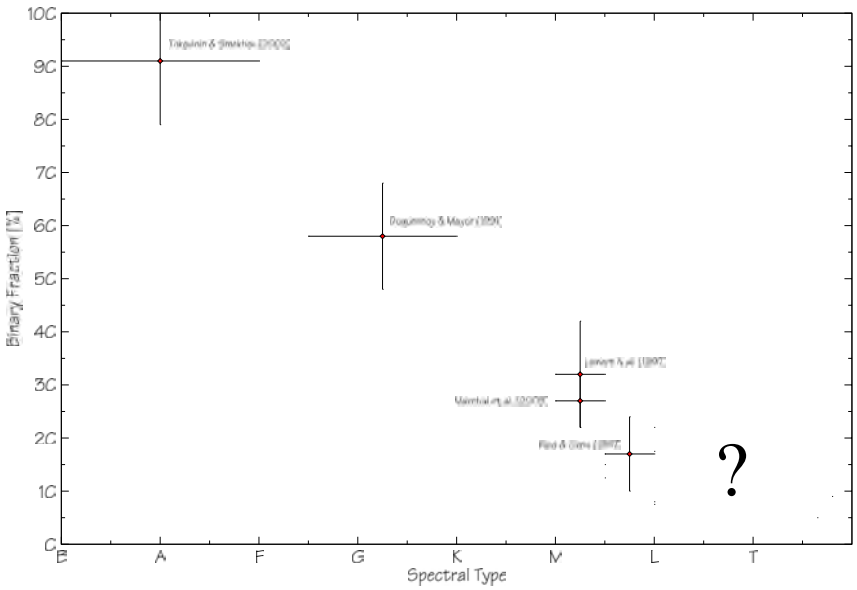

Figure 1 How does multiplicity depend on the spectral class ?

by Martín et al. (2000b). Dynamical masses for brown dwarfs of different ages are very much needed, as the mass estimates currently depend on untested theoretical evolutionary tracks, model atmospheres, and assumptions on the internal structure of brown dwarfs. In particular and as mentioned in Section 3.2 of the previous chapter, a brown dwarf with a given age and mass might have colours and luminosity very similar to that of a younger brown dwarf with a lower mass. This degeneracy in the mass-luminosity relation for substellar objects makes it very hard to pin down the physical properties of brown dwarfs, and to achieve the interplay between observation and theory which is necessary in order to improve, adapt, fine-tune models, and to guide the interpretation of the observations. A search for binary brown dwarfs, and a detailed study of their properties directly addresses these questions. Dynamical masses, which are model-independent, are therefore highly required.

3 Models of atmospheres of ultracool dwarfs

As mentioned above, theoretical models and evolutionary tracks have not been calibrated yet by observation, and the characteristics of an ultracool dwarf of a given age and mass are very much model dependent. By measuring dynamical masses independently from any model, we should be able to calibrate them and therefore be able to understand the physical properties of this class of objects (inner structure, dust formation, settling and depletion of refractory elements, and on the underlying opacities). Such a study will provide a more accurate picture of the differential evolution at the substellar transition for objects with the same age, but differing masses.

4 Goals and strategy of the thesis project

4.1 Statistical properties of multiple systems

The first part of this thesis focuses on the statistical properties of binaries in two different environments and ages: 1) in the field, and 2) in the Pleiades Open Cluster. Using high angular resolution instruments, the goal was to resolve visual multiple systems in order to derive the main statistical properties of visual binaries: the binary fraction, the distribution of separation, and the distribution of mass ratio. We aimed at looking in two different environments in order to see if these properties depends on: 1) the environment (presence or absence of neighbours) 2) the age (well known and relatively young in the Pleiades, unknown but usually older in the field). A complete study would have included observations in an even younger environment, such as a star forming region. The lack of time and of data did not allow me to perform a detailed study in a star forming region, but we could nevertheless study in details one interesting and peculiar binary brown dwarf in the R-CrA star forming region.

Advantages and disadvantages of field very low mass stars and brown dwarfs

Nearby free-floating brown dwarfs do not form a coeval sample, but they are close enough to measure their distance (angular parallax) precisely, and – by using high angular resolution instruments – it is possible to detect and resolve binary brown dwarfs with separations down to 0.4 A.U. ($0\farcs06$ at 7 pc). The corresponding orbital periods can be as short as a couple of years, and are therefore ideal for follow-up observations in order to determine the total dynamical mass. On the other hand, since their ages cannot be easily and independently constrained, they are not ideally suited for the calibration of evolutionary models.

Advantages and disadvantages of Pleiades very low mass stars and brown dwarfs

The Pleiades, the first cluster in which a significant population of (coeval) brown dwarfs was identified, is at a distance of 135 pc. This makes it hard to detect and resolve visual binary brown dwarfs with separations less than $\sim$6.5 A.U ($0\farcs05$ at 135 pc). Orbital periods of resolved brown dwarf binaries in the Pleiades will be excessively long ($\geq$ several 100 yrs), making it impractical to compute their orbits and to derive dynamical masses. But with the age and the distance of the Pleiades cluster being well known, the masses and effective temperatures of the member objects can directly be obtained using the most recent evolutionary models.

4.2 Physical properties of binary brown dwarfs

After we had discovered enough multiple systems, it was time to study their individual properties, and see how the physical properties of very low mass stars and brown dwarfs depend on the age or the mass.

Physical properties of the individual components

Binaries offer a great advantage for the study of the physical properties: even if the age is not well constrained, both components of each binary are expected to be coeval, removing part of the above mentioned degeneracy in the mass-luminosity (age-temperature) relation. In one shot, one can thus see how the properties of very low mass stars and brown dwarfs depend on the mass at a given age. We thus aimed at studying the physical properties of the individual component

of several multiple systems. In order to do so we decided to take advantage of the very high angular resolution of HST to obtain spatially resolved optical spectra of four multiple systems.

Determination of the dynamical mass

In our sample we had the chance to find a short period binary. This object represented a unique chance to follow up the companion in its orbit and to determine, for the first time, the total mass of the system. The object is a pair of field L dwarfs. The spectroscopic orbit could unfortunately not be measured, because the rotational velocity of the components is too fast and covers the Doppler shifts of spectral lines. We could estimate the individual masses only using theoretical evolutionary tracks. Although this particular object will not allow us to constrain the models yet, it gives promising results for the near future.

Duplicity is not enough

Although many questions remain unanswered regarding the properties of binaries among very low mass objects, one can wonder if this class of objects is also able to form triple, quadruple, etc... systems stable enough that we can observe them. Although the frequency of higher orders multiple systems ($n \geq 2$) and the probability to observe one must be very low, our high angular resolution observations with HST led us to the discovery of a very good triple system candidate consisting of brown dwarfs. If confirmed by higher angular resolution observations, this would be the first triple system of brown dwarfs reported to date, opening a new field for investigations, and giving new constraints on the models of formation and evolution.

Part I

Statistical properties of binary ultracool dwarfs

Chapter 1

Ultracool dwarfs in the field

In order to look for multiple systems and measure their statistical properties, we performed a search for visual binaries among a sample of ultraccol dwarfs using the high angular resolution provided by HST and its WFPC2 Planetary Camera.

1.1 Observations

1.1.1 Sample

The initial sample consists primarily of 34 objects detected by the near-infrared sky surveys DENIS, 2MASS and SDSS. They have been selected by analysing their positions in a colour-magnitude diagram, looking for the reddest objects.

In order to increase the sample of objects and the quality of the statistical study, the total sample presented in this work put together data from program (GO8720, P.I. Brandner) with public data from the HST archive, coming from programs GO8146 (P.I. Reid), including 21 objects (Reid et al. 2001), and program GO8581 (P.I. Reid) (Gizis et al. 2003), including 84 objects. The total sample thus had 134 objects.

The complete list of targets of the program is shown in Table 1.1. Eleven of these objects were already previously identified as binary brown dwarfs.

Table 1.1. List of Targets

Name	R.A [a]	Dec [a]	SpT	I	J	H	K	Obs. Date	Dist.[c]
			GO8720						
DENIS-PJ020529.0-115925 *	02 05 29.0	-11 59 25	L7	18.30	14.43	13.61	13.00	2000-10-28	19.8 •
DENIS-PJ024351.0-543219	02 43 51.0	-54 32 19	M9	17.60	14.13	···	12.93	2001-07-02	34.4
DENIS-P030149-590302	03 01 49.0	-59 03 02	∼L0 [b]	16.84	13.71	···	12.56	2001-03-14	31.3
DENIS-PJ031433.1-462339	03 14 33.1	-46 23 39	∼L0 [b]	17.99	14.88	···	13.71	2001-06-12	54.7
DENIS-P035726.9-441730 **	03 57 26.9	-44 17 30	∼L3 [b]	18.07	14.58	···	12.91	2001-04-07	22.2
DENIS-PJ042655.9-573551	04 26 55.9	-57 35 51	∼L1 [b]	18.45	15.28	···	···	2001-03-03	62.3
DENIS-P044111.3+010554	04 41 11.3	+01 05 54	∼L0 [b]	19.38	16.27	···	···	2001-01-14	103.7
DENIS-PJ090957.1-065806	09 09 57.1	-06 58 06	L0	17.21	13.9	13.09	12.55	2000-10-29	26.4
DENIS-P100428.3-114648 **	10 04 28.3	-11 46 48	∼L0 [b]	18.0	14.9	···	13.67	2000-10-27	46.8
DENIS-P101621.9-271428	10 16 21.9	-27 14 28	∼L2 [b]	18.45	15.10	···	···	2000-10-22	47.1
DENIS-P104731.1-181558	10 47 31.1	-18 15 58	L2.5	17.75	14.24	···	12.88	2001-07-27	20.9
DENIS-P104814.7-395606	10 48 14.7	-39 56 06	∼L0 [b]	12.67	9.59	···	8.58	2001-04-07	4.9
2MASSWJ1145572+231730	11 45 57.2	+23 17 30	L1.5	18.62	15.37	14.52	13.92	2001-04-04	41.1
DENIS-PJ115442.2-340039	11 54 42.2	-34 00 39	∼L4 [b]	17.90	14.26	···	12.64	2001-04-07	20.9
DENIS-P121612.1-125731	12 16 12.1	-12 57 31	∼L1 [b]	18.30	15.11	···	···	2001-03-04	56.5
DENIS-PJ122813.8-154711 *	12 28 15.2	-15 47 34	L5	18.19	14.43	···	12.73	2001-03-04	20.2 •
DENIS-PJ122821.6-241541	12 28 21.6	-24 15 41	∼L5 [b]	18.00	14.28	13.4	12.71	2001-02-27	20.2
DENIS-PJ131500.9-251302	13 15 00.9	-25 13 02	∼M9 [b]	18.21	15.16	···	···	2001-03-29	65.3
2MASSW1342236+175156	13 42 23.6	+17 51 56	L2.5	19.81	16.06	15.12	14.59	2000-11-23	48.2
2MASSIJ1346464-003150	13 46 46.4	-00 31 50	T	20.0	15.86	16.05	15.74	2001-03-15	15.5
DENIS-PJ141217.1-043358	14 12 17.1	-04 33 58	∼L5 [b]	18.78	15.05	···	13.61	2001-03-27	25.7
2MASSWJ1439409+182637	14 39 40.9	+18 26 37	L1	19.87	16.21	15.47	14.53	2001-03-26	65.4
SDSS144001.8+002145.8	14 40 01.8	+00 21 45.8	L1	18.8	15.9	15.1	14.6	2001-01-28	101.1
DENIS-PJ144137.3-094559 *	14 41 37.3	-09 45 59	L1	17.32	14.25	···	12.37	2001-01-16	29.2
DENIS-PJ161928.3+005012	16 19 28.3	+00 50 12	∼L2 [b]	17.79	14.40	···	13.01	2001-06-02	32.4
DENIS-PJ191903.9-413433	19 19 03.9	-41 34 33	∼L3 [b]	19.4	15.9	···	···	2000-08-03	55.6
DENIS-PJ202333.6-181500	20 23 33.6	-18 15 00	∼L3 [b]	18.50	15.0	···	···	2001-03-24	36.7
DENIS-PJ221538.2-080912	22 15 38.2	-08 09 12	∼L1 [b]	17.86	14.56	···	13.26	2001-06-28	39.0
DENIS-PJ232931.7-540858	23 29 31.7	-54 08 58	M8 [b]	18.18	15.15	···	13.53	2001-07-03	64.3
			GO8146						
2MASSW003616+182110	00 36 16.0	+18 21 10	L3.5	16.0	12.44	11.58	11.03	2000-02-15	08.7 •
2MASSW0708213+295035	07 08 21.3	+29 50 35	L5	20.2	16.75	15.54	14.69	2000-03-23	44.8
2MASSW0740096+321203	07 40 09.6	+32 12 03	L4.5	19.6	16.2	14.8	14.2	2000-03-27	37.6
2MASSW0746425+200032 *	07 46 42.5	+20 00 32	L0.5	15.1	11.7	11.0	10.5	2000-04-15	12.3 •
2MASSW0820299+450031	08 20 29.9	+45 00 31	L5	20.0	16.3	15.0	14.2	2000-04-24	36.4
2MASSW0825196+211552	08 25 19.6	+21 15 52	L7.5	18.9	15.1	13.8	13.0	2000-03-25	10.7 •
2MASSW0850359+105715 *	08 50 35.9	+10 57 15	L6	···	16.5	15.2	14.5	2000-02-01	41.0 •

Table 1.1—Continued

Name	R.A [a]	Dec [a]	SpT	I	J	H	K	Obs. Date	Dist.[c]
2MASSW0913032+184150	09 13 03.2	+18 41 50	L3	19.4	15.9	14.8	14.2	2000-04-05	41.4
2MASSW0920122+351742 *	09 20 12.2	+35 17 42	L6.5	19.4	15.6	14.7	13.9	2000-02-09	20.1
2MASSW0928397-160312	09 28 39.7	-16 03 12	L2	18.8	15.3	14.3	13.6	2000-04-28	36.8
2MASSW1029216+162652	10 29 21.6	+16 26 52	L2.5	···	14.3	13.3	12.6	2000-03-06	21.4
2MASSW1123556+412228	11 23 55.6	+41 22 28	L2.5	19.6	16.1	15.1	14.3	2000-04-19	21.7 •
2MASSW1146344+223052 *	11 46 34.4	+22 30 52	L3	···	14.2	13.2	12.6	2000-04-28	27.2 •
2MASSW1155008+230705	11 55 00.8	+23 07 05	L4	19.5	15.8	14.7	14.1	2000-03-18	33.8
2MASSW132855+211449	13 28 55.0	+21 14 49	L5	19.8	16.1	16.0	14.3	2000-04-23	32.2 •
2MASSW1338261+414034	13 38 26.1	+41 40 34	L2.5	17.6	14.2	13.3	12.8	2000-04-25	20.5
2MASSW1343167+394508	13 43 16.7	+39 45 08	L5	19.8	16.2	14.9	14.1	2000-04-21	34.7
2MASSW1439284+192915	14 39 28.4	+19 29 15	L1	16.1	12.8	12.0	11.6	2000-03-22	14.4 •
2MASSW1507476-162738	15 07 47.6	-16 27 38	L5	17.0	12.8	11.9	11.3	2000-02-24	07.3 •
2MASSW1632291+190440	16 32 29.1	+19 04 40	L8	19.7	15.9	14.6	14.0	2000-04-20	15.2 •
2MASSW1726000+153819	17 26 00.0	+15 38 19	L2	19.4	15.7	14.5	13.6	2000-03-24	44.2
			GO8581						
2MASSW0010036+343609	00 10 03.6	+34 36 09	M8	18.5	15.6	15.1	14.4	2001-01-20	79.1
SDSS0019117+0030179	00 19 11.7	+00 30 17.9	L1	18.4	14.9	14.2	13.6	2001-07-09	35.8
2MASSW0028394+150141	00 28 39.4	+15 01 41	L4.5	20.0	16.5	15.3	14.6	2001-01-14	43.2
2MASSW0030300-145033	00 30 30.0	-14 50 33	L7	18.6	16.8	15.4	14.4	2001-01-13	33.5
2MASSW0033239-152131	00 33 23.9	-15 21 30.9	···	18.3	···	···	···	2001-05-13	···
2MASSW0208183+254253	02 08 18.3	+25 42 53	L1	17.7	14.0	13.1	12.6	2000-08-26	23.6
2MASSW0224366+253704	02 24 36.6	+25 37 04	L2	19.7	16.6	15.4	14.7	2001-01-09	66.9
2MASSW0326422-210205	03 26 42.2	-21 02 05	L3.5[b]	19.9	16.11	14.77	13.88	2000-12-30	32.2 •
2MASSW0328426+230205	03 28 42.6	+23 02 05	L8	20.3	16.7	15.6	14.8	2001-02-28	27.3
SDSS0330351-002534	03 30 35.1	-00 25 34	L2	19.0	15.29	14.42	13.83	2001-06-30	36.6
2MASSW0335020+234235	03 35 02.0	+23 42 35	∼L2[b]	15.7	12.26	11.65	11.26	2001-07-21	11.3
2MASSW0337036-175807	03 37 03.6	-17 58 07	L4.5	19.4	15.6	14.4	13.6	2000-12-25	28.5
SDSS0344089+011125	03 44 08.9	+01 11 25.0	···	18.2	···	···	···	2001-07-12	···
2MASSW0345432+254023	03 45 43.2	+25 40 23	L0	17.7	14.0	13.2	12.7	2001-03-27	26.9 •
2MASSW0350573+181806	03 50 57.3	+18 18 06	∼L2[b]	16.4	13.0	12.2	11.8	2001-02-26	16.8
2MASSW0355419+225701	03 55 41.9	+22 57 01	L3	19.6	16.1	15.0	14.2	2000-08-25	45.4
SDSS0539519-005901	05 39 51.9	-00 59 01	L5	18.0	14.02	13.09	12.51	2000-11-27	12.7
2MASSW0753321+291711	07 53 32.1	+29 17 11	L2	19.0	15.5	14.5	13.8	2000-09-08	40.3
2MASSW0801405+462850	08 01 40.5	+46 28 50	L6.5	19.7	16.3	15.4	14.5	2001-03-08	28.7
2MASSW0829570+265510	08 29 57.0	+26 55 10	L6.5	20.6	17.0	15.8	14.9	2001-04-18	39.7
2MASSW0832045-012835	08 32 04.5	-01 28 35	L1.5	17.9	14.1	13.3	12.7	2000-09-23	22.9
2MASSW0856479+223518**	08 56 47.9	+22 35 18	L3	19.2	15.65	14.58	13.92	2001-04-24	34.7
2MASSW0914188+223813	09 14 18.8	+22 38 13	∼L1[b]	18.6	15.30	14.40	13.90	2001-04-07	54.8

Table 1.1—Continued

Name	R.A [a]	Dec [a]	SpT	I	J	H	K	Obs. Date	Dist.[c]
2MASSW0951054+355802	09 51 05.4	+35 58 02	L6	20.7	17.1	15.8	15.1	2001-01-26	44.9
2MASSW1017075+130839**	10 17 07.5	+13 08 39	L3	17.8	14.1	13.2	12.7	2001-04-16	21.4
SDSS1043251+000148	10 43 25.1	+00 01 48	L3	19.3	15.95	15.17	14.53	2001-05-02	42.4
2MASSW1102337-235945	11 02 33.7	-23 59 45	L4.5	20.4	17.0	15.6	14.8	2001-05-10	54.3
2MASSW1104012+195921	11 04 01.2	+19 59 21	L4.5	18.3	14.4	13.5	13.0	2001-04-26	16.4
2MASSW1108307+683017	11 08 30.7	+68 30 17	L1	17.2	13.31	12.2	11.92	2000-10-02	17.2
2MASSW1112256+354813**	11 12 25.6	+35 48 13	L4.5	18.5	14.6	13.5	12.7	2001-02-14	21.7 •
2MASSW1127534+741107**	11 27 53.4	+74 11 07	∼L2[b]	16.5	13.1	12.4	12.0	2001-05-05	14.6
2MASSW1239194+202952	12 39 19.4	+20 29 52.0	···	17.8	···	···	···	2001-05-13	···
2MASSW1239272+551537**	12 39 27.2	+55 15 37	L5	18.6	14.7	13.5	12.7	2001-03-18	21.3
2MASSW1311391+803222**	13 11 39.1	+80 32 22	∼L2[b]	16.2	12.8	12.1	11.7	2000-07-30	13.7
2MASSW1403223+300754	14 03 22.3	+30 07 54	M8.5	16.3	12.7	12.0	11.6	2001-06-14	19.2
2MASSW1411175+393636	14 11 17.5	+39 36 36	L1.5	18.2	14.7	13.8	13.3	2000-09-19	30.2
2MASSW1412244+163312	14 12 24.4	+16 33 12	L0.5	17.6	13.89	13.06	12.59	2000-09-02	24.3
2MASSW1426316+155701*	14 26 31.6	+15 57 01.3	M9	16.5	12.87	12.18	11.71	2001-07-19	26.7
2MASSW1430435+291540**	14 30 43.5	+29 15 40	L2	18.0	14.3	13.4	12.7	2001-04-19	29.4
2MASSW1434264+194050	14 34 26.4	+19 40 50.0	···	18.5	···	···	···	2001-05-11	···
SDSS1435172-0046129	14 35 17.2	-00 46 12.9	L0	19.7	16.5	15.6	15.3	2001-07-23	87.5
SDSS1435357-004347	14 35 35.7	-00 43 47	L3	19.2	16.5	15.7	15.0	2001-05-11	54.6
2MASSW1438549-130910	14 38 54.9	-13 09 10	L3	19.1	15.5	14.5	13.9	2001-03-12	34.5
2MASSW1438082+640836	14 38 08.2	+64 08 36	∼L6[b]	16.8	12.92	12.03	11.57	2001-03-10	7.2
2MASSW1449378+235537**	14 49 37.8	+23 55 37	L0	18.9	15.6	15.0	14.5	2000-12-21	63.7
2MASSW1457396+451716	14 57 39.6	+45 17 16	∼L3[b]	16.7	13.1	12.4	11.9	2000-10-31	13.1
2MASSW1506544+132106	15 06 54.4	+13 21 06	L3	17.4	13.4	12.4	11.7	2001-05-09	13.1
SDSS151547.2-0030597	15 15 47.2	-00 30 59.7	···	17.5	···	···	···	2001-05-06	···
2MASSW1526140+204341	15 26 14.0	+20 43 41	L7	19.1	15.6	14.5	13.9	2001-05-09	19.2
SDSS154831.7+0029415	15 48 31.7	-00 29 41.5	···	18.5	···	···	···	2001-05-30	···
2MASSW1550382+3041037	15 50 38.2	+30 41 03.7	···	16.3	···	···	···	2001-05-10	···
2MASSW1551066+645704	15 51 06.6	+64 57 04	∼L3[b]	16.5	12.9	12.1	11.7	2000-09-17	12.0
2MASSW1600054+170832**	16 00 05.4	+17 08 32	L1.5	19.3	16.1	15.1	14.7	2001-01-14	60.6
2MASSW1627279+810507	16 27 27.9	+81 05 07	∼L5[b]	16.8	13.0	12.3	11.9	2001-03-15	19.0
2MASSW1635191+422305	16 35 19.1	+42 23 05	∼L3[b]	16.5	12.9	12.2	11.8	2001-05-12	12.0
SDSS1653297+6231365	16 53 29.7	+62 31 36.5	L3	18.1	15.1	14.4	13.9	2001-05-04	28.7
2MASSW1656188+283506	16 56 18.8	+28 35 06	L4.5	20.3	17.1	15.9	15.0	2001-04-25	56.9
2MASSW1707333+430130	17 07 33.3	+43 01 30	L0	17.6	14.0	13.2	12.7	2001-05-13	27.7
2MASSW1707183+6439334	17 07 18.3	+64 39 33.4	···	16.3	···	···	···	2001-05-13	···
2MASSW1710254+210715	17 10 25.4	+21 07 15	∼M8[b]	18.6	15.87	15.02	14.46	2001-03-19	106.7
2MASSW1711457+223204	17 11 45.7	+22 32 04	L6.5	20.4	17.1	15.8	14.7	2001-03-20	41.6

1.1.2 Observationnal strategy and techniques

The observations occurred between February 2000 and August 2001 during HST Cycles 8 and 9. They have been carried out in snapshot mode. Each object was observed with the Planetary Camera of HST/WFPC2, in the F675W (600 s) and F814W (300 s) for our own program, in the F606W (100 s) and F814W (300+350 s) filters for program GO8146 (Cycle 8, P.I. Reid, see Reid et al. 2001) and in the F814W (100 s, 200 s or 400 s) and F1042M (500 s) filters for program GO8581 (Cycle 9, P.I. Reid, see Gizis et al. 2003). Some objects have been observed twice : once during our own HST program and the second time during HST program GO9157 (P.I. Martín). Our targets are very red, thus the observations in F814W were sensitive to even lower mass companions than the observations in F675W, despite the shorter exposure time and the lower quantum efficiency of WFPC2 at longer wavelengths. For our program (GO8720), only one exposure was taken in each filter for each object, thus not allowing to reject cosmic rays automatically. This choice was done to minimise overheads and maximise exposure times.

1.2 Data analysis

1.2.1 Identification of the multiple systems

We processed the data in two steps. We first identified the multiple systems either directly when resolved or by performing a detailed PSF analysis. Taking advantage of the extremely stable PSF of HST/WFPC2, we performed a PSF subtraction on each target using 9 different unresolved objects from programs GO8720 (P.I. Brandner, Bouy et al. 2003) and GO8581 (P.I. Reid, Gizis et al. 2003), and 1 synthetic PSF obtained with *Tiny Tim* (Krist & Hook 2003) as reference PSF stars. Using this technique, we tried to define a criterium that would allow to determine quantitatively if the secondary is a multiple system or not. We thus performed a detailed PSF analysis of all the WFPC2 images of programs GO8720, GO8146 (P.I. Reid, Reid et al. 2001) and GO8581. These three samples have the great advantage to be homogeneous (all used the WFPC2/PC with the F814W filter), and were all dedicated to the search for multiple systems among very low mass stars and brown dwarfs.

The relative intensity of the residuals, defined as the integrated intensity of the residuals after PSF subtraction, divided by the integrated intensity of the object as expressed in equation 1.1, appears to be a powerful criterium to identify binary candidates.

$$\mathcal{R}.\mathcal{I} = \frac{\sum_{i=1}^{n} \mathcal{F}_R^2(i)}{\sum_{i=1}^{n} \mathcal{F}_O^2(i)} \tag{1.1}$$

where: n is the number of pixels, $\mathcal{F}_R(i)$ is the flux in pixel i after PSF subtraction, and $\mathcal{F}_O(i)$ is the flux in pixel i before PSF subtraction.

Figure 1.1 shows that $\mathcal{R}.\mathcal{I}$ is very low and very stable for unresolved objects, while it is always higher than $\sim$3-σ above the median value in the case of multiple systems. This technique found easily and automatically all the multiple systems present in these samples (see Reid et al. 2001; Bouy et al. 2003; Gizis et al. 2003), except one (2MASSW J0856479+223518). This latter multiple system is indeed a good example to illustrate the limitations of this technique. 2MASSW J0856479+223518 is a very close binary (δ=0.″1) with a relatively large difference of magnitude (ΔMag=2.8 mag, see Section 1.5.5). The relative intensity of the residuals after PSF

Table 1.1—Continued

Name	R.A [a]	Dec [a]	SpT	I	J	H	K	Obs. Date	Dist.[c]
SDSS1723287+6406233	17 23 28.7	+64 06 23.3	···	19.1	···	···	···	2001-05-30	···
2MASSW1728114+394859**	17 28 11.4	+39 48 59	L7	19.6	16.0	14.8	13.9	2000-08-12	20.4
2MASSW1743349+212711	17 43 34.9	+21 27 11	L2.5	19.3	15.80	14.78	14.29	2001-01-24	42.8
2MASSW1743348+584411	17 43 34.8	+58 44 11	L0.5	17.7	14.02	13.15	12.67	2001-06-15	25.8
2MASSW1841086+311727	18 41 08.6	+31 17 27	L4	19.6	16.1	15.0	14.2	2001-03-08	38.8
2MASSW2054358+151904	20 54 35.8	+15 19 04	L1	19.6	16.5	15.6	14.8	2001-05-03	74.8
2MASSW2057153+171515	20 57 15.3	+17 15 15	L1.5	19.4	16.1	15.2	14.6	2001-05-02	57.5
2MASSW2101154+175658**	21 01 15.4	+17 56 58	L7.5	20.1	16.87	15.70	15.04	2001-05-07	23.2
2MASSW2140293+162518*	21 40 29.3	+16 25 18	∼L2[b]	16.4	12.9	12.3	11.8	2001-05-31	12.9
2MASSW2147436+143131**	21 47 43.6	+14 31 31	∼L2[b]	17.3	13.8	13.1	12.7	2000-10-09	21.8
2MASSW2158045-155009	21 58 04.5	-15 50 09	L4	18.8	14.9	13.9	13.1	2000-10-30	22.3
2MASSW2206449-421720	22 06 44.9	-42 17 20	L2	19.2	15.6	14.5	13.6	2001-03-22	42.2
2MASSW2206228-204705*	22 06 22.8	-20 47 05	M8	16.0	12.4	11.7	11.3	2000-08-13	22.2 •
2MASSW2208136+292121	22 08 13.6	+29 21 21	L2	19.5	15.82	14.83	14.09	2000-10-12	46.7
2MASSW2234139+235955	22 34 13.9	+23 59 55	M9.5	16.5	13.2	12.4	11.8	2001-01-14	20.7
2MASSW2242531+254257	22 42 53.1	+25 42 57	<M5[b]	18.3	14.8	13.8	13.0	2001-04-26	···
2MASSW2244316+204343	22 44 31.6	+20 43 43	L6.5	20.1	16.53	14.97	13.97	2001-05-09	11.3 •
2MASSW2306292-050227	23 06 29.2	-05 02 27	∼L4[b]	15.1	11.37	10.72	10.29	2000-08-18	8.6
2MASSW2309462+154905	23 09 46.2	+15 49 05	···	18.2	···	···	···	2000-10-10	···
2MASSW2331016-040619*	23 31 01.6	-04 06 19	∼L2[b]	16.3	12.9	12.3	11.9	2001-05-06	26.2 •
SDSS2335583-001304**	23 35 58.3	-00 13 04.0	···	18.9	···	···	···	2001-06-29	62
2MASSW2349489+122438	23 49 48.9	+12 24 38	∼L4[b]	16.2	12.6	12.0	11.6	2001-05-13	19.2

* indicates the previously known binaries

** indicates the new multiple systems candidates presented in this work

[a] J2000

[b] Spectral Types estimated using the SpT vs. (I-J) relation given in Dahn et al. (2002)

[c] Distances in pc estimated as explained in the text or by trigonometric parallax (Dahn et al. 2002; Perryman et al. 1997) when available (these latter cases are indicated with a sign •)

subtraction of the primary, corresponding roughly to the ratio of the intensity of the secondary over that of the primary, is therefore of the order of a few percents only (ΔMag=2.8 mag is equivalent to a flux ratio of f_B/f_A ~0.07). The relative intensity of the residuals after PSF subtraction is therefore a good method to find multiple systems with moderate differences of magnitude. As a sanity check, all images have been inspected manually to confirm the mutliplicity of objects found by this method and to ensure that we did not miss any candidate. The method proves to be very efficient, since all the candidates found this way have been confirmed by the visual check. Few objects had residuals just at or just above the limit, but a more careful visual check of the images and of the residuals shows that they were due either to bad pixels or to much lower S/N in the image than the S/N of the PSF stars used for subtraction. Although they cannot be ruled out as possible very close binary candidates, we will not include them in the rest of this study.

Figure 1.2 is a gallery of all the multiple systems identified this way, plus CFHT-PL-18.

1.2.2 Relative astrometry and photometry with WFPC2: PSF fitting

The PSF of the HST at these wavelengths has a core of about 0.″070, whereas the pixelscale is 0.″0455 (Biretta 2002). The PSF is therefore badly undersampled. Nyquist sampling is generally thought to be required to enable precise astrometric analysis, but fortunately we do not need Nyquist sampling to be able to measure the precise positions of the objects in the images. The PSF is indeed not so sharp that all of a star's flux falls within a single pixel. If a reasonnable amount of flux falls in the surrounding pixels, we have enough information to measure accurate positions, by correlating not only one pixel but many more. Shifting the object's position by a small amount redistributes the light from one pixel to another. The program I wrote to measure the relative astrometry and photometry of the multiple systems is based on this idea.

A single point source can be described by only three parameters: the position of its centroid (x, y), and its total flux (f). In the case of a binary, the system must therefore be described by 6 parameters. The custom made program used here makes a non-linear fit of the binary system, fitting both components at the same time. To make the fit, it uses different PSF of unresolved stars from throughout the sample and for each of them compute a model of the binary system (see Figure 1.3). A minimum–χ^2 between the model and the binary system gives the best values for the six parameters. In order to minimise the effects due to the slight position sensitivity of the PSF shape in the detector and the slight change of HST focus from one orbit to another, the program uses a library of eight different PSF stars in each filter. For each object, the fit was performed once with each PSF and the final result obtained by calculating the mean of the eight different values. As eight PSF stars were not available in every field of view, the program used the same library of PSF stars to analyse all the images. Comparison with analysis of images where 8 PSF stars were present in the field showed that this has no significant effect on the accuracy of the results. The systematic errors and uncertainties associated to that method are discussed in details in Annex A. Figures 1.5 and 1.4 gives an overview of the results and limitations of the method.

1.3 Accuracy of the results and limits of the analysis

An overview of the results is given in Table 1.2 and Figure 1.5, and an example is given in Figure 1.3. The uncertainties given in Table 1.2 correspond to the 1-σ uncertainties calculated as explained in Annex A. As the observations in the F814W filter offer a much better S/N than in the F675W and F1042M filters, and a much better sampling than the F675W (the diffraction

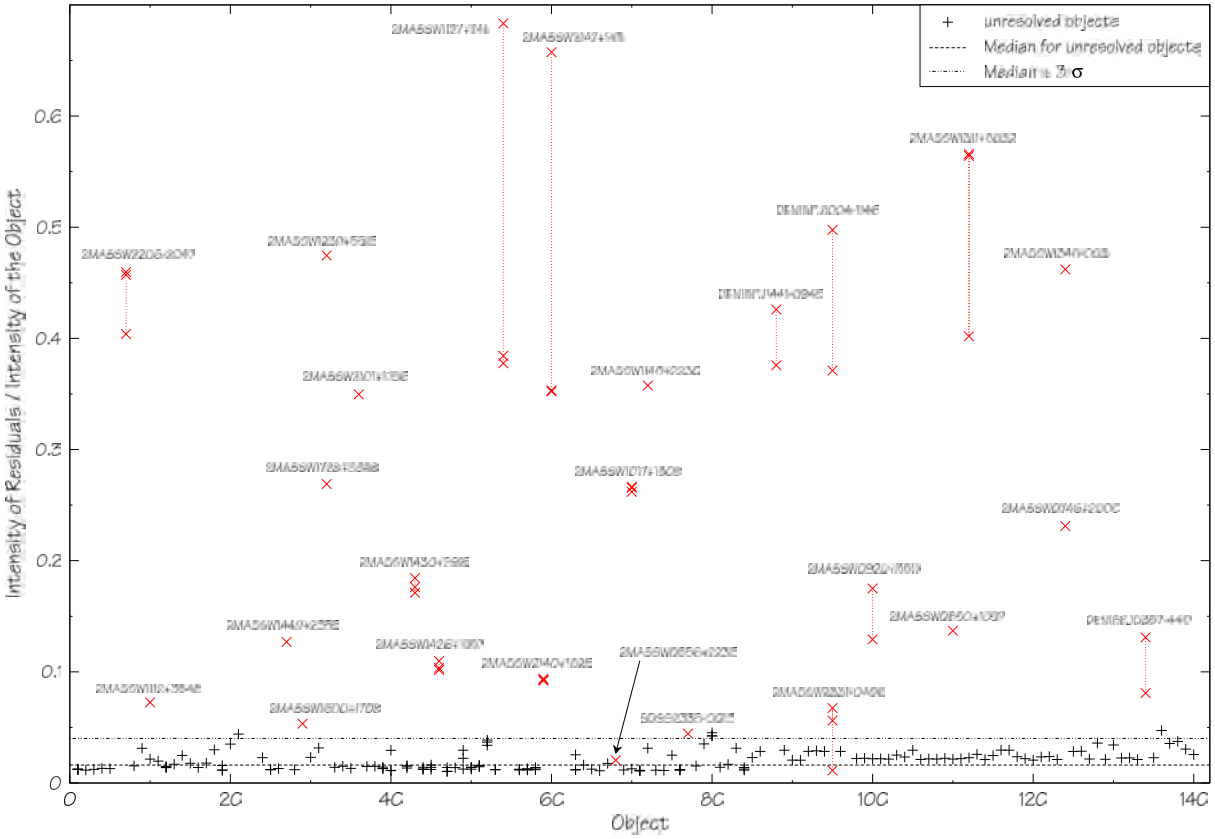

Figure 1.1 Relative intensity of the residuals after PSF subtraction on the field ultraccol dwarfs of our sample. Comparison with unresolved objects (black plus), visually resolved binaries (red crosses, linked by a dot line when corresponding to the same object in different images). The relative intensity of the residuals for unresolved objects is almost always smaller than 4.0% (=3-σ above the median), with a median value at 1.5%, while the residuals of visually resolved binaries are always greater than 4.0%, except in the case of 2MASSW J0856479+223518. This latter object is very peculiar since it is very close and it has a much smaller flux ratio than any other object, explaining why the method is inconclusive in its case. Few objects are just above the limit, but a careful visual check show that their are not visual binaries. The relative intensity of the residuals appears to be a good indicator to detect possible multiple systems.

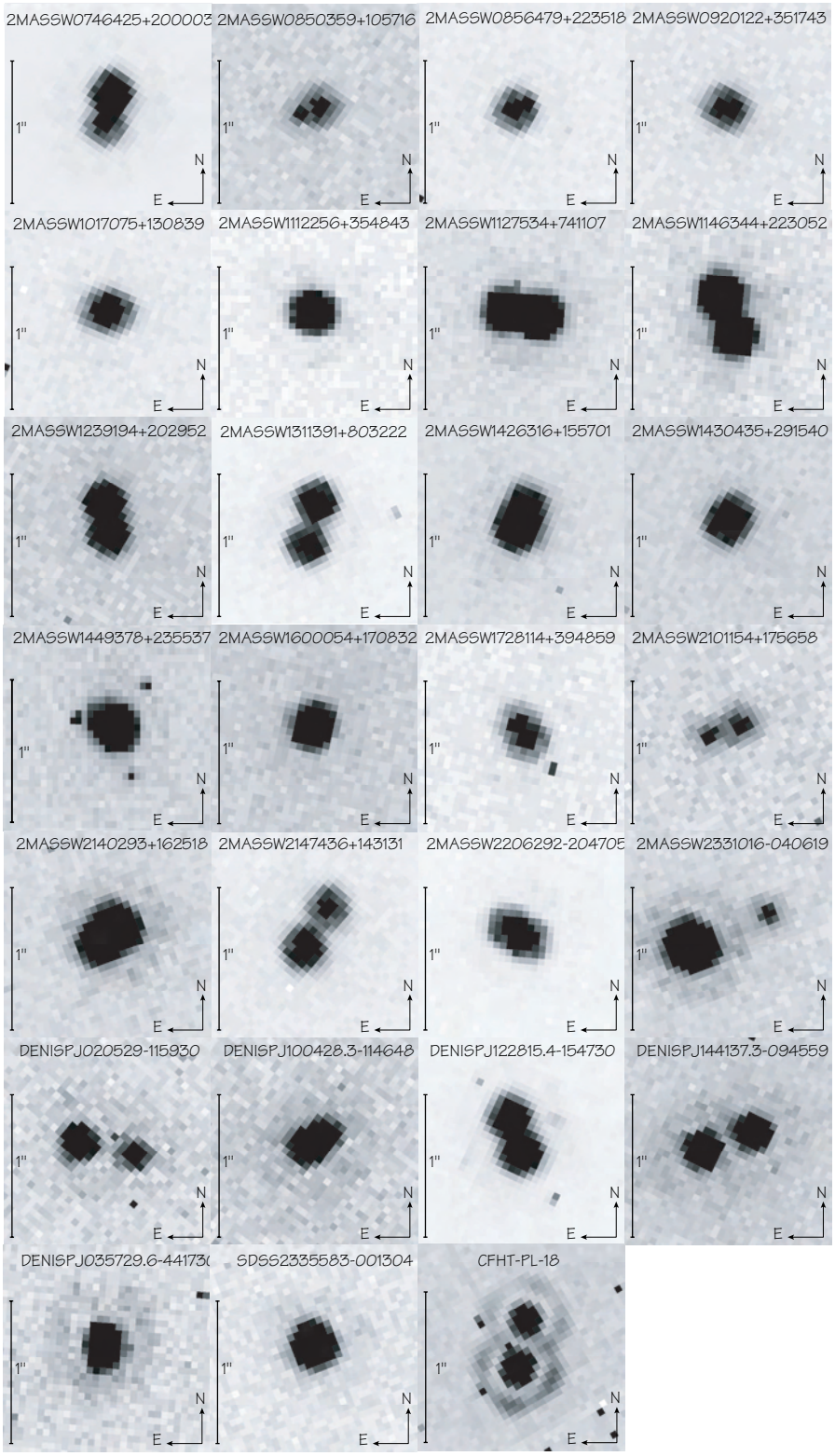

Figure 1.2 Mosaic of the 26 binaries and binary candidates presented in this paper (HST/WFPC2, F814W filter) and CFHT-PL-18 (Martín et al. 1998, HST/NICMOS, F165W filter)

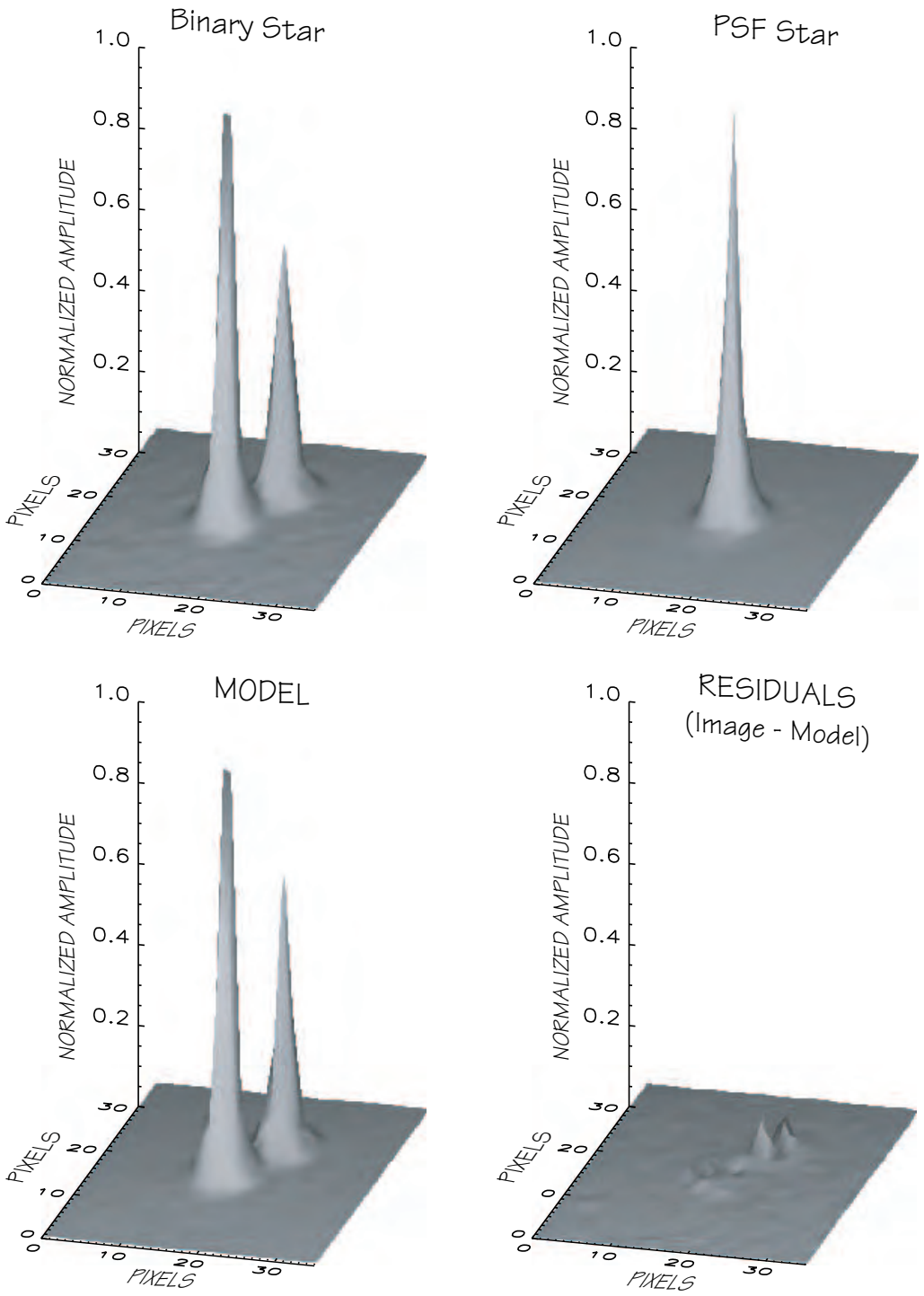

Figure 1.3 Surface plots of the PSF fitting. Top left panel : Binary system observed with WFPC2-PC. Top right panel : PSF star from the field observed with the same settings and used to modelize the binary system. Bottom left panel : Model of the binary system built with the PSF Star. Bottom right panel : Residuals after subtraction of the model - All amplitudes are normalized, and sky has been subtracted. The images were obtained in the F814W filter.

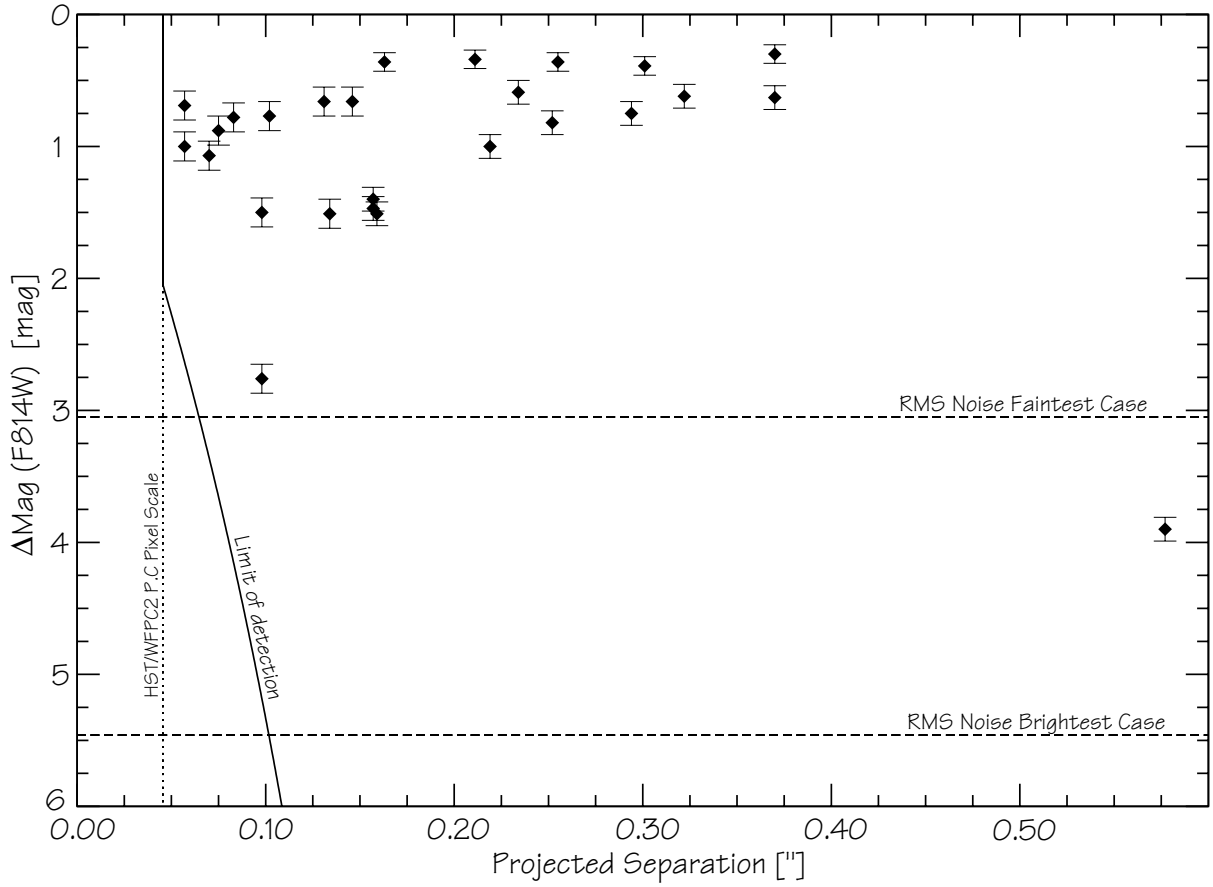

Figure 1.4 Limits of detection. The largest difference of magnitude we were able to detect is shown here as a function of the angular separation. At separations close to the pixel scale, the detection of companions is limited by the contrast against the bright primary. At larger separations, the detection is background limited. The full line represents the HST/WFPC2 limit of detection and the 2 dashed lines the 3-σ RMS noise in the faintest and brightest cases. The limit of detection has been computed by calculating the average of the 3-σ RMS noise on the radial profile of several unresolved objects. The results obtained for the 26 binaries reported in this paper are represented by filled diamonds with their uncertainties.

limit is indeed 0.″0703 in the F675W filter, and 0.″0860 in the F814W filter, and the pixel scale of the WFPC2/PC camera is 0.″0455), they are considered more accurate.

Table 1.2. Results of the PSF fitting

Name	Date of Obs.	Sep. (mas) [d]	P.A (°) [d]	Δmag[d]	mag(A)[e]	Filter
			GO8720			
DENISPJ0205-1159	2000-10-28	409 [b]	259.7 [b]	1.47±0.19	20.75±0.26	F675W
	2000-10-28	398 [b]	257.9 [b]	0.65±0.16	18.32±0.24	F814W
	2001-07-08	370.0	255.8 ± 0.3	0.63±0.09	18.58±0.15	F814W
DENISPJ0357-4417	2001-04-07	97.0	174 ± 1.2	1.23±0.11	20.37±0.18	F675W
	2001-04-07	98.1	174.7± 1.2	1.50±0.11	17.94±0.18	F814W
DENISPJ1004-1146	2000-10-27	146.0	306.1 ± 1.2	0.25±0.07	20.88±0.18	F675W
	2000-10-27	146.0	304.5 ±1.2	0.66±0.11	18.40±0.18	F814W
DENISPS1228-1547	2001-03-04	264 [a]	21.5 ± 1.0	0.53±0.09	20.52±0.15	F675W
	2001-03-04	246 [a]	23.1 ± 2.0	0.44±0.09	18.37±0.15	F814W
	2001-06-16	255.4	18.3 ± 0.3	0.36±0.07	18.34±0.14	F814W
DENISPJ1441-0945	2001-01-16	374.0	290.4 ± 0.3	0.63±0.09	20.05±0.15	F675W
	2001-01-16	375.1	290.3± 0.3	0.37±0.07	17.84±0.14	F814W
	2001-05-22	370.2	290.8± 0.3	0.30±0.07	17.82±0.14	F814W
			GO8146			
2MASSW0746+2000	2000-04-15	219.0	168.8 ± 0.3	1.0±0.09	15.41±0.15	F814W
2MASSW0850+1057	2000-02-01	157.2	114.7 ± 0.3	1.47±0.09	20.29±0.15	F814W
2MASSW0920+3517	2000-02-09	75.1	248.5 ± 1.2	0.88±0.11	19.83±0.18	F814W
2MASSW1146+2230	2000-04-28	294.1	199.5 ± 0.3	0.75±0.09	18.17±0.15	F814W
			GO8581			
2MASSW1239+5515	2001-03-18	211.0	187.6 ± 0.3	0.34±0.07	18.86±0.15	F814W
	2001-03-18	210.1	184.2 ± 0.3	0.54±0.09	14.62±0.15	F1042M
2MASSW1311+8032	2000-07-30	300.8	167.2 ± 0.3	0.39±0.07	16.00±0.17	F814W
	2000-07-30	300.0	167.3 ± 0.3	0.45±0.09	13.65±0.17	F1042M
2MASSW1426+1557	2001-07-19	157.1	339.9 ± 0.3	1.40±0.09	16.15±0.17	F814W
	2001-07-19	154.2	340.1 ± 0.3	1.30±0.09	13.99±0.17	F1042M
2MASSW1430+2915	2001-04-19	83.0	327.1 ± 1.2	0.78±0.11	18.16±0.18	F814W

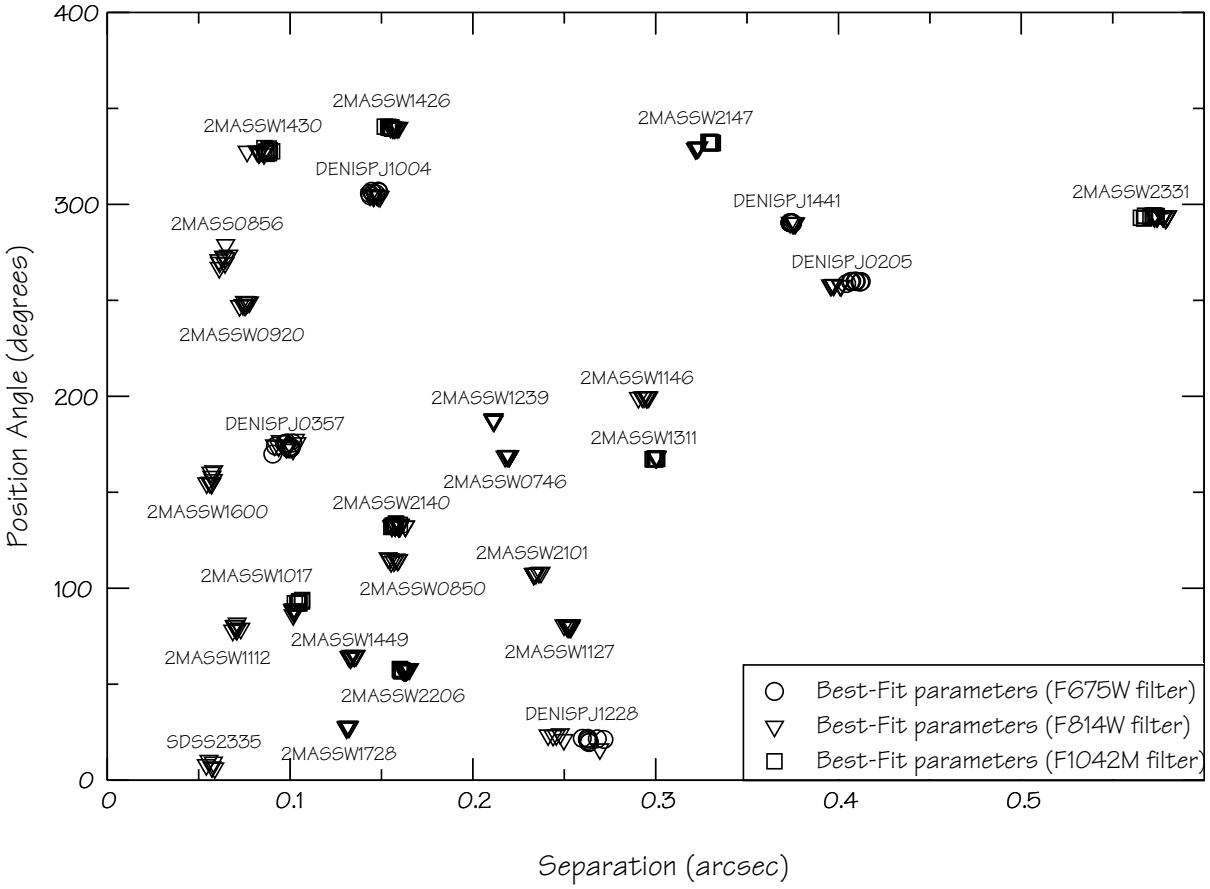

Figure 1.5 Best Fit parameters (separation and position angle) obtained for each object using different PSF stars for the fit. The eight values in each filters have been obtained using the library of eight different PSF stars. The parameters derived using the PSF fitting are in very good agreement for most of the objects, even at the smallest separations. The slight dispersion of the values for DENIS1228, DENIS0205 are explained respectively in paragraphs 1.5.12 and 1.5.1 and Chapter 3. One can notice that the values in the F814W filter are usually less dispersed than in the F675W filter (worse S/N, worse sampling and coarser PSF).

Only the values obtained with the F814W filter are therefore used to compute the final parameters given in Table 1.2. For the data from the archive only the F814W and/or F1042M filters are available (the objects were too faint in the F606W filter).

The PSF at these wavelengths is under-sampled by the $0\farcs0455$ pix^{-1} plate scale of the Planetary Camera, thus not allowing to use deconvolution in the Fourier space. By using non-linear PSF fitting as described above, it is possible to push the limit of detection down to $\sim 0\farcs060$ arcsec for non-equal luminosity systems. Figure 1.4 shows that we should have been able to detect all the binary systems with differences of magnitudes between $1.5 \leq \Delta m_{F814W} \leq 3.0$ mag easily even in the faintest cases, and binary systems with differences of magnitudes between $3.0 \leq \Delta m_{F814W} \leq 5.5$ mag in the brightest cases.

Table 1.2—Continued

Name	Date of Obs.	Sep. (mas) [d]	P.A (°) [d]	Δmag[d]	mag(A)[e]	Filter
	2001-04-19	88.0	327.5 ± 1.2	0.76±0.11	15.13±0.18	F1042M
2MASSW1449+2355	2000-12-21	134.0	64.4 ± 1.2	1.51±0.11	18.93±0.18	F814W
	2000-12-21	129.0	63.4 ± 1.2	1.08±0.11	15.17±0.18	F1042M
2MASSW1600+1708	2001-01-14	57.0	156.2 ± 1.2	0.69±0.11	19.81±0.17	F814W
2MASSW1728+3948	2000-08-12	131.3	27.6 ± 1.2	0.66±0.11	20.25±0.17	F814W
2MASSW2101+1756	2001-05-07	234.3	107.7 ± 0.3	0.59±0.09	20.84±0.17	F814W
2MASSW2140+1625	2001-05-31	159.0	132.4 ± 0.3	1.51±0.09	16.04±0.17	F814W
	2000-05-31	157	132.8 ± 0.3	1.38±0.09	13.78±0.17	F1042M
2MASSW2147+1431	2000-10-09	322.7	329.5 ± 0.3	0.62±0.09	17.38±0.17	F814W
	2000-10-09	333[c]	332[c]	0.75±0.28[c]	14.67±0.30	F1042M
2MASSW2206-2047	2000-08-13	163.0	57.5 ± 0.3	0.36±0.07	15.69±0.14	F814W
	2000-08-13	160.7	57.2 ± 0.3	0.30±0.07	13.84±0.14	F1042M
2MASSW2331-0406	2001-05-06	577.0	293.7 ± 0.3	3.90±0.09	15.63±0.17	F814W
	2000-05-06	570.0	293.7 ± 0.3	3.54±0.09	13.63±0.17	F1042M
SDSS2335583-001304	2001-06-29	56.8	8.1 ± 1.2	1.00±0.11	19.18±0.18	F814W

[a]The object was observed in a corner of the HST/WF, where the pixel scale is coarser and the distortions higher, hence implying higher uncertainties, explaining the discrepancy between the values obtained in the two filters

[b]The secondary fell on a boundary between two pixels and was very elongated on both images, thus increasing the uncertainties and explaining the discrepancy between the values obtained in the two filters. As the image in the F814W were more sensitive and as the secondary is brighter in that band, we hereafter keep the corresponding value as final result

[c]A cosmic ray event fall too close to the primary to allow precise measurements

[d]1σ uncertainties: refer to the description given in section 1.2.2, unless a different value is specified in the table.

[e]The uncertainties on these values includes both the uncertainties on the measure of the magnitude of the whole system and the uncertainties on the difference of magnitude.

1.4 Photometry, Spectral Classification and Distances

An overview of values of photometry, spectral types, and distances for all the targets of the sample is given in Tables 1.1, 1.3, 1.5 and 1.4. The I,J,K_s values of the DENIS objects come from the DENIS survey. The J,H,K_s values of the 2MASS and some SDSS objects come from the 2MASS survey (Kirkpatrick et al. 2000) and from Davy Kirkpatrick's on-line archive of L and T dwarfs[3] . The I values of the 2MASS and SDSS targets have been calculated as follow : using the F675W and F814W magnitudes obtained in the data (see Tables 1.3,1.5 and 1.4) and the I magnitudes of the DENIS objects of our program (see Table 1.1), one can derive the following relation:

$$I_{DENIS} = -0.81 + 1.02 \times m_{F814W} + 0.28 \times (m_{F675W} - m_{F814W}) \quad (1.2)$$

with a dispersion of 0.18 mag (thus of the same order than the uncertainties on the DENIS magnitudes themselves) and used it to compute the I magnitudes[4] given in Table 1.1.

The magnitudes have been measured with standard procedures using the aperture photometry task *phot* in IRAF, with sky subtraction and a 3-σ rejection. We used a recommended aperture of 0.″5 in the case of unresolved objects (Baggett et al. 2002), and an aperture of 1.″365 (30 pixels) in the case of binaries, to measure the total flux of the system. The counts were transformed to magnitudes using the relation : $m[mag] = -2.5 \cdot log(counts/exp) + ZP - 0.1$ for the unresolved objects, where *counts* is the number of counts measured with IRAF, *exp* the exposure time, ZP the Vega Zero Point magnitude ($ZP_{F675W} = 22.042$ mag, $ZP_{F814W} = 21.639$ mag, and $ZP_{F1042M} = 16.148$ mag, Baggett et al. (2002)) and -0.1 is to correct from the finite to infinite aperture, according to the HST data handbook, and the relation: $m[mag] = -2.5 \cdot log(counts/exp) + ZP - 0.028$ in the case of binaries, where -0.028 is the correction evaluated as suggested in the HST data Handbook to correct from the finite to infinite aperture in that case. For multiple systems, the magnitude of each component were deduced using the values of flux ratios obtained with the PSF fitting. In many cases only one image was available, thus not allowing to remove cosmic ray events automatically. Nevertheless cosmic rays should not have influenced our photometry significantly since we would have been able to detect any cosmic ray event too close to the object to be removed by the 3-σ automatic rejection. This situation happened in only one case (2MASSW J2147437+143131, F1042M filter). All the cosmic ray events sufficiently far away from the object have been corrected by the 3-σ automatic rejection of the IRAF *phot* task. The results are given in Tables 1.2, 1.3, 1.5 and 1.4. Uncertainties for the unresolved objects are 0.1 mag.

A few DENIS objects and most 2MASS and SDSS objects had accurate values of spectral types found in Davy Kirkpatrick's on-line archive of L and T dwarfs, and obtained through spectroscopic measurements. For the other objects, we used the Dahn et al. (2002) spectral type vs. $(I - J)$ colour relation to deduce the spectral types given in Table 1.1. These latter spectral types will have to be confirmed by spectroscopic measurements. The sample thus covers a large range of spectral types, going from ∼M8 to ∼L8.

Two efforts by the United States Naval Observatory and by an Australian group led by Chris Tinney are currently under way in order to derive precise angular parallaxes for these objects. Some of the targets already have published angular parallaxes and distances (Dahn et al. 2002). For the unresolved objects without published trigonometric parallax, the photometric parallax was evaluated using the Dahn et al. (2002) M_J vs. Spectral Type relation when both J and

[3] *http://spider.ipac.caltech.edu/staff/davy/ARCHIVE/*

[4] I_{DENIS} is very close to the $I_{Cousins}$ (Delfosse X., PhD thesis, Universite Joseph Fourier, Grenoble, 1997)

Table 1.3. Photometry of the unresolved objects of program GO8720

Name[a]	m_{F814W} [b]	m_{F675W} [b]
DENISPJ0243-5432	17.1	19.5
DENISPJ0301-5903	16.6	19.2
DENISPJ0314-4623	17.9	···
DENISPJ0426-5735	18.3	19.9
DENISPJ0441-0211	18.7	20.7
DENISPJ1016-2714	18.0	20.4
DENISPJ1047-1815	17.4	19.8
DENISPJ1048-3956	12.4	15.1
2MASSWJ1145+2317	18.6	20.6
DENISPJ1154-3400	17.6	19.8
DENISPJ1216-1257	18.0	20.0
DENISPJ1315-2513	18.1	20.7
2MASSWJ1342+1751	19.2	21.6
2MASSIJ1346-0031	20.8	22.9
DENISPJ1412-0433	18.2	20.8
2MASSWJ1439+1826	19.4	···
SDSSJ1440+0021	19.2	21.5
DENISPJ1619+0050	17.6	20.0
DENISPJ1919-4134	20.0	···
DENISPJ2023-1815	18.0	19.5
DENISPJ2215-0809	17.9	20.0
DENISPJ2329-5408	18.3	20.4

[a]Not all object were bright enough to do photometry.

[b]Uncertainties on these values are ∼0.1 mag

spectral type where available, and the Dahn et al. (2002) M_J vs. $(I-J)$ relation in the other cases. For the multiple systems, the distance was evaluated using the Dahn et al. (2002) M_I vs. Spectral Type relation and then multiplied the photometric distance obtained by a correction factor of $\sqrt{1+f}$, were f is the flux ratio (defined as f_{sec}/f_{prim}; in the F814W∼I_C filter), to correct for the bias introduced by the multiplicity. These results indicate that the ultra-cool dwarfs in the sample are at distances between 7 pc and 105 pc (cf. Table 1.1). Some SDSS objects had no published values of spectral types and J,H,K_S magnitudes. For these objects we used the SDSS photometry obtained from the public SDSS data release and the M_{i^*} vs (i^*-J) relation quoted in Hawley et al. (2002) (see section 5.4, and their equation 3).

Table 1.4. Photometry of the unresolved objects of program GO8146

Name	m_{F814W} [a]
2MASSW0036+1821	15.9
2MASSW0708+2950	20.4
2MASSW0740+3212	19.7
2MASSW0820+4500	20.1
2MASSW0825+2115	18.8
2MASSW0913+1841	19.3
2MASSW0928-1603	18.7
2MASSW1123+4122	19.6
2MASSW1155+2307	19.5
2MASSW1328+2114	19.9
2MASSW1338+4140	17.5
2MASSW1343+3945	19.9
2MASSW1439+1929	16.0
2MASSW1507-1627	16.4
2MASSW1632+1904	19.7
2MASSW1726+1538	19.3

[a]Uncertainties on these values are ∼0.1 mag

Table 1.5. Photometry of the unresolved objects of program GO8581

Name[a]	m_{F814W} [b]	m_{F1042M} [b]
SDSS0019+0030	18.1	16.0
SDSS0344+0111	17.8	14.6
SDSS1043+0001	19.2	···
SDSS1435-0043	19.7	···
SDSS1435-0046	19.1	···
SDSS1548-0029	18.2	16.6
SDSS1653+6231	17.7	15.3
SDSS1723+6406	18.9	···
SDSS0330-0025	18.8	16.4
SDSS0539-0059	17.5	15.0
SDSS1515-0030	17.0	15.0
2MASS0326-2102	20.0	···
2MASSW0010+3436	18.1	16.3
2MASSW0028+1501	20.1	17.5
2MASSW0030-1450	18.3	···
2MASSW0033-1521	18.0	···
2MASSW0208+2542	17.2	15.0
2MASSW0224+2537	19.7	···
2MASSW0328+2302	20.4	16.5
2MASSW0335+2342	14.7	12.8
2MASSW0337-1758	19.4	16.3
2MASSW0345+2540	17.2	14.8
2MASSW0350+1818	15.6	13.6
2MASSW0355+2257	19.6	···
2MASSW0753+2917	18.8	16.6
2MASSW0801+4628	19.6	16.4
2MASSW0829+2655	20.8	18.2
2MASSW0832-0128	17.4	14.9
2MASSW0914+2238	18.4	16.0
2MASSW0951+3558	21.0	···
2MASSW1102-2359	20.5	···
2MASSW1104+1959	17.9	15.8
2MASSW1108+6830	16.6	···
2MASSW1239+2029	17.3	15.2
2MASSW1403+3007	15.4	13.4
2MASSW1411+3936	17.8	15.5
2MASSW1412+1633	17.0	14.9
2MASSW1434+1940	18.1	15.1

1.5 Results for the individual objects

1.5.1 DENIS-P J020529.0-115925

DENIS-P J020529.0-115925 is a peculiar object. We strongly suspect it to be a triple system. The results and the properties of DENIS-P J020529-115930 will be presented in details in Part II, Section 3, but a brief summary of general properties is reported here for completness. DENIS-P J020529-115930 is a L7V brown dwarf in the Kirkpatrick classification scheme (L5 in the Martín classification scheme). It has been discovered by Delfosse et al. (1997), and announced as a binary by Koerner et al. (1999), on the basis of K band observations at Keck ($0\farcs51\pm0\farcs02$ and $106°\pm5°$in July 1997, and $0\farcs51\pm0\farcs02$ and $72°\pm10°$ in January 1999). This object has also been observed in the 2MASS survey and is reported as 2MASSW J0205293-115930. Leggett et al. (2001) observed it in the IR with UKIRT on September 1999, and report a separation of $0\farcs35$ $\pm0\farcs03$ and a position angle of $77°\pm4°$.

Delfosse et al. (1997), McLean et al. (2001) and Burgasser et al. (2003) report the detection of methane absorption band in their IR spectra, which would imply a mass below the stellar limit, and an effective temperature below 1800 K, as stated by Schweitzer et al. (2002). Basri et al. (2000) estimated this temperature to be $T_{eff} = 1700 \sim 1800$ K. Tokunaga & Kobayashi (1999) also observed absorption feature in the spectra but attributed it to H_2 rather than CH_4.

1.5.2 DENIS-P J035726.9-441730

DENIS-P J035729.6-441730 is one of the new binary system candidates discovered in this survey. It consists of a very close binary, with a separation of 98±2.8 mas and a position angle of 174.7±1.2°. The differences of magnitude are $\Delta m_{F675W} = 1.23 \pm 0.11$ mag and $\Delta m_{F814W} = 1.50 \pm 0.11$ mag, suggesting that the two components have slightly different masses. Despite the very small separation, (we are here very close to WFPC2/PC pixel scale), the values obtained for the separation and the position angle in the two filters are in very good agreement one with each other (cf. Figure 1.5). The companion appears clearly after PSF fitting (see Figure 1.7).

As described in section 1.4, its photometric distance corrected for multiplicity was evaluated at 22.2 pc. To the projected separation of $22.2 \times 0.098 = 2.2$ A.U should correspond a semi-major axis of $2.2 \times 1.26 = 2.8$ A.U. Assuming a face-on orbit, with a total mass of ~ 0.20 $M_\odot$ (masses are here unknown and we assume masses of about ~ 0.1 $M_\odot$ for each component), and a semi-major axis of 2.8 A.U, the period of this system would be ~ 10.5 years.

The physical properties of the individual components of DENIS-P J035726.9-441730 will be studied in more details in Section 1.2.4 of Chapter 1 in Part II.

1.5.3 2MASSW J0746425+2000032

2MASSW J0746425+2000032 is also a very peculiar object of our sample, since we were able to follow the secondary on its orbit and obtain the dynamical mass of the system. A more detailed presentation of the results concerning this object will be given in Part II, Chapter 2, but a brief summary of general properties is reported here for completness.

2MASSW J0746425+2000032 (spectral type L0.5 (Kirkpatrick et al. 2000)) has been discovered by Kirkpatrick et al. (2000), and was suggested to be a binary by Reid et al. (2000) based on its position in a colour-magnitude diagram. It has been confirmed as a multiple system by Reid et al. (2001), with a separation of $0\farcs22$ and a position angle of 15°.

The distance of 2MASSW J0746425+2000032 was estimated by trigonometric parallax measurements to be 12.21±0.05 pc.

Table 1.5—Continued

Name[a]	m_{F814W} [b]	m_{F1042M} [b]
2MASSW1438-1309	19.0	17.0
2MASSW1438+6408	16.0	13.8
2MASSW1457+4517	16.0	13.9
2MASSW1506+1321	16.8	14.5
2MASSW1526+2043	18.9	16.5
2MASSW1550+3041	15.4	13.3
2MASSW1551+6457	15.8	13.6
2MASSW1627+8105	16.0	13.7
2MASSW1635+4223	15.7	12.2
2MASSW1656+2835	20.5	···
2MASSW1707+4301	17.1	14.9
2MASSW1707+6439	15.4	13.3
2MASSW1710+2107	18.4	15.8
2MASSW1711+2232	20.5	···
2MASSW1743+2127	19.2	···
2MASSW1743+5844	17.2	14.1
2MASSW1841+3117	19.5	16.8
2MASSW2054+1519	19.6	···
2MASSW2057+1715	19.3	17.1
2MASSW2158-1550	18.5	14.9
2MASSW2206-4217	19.1	15.8
2MASSW2208+2921	19.4	···
2MASSW2234+2359	16.3	14.1
2MASSW2242+2542	18.0	15.2
2MASSW2244+2043	20.2	···
2MASSW2306-0502	14.0	12.0
2MASSW2309+1549	17.8	15.8
2MASSW2349+1224	15.3	13.2

[a]Not all object were bright enough to do photometry.

[b]Uncertainties on these values are ∼0.1 mag

1.5.4 2MASSW J0850359+105716

2MASSW J0850359+105716 was a known binary brown dwarf (Reid et al. 2001) of spectral type L6 in the Kirkpatrick classification scheme (L5 in the Martín classification scheme) implying $T_{eff} < 1800$ K. This object shows a strong lithium line (Kirkpatrick et al. 1999) implying a mass $M \leq 0.06\ M_{\odot}$. Its distance (25.6 pc) and proper motion ($\mu = 144.7 \pm 2.0$ mas/yr) were estimated by USNO parallax measurements (Dahn et al. 2002). Reid et al. (2001) measured a separation of $0\farcs16$ and a position angle of 250°on the 1^{rst} of February 2001 using HST/WFPC2. On the same data set we measured a separation of 157±2.8 mas and a position angle of 114.7±0.3°(cf. Figure 1.5). There is again a discrepancy between the values measured for the position angle. Figure 1.2 shows the image of 2MASSW J0850359+105716 and its orientation.

We measured a difference of magnitude of $\Delta m_{F814W} = 1.47 \pm 0.09$ mag. This implies again a slight difference in the masses of the two components. On the same set of data Reid et al. (2001) measured a difference of magnitude of $\Delta I = 1.34$ mag, in good agreement with our value. Assuming a semi-major axis of $0.157 \times 41.0 \times 1.26 = 8.1$ A.U, with an assumed total mass of ~ 0.14 $M_{\odot}$ (masses of the two components are unknown, but the presence of lithium in a L5 dwarf implies a mass less than 0.06 $M_{\odot}$ for one of them at least), the period of this system would be ∼61.6 years.

1.5.5 2MASSW J0856479+223518

2MASSW J0856479+223518 is a good candidate binary we report in this study. It has been observed on the 24th of April 2001 in the F814W and F1042M filters, but was not resolved in the latter one. We measured a separation of 98±9 mas and a position angle of 275±2.0 °. The difference of magnitude is $\Delta m_{F814W} = 2.76 \pm 0.11$ mag, suggesting that the two components have probably different masses. This large difference of magnitudes at such a small separation makes it very difficult to measure precisely the different parameters, explaining the higher uncertainties on the values. Nevertheless the two centroids appear clearly on the image (cf. Figure 1.6) and the PSF fitting makes appear a faint but obvious companion (see Figure 1.7). As we reach here the limit of detection of our method, the multiplicity of this object should be considered with caution and further followup observations with higher spatial resolution are required in order to confirmed that it is a real binary.

As described in section 1.4, we evaluated a photometric distance corrected for the multiplicity of $d = 34.7$ pc, which leads to a semi-major axis of 4.4 A.U, and with a total mass of ~ 0.20 $M_{\odot}$, to a period of ~ 20.8 years (masses are here unknown and we assume masses of about ~ 0.1 $M_{\odot}$ for each component).

1.5.6 2MASSW J0920122+351743

2MASSW J0920122+351743 (L6.5) has been identified as a brown dwarf by Kirkpatrick et al. (2000) and as a binary by Reid et al. (2001). Nakajima et al. (2001) report the observation of methane in the H and K bands, which makes more difficult the definition of the transition between L and T dwarfs.

For that object, Reid et al. (2001) report a separation of 75 mas and a position angle of 90°on the 2nd of September 2000. On the same set of data we measured a separation of 75±2.8 mas and a position angle of 248.5±1.2°(cf. Figure 1.5 and 1.2). Once again there is a discrepancy in the position angle. Figure 1.2 shows the image of 2MASSW J0920122+351743 and its orientation. We measured a difference of magnitude $\Delta m_{F814W} = 0.88 \pm 0.11$ mag. On the same set of data Reid et al. (2001) measured a difference of magnitude of $\Delta I = 0.44$ mag, lower than the one we

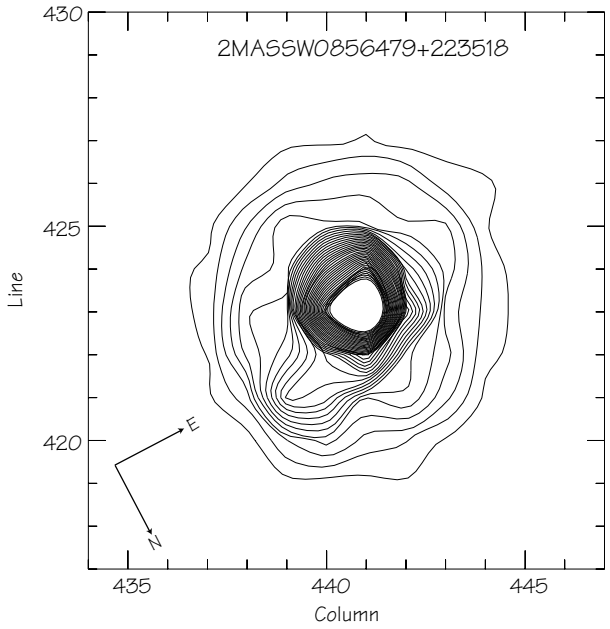

Figure 1.6 Contour plot of 2MASS0856+2235 obtained with HST/WFPC2. We measured a position angle of 275±2.0°and a separation of 98±9 mas. The two centroids appear clearly.

measure, but the uncertainties are not given. Considering only our uncertainties, the two values are different by 4-σ.

This makes of 2MASSW J0920122+351743 one of the closest resolved binaries observed in the sample. Figure 1.7 shows the companion clearly appearing after PSF fitting. Kirkpatrick et al. (2000) estimated a distance of 21 pc for the unresolved system. Using our photometric measurement we derive a distance of 16.7 pc. Correcting for multiplicity it gives a distance of 20.1 pc for the multiple system. We can estimate the semi-major axis to be about 1.9 A.U.

Assuming a total mass of ~ 0.14 $M_{\odot}$ (masses of the two components are unknown, but the presence of methane in this L6.5 dwarf implies a mass of less than 0.07 $M_{\odot}$), and a semi-major axis of 1.9 A.U, the period of this system would be ∼7.2 years.

1.5.7 DENIS-P J100428.3-114648

DENIS-P J100428.3-114648 is a new binary system candidate with a separation of 146±2.8 mas and position angle of 304.5±1.2°. It has also been reported in the 2MASS Survey as 2MASSW J1004282-114648. The differences of magnitudes are $\Delta m_{F675W} = 0.25 \pm 0.07$ mag and $\Delta m_{F814W} = 0.66 \pm 0.11$ mag. Once again the agreement between the values for separation and position angle obtained in the two filters is very good (cf. Figure 1.5). As explained in section 1.4, we estimated its photometric distance corrected for binarity to be 46.8 pc.

Assuming a semi-major axis of 8.6 A.U, with a total mass of ~ 0.20 $M_{\odot}$ (masses are here unknown and we assume masses of about ~ 0.1 $M_{\odot}$ for each component), the period of this system would be ~ 56.5 years.

The physical properties of the individual components of DENIS-P J100428.3-114648 will be studied in more details in Section 1.2.5 of Chapter 1 in Part II.

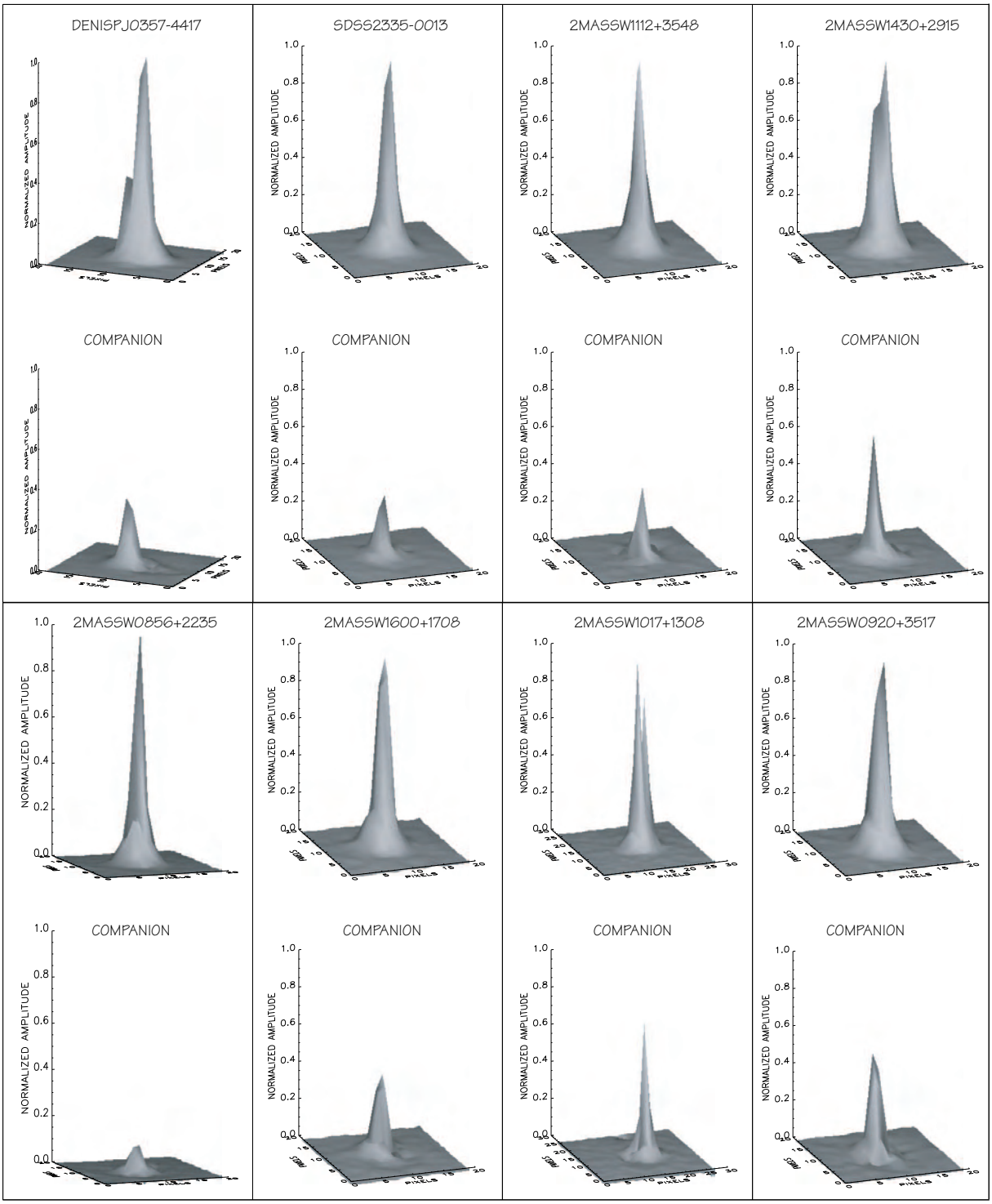

Figure 1.7 Surface plots representing the closest binary candidates of the sample and their companion. The companion appears after subtraction of the primary using the PSF fitting. All these plots correspond to the F814W images. Amplitudes are normalized and sky has been subtracted. Even if the separations are very small, the companions appear clearly after the PSF subtraction.

1.5.8 2MASSW J1017075+130839

2MASSW J1017075+130839 has been observed on the 16th of April 2001 in the F1042M and F814W filters. We measure a separation of 104±2.8 mas and a position angle of 92.6±1.2°. The difference of magnitude are $\Delta m_{F1042M} = 0.74 \pm 0.11$ mag, and $\Delta m_{F814W} = 0.77 \pm 0.11$ mag, suggesting that the two components have probably similar masses.

We evaluated the photometric distance corrected for binarity at $\sim$ 21.4 pc. Assuming a semi-major axis of 2.9 A.U, with a total mass of ~ 0.20 $M_\odot$ (masses are here unknown and we assume masses of about ~ 0.1 $M_\odot$ for each component), the period of this system would be $\sim$ 11.0 years.

1.5.9 2MASSW J1112257+354813

2MASSW J1112257+354813 has been observed on the 14th of February 2001 in the F814W and F1042M filters. For this object we measure a separation of 70±2.8 mas and a position angle of 79.6±1.2°. The differences of magnitude are $\Delta m_{F814W} = 1.07 \pm 0.11$ mag and $\Delta m_{F1042M} = 1.04 \pm 0.11$ mag. Figure 1.7 shows the companion appearing clearly after PSF fitting.

This object is particularly interesting since 2MASSW J1112257+354813 is also known as Gl 417B, confirmed as a L-dwarf and as companion of the G0-dwarf Gl 417A by Kirkpatrick et al. (2001), who measured a separation between the G-dwarf primary and the 2MASSW J1112257+354813 unresolved system of $90\farcs0$ and a position angle of 245 degrees. As stated by Harrington (1968) and then Szebehely & Zare (1977) in their analytical study, triple systems with moderate eccentricity are stable for ratios between the semi-major axes of the outer (a_2) and the inner orbits (a_1) greater than $a_2/a_1 \geq$3.2. Assuming that the orbits of 2MASSW J1112257+354813 around Gl 417A components have moderate eccentricities, the system would fit well above the stability criterium, with a ratio between $a_2/a_1 = 90/0.070 \sim 1300$. Kirkpatrick et al. (2001) estimated an age of 0.08-0.3 Gyr for the G-dwarf primary and, assuming that the primary and its companions are coeval, they computed a mass of $0.035\pm0.015 M_\odot$ for 2MASSW J1112257+354813, well below the hydrogen burning limit. The G-dwarf primary appears clearly on the HST/WFPC2 image and saturates completely one of the four CCD of the HST/WFPC2 camera.

This triple system is thus similar to Gl 569Bab (Martín et al. 2000b; Kenworthy et al. 2001) and HD130948 (Potter et al. 2002) (see Table 1.6).

The distance of the G-dwarf primary has been evaluated by trigonometric parallax (π =46.04 mas or d=21.7 pc; Hipparcos, Perryman et al. (1997)) and Kirkpatrick et al. (2000) assigned a spectral type of L4.5. Assuming a semi-major axis of $1.26 \times 21.7 \times 0.070 = 1.9$ A.U, with a total mass of ~ 0.20 $M_\odot$ (masses are here unknown and we assume masses of about ~ 0.1 $M_\odot$ for each component), the period of this system would be $\sim$ 5.8 years only. As its distance is known precisely, and as its age can be constrained by studying the G-dwarf primary, this system is a very good and very promising candidate to constrain theory and the mass/luminosity function.

1.5.10 2MASSW J1127534+741107

2MASSW J1127534+741107 is a M8.0 dwarf (Gizis et al. 2000) and also one of the 15 new binary candidates we report in this study. It has been observed on the 5th of May 2001 in the F1042M and F814W filters. We measure a separation of 252.5±2.8 mas and a position angle of 79.9±0.3°. The differences of magnitude between the primary and the secondary are $\Delta m_{F1042M} = 0.39 \pm 0.07$ mag and $\Delta m_{F814W} = 0.82 \pm 0.09$ mag, suggesting that the two components have probably similar masses.

Table 1.6. Ultra-cool Dwarfs Binaries associated to another star

Name	Name of the primary	Distance[a] (pc)	Sep. (A/B) (A.U)	Sep. (B/C) (A.U)	Period (B/C)[b] (yrs)
2MASSW1112+3548	Gl 417	21.7	1953	1.5	5.8
Gliese 569B	Gliese 569A	9.8	49	1.1	2.9
HD 130948BC	HD 130948	17.9	47.2	2.4	10

[a]Hipparcos trigonometric parallax of the Primary (Perryman et al. 1997)

[b]This period is just an estimate, calculated as explained in the text.

We evaluated the photometric distance corrected for multiplicity at 14.6 pc. Assuming a semi-major axis of 4.8 A.U, with a total mass of ~ 0.20 $M_\odot$ (masses are here unknown and we assume again masses of about ~ 0.1 $M_\odot$ for each component), the period of this system would be ~ 23.5 years.

1.5.11 2MASSW J1146344+223052

2MASSW J1146344+223052 has been discovered as a L3 dwarf by Kirkpatrick et al. (1999) and as a binary by Koerner et al. (1999). It shows lithium lines and Basri et al. (2000) estimated its effective temperature to 1950 K. Its distance (27.2 pc) has been measured by trigonometric parallax (Dahn et al. 2002). Reid et al. (2001) measured a separation of $0\farcs29$ and a position angle of 199.5°. On the same set of data we measured a separation of 294±2.8 mas and a position angle of 199.5±0.3°(cf. Figure 1.5). This time both position angle and separation are in agreement with the values given by Reid et al. (2001). We also measured a difference of magnitude $\Delta m_{F814W} = 0.75 \pm 0.09$ mag. On the same set of data Reid et al. (2001) measured a difference of magnitude of $\Delta I = 0.31$ mag, again smaller than the one we measure, but the uncertainties are not given. Considering only our uncertainties, the two measurements are different by 5-σ. Such a difference is much larger than the uncertainties on our measurement, as explained in section 1.2.2, especially considering that with a separation of $\sim 0\farcs29$ and a difference of magnitude less than 1.0, 2MASSW J1146344+223052 was an "easy" case for the PSF fitting program.

Assuming a semi-major axis of 10.1 A.U, with a total mass of ~ 0.12 $M_\odot$ (masses of the two components are unknown, but the presence of lithium in a L7 dwarf implies a mass equal or less than 0.06 $M_\odot$), the period of this system would be ~ 92.6 years.

1.5.12 DENIS-P J122813.8-154711

DENIS-P J122813.8-154711 has been discovered by Delfosse et al. (1997) and resolved for the first time by Martín et al. (1999a). It is a L4.5 brown dwarf in the Martín classification scheme and a L5 in the Kirkpatrick classification scheme (Kirkpatrick et al. 1999). This object has been observed and studied several times. We provide a summary of the astrometric and photometric measurements in Table 1.7.

This object has also been observed in the 2MASS survey and is reported as 2MASSW J-1228152-154734. The designations are different mostly because the DENIS astrometric pipeline

used at the time of discovery was not the final version and the uncertainties of the astrometry were high.

Lithium absorption has been reported by both Martín et al. (1997) and Tinney et al. (1997), implying a mass M $\leq$ 0.06 $M_\odot$. DENIS-P J122813.8-154711 was the second field brown dwarf to be confirmed by the lithium test.

For this object again we had two sets of data. The results obtained with the first set are not very accurate because of coordinate mismatch. The target fell in a corner of one of the Wide Field Camera of WFPC2 instead of in the centre of the Planetary Camera (PC), where the distortions are more important and the pixel scale coarser, implying a worse sampling of the PSF and thus higher uncertainties. Thus the results in the two filters are not in very good agreement (cf. Table 1.7 and Figure 1.5). The second set of data was much better since the target was in the centre of the PC and the exposure time was 1700s instead of 300s, spread over several exposures and allowing to reject cosmic rays easily. The accuracy of the result is then very good. The differences of magnitude in both filters indicate that the two components are probably very similar : $\Delta m_{F814W} = 0.36 \pm 0.07$ mag and $\Delta m_{F675W} = 0.53 \pm 0.09$ mag.

DENIS-P J122813.8-154711 has been observed now over more than 5 years, and we have astrometric data related to the binary spread over more than 3 years. Within a few years we should thus be able to compute orbital parameters and dynamical masses. The motion of DENIS-P J122813.8-154711-B is already obvious. We see in Table 1.7 a separation change by $\sim 8\%$ and a position angle change by 23 degrees in three years. If we assume a semimajor axis of 6.6 A.U, and a total mass of 0.12 $M_\odot$, we find an orbital period of $\sim$ 49 years.

1.5.13 2MASSW J1239272+551537

2MASSW J1239272+551537 has been observed on the 18th of March 2001 in the F814W filter. We measure a separation of 211±2.8 mas and a position angle of 187.6±0.3°. The difference of flux between the primary and the secondary is $\Delta m_{F814W} = 0.34 \pm 0.07$ mag and $\Delta m_{F1042M} = 0.54 \pm 0.09$ mag, suggesting that the two components might have very similar masses. The whole system is classified as L5 by Kirkpatrick et al. (2000), who also evaluated the photometric distance of the whole system considering it was a single object (17 pc). From our photometric measurement we calculate a distance (corrected for the multiplicity) of 21.3 pc. Assuming a semi-major axis of 5.9 A.U, with a total mass of $\sim$ 0.20 $M_\odot$ (masses are here unknown and we assume masses of about $\sim$ 0.1 $M_\odot$ for each component), the period of this system would be $\sim$ 32.0 years.

1.5.14 2MASSW J1311392+8032222

2MASSW J1311392+8032222 is a M8.0 dwarf (Gizis et al. 2000) and has been observed on the 30th of July 2000 in the F1042M and F814W filters. We measure a separation of 300±2.8 mas and a position angle of 167.3±0.3°. The difference of flux between the primary and the secondary is $\Delta m_{F1042M} = 0.45 \pm 0.09$ mag and $\Delta m_{F814W} = 0.0.39 \pm 0.07$ mag, suggesting that the two components have similar masses.

We evaluate a photometric distance corrected for binarity of 13.7 pc. Assuming a semi-major axis of 5.5 A.U, with a total mass of $\sim$ 0.20 $M_\odot$ (masses are here unknown and we assume masses of about $\sim$ 0.1 $M_\odot$ for each component), the period of this system would be $\sim$ 28.8 years.

The physical properties of the individual components of 2MASSW J1311392+8032222 will be studied in more details in Section 1.2.2 of Chapter 1 in Part II.

Table 1.7. Avalaible measurements on DENIS-P J122815.4-154730

DENIS-P J122815.4-154730			Ref.
Separation (mas) :	P.A (°) :	Date :	
275 ± 2	41.0 ± 0.2	02-06-1998	(1)
246 ± 20 [a]	23 ± 2 [a]	03-04-2001	(4)
255.4 ± 2.8	18.3 ± 0.3	16-06-2001	(4)
Distance (pc) :	18 ± 4		(1)
	20.2 ± 1		(2)
Proper Motion (mas/yr) :	$\mu = 224 \pm 1.3$		(2)
	$P.A = 143.3 \pm 0.3$		(2)
Parallax (mas) :	49.4 ± 1.9		(2)
$v.sin(i)$ $(km.s^{-1})$:	22 ± 2.5		(3)

References. — (1) Martín et al. (1999a), (2) Dahn et al. (2002), (3) Basri et al. (2000), (4) this work.

[a]The object was observed in a corner of the HST/WF, where the pixel scale is coarser and the distortions higher, hence implying higher uncertainties

1.5.15 2MASSW J1426316+155701

2MASSW J1426316+155701 is a M9 dwarf and has been reported as a binary for the first time by Close et al. (2002a,b) with Hokupa'a/Gemini. On the 22nd of September 2001, they measured a separation of 152±6 mas and a position angle of 344.1±0.7°. They estimated an age of $0.8^{+6.7}_{-0.2}$ Gyr and a photometric distance of 23.6 ± 6.0 pc, giving a separation of 3.6 ± 0.9 A.U and a period of 17^{+10}_{-7} years. They also estimated the mass of the whole system $M_{tot} = 0.140^{+0.011}_{-0.026}\ M_{\odot}$ as well as the masses of each components : $M_A = 0.074^{+0.011}_{-0.005}\ M_{\odot}$ at the limit of the Hydrogen burning limit for the primary and $M_B = 0.066^{+0.015}_{-0.006}\ M_{\odot}$ for the secondary.

On the 17th of July 2001 we measured a separation of 157.1±2.8 mas and a position angle of 339.9±0.3°. We also estimate a photometric distance corrected for binarity of 26.7 pc. These values are close to the one of Close et al. (2002b) taken ∼2 months later (within 1-σ). Gizis et al. (2000) measured a proper motion of μ =0.″121/yr, implying 20 mas of motion between the observations, confirming that the system is a common proper motion pair. We also measured differences of magnitudes of $\Delta m_{F814W} = 1.40 \pm 0.09$ mag, and $\Delta m_{F1042M} = 1.30 \pm 0.09$ mag. Assuming a total mass of $0.14 M_{\odot}$ as given by Close et al. (2002a,b) and a semi-major axis of 4.3 A.U, we estimate the period of this system to be 33.3 years.

The physical properties of the individual components of 2MASSW J1426316+155701 will be studied in more details in Section 1.2.3 of Chapter 1 in Part II.

1.5.16 2MASSW J1430436+291541

2MASSW J1430436+291541 has been observed on the 19th of April 2001 in the F1042M and F814W filters. We measure a separation of 88±2.8 mas and a position angle of 327.5 ±1.2°. The difference of flux between the primary and the secondary is $\Delta m_{F1042M} = 0.76 \pm 0.11$ mag and $\Delta m_{F814W} = 0.78 \pm 0.11$ mag, suggesting that the two components have slightly similar masses. The companion appears clearly after PSF fitting, as shown in Figure 1.7.

We evaluated the distance (corrected for multiplicity) of 29.4 pc. Assuming a semi-major axis of 3.4 A.U, with a total mass of ∼ 0.20 $M_{\odot}$ (masses are here unknown and we assume masses of about ∼ 0.1 $M_{\odot}$ for each component), the period of this system would be ∼ 13.9 years.

1.5.17 DENIS-P J144137.3-094559

DENIS-P J144137.3-094559 is a binary brown dwarf of spectral type L1 (Martín et al. 1999b), first resolved in February 2000 with Keck/NIRC. It has been observed with Keck by Stephens et al. (2001) on the 13th of April 2000 and resolved with a separation of 0.42 arcsec. Kirkpatrick et al. (2000) deduced a distance of 25.5 pc using photometric measurements, considering a single object. We estimate a photometric distance corrected for multiplicity of 29.2 pc.

For this object we had two epochs of data, one from our HST program (two filters) and one from an on going program (GO9157).

In the first set of data obtained on the 16th of January 2001 we measured a separation of 375±2.8 mas and a position angle of 290.3±0.3°. The values obtained in both filters are again in very good agreement (cf. Figure 1.5). We measured $\Delta m_{F675W} = 0.63 \pm 0.09$ mag and $\Delta m_{F814W} = 0.37 \pm 0.07$ mag. In the second set of data, obtained four months later on the 22nd of May 2001, we measured a separation of 370±2.8 mas, a position angle of 290.8±0.3°, and a difference of magnitude $\Delta m_{F814} = 0.30 \pm 0.07$. These data are in good agreement with the previous one. Assuming a semi-major axis of 14.1 A.U, with a total mass of ∼ 0.2 $M_{\odot}$ (masses

are here unknown and we assume masses of about ~ 0.1 $M_\odot$ for each component), the period of this system would be ~ 118 years.

1.5.18 2MASSW J1449378+235537

2MASSW J1449378+235537 is another of the new binary candidates we report in this study. The spectral type of the whole system is L0 (Kirkpatrick et al. 2000). It has been observed on the 21st of December 2000 in the F814W and F1042M filters. We measure a separation of 134±2.8 mas and a position angle of 64.4±1.2°. The difference of flux between the primary and the secondary is $\Delta m_{F814W} = 1.51 \pm 0.11$ mag and $\Delta m_{F1042M} = 1.08 \pm 0.11$ mag, suggesting that the secondary is redder than the primary.

Kirkpatrick et al. (2000) evaluated the photometric distance of the unresolved system to 62 pc. From our photometric measurements we estimate a photometric distance corrected for binarity of 63.7 pc. Assuming a semi-major axis of 11.0 A.U, with a total mass of ~ 0.20 $M_\odot$, the period of this system would be ~ 81.1 years.

1.5.19 2MASSW J1600054+170832

2MASSW J1600054+170832 is a L1.5 dwarf according to Kirkpatrick et al. (2000). It has been observed on the 14th of January 2001 in the F814W and F1042M filters. We measure a separation of 57±2.8 mas and a position angle of 156.2±1.2°. The difference of flux between the primary and the secondary is $\Delta m_{F814W} = 0.69 \pm 0.11$ mag. At such a close separation, it might be better to consider 2- or 3-σ uncertainties on these values, since we reach here the very limit of resolution of the WFPC2/PC camera. Nevertheless, the companion appears once again clearly after PSF subtraction (see Figure 1.7). The object was too faint for PSF fitting in the F1042M filter.

Kirkpatrick et al. (2000) evaluated the photometric distance of the unresolved system to 62 pc. We estimate a photometric distance (corrected for multiplicity) of the primary of 60.6 pc. Assuming a semi-major axis of 4.3 A.U, with a total mass of ~ 0.20 $M_\odot$ (masses are here unknown and we assume masses of about ~ 0.1 $M_\odot$ for each component), the period of this system would be ~ 19.9 years.

1.5.20 2MASSW J1728114+394859

2MASSW J1728114+394859 is also one of the new binary candidates. The spectral type of the whole system is L7 (Kirkpatrick et al. 2000). It has been observed on the 12th of August 2000 in the F814W and F1042M filters. We measure a separation of 131.3±2.8 mas and a position angle of 27.6±1.2°. The difference of flux between the primary and the secondary in this range of wavelength is $\Delta m_{F814W} = 0.66 \pm 0.11$ mag, suggesting that the two components have similar masses. This object was also too faint for PSF fitting in the F1042M filter.

Kirkpatrick et al. (2000) evaluated the photometric distance of the unresolved system (20 pc). We estimate the photometric distance (corrected for multiplicity) at 20.4 pc. Assuming a semi-major axis of 3.4 A.U, with a total mass of ~ 0.20 $M_\odot$, the period of this system would be $\sim$ 13.8 years.

1.5.21 2MASSW J2101154+175658

2MASSW J2101154+175658 is a L7.5 dwarf according to Kirkpatrick et al. (2000) and is a new binary we report in this study. It has been observed on the 7th of May 2001 in the F814W filter.

We measure a separation of 234.3±2.8 mas and a position angle of 107.7°±0.3°. The difference of flux between the primary and the secondary is $\Delta m_{F814W} = 0.59 \pm 0.09$ mag, suggesting that the two components have similar masses. The object was too faint in the F1042M filter to be able to use the PSF fitting.

Kirkpatrick et al. (2000) evaluated its distance at 29 pc, considering a single object. We estimate the corrected photometric distance to be 23.2 pc. Assuming a total mass of ~ 0.20 $M_\odot$ (masses are here unknown and we assume masses of about ~ 0.1 $M_\odot$ for each component), and a semi-major axis of 7.1 A.U, the period of this system would be ~ 41.9 years.

1.5.22 2MASSW J2140293+162518

2MASSW J2140293+162518 has been reported as a binary for the first time by Close et al. (2002a,b) with Hokupa'a/Gemini. On the 22nd of September 2001, they measured a separation of 155 ± 5 mas and a position angle of 134.3 ± 0.5 degrees. They estimated an age of $3.0^{+4.5}_{-2.4}$ Gyr and a photometric distance of 23.9 ± 6.0 pc, leading to a separation of 3.7 ± 0.9 A.U and a period of 18^{+10}_{-7} years. They also estimated the mass of the whole system $M_{tot} = 0.162^{+0.008}_{-0.018}$ $M_\odot$ as well as the masses of each components : $M_A = 0.087^{+0.008}_{-0.017}$ $M_\odot$ for the primary and $M_B = 0.075^{+0.007}_{-0.018}$ $M_\odot$ for the secondary, at the limit of the Hydrogen burning limit. From their colours they estimated the spectral types of each component : M8.5 ± 1.5 for the primary and L0 ± 1.5 for the secondary.

On this object we had data from the HST public archive (GO8581, P.I. Reid). The object was observed on the 21st of May 2001, in the PC chip of WFPC2 in two filters (F814W and F1042M), almost four months before Close et al. (2002a) reported it. On this set of data we measure a separation of 159.0 ± 2.8 mas and a position angle of 132.4 ± 0.3 degrees, as well as difference of magnitude of $\Delta m_{F814W} = 1.51 \pm 0.11$ mag, and $\Delta m_{F1042M} = 1.38 \pm 0.11$ mag. These values are in agreement with the values given by Close et al. (2002b) within 3-σ. We estimate a photometric distance of 12.9 pc. Considering a semi-major axis of 2.6 A.U and a total mass of 0.16 $M_\odot$ as calculated by Close et al. (2002b), the period of this system would be 10.5 years. Gizis et al. (2000) measured a proper motion of μ_α =-0.″008/yr and μ_δ =-0.″102/yr implying 35 mas of motion between the observations. Although the uncertainties on their astrometry are relatively high, the system is likely to be a common proper motion pair. Better astrometric measurements are required in order to confirm the multiplicity of this object.

1.5.23 2MASSW J2147437+143131

2MASSW J2147437+143131 is a M8.0 ultra-cool dwarf (Gizis et al. 2000). It has been observed on the 9th of October 2000 in the F1042M and F814W filters. We measure a separation of 322 ± 2.8 mas, a position angle of 329.5 ± 0.3 degrees and a difference of magnitude in the F814W filter of $\Delta m_{F814W} = 0.62 \pm 0.09$ mag. We were not able to measure accurately the parameters in the F1042M filter due to a a cosmic ray event very close to the primary. We were only able to evaluate a difference of magnitude of $\Delta m_{F1042M} = 0.75 \pm 0.28$ mag.

The photometric distance given by Gizis et al. (2000) is 22.9 pc considering a single object. From our measurements we estimate a photometric distance corrected for multiplicity of 21.8 pc. Thus assuming a total mass of ~ 0.20 $M_\odot$ (masses are here unknown and we assume masses of about ~ 0.1 $M_\odot$ for each component), and a semi-major axis of 9.1 A.U, the period of this system would be ~ 61.7 years.

1.5.24 2MASSW J2206228-204705

2MASSW J2206228-204705 has also been reported as a binary for the first time by Close et al. (2002a,b) with Hokupa'a/Gemini. On the 22nd of September 2001, they measured a separation of 168 ± 7 mas and a position angle of 68.2 ± 0.5 degrees. They estimated an age of $3.0^{+4.5}_{-2.4}$ Gyr and a photometric distance of 24.68 ± 6.8 pc, giving a separation of 4.1 ± 1.1 A.U and a period of 20^{+9}_{-7} years. They also estimated the mass of the whole system $M_{tot} = 0.178^{+0.008}_{-0.014}$ $M_\odot$ as well as the masses of each components : $M_A = 0.090^{+0.008}_{-0.014}$ $M_\odot$ for the primary and $M_B = 0.088^{+0.008}_{-0.014}$ $M_\odot$ for the secondary. From their colours they estimated the spectral types of each component : M8.0 $\pm$ 1.5 for the primary and M8.5 $\pm$ 1.5 for the secondary. Kirkpatrick et al. (2000) assigned M8 to the whole system.

We used again data from the HST public archive (GO8581, P.I. Reid). The object was observed on the 13th of August 2000, in the PC chip of WFPC2 in two filters (F814W and F1042M), almost fourteen months before Close et al. (2002a) reported it. On this set of data we measure a separation of 160.7 ± 2.8 mas and a position angle of 57.2 ± 0.3 degrees, as well as difference of magnitude of $\Delta m_{F814W} = 0.36 \pm 0.07$ mag, and $\Delta m_{F1042M} = 0.30 \pm 0.07$ mag.

From our photometric measurement, we estimate a distance (corrected for multiplicity) of 22.2 pc. Considering a semi-major axis of 4.5 A.U and a total mass of 0.178 $M_\odot$ the period of this system would be 22.6 years. If we consider the little motion we observe between the two epochs (11 degrees in 14 months), and assuming a circular face-on orbit, it gives a period of 33 years which is of the same order of the previous estimation (and in good agreement since the orbit is probably not circular face-on).

Gizis et al. (2000) measured a proper motion of $\mu = 0\farcs065$/yr, implying 76 mas of motion between the observations. Although the uncertainties on their astrometry are relatively high, the system is likely to be a common proper motion pair. Better astrometric measurements are required in order to confirm the multiplicity of this object.

1.5.25 2MASSW J2331016-040618

2MASSW J2331016-040618 has also been reported as a binary for the first time by Close et al. (2002a,b) with Hokupa'a/Gemini. On the 22nd of September 2001, they measured a separation of 573 ± 8 mas and a position angle of 302.6 ± 0.4 degrees. They estimated an age of $5.0^{+2.5}_{-4.4}$ Gyr and a photometric distance of 25.2 ± 6.8 pc, thus giving a separation of 14.4 ± 3.9 A.U and a period of 139^{+86}_{-57} years. They also estimated the mass of the whole system $M_{tot} = 0.153^{+0.008}_{-0.020}$ $M_\odot$ as well as the masses of each components : $M_A = 0.091^{+0.008}_{-0.013}$ $M_\odot$ for the primary and $M_B = 0.062^{+0.010}_{-0.020}$ $M_\odot$ for the secondary, thus clearly below the sub-stellar limit. From their colours they estimated the spectral types of each component : M8.0 $\pm$ 1.5 for the primary and L3 $\pm$ 1.5 for the secondary. This object is very peculiar because the differences of magnitudes between the primary and the secondary are really high in the infrared. Close et al. (2002b) measured $\Delta K = 2.38 \pm 0.16$ mag.

We used data from the HST public archive (GO8581, P.I. Reid). The object was observed on the 6th of May 2001, in the PC chip of WFPC2 in two filters (F814W and F1042M), almost 4.5 months before Close et al. (2002a) reported it. On this set of data we measure a separation of 577 ± 2.8 mas and a position angle of 293.7 ± 0.3 degrees, as well as difference of magnitude of $\Delta m_{F814W} = 3.90 \pm 0.09$ mag, and $\Delta m_{F1042M} = 3.54 \pm 0.09$ mag. The results we obtain in the two filters are slightly different but still in agreement within 3-σ (cf. Table 1.2). Our value for the separation is in good agreement with the values given by Close et al. (2002b) but the difference in the values for the position angle is larger. Even if the difference of magnitude is

high, the separation is large enough to let us trust the results we obtained with our PSF fitting method with the accuracy of 0.″0028 for the separation and 0.3° for the P.A, as explained in section 1.2.2.

Gizis et al. (2000) measured a proper motion of μ_α =0.″401/yr and μ_δ =-0.″231/yr, implying a motion of 0.″150 in right ascension and -0.″087 in declination between the observations, whereas the variation of position angle occurs in the opposite direction, confirming that the system is a common proper motion pair.

On the basis of distance and proper motions consistencies, Gizis et al. (2000) suggested that 2MASSW J2331016-040618 is associated to the F8 dwarf HD221356. The distance (26.2 pc) and proper motion (μ_α = 178.65 mas/yr and μ_δ = −192.79 mas/yr) of HD221356 have been measured precisely by Hipparcos. The distances of the two objects are very similar (26.2 pc for the M-dwarf and 26.24 for the F-dwarf) but the proper motions measured by Gizis et al. (2000) and Hipparcos (Perryman et al. 1997) are very different : more than 220 mas/yr of difference for μ_α and almost 40 mas/yr for μ_δ. We then suggest that these two objects are not linked on the basis of proper motion discrepancy. HD221356 does not appear on the HST images we used, thus not allowing to check for second epoch data. It might nevertheless be interesting to get second epoch data in the future to confirm the values of proper motion of 2MASSW J2331016-040618 given by Gizis et al. (2000). We therefore consider that 2MASSW J2331016-040618 is a field binary ultra-cool dwarf.

We estimate a photometric distance corrected for the binarity of 26.2 pc. Considering a semi-major axis of 19.0 A.U, and a total mass of 0.153 $M_\odot$, the period of this system would be 211 years.

1.5.26 SDSS2335583-001304

SDSS2335583-001304 is a new very close binary system candidate. We measured a separation of 56.8±2.8 mas and a position angle of ∼8.1°±1.2°. The system is so close that it was not resolved in the F1042M filter. We are here very close to the HST/WFPC2 pixel scale and already below the sampling limit, thus second epoch data with higher resolution will be necessary in order to confirm the multiplicity of this object. The difference of magnitude in the F814W is : $\Delta m_{F814W} = 1.00 \pm 0.11$ mag. This value should be considered with caution, since we reach here the limits of resolution of HST/WFPC2. It might thus be better to consider 2- or 3-σ uncertainties.

Nevertheless the clear elongation of the object in the image as well as the companion that appears clearly after PSF fitting as shown in Figure 1.7 allow us to conclude that SDSS2335583-001304 is a good candidate multiple system.

Unfortunately the only photometric value available is the one we measured, thus not allowing to compute the photometric distance.

Assuming a circular face-on orbit at a distance of 62 pc, with a total mass of ∼ 0.20 $M_\odot$ (masses are here unknown and we assume masses of about ∼ 0.1 $M_\odot$ for each component), and a radius of 3.5 A.U, the period of this system would be ∼ 14.5 years

1.6 Analysis

1.6.1 Binary frequency

26 of the 134 targets in the sample appear to be multiple systems (see Figure 1.2). Fifteen of these still have to be confirmed by second epoch data, but given the relatively low star density, we will

consider that these objects are almost certainly binary systems. 2MASSW J1112256+354813 is associated to a G-dwarf in a triple system, and thus is not a field binary and we therefore remove it from the statistics. We then hereafter count 25 field binaries. Eleven binary systems were already known and thus confirmed by second and sometimes third epoch data.

Our observed binary frequency is based on the fact that we know 25 binaries in a sample of 133 ultra-cool dwarfs. This corresponds to an observed binary fraction of $18.8 \pm 3.7\%$. This value is only indicative and not related to any physical value for the following reasons:

1. First because our detection was limited to binaries with differences of magnitude Δm_{F814W} less than 3 mag (5.5 mag in the best cases, ∼4 mag in average, cf. Figure A.1, page 164). We thus missed all the multiple systems for which the companion was too faint in comparison with the primary. Nevertheless, as shown in Figures A.1 (page 164) and 1.10 and as explained in section 1.6.3, our observations suggest a strong preference for nearly equal luminosity systems. We therefore go on the assumption that multiple systems with high differences of magnitudes are rare among ultra-cool dwarfs and that we do not miss a significant number of such multiple systems in our study except if there is a bimodal distribution of mass ratio with a second peak at small mass ratio.

2. Second because the sample selection introduced a bias, since we did not choose the targets completely randomly among field brown dwarfs: some were selected from their colours and brightnesses. The sample is thus limited in magnitudes rather than in distances, and this introduces a bias: the multiple systems are detected at larger distances than simple one, and their spatial density is thus overestimated. To be able to evaluate more precisely the binary fraction we have been analysing the sample in order to find at which limiting distance the sample cannot be considered as a complete volume-limited sample. As the sample is made of objects coming from different surveys (DENIS, 2MASS ans SDSS), we had to take their respective limits of completeness into account. The DENIS survey is complete until objects with I≤18 mag (Delfosse et al. 1999). For a typical ultra-cool dwarf of spectral type L5 (latest DENIS spectral type of the sample, except DENIS0205-1159), it corresponds to an absolute magnitude of $M_I \sim 17$ mag (according to the M_I vs. Spectral Type relation given in Dahn et al. 2002), and to a distance of ∼ 16 pc. We consider for our study that the 2MASS survey has a limit of completeness of K≤14.5 mag. For a typical ultra-cool dwarf of spectral type L8, this corresponds to an absolute magnitude M_K ∼13 mag, and to a distance of ∼20 pc. We can therefore as a first approximation consider that the sample was very close to a volume limited sample until 16 pc for the DENIS objects and until 20 pc for the 2MASS objects. As the SDSS objects represent only a very small number of objects in the sample, as many of them were also observed in the 2MASS survey and as they are all further away than 20 pc, they do not count in the statistical study hereafter. Figure 1.8 shows that on the range 0∼20 pc (distance corrected for the resolved multiple systems), the sample behaves almost like a volume limited sample and the number of objects increases like d^3. After 20 pc, the sample behaves indeed more like a magnitude limited sample and the number of objects decreases roughly like d^{-2}. All these considerations suggest us that in order to make a better statistical study, we should consider only the DENIS objects of the sample that are closer than 16 pc and the 2MASS objects that are closer than 20 pc. Only one DENIS object (no binary) and twenty five 2MASS objects (including four multiple systems) are thus included in the statistical sample defined as explained above. This makes a binary fraction of ∼ 15%.

3. Finally because the detections are limited to objects with separations greater than ∼ 0.060

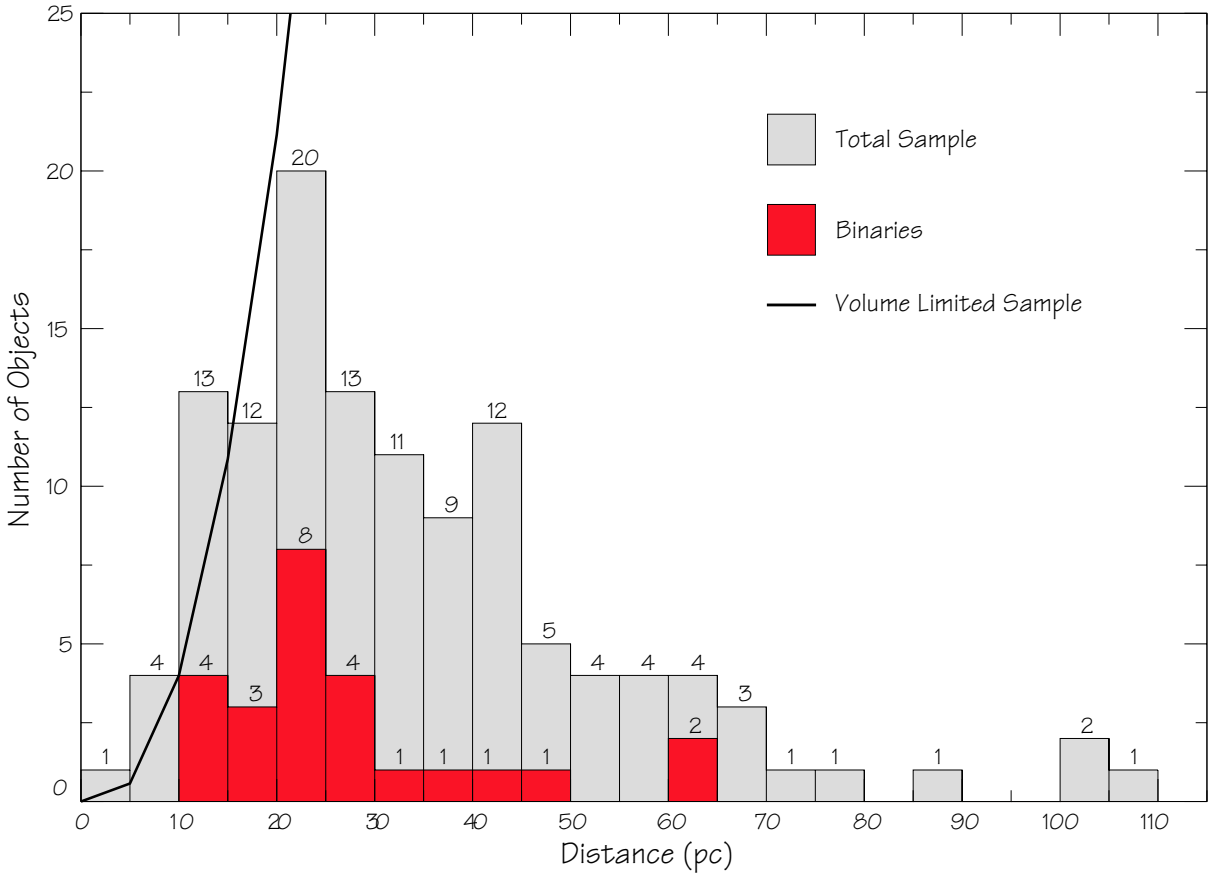

Figure 1.8 Distribution of separation in the sample. The total sample is represented in light grey and the binaries alone are over-plotted in dark grey. We also over-plot the expected distribution for a volume limited sample. The sample is roughly limited in magnitude. For the statistical study, we therefore consider only the DENIS objects at distances less than 16 pc and the 2MASS objects closer than 20 pc.

arcsec. We therefore missed all the binaries with separations less than this value. This effect becomes stronger with increasing distances. At a distance of 20 pc, it corresponds to physical separations of 1.2 A.U. The value given above is then probably a lower limit of the exact binary fraction.

Another way to estimate the bias corrected binary frequency is to apply a correction to the observed binary frequency as described in Burgasser et al. (2003) (see their equations 4 and 5). If we go on the assumption that the total sample is purely magnitude limited, and that the correction factor for the increase of volume sampled for binaries is between $1.86 \leq \alpha \leq 2.83$ (see section 1.6.3), the corrected binary fraction is $7.6^{+5.9}_{-1.7}\%$. As we observe a preference for nearly equal luminosity systems (see section 1.6.3), α must be closer to 2.83 than to 1.86. The value given above therefore corresponds to α =2.83, but its uncertainties includes the uncertainties on α and on the observed binary fraction. This result is of the same order than the previous one and in good agreement within the uncertainties. However, the two methods presented here to correct the observed binary frequency take in account only the bias for visual binaries resolved by HST, and not for the spectroscopic binaries of the sample that we miss. Indeed in order

to construct our "volume limited" sample we correct the photometric distances of the identified HST visual binaries, but not those of undetected spectroscopic binaries. The same is true for the Burgasser et al. (2003) method; in their equation 4, only the volume sampled for HST visual binaries is corrected. As result, the denominator of the binary fraction, which is the total number of systems (single and multiple), is overestimated because the bias for multiplicity is not corrected for all the multiple systems, and the binary fraction is therefore under-estimated.

Nevertheless, this sample of 134 objects is the largest studied to date, with the highest spatial resolution available. We found 15 new binary candidates (to be added to the 11 previously known). This allows us to make a meaningful statistical study over a sufficiently large number of objects. Although it is biased, we can already make some preliminary comments on the results, keeping in mind the limitations of this study.

With these considerations we obtain a HST visual binary fraction among ultra-cool dwarfs of $7 - 10\%$. But even in these conditions and with these precautions the sample is not a purely volume limited sample and the results will not be as accurate as the one we could get with a statistically well defined sample.

1.6.2 Distribution of Separations

Figure 1.9 shows the distribution of separations. It shows evidence of a lack of binaries with separations wider than $\sim$ 15 A.U. This was already mentioned as the possible "brown dwarf wide binary desert" by Martín (2000).

This is certainly not an artifact of incompleteness in the observations since this separation corresponds to $\sim 0\farcs5$ (at an average distance of $\sim$ 20 pc), where multiple systems can easily be detected either by HST/WFPC2 for the faintest companions or 2MASS and DENIS in the brighter and wider cases (the resolutions of the 2MASS and DENIS surveys are $\sim 2\farcs0$, corresponding to $\sim$ 40 A.U semi-major axis at 20 pc). Figure 1.9 shows clearly that all the objects have angular separations well below these limits. We estimate that we should have been able to detect every companion candidate within $4\farcs0$ of the targets (within the limits of flux ratio mentioned in Section 1.6.3). We have been looking for wide companions by comparing the colours of the objects in the WFPC2 field of view, and found only very few candidates with colours very similar to those of the associated targets. The colours similarity being a poor constraint (especially with the HST filters used in this study), the probability that these objects are physically associated to the corresponding targets is very low. One object from the literature (CFHT-Pl-18, cf. Table 1.9) is currently known to have a wider separation (35 A.U), but even in this case the separation does not exceed a few tens of A.U. This indicates that these objects can exist but are probably very rare, and probably do not have separations greater than a few tens of A.U.

1.6.3 Luminosity ratios

Figure A.1 and 1.10 also suggest that there is a lack of binary systems with large differences of magnitudes, corresponding to unequal luminosities. Most of the values of differences of magnitudes are homogeneously spread between $0.1 \leq \Delta m_{F814W} \leq 2.0$ mag. Only two systems have $\Delta m_{F814W} > 2.5$ mag. As explained in Section 1.2.2, this is probably not an artifact of incompleteness, because even if the sample is magnitude limited (in a magnitude limited sample, the selection bias is stronger for the equal luminosity systems, since the systems with unequal luminosities are detected in a smaller volume) Figure 1.10 shows that we should have been able to detect all the binary systems with differences of magnitudes between $1.5 \leq \Delta m_{F814W} \leq 3.0$ mag

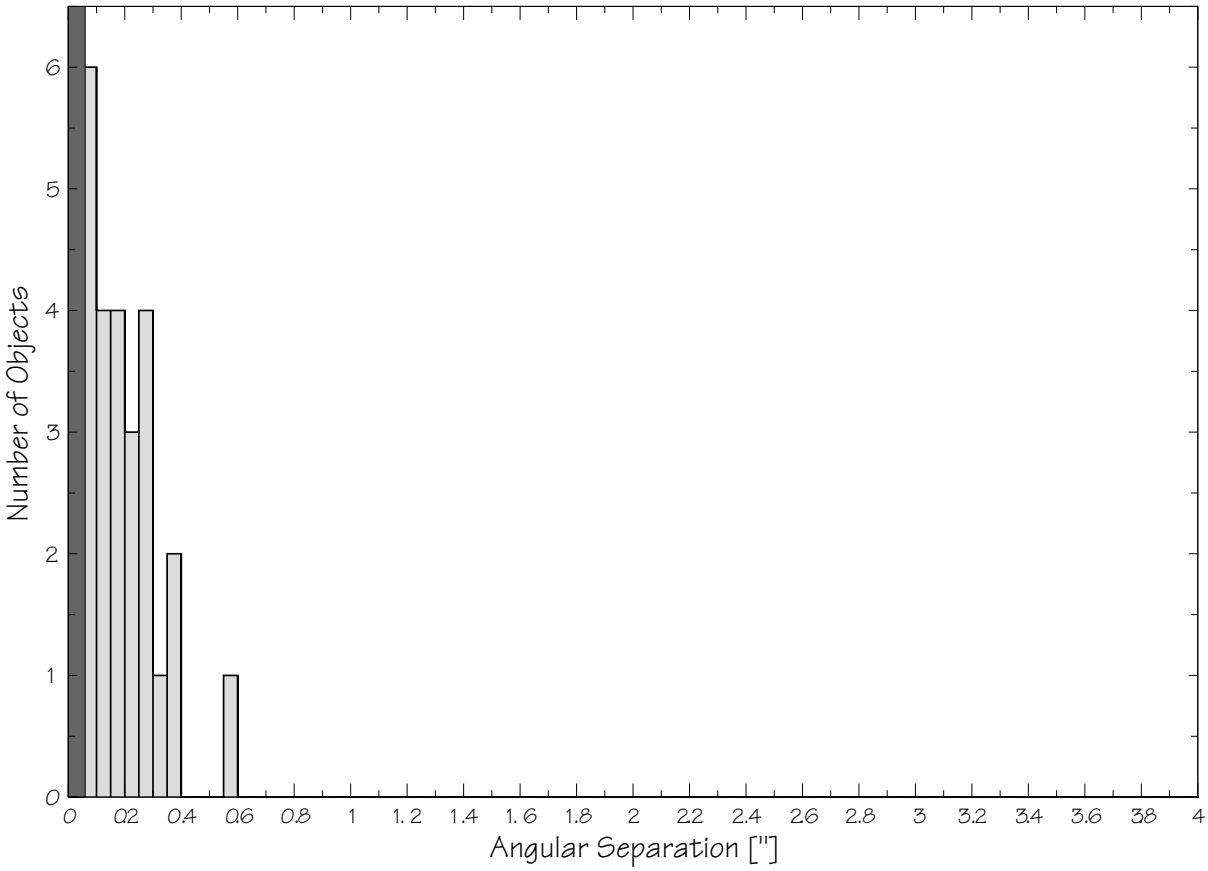

Figure 1.9 Distribution of angular separations of the binaries presented in this paper. There is an evident absence of systems with separation larger than $0\farcs6$. The observations were limited to $0\farcs060$ in the lower part (dark grey region) and $\sim 4\farcs0$ for the upper part.

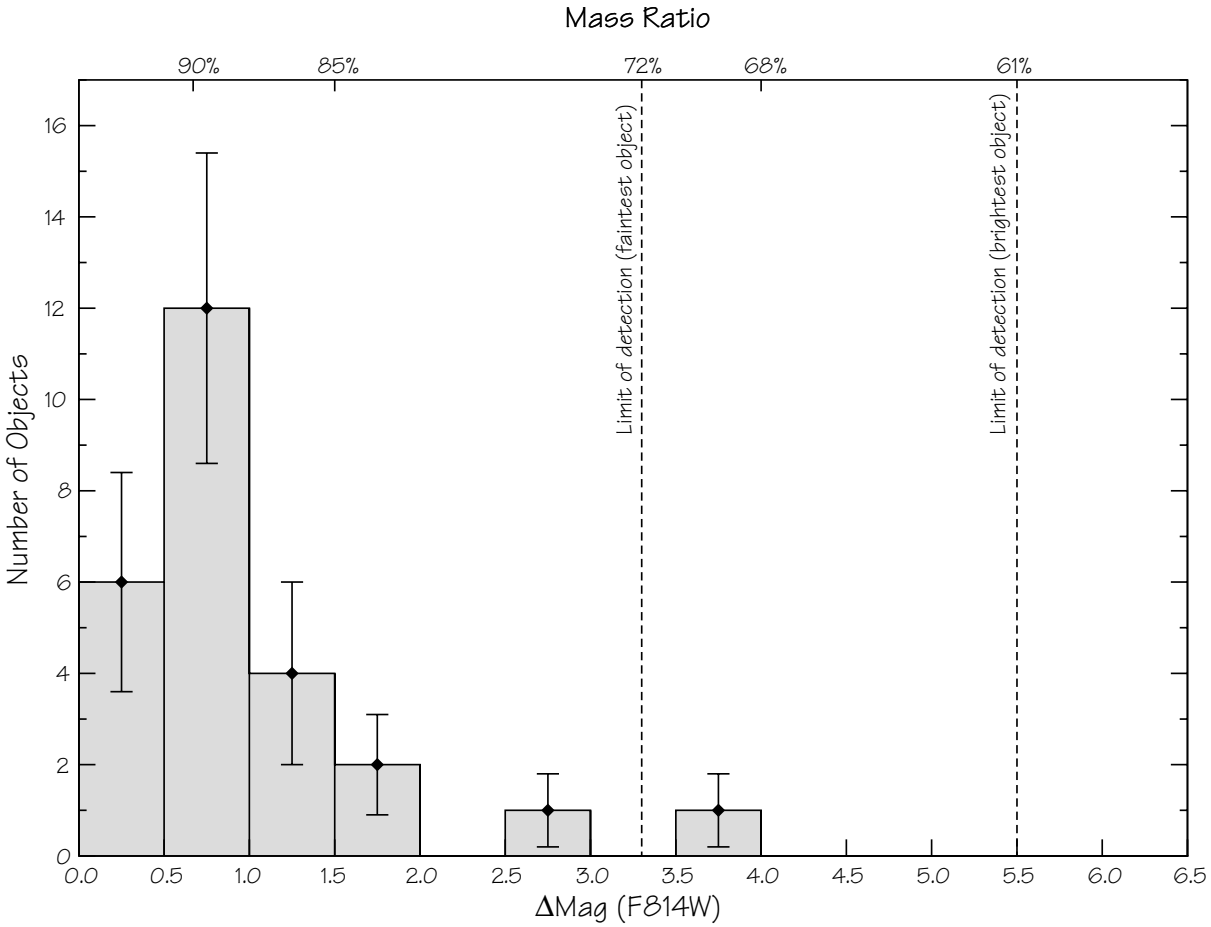

Figure 1.10 Distribution of difference of magnitude in the F814W ($\sim$ I) Filter. Although we would have been able to detect objects with $\Delta m_{F814W} < 3.3$ easily, we observe a clear lack of systems with $\Delta m_{F814W} > 2.0$, corresponding to a mass ratio of 85% (the mass ratios indicated here correspond to the one given by the Chabrier et al. (2000) models for a primary of 0.1 $M_{\odot}$ and an age of 1 Gyr, cf. Table 1.8).

easily even in the faintest cases, and binary systems with differences of magnitudes between $3.0 \leq \Delta m_{F814W} \leq 5.5$ mag in the brightest cases.

Binaries with a flux ratio $f = f_2/f_1$ can be detected $\sqrt{1+f}$ times further away. Therefore the higher ($\sim$ 1) the flux ratio is, the larger the sampled volume is. This is an another well known effect of the bias introduced by the multiplicity: the number of equal mass binaries is over-estimated in comparison with the number of binaries with large differences of magnitudes. This effect is maximum for equal mass binaries compared to binaries with mass ratio close to zero. The volume sampled for equal mass binaries is then 2.83 times larger than the volume sampled for systems with mass ratio close to zero. In our study we find a factor of $24/2 = 12$ times more systems with $0.1 \leq \Delta m_{F814W} \leq 2.0$ mag than system with $2.0 \leq \Delta m_{F814W} \leq 5.5$ (see Figure 1.10). Such a very large ratio can not be explained by this bias.

1.6.4 Colours

A colour-magnitude diagram (F814W vs. (F675W-F814W) $\sim$ I vs. R-I) of the sample of the GO8720 program is given in Figure 1.11. Plotted are the single or unresolved targets, as well as the multiple systems represented by three points : one point for the whole system and two linked points for the two individual components. Figure 1.11 shows clearly that the multiple systems include some of the reddest objects of the sample. The slopes of the lines joining the primary and the secondary might indicate that for two objects the secondary is bluer (higher R-I), whereas for the three other it is redder. This might be explained by dust effects as described in the DUSTY model (Allard et al. 2001; Chabrier et al. 2000), but could also be due to the relatively high uncertainties on the flux ratios and the corresponding uncertainties on the magnitudes of the two components.

A colour-magnitude diagram (F814W vs. (F814W-F1042M) $\sim$ I vs. I-z) of the sample of the GO8581 program is given in Figure 1.12. Not all the 15 binaries found in this sample were bright enough in the F1042M filter to be able to do the PSF fitting, thus not allowing to measure the flux ratios.

1.7 Discussion

This study allows us to point out three important results: the frequency of binaries, the lack of binaries with separations greater than 15 A.U and the possible preference for equal-mass systems. We will now discuss these results in the context of current scenarios of formation and evolution of free-floating ultra-cool dwarfs.

1.7.1 Binary frequency

As shown in Figure 1.13, the value we found for the binary frequency (10$\sim$15%) is much lower than the values given by Duquennoy & Mayor (1991) for G dwarfs ($\sim$ 57%), and by Reid & Gizis (1997b) or Marchal et al. (2003) for the early M dwarfs ($31 - 35\%$) considering that this latter values covers larger ranges of mass ratios and separations whereas we were limited in both cases. If we compare with only the G and M stellar systems having a separation $2.1 \leq a \leq 140$ A.U (corresponding to respectively $0\farcs060$ and $4\farcs0$ at the average distance of our sample: 35 pc) we find roughly $\sim$ 30% in the Duquennoy & Mayor (1991) distribution, which is still much higher than the one we give here for ultracool dwarfs (spectral types between M7 and L8). For comparison, in Figure 1.14 we combine a plot of the 25 field binary ultracool dwarfs presented here, with the distribution of separations given by Duquennoy & Mayor (1991) for the G-dwarfs. In the left part of our histogram we missed the binaries with separations smaller than $\sim 0\farcs060$. Even if it is not correct to compare directly both distributions (the Duquennoy & Mayor (1991) distribution was indeed corrected for biases whereas the distribution of the 25 binaries is not corrected at all), we can note the absence of systems with separations greater than 15 A.U, and the strong peak between $4 \sim 8$ A.U, instead of ~ 30 A.U for the G dwarfs.

In a recent study Burgasser et al. (2003) report an observed binary frequency among T dwarfs of 20^{+17}_{-7}% (2 multiple systems over a sample of 20 objects) corresponding to a biased corrected fraction of 9^{+15}_{-4}%. This number is in good agreement with the one we report here for late-M and L dwarfs. They also computed a bias corrected value of the binary fraction of late-M and L dwarfs of the sample of Reid et al. (2001) (HST program GO8146, 4 multiple objects among 20 targets) and, assuming it was a purely magnitude limited sample, they estimated a fraction of binary of the same order (9^{+11}_{-4}%) (see section 1.6.1 for a detailed discussion on the

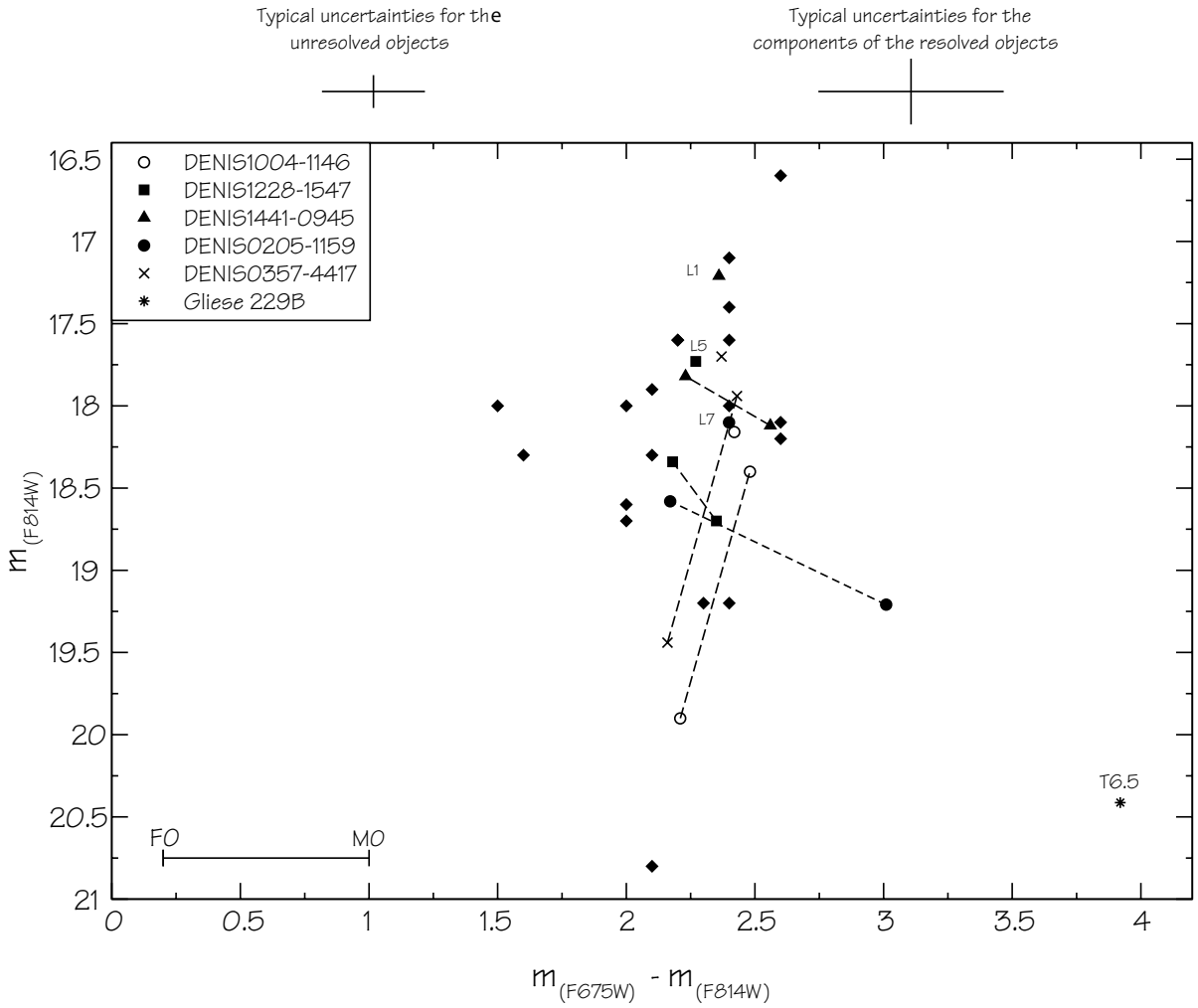

Figure 1.11 Colour Magnitude diagram of the sample (GO8720). Single or unresolved objects are represented by filled diamonds. Binary systems are represented by various symbols. For each binary system, both the binary system and the two components are represented (same symbol), these latter two are joined by a dashed line. The T-dwarf Gl229B is represented (by an asterisk) in addition for comparison between M, L and T-dwarfs. Values for Gl229B from Golimowski et al. (1998). Not all objects were available in both filters (see Tables 1.2 and 1.3). Spectral types of some objects were available (cf. Table 1.1).

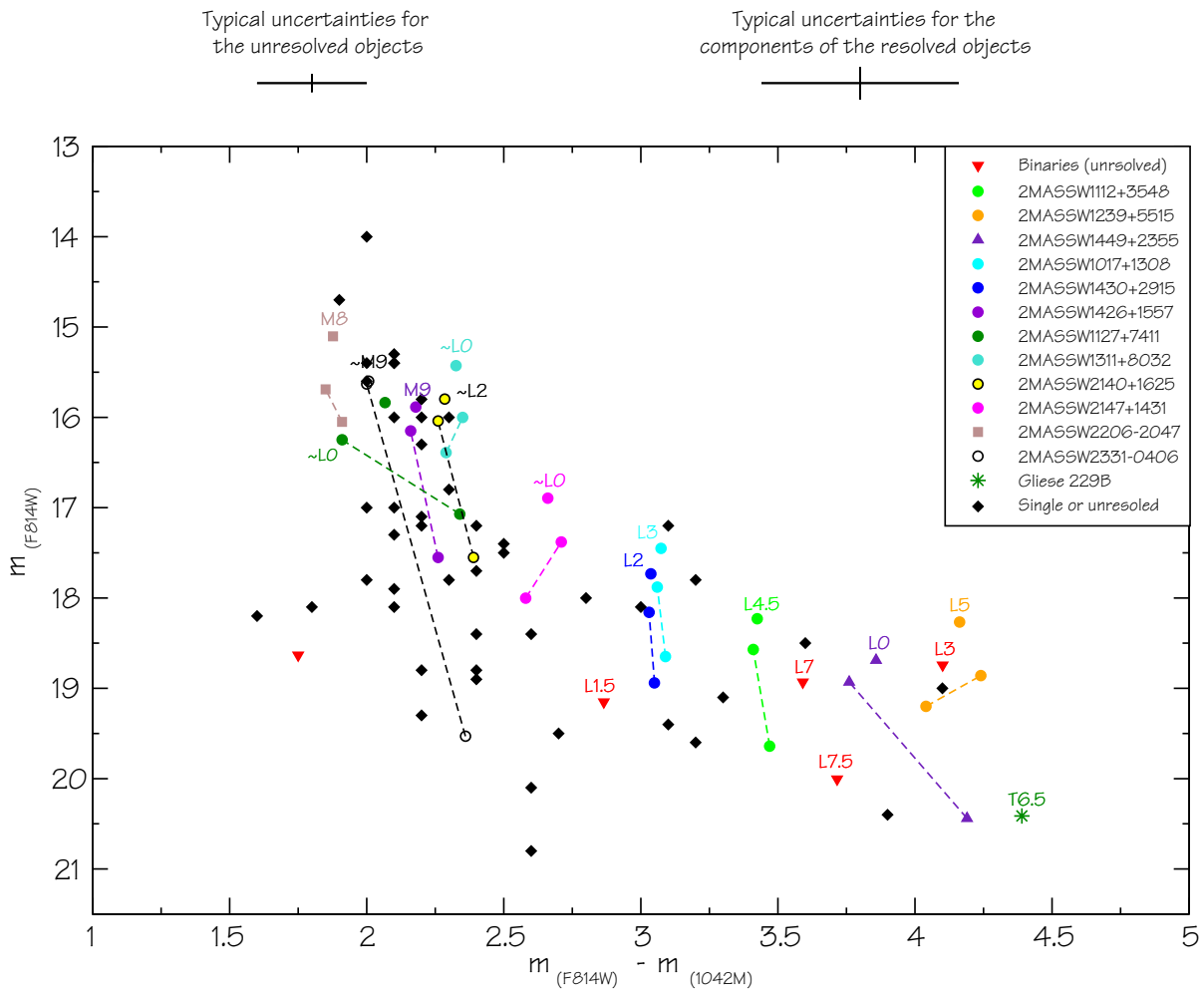

Figure 1.12 Colour Magnitude diagram of the sample (GO8581). Some multiple systems were unresolved or too faint in the F0142M filter, thus not allowing to measure the flux ratios. These latter cases are represented by a red triangle. The binaries resolved in both filters are represented with 3 points like in Fig. 1.11. Typical uncertainties are given for the unresolved objects and for the components of the multiple systems. The T-dwarf Gl229B is represented (asterisk) in addition for comparison between late M, L and T-dwarfs. Values for Gl229B from Golimowski et al. (1998). (see Tables 1.2 and 1.5 for the detailed values of magnitudes)

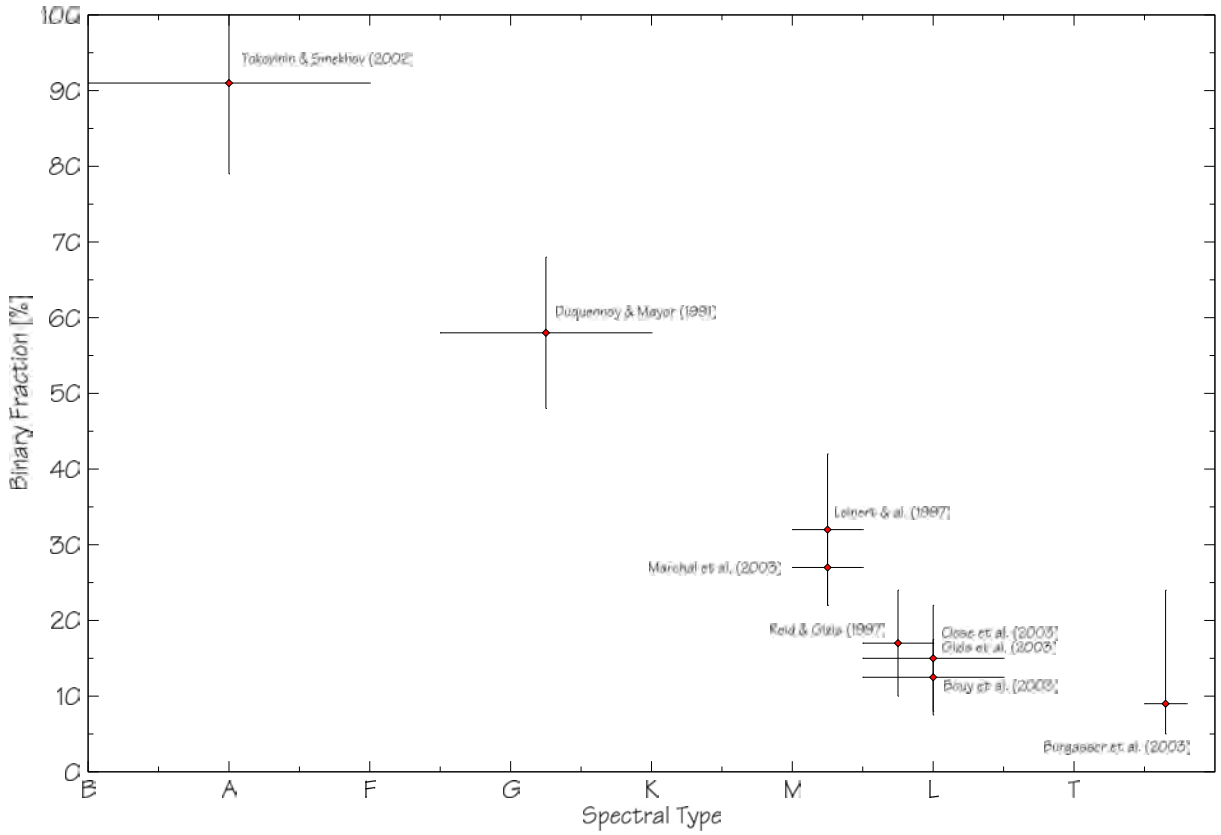

Figure 1.13 Binary frequency as a function of spectral type. Comparison of results obtained by several authors. Although it is not strictly rigorous to compare these values that were obtained under different conditions, there seems to be a trend fo decreasing binary fraction with increasing spectral type. See also Figure 1 of the Introduction (page 14).

difficulty to correct properly the bias). The results are again in good agreement within 1-σ. Our binary fraction is based on a total sample 6.65 larger than the samples of T-dwarfs and L-dwarfs they present, including the sample of L-dwarfs of Reid et al. (2001).

The binary frequency we report here gives also strong constraints on the models of formation. In particular such a high rate of multiple systems cannot be explained by the hydrodynamical simulations of Delgado-Donate et al. (2003); Bate et al. (2002) that predict very few binary ultra-cool dwarfs. They report that their models of formation and evolution predict a very low frequency of binaries among very low mass stars and brown dwarfs ($\leq 5\%$), because in most of the cases the dynamical interactions involved in the ejection of the ultracool dwarfs lead to the disruption of the multiple systems. Their important results obtained using high-resolution hydrodynamical simulations of 5 bodies star forming regions (Delgado-Donate et al. 2003) and star formation from the fragmentation of turbulent molecular clouds (Bate et al. 2002) are thus in contradiction with the results we present here on that point. Indeed, even if the binary frequency we report here is not much higher than the upper limit predicted by these models, we have to keep in mind that our value is a lower limit since we did not take in account the spectroscopic binaries. We will discuss the impacts of our result on the models of formation in more details in Part III. The binary frequency we present here should allow to constrain better the properties of the initial molecular clouds in which ultra-cool dwarfs are supposed to form.

1.7.2 The brown dwarf wide binary desert

The lack of binaries with wide separations that we observe for ultra-cool and brown dwarfs suggest that there are major differences in the formation and evolution processes of these ultra-cool objects in comparison with stars. Whereas they cannot explain the binary frequency we report here, the models of ejection (Delgado-Donate et al. 2003; Bate et al. 2002; Durisen et al. 2001) are consistent with the wide binary desert. Only a close binary might indeed be able to survive during the disruption process. As we observe a relatively high rate of binaries, it is more likely that the observed desert might be the consequence of several effects: both formation peculiarities and later evolution processes, such as disruption due to the gravitational interaction with neighbouring stars and/or molecular clouds (see Burgasser et al. (2003) for a discussion on this last point). These results are consistent with the previous results presented by Reid et al. (2001); Close et al. (2003, 2002b). We will also discuss this point in more details in Part III.

1.7.3 Distribution of Mass Ratios

The transformation of flux ratio to mass ratio is not straightforward, because the ages of various individual systems can be very different, and second because of the degeneracy in the mass-luminosity (age-temperature) relation in the case of brown dwarfs. Luminosities and effective temperatures of brown dwarfs are indeed function of both age and mass (Burrows et al. 1997; Chabrier et al. 2000). But since the two components of a binary system can be assumed to be coeval, a difference in the luminosity must be associated to a difference in mass.

As we observe a strong lack of binaries between $1.5 \leq \Delta m_{F814W} \leq 2.5$ mag (see Fig. 1.10), and if we consider that the sample covers a randomly large range of ages (typically between 0.5 Gyr and 10 Gyrs), we can suggest that this might be evidence of a preference for equal-mass systems, as it was thought before. Indeed Table 1.8 shows that the mass ratios corresponding to $\Delta m_{F814W} = 1.5$ mag for ages between 0.5 Gyr and 5.0 Gyrs are ranging between 75% and 95%, whereas mass ratios corresponding to $\Delta m_{F814W} = 4.0$ mag are ranging between 55% and 74% (Chabrier et al. 2000). If we consider a coeval binary system with a primary

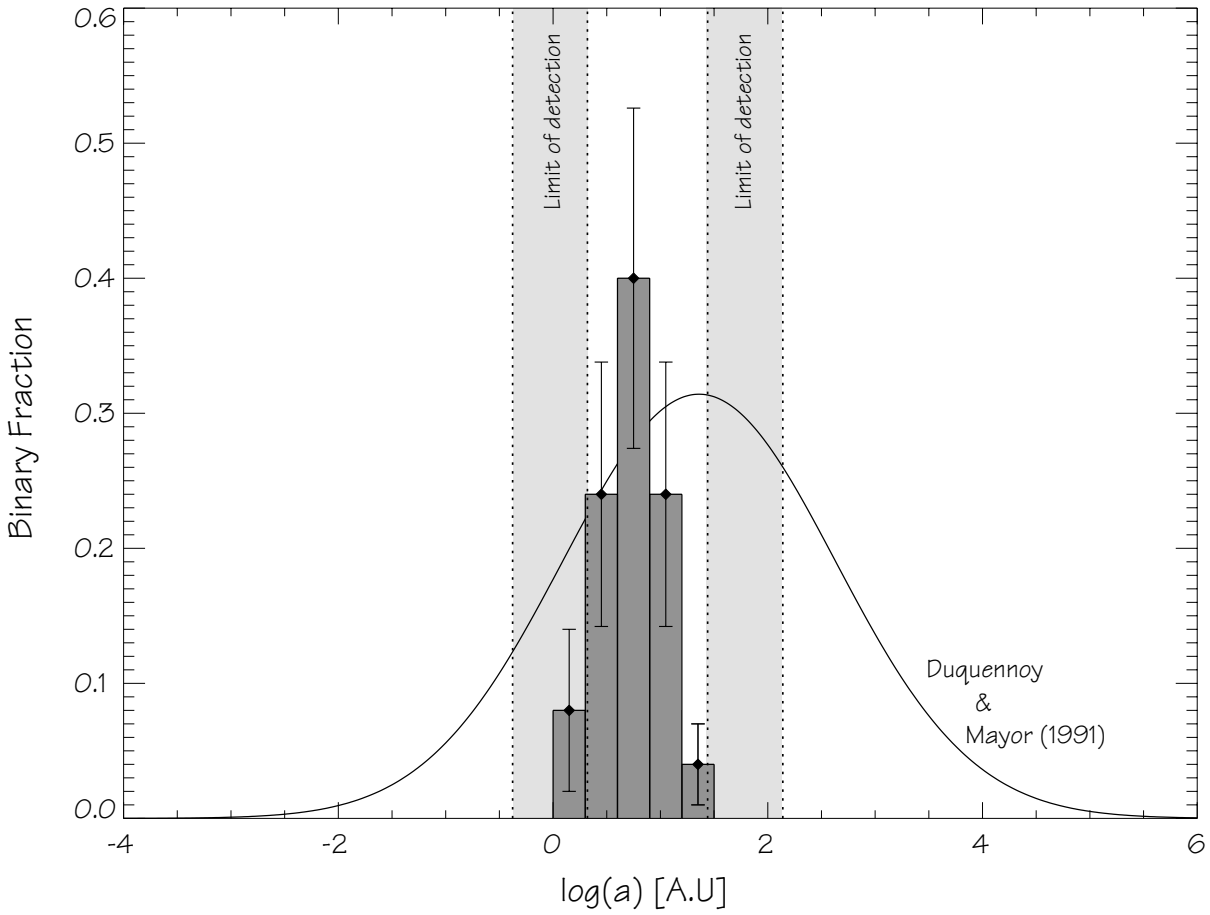

Figure 1.14 Distribution of separations of the 25 binaries presented in this paper, compared with the Duquennoy & Mayor (1991) distribution of G-dwarf. The upper and lower limits of detection are in the grey regions. These regions have been calculated considering an upper limit in the distance at 35 pc (average distance of the sample) with corresponding maximum limits of detection of 4.″0 and 0.″06 and a lower limit at 7 pc (closest distance of our sample) with minimum limits of detection of 4.″0 and 0.″060. Even if it is not correct to compare both distributions (the distribution of ultra-cool binaries was not corrected for bias) the lack of binaries wider than 15 A.U and the strong peak around 4∼8 pc appear clearly, although wider binaries should have been identified despite the selection biases.

Table 1.8. Examples of mass ratios based on the DUSTY model

Δm_{F814W}	1.5	3.0	4.0	5.5
Age	M_2/M_1	M_2/M_1	M_2/M_1	M_2/M_1
0.5 Gyr	75%	62%	55%	45%
1.0 Gyr	85%	73%	68%	61%
5.0 Gyrs	95%	77%	74%	71%

Note. — Examples of mass ratios based on the DUSTY model convolved with the HST/WFPC F814W filter, corresponding to luminosity ratios of $\Delta m_{F814W} = 1.5$, 3.0, 4.0, and 5.5 mag, for a primary of 0.1 $M_\odot$, according to the DUSTY model of Chabrier et al. (2000)

with $T_{eff}(A) = 2012$K, 1Gyr and M_A=0.07$M_\odot$, a difference of magnitude $\Delta m_{F814W} = 3$ mag corresponds to a secondary with $T_{eff}(B) \sim 1600$K and M_B=0.06$M_\odot$, whereas a a difference of magnitude $\Delta m_{F814W} = 5.5$ mag corresponds to a secondary with $T_{eff}(B) \sim 1500$K and M_B=0.052$M_\odot$. These examples illustrates the limits we were able to reach in our study.

It is also interesting to mention that this lack is similar to the deficiency of low mass ratios among binary early-M dwarfs in comparison with G dwarfs reported by Fischer & Marcy (1992) and to the excess of near equal mass M-dwarf binary systems in comparison with G dwarfs systems reported by Reid & Gizis (1997b). All these observations suggest different formation mechanisms and/or different processes of evolution.

The survey is of course biased by the limited sensitivity at smaller separations/lower flux ratios, but nevertheless covers a relatively large dynamic and resolution range. Because of these limits of detection we cannot exclude the possibility of a multi-modal distribution of mass ratio, even if this scenario appears very unlikely in the current context of models of formation and evolution. It is important to remember that we were not able to detect systems with Δm_{F814W} greater than 5.5 mag, corresponding to systems with mass ratios of about 45%, 61%, 71% respectively at the ages of 0.5, 1.0 and 5 Gyrs and for a primary mass of 0.1 $M_\odot$ (according to the DUSTY models of Chabrier et al. (2000), cf. Table 1.8).

Table 1.9. Resolved Field Ultra-cool Dwarfs Binaries

Name	Distance (pc)	Sep. (A.U)	Semi-major axis[c](A.U)	Period[d] (yrs)
DENISPJ0205-1159	19.8	7.3	9.2	74.6
DENISPJ0357-4417	22.2 [b]	2.2	2.8	10.5
2MASSW0746+2000	12.3	2.7	3.4	14.0
2MASSW0850+1057	41.0	6.4	8.1	61.6
2MASSW0856+2235	34.7 [b]	3.5	4.4	20.8
2MASSW0920+3517	20.1 [b]	1.5	1.9	7.2
DENISPJ1004-1146	46.8[b]	6.8	8.6	56.5
2MASSW1017+1308	21.4 [b]	2.3	2.9	11.0
2MASSW1127+7411	14.6 [b]	3.8	4.8	23.5
2MASSW1146+2230	27.2	8.0	10.1	92.6
DENISPS1228-1547	20.2	5.1	6.6	49.0
2MASSW1239+5515	21.3 [b]	4.7	5.9	32.0
2MASSW1311+8032	13.7 [b]	4.4	5.5	28.7
2MASSW1426+1557	26.7 [b]	4.3	5.4	33.3
2MASSW1430+2915	29.4 [b]	2.7	3.4	13.9
DENISPJ1441-0945	29.2[b]	11.2	14.1	118.0
2MASSW1449+2355	63.7 [b]	8.7	11.0	81.1
2MASSW1600+1708	60.6 [b]	3.4	4.3	19.9
2MASSW1728+3948	20.4 [b]	2.8	3.4	13.8
2MASSW2101+1756	23.2 [b]	5.6	7.1	41.9
2MASSW2140+1625	12.9 [b]	2.1	2.6	10.5
2MASSW2147+1431	21.8 [b]	7.2	9.1	61.7
2MASSW2206-2047	22.2 [b]	3.6	4.5	22.6
2MASSW2331-0406	26.2	15.1	19.0	211.0
SDSS2335-0013	20 [a]	1.1	1.4	3.7
CFHT-PL-18	105 [b]	35.0	44.1	641

[a]The distance cannot be estimated by any method. We assume an average distance of 20 pc.

[b]Photometric distances evaluated as explained in section 1.4.

[c]Semi-major axis calculated by multiplying the projected separation by the correction factor 1.26 as explained in Fischer & Marcy (1992), in order to take in account inclination, orbital angle, etc.

[d]This period is just an estimate, calculated as explained in the text.

Chapter 2

Ultracool dwarfs in a young open cluster: the Pleiades

2.1 Introduction: The Pleiades

Photometric surveys to look for brown dwarfs in young stellar clusters proved to be very successful. The advantage of working with young open clusters is that both the age and distance are precisely known so that brown dwarfs candidates are easily identified from their position in colour-magnitude diagrams, relative to the expected position of the cluster's sub-stellar isochrone (Moraux et al. 2003). Also, still using theoretical models Chabrier et al. (2000), the magnitude of the object can be readily converted to a mass (given the age and distance of the cluster) and the resulting IMF estimated. In the following study, we obtained high angular resolution images of a sample of brown dwarfs in the Pleiades cluster in order to investigate the occurrence of multiple systems among sub-stellar objects, and its implications on:

1. the formation and evolution processes of brown dwarfs
2. the properties of these multiple systems in comparison with that in the field and in star forming regions.

The Pleiades, in which we did the study, is one of the best studied open clusters. Its age (120 Myr) and distance (d=135 pc, see e.g Pan et al. 2004; Munari et al. 2004) are well known and its IMF has been well studied over the stellar mass range. All the targets come from the same forming region: they had the same initial conditions and are now following identical evolutionary paths, which is not the case of field brown dwarfs for which in general we do not know neither the age nor the distance precisely. Moreover, the Pleiades cluster offers many advantages for our study in comparison with other clusters, star forming regions or associations. First of all, because we have a relatively large sample of confirmed brown dwarfs, which is of prime importance in order to make a good statistical study. This was not the case of star forming regions or other associations where only few brown dwarfs were confirmed at the time of this study. Second, this sample is homogeneous in age and distance, and is not too far away to exclude a search for close visual binaries. All this considerations make this cluster the ideal place for a complementary study to the field ultracool dwarfs.

In a first attempt to investigate brown dwarf binaries, Martín et al. (2000a) surveyed 34 very low mass Pleiades members with HST/NICMOS and HST/WFPC2. They failed to find any companion at a resolution of $0\farcs2$ or larger (27 A.U, NICMOS) and only few (4) at a resolution of $\sim 0\farcs060$ or larger (8.1 A.U at 135 pc, WFPC2/PC).

2.2 WFPC2 search for multiple systems in the Pleiades

*Note: T*he WFPC2-PC study presented in this chapter has been conducted and lead by Prof. E. L. Martín (I.A.C), who invited me to participate. The results presented here have been published by Prof. Martín and a list of collaborators including myself in a refereed article (Martín et al. 2003). My work in this study consisted mainly in the identification of the multiple systems and the analysis of their astrometric and photometric properties. With the permission of Prof. E. L. Martín, I will therefore often refer to and quote the sections of the article of Martín et al. (2003) corresponding to the work I have done. The ACS study happened after an interval of two years after the WFPC2 one.

2.2.1 Observations

We used the unique high angular resolution provided by HST/WFPC2 (program SNAP-8701, P.I. Martín). The observations we performed with HST/WFPC2 provide angular resolution down to $\sim 0''.060$ ($\sim$8.1 A.U), i.e more than 3 times better than the NICMOS study of Martín et al. (2000a). This allows us to investigate very close companions.

2.2.2 Sample

The targets were compiled from several lists of very low-mass ($M<0.1\ M_{\odot}$) candidate members. We used the informations provided in the works of Martín et al. (1996); Martín et al. (1998); Rebolo et al. (1996); Zapatero Osorio et al. (1997) for Calar objects; Zapatero Osorio et al. (1999) for Roque objects; Bouvier et al. (1998); Stauffer et al. (1998); Martín et al. (2000a) for CFHT-PL objects; Hambly et al. (1999) for IPMBD objects; and Festin (1998b,a) for NPL objects. These compilations include most of the known Pleiades very low mass stars and brown dwarf candidates that had not been previously observed with HST. Of the 29 objects proposed for this program, 26 have been observed. One of them turned out to be a duplication because NPL 40 is the same object as Roque 33. This object was observed twice. The remaining 3 Pleiades targets were not scheduled for observation.

Table 2.1 gives an overview of the sample.

2.2.3 Observational strategies and techniques

Observations were carried out between July 2000 and August 2001 as part of the HST Snapshot program designed to fill short intervals between accepted GO observations (SNAP-8701, HST Cycle 9, P.I Martín). Each brown dwarf candidate was centered in the PC chip of the WFPC2. With a plate-scale of $0''.0455$ per pixel, the PC has a field of view of $36''$ in diameter. Assuming a distance of 135 pc for the Pleiades, this provides a maximum physical separation of 2430 A.U from each brown dwarf candidate to search for companions. The observations were made in two broadband filters, the F814W and the F785LP with central wavelengths at 862.1 nm and 792.4 nm respectively. The filters were chosen to provide high throughput and a clear colour separation between brown dwarfs and background stars and galaxies. Two exposures were taken in each filter to allow for proper cosmic ray rejection, yielding to total integration times of 600 s and 280 s in the F814W and F785LP filters, respectively.

Table 2.1. Pleiades WFPC2 sample

Name	R.A[b]	Dec.[a]	F785LP	F814W	I_C[a]	$R-I_C$[a]	SpT[a]	Li ?[a]	PMM[a]	Member ?
Cl* Melotte 22 CALAR 3	03 51 26.1	+23 45 20	19.00	18.19	19.00	2.50	M8	Y	Y	Y
Cl* Melotte 22 CFHT-Pl 9	03 49 15.2	+24 36 23	17.74	17.05	17.71	2.18	M6.5	N	Y	Y
Cl* Melotte 22 CFHT-Pl 10	03 44 32.4	+25 25 18	17.81	17.12	17.82	2.21	M6.5	N	Y	Y
Cl* Melotte 22 CFHT-Pl 12	03 53 55.2	+23 23 37	17.93	17.14	18.00	2.47	M8	Y	Y	Y
Cl* Melotte 22 CFHT-Pl 15	03 55 12.6	+23 17 38	18.73	17.96	18.62	2.34	M7	Y	N	Y
Cl* Melotte 22 CFHT-Pl 19	03 45 33.2	+25 34 30	18.99	18.30	18.92	2.51	···	···	N	N
Cl* Melotte 22 HHJ 3	03 48 50.4	+22 44 30.	18.00	17.25	18.07	···	···	···	Y	Y
Cl* Melotte 22 IPMBD 21	03 49 16.15	+26 49 03.6	17.85	17.15	17.85	···	···	···	Y	Y
Cl* Melotte 22 IPMBD 22	03 49 33.03	+26 50 43.0	17.86	17.20	17.90	···	···	···	Y	Y
Cl* Melotte 22 IPMBD 25	03 46 26.06	+24 05 09.9	17.67	16.97	17.82	···	···	···	Y	Y
Cl* Melotte 22 IPMBD 26	03 47 15.17	+25 24 19.2	18.04	17.40	18.11	···	···	···	Y	Y
Cl* Melotte 22 IPMBD 29	03 45 31.33	+24 52 47.8	18.38	17.49	18.35	···	···	···	Y	Y
Cl* Melotte 22 IPMBD 43	03 39 17.03	+22 27 11.5	18.06	17.33	18.1:	···	···	···	Y	Y
Cl* Melotte 22 NPl 36	03 47 50.4	+23 54 49	18.56	17.79	18.66	···	M7.5	···	···	···
Cl* Melotte 22 NPl 38	03 47 50.4	+23 54 49	19.20	18.38	19.18	···	M8	···	···	···
Cl* Melotte 22 NPl 40	03 48 49.0	+24 20 25	20.39	19.65	20.26	···	M9.5	···	···	···
Cl* Melotte 22 NPl 43	03 48 27.36	+23 46 20.3	21.77	21.05	21.79	···	···	···	···	···
Cl* Melotte 22 ROQUE 5	03 44 22.4	+23 39 01	20.05	19.29	19.71	···	M9	···	Y	Y
Cl* Melotte 22 ROQUE 7	03 43 40.3	+24 30 12	19.39	18.68	19.50	2.61	M8.5	···	Y	Y
Cl* Melotte 22 ROQUE 18	03 45 52.6	+23 43 17	21.41	20.85	21.11	···	···	···	···	···
Cl* Melotte 22 ROQUE 20	03 48 43.7	+22 40 46	21.62	22.31	22.2:	···	···	···	···	···
Cl* Melotte 22 ROQUE 23	03 47 05.0	+23 55 48	22.01	21.73	21.75	···	···	···	···	···
Cl* Melotte 22 ROQUE 24	03 43 21.4	+24 34 42	22.14	21.02	21.56	···	···	···	···	···
Cl* Melotte 22 ROQUE 30	03 50 16.0	+24 08 35	20.92	20.40	20.31	···	···	···	···	···

Note. — Multiple systems are indicated in bold face

[a]The R_C and I_C photometric data, spectral types, lithium detections and proper motion memberships come from the literature cited in the text.

[b]J2000

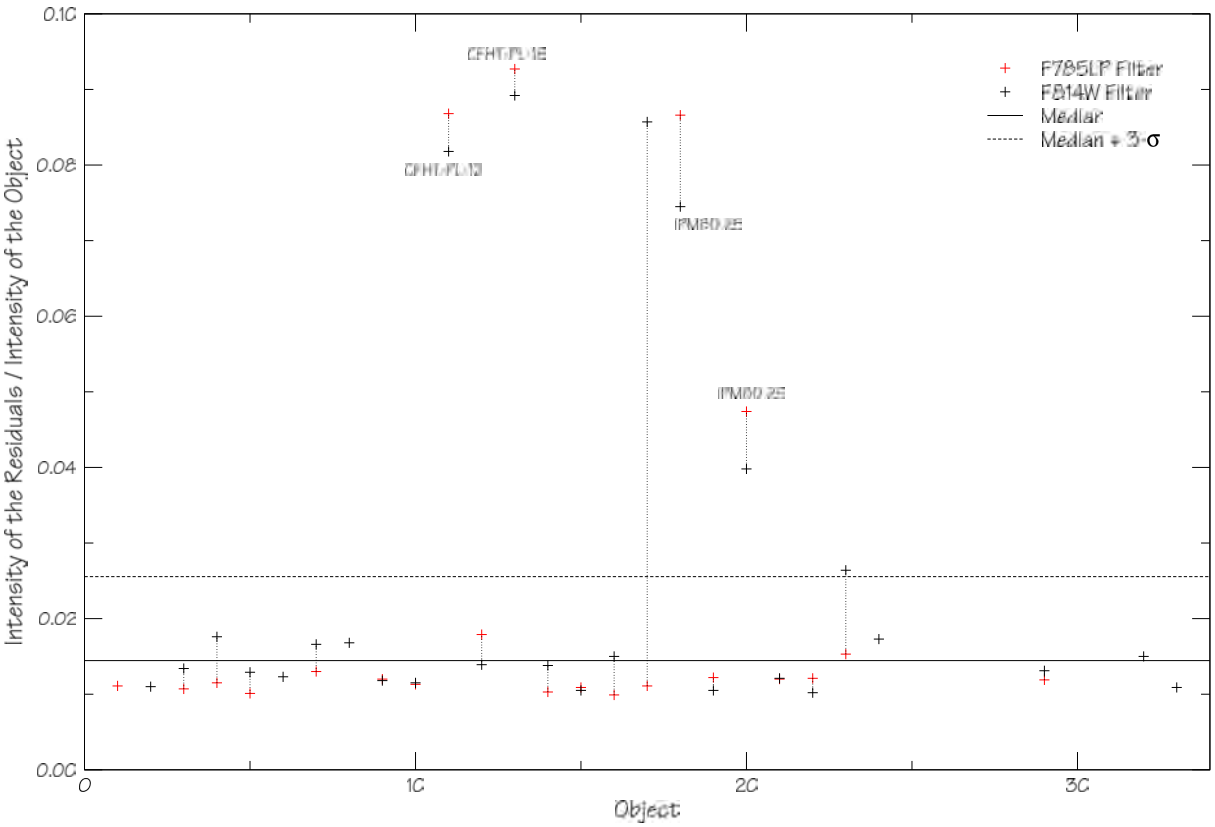

Figure 2.1 Relative intensity of the residuals after PSF subtraction on the Pleiades ultracool dwarfs of our WFPC2-PC sample. The black plus indicate the results in the F814W filter, and the red plus the results in the F785LP filter. Results for the same objects are linked by a dotted line. The median value and 3-σ above the median are indicated. Objects below 3-σ above the median value are considered as unresolved. Two objects have great residuals in the F814W filter, but normal residuals in the F785LP filter. A visual check confirms that the elongation seen in the F814W images is due to a cosmic ray or bad pixel.

2.2.4 Data analysis

Identification of the multiple systems

We searched for and identified the binary candidates using the same technique as for field ultracool dwarfs, as described in Section 1.2.1 of Chapter 1 in this Part.

As shown by Figure 2.1, we found 4 binary candidates in the WFPC2-PC sample. One object (HHCJ4) has great residuals in the F814W filter, but normal residuals in the F785LP filter. A visual check confirm that the elongation seen in the F814W image is due to a cosmic ray or bad pixel.

PSF Fitting

The WFPC2-PC data have been processed with PSF fitting exactly as described in Section 1.2.2 of Chapter 1 in this Part. The calibrations of the PSF fitting program are presented in Annex A.

2.3 ACS search for multiple systems in the Pleiades

2.3.1 Observations

In order to refine the WFPC2 study, we used the higher angular resolution provided by ACS-HRC (program SNAP-9831, P.I. Bouy). An ESO/VLT-NACO proposal had been rejected because the Pleiades are too low in the Chilean sky to make an efficient use of this Adaptive Optic System, which would have been the only one currently able to compete with HST/ACS spatial resolution. Keck/AO was indeed limited to NGS brighter than 12 in the visible, much too low in the case of our study, and Subaru/AO does not provide a resolution below 0.″2, which is about 5 times worse than HST/ACS. Using PSF fitting, the observations we performed with HST/ACS allow us to resolve multiple systems with separations as low as ∼0.″040 (∼5.4 A.U), i.e more than 5 times better than the NICMOS study of Martín et al. (2000a) and 1.5 times as good as the WFPC2/PC study. Moreover, the sensitivity of HST/ACS in the chosen filter is ∼5 times greater than the WFPC2/PC (see Biretta 2002, and Chapter 1). This allows us to investigate very close companions and very small mass ratios between the companion and the primary.

2.3.2 Sample

The sample consists of 32 very low mass stars and brown dwarfs (spectral types later than M7) in the magnitude range I=18.0 mag to I=22.9 mag, identified from deep, wide-field surveys of the Pleiades cluster (Moraux et al. 2003, 2001; Bouvier et al. 1998), and different from the WFPC2-PC sample, apart from 4 objects (the binaries CFHT-PL-12 and IPMBD 29, and CFHT-PL-15 and IPMBD 25). All the targets have been identified as brown dwarfs using near-infrared and optical photometry analysis and/or spectroscopy. The sample covers a mass range from 0.025 to 0.080 $M_{\odot}$ and is shown in Figure 2.2 enclosed and Table 2.2. The membership of our targets has been already confirmed by proper motion measurements or photometry (Moraux et al. 2001, 2003).

2.3.3 Observational strategies and techniques

Observations were carried out during cycle 12 between July 2003 and August 2004 as part of the HST Snapshot SNAP-9831 program. Each object was observed in the F814W filter, which provides the best compromise between the efficiency, the sensitivity to our cold objects, and the S/N ratio. Only one band was obtained in order to maximize exposure times, minimize the visit times and thus optimize schedulability.

Diffraction limited imaging with ACS-HRC at 814 nm gives us a spatial resolution of 0.″085. With its 0.″027 pixel scale, the ACS-HRC thus provides the required critical sampling of the PSF, which was not the case of the WFPC2/PC camera. Using PSF fitting, we are thus able to resolve even closer companions than in the case of WFPC2. Integration times were 400 s, spread over 4 exposures in CR-SPLIT mode (Pavlovsky et al. 2003). Figure 2.4 shows that we were sensitive to companions 5.9 mag fainter than their primary (3-σ detection limit), corresponding to a lower limit on the mass ratio between 0.4 and 0.7 depending on the brightness of the primary.

Seventeen objects among the 33 submitted have been observed, but in 2 cases a problem with the guidance sensor resulted in moved exposures, as shown in Figure 2.3. The corresponding images are useless. We thus obtained images for 15 targets, 2 of which were already known binaries.

Table 2.2. Pleiades ACS sample

Name	R.A (2000)	Dec. (2000)
Cl* Melotte 22 CFHT-Pl 11	03 47 39.0	+24 36 22.1
Cl* Melotte 22 CFHT-Pl 12⋆	03 53 55.1	+23 23 36.4
Cl* Melotte 22 CFHT-Pl 13	03 52 06.72	+24 16 00.76
Cl* Melotte 22 CFHT-Pl 15	03 55 12.5	+23 17 38.0
Cl* Melotte 22 CFHT-Pl 16	03 44 35.3	+25 13 44.0
Cl* Melotte 22 CFHT-Pl 17	03 43 00.2	+24 43 52.1
Cl* Melotte 22 CFHT-Pl 21	03 51 25.6	+23 45 21.2
Cl* Melotte 22 CFHT-Pl 23	03 52 18.64	+24 04 28.41
Cl* Melotte 22 CFHT-Pl 24	03 43 40.29	+24 30 11.34
Cl* Melotte 22 CFHT-Pl 25	03 54 05.37	+23 33 59.47
Cl* Melotte 22 CFHT-Pl-IZ 10	03 51 44.97	+23 26 39.47
Cl* Melotte 22 CFHT-Pl-IZ 1262	03 44 27.27	+25 44 41.28
Cl* Melotte 22 CFHT-Pl-IZ 13	03 55 04.4	+26 15 49.3
Cl* Melotte 22 CFHT-Pl-IZ 14	03 53 32.39	+26 07 01.2
Cl* Melotte 22 CFHT-Pl-IZ 2141	03 44 31.29	+25 35 14.42
Cl* Melotte 22 CFHT-Pl-IZ 161	03 51 29.43	+24 00 36.79
Cl* Melotte 22 CFHT-Pl-IZ 17	03 51 26.69	+23 30 10.65
Cl* Melotte 22 CFHT-Pl-IZ 19	03 56 16.37	+23 54 51.44
Cl* Melotte 22 CFHT-Pl-IZ 2	03 55 23.07	+24 49 05.01
Cl* Melotte 22 CFHT-Pl-IZ 21	03 55 27.66	+25 49 40.72
Cl* Melotte 22 CFHT-Pl-IZ 23	03 51 33.48	+24 10 14.16
Cl* Melotte 22 CFHT-Pl-IZ 25	03 52 44.3	+24 24 50.04
Cl* Melotte 22 CFHT-Pl-IZ 26	03 44 48.66	+25 39 17.52
Cl* Melotte 22 CFHT-Pl-IZ 28	03 54 14.03	+23 17 51.39
Cl* Melotte 22 CFHT-Pl-IZ 29	03 49 45.29	+26 50 49.88
Cl* Melotte 22 CFHT-Pl-IZ 300	03 51 15.6	+23 47 05.38
Cl* Melotte 22 CFHT-Pl-IZ 31	03 51 47.65	+24 39 59.51
Cl* Melotte 22 CFHT-Pl-IZ 4	03 41 40.92	+25 54 23.0
Cl* Melotte 22 CFHT-Pl-IZ 51	03 46 36.24	+25 33 36.21
Cl* Melotte 22 CFHT-Pl-IZ 7	03 48 12.13	+25 54 28.4
Cl* Melotte 22 IPMBD 25⋆	03 46 26.1	+24 05 10.0
Cl* Melotte 22 IPMBD 29⋆	03 45 31.3	+24 52 48.0

Note. — Observed objects are indicated in bold face, and the ⋆ symbol indicates the binaries.

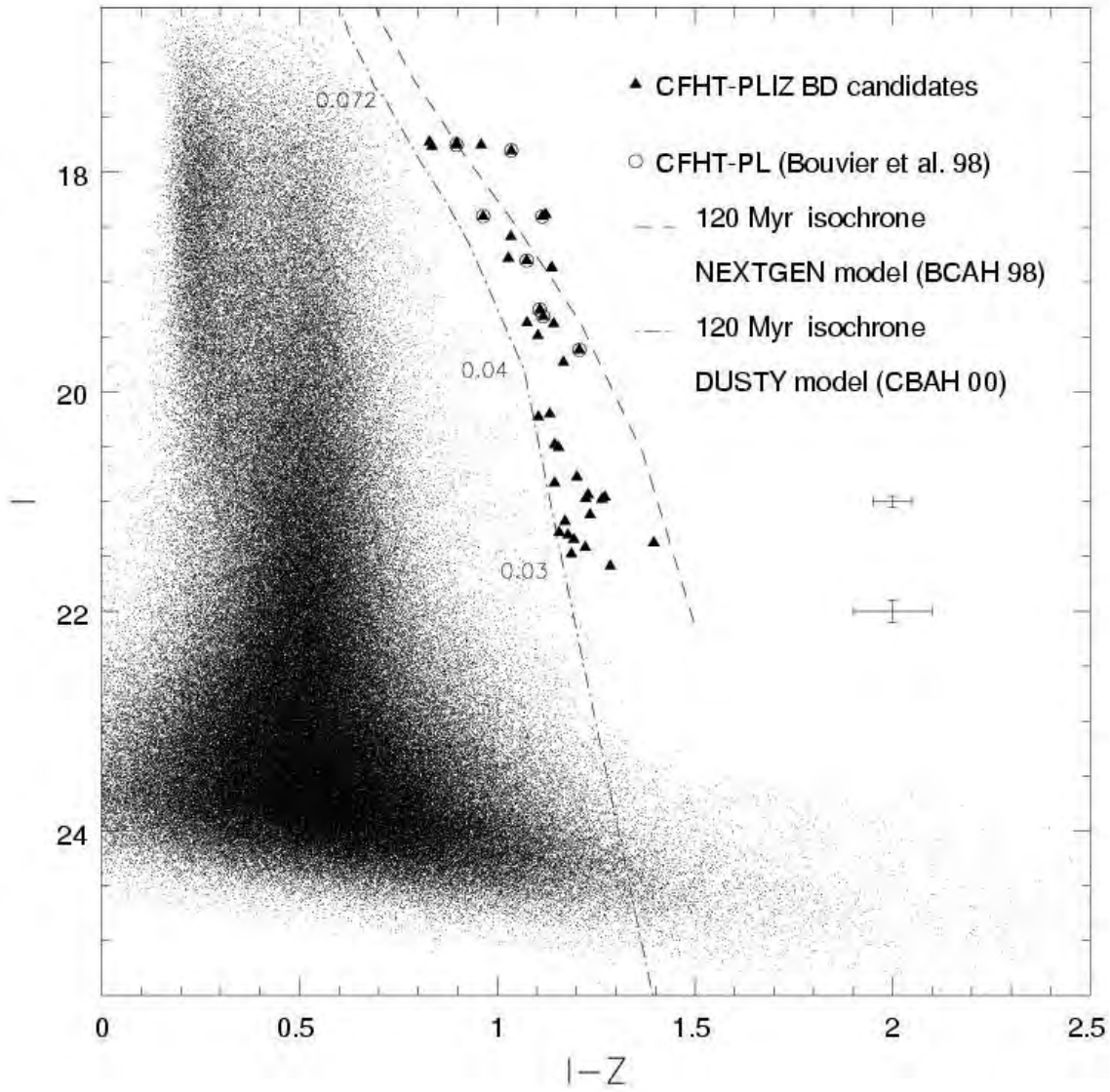

Figure 2.2 (I vs I-Z) colour-magnitude diagram. The small dots represents the field stars. Brown dwarfs down to $0.03M_{\odot}$ are shown as filled triangles and/or open circles. Courtesy Estelle Moraux, from Moraux et al. (2003)

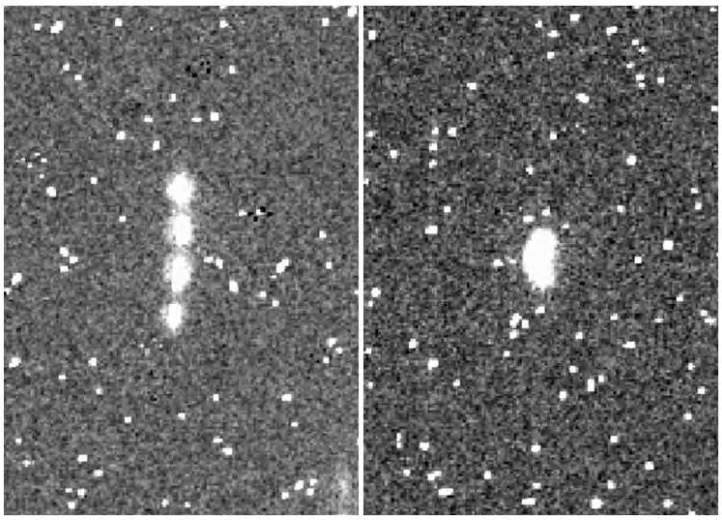

Figure 2.3 A problem in the FGS during the acquisition resulted in moved and useless exposures. Left panel: CFHT-Pl-23; Right Panel: CFHT-Pl-24.

2.3.4 Data Analysis

Search for the multiple systems

All images have been inspected manually in order to look for elongation. Figure 2.5 shows the contour plots of each of the targets. The two previously known binaries (CFHT-PL-12 and IPMBD-29) appears clearly elongated. Some objects appeared to have possible companions which, after further analysis, turned to be cosmic rays, as indicated on Figure 2.5. We also performed PSF subtraction as for the WFPC2 sample. No new binary was found among the 13 new objects.

PSF fitting

The ACS-HRC data have been processed with the same PSF fitting program described in Section 1.2.2 of Chapter 1 in this Part, adapted to ACS-HRC. The calibration of the PSF fitting program for ACS-HRC data are presented in Annex B.

2.4 Results for the individual objects

We confirm the 2 binaries found previously in the WFPC2 study, and report 0 new binary in the range $0\farcs045$–$0\farcs26$, and $18<I_C<22.8$.

Considering the relatively high proper motion of the Pleiades cluster, and the small relative motion of their respective components (see Tables 2.3 and 2.4), we conclude that CFHT-PL-12AB and IPMBD-29AB have common proper motion.

2.4.1 Cl* Melotte 22 CFHT-Pl 12

Cl* Melotte 22 CFHT-Pl 12 is a binary with a separation of $0\farcs062\pm0\farcs002$ and a P.A of $266.7\pm1.7°$ (14th November 2000), corresponding to a physical separation of 8.4 A.U at 135 pc. Correcting

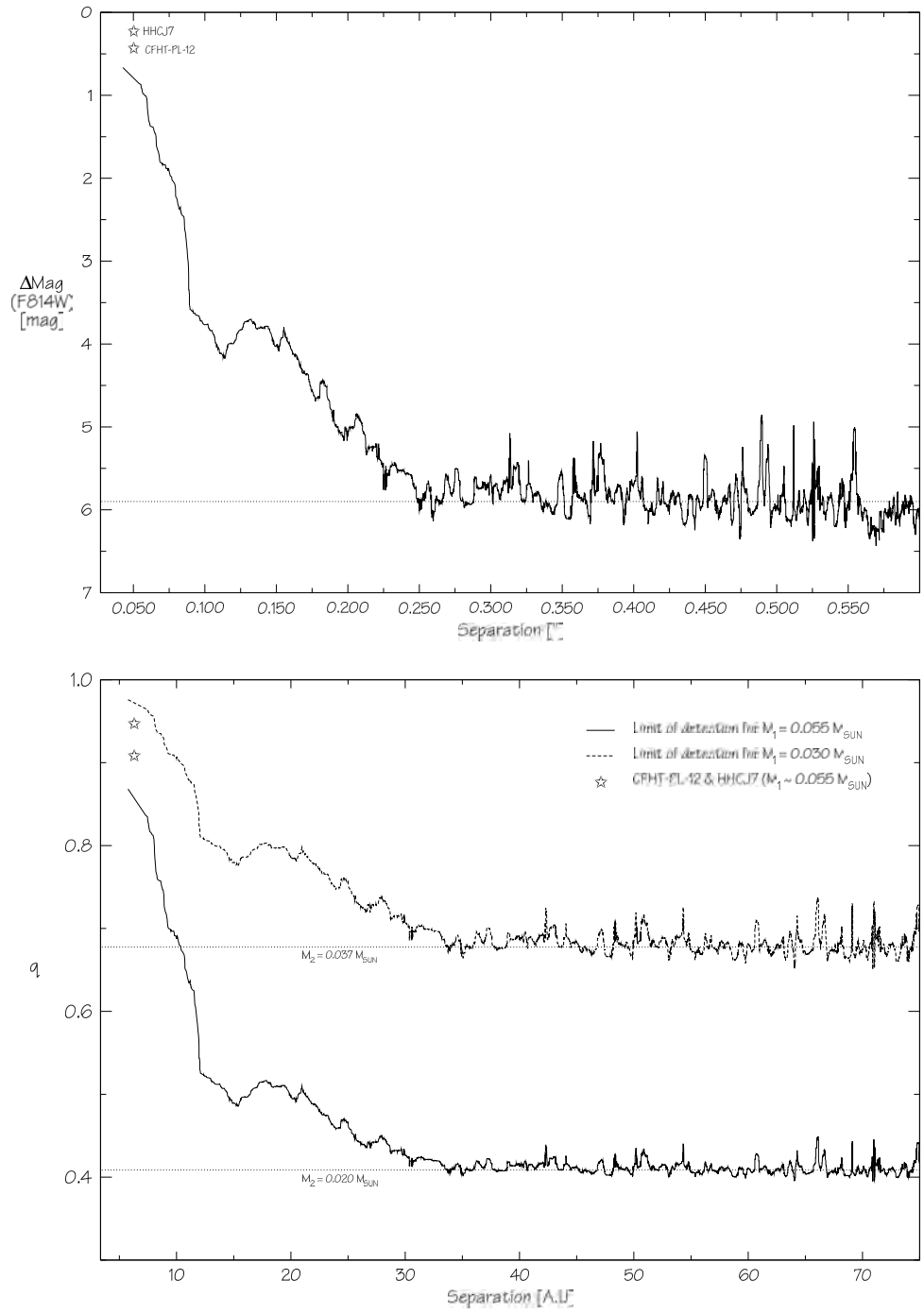

Figure 2.4 Limit of detection of our ACS/HRC observations.
Top panel: ΔMag vs angular separation. The curve represent the largest detectable difference of magnitude in the F814W band between the primary and the secondary, as a function of the projected separation. The curve was computed from the average of the 3-σ noise measurements in the images. At separation greater than $0''.250$, we were sensitive to companions 5.9 magnitudes fainter than the primary. The two stars indicate the two resolved binaries in this sample.
Bottom Panel: Same as top panel, but for the mass ratio vs the physical separation. The mass ratios have been computed for 2 different masses of the primary characteristic of our sample, using the top panel curve and DUSTY models for the mass-luminosity relation. The physical separations have been calculated assuming an average distance of 135 pc.

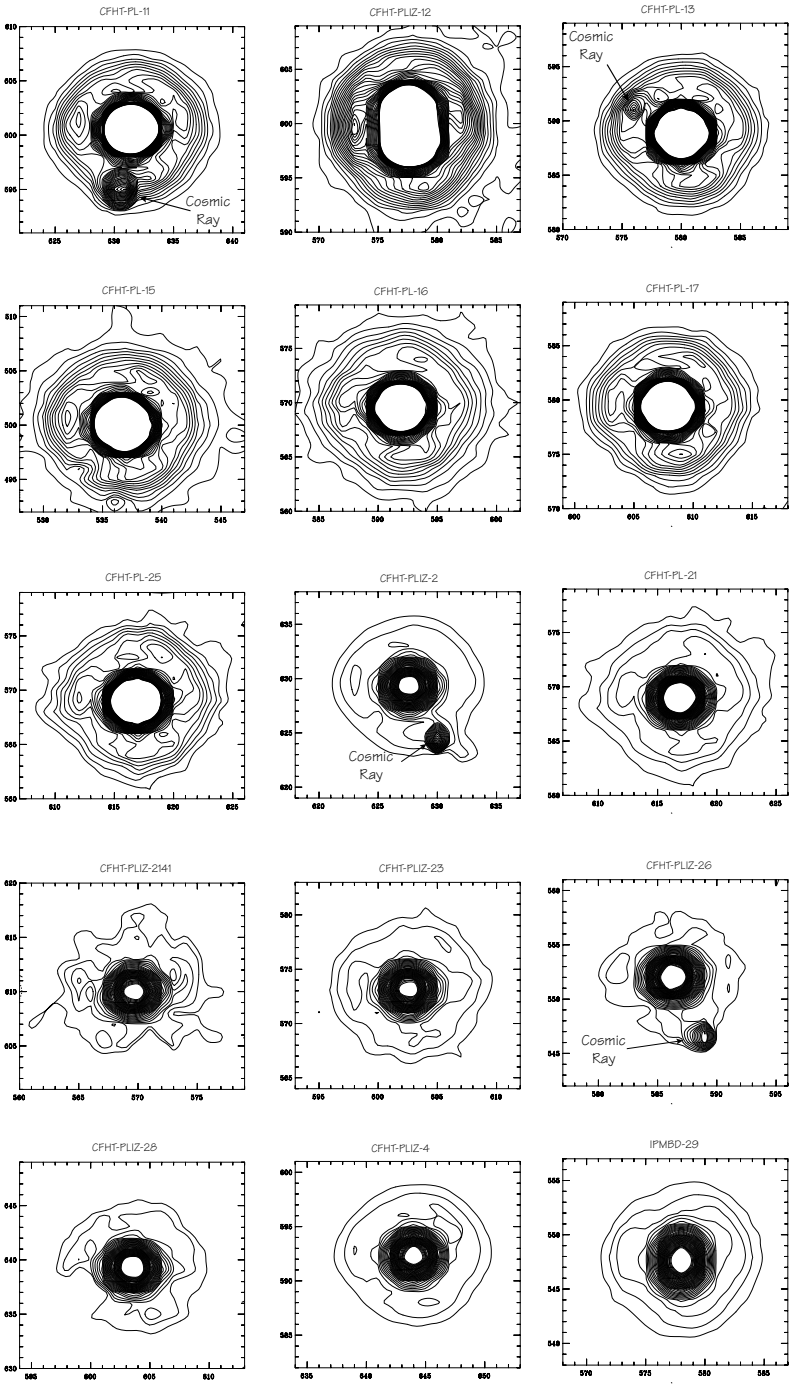

Figure 2.5 Contour plot of each of the targets of the ACS sample. Some cosmic rays are indicated.

Table 2.3. Relative Astrometry and photometry of Cl* Melotte 22 CFHT-PL 12

Date DD/MM/YYYY	Instrument	Sep. [mas]	P.A [°]	ΔMag	Filter
14/11/2000	WFPC2	62±3	266.7±4.5	0.98±0.15	F814W
07/11/2003	ACS	50±3	251.4±0.75	0.43±0.15	F814W

Note. — The difference of magnitude is different at the two epochs. They agree within 2-σ, but the WFPC2 value should be considered with more caution than the ACS value. The ACS image is indeed much better sampled (the pixel-scale of ACS is twice as good as that of WFPC2). We therefore consider that the ACS value is more accurate.

for a statistical factor of 1.26 as explained in Fischer & Marcy (1992), it leads to a semi-major axis of 10.5 A.U. Its proper motion and the presence of Li absorption in its spectrum indicate that it is substellar and belongs to the Pleiades cluster. Table 2.6 gives a summary of its astrometric and photometric properties. Using the NextGen models for the primary and the DUSTY models for the fainter (and therefore cooler) secondary and assuming an age of 120 Myr, we can estimate the masses of each component to be M_A=0.054 $M_\odot$ and M_B=0.038 $M_\odot$, corresponding to a mass ratio of $q = 0.7$. According to Kepler's laws (Kepler 1609), the corresponding period is ∼112 years. Considering a face-on circular orbit, the small relative motion of 5.1° in 3 years corresponds to an orbital period of ∼70 years. This is of the same order of magnitude as the more precise orbital period derived from the masses and the semi-major axis, and provides a sanity check.

2.4.2 Cl* Melotte 22 CFHT-Pl 19

Cl* Melotte 22 CFHT-Pl 19 is a binary with a separation of 0.″066±0.″003 and a position angle of 262.7±1.8°on the 21rst of September 2000. Proper motion measurements later than our study by Moraux et al. (2001) indicate that it is not a member of the Pleiades cluster. It is unlikely that the binarity has affected the proper motion measurement of Moraux et al. (2001). Furthermore, its position in the H-R diagram is not consistent with being a cluster binary (Martín et al. 2000a). We report here the properties of this object for completeness but we will not include it in the further statistical analysis.

2.4.3 Cl* Melotte 22 IPMBD 25

Cl* Melotte 22 IPMBD 25 was confirmed as a Pleiades member via proper motion measurements by Hambly et al. (1999), and the detection of Li later by Martín et al. (2003). It is a binary with

a separation of 0.″094±0.″003 and P.A of 340.5±2.1°(11th September 2000), corresponding to a physical separation of 16.0 A.U at 135 pc. Correcting for a statistical factor of 1.26 as explained in Fischer & Marcy (1992), it leads to a semi-major axis of 14.8 A.U. Its proper motion and the presence of Li absorption in its spectrum indicate that it is substellar and belongs to the Pleiades cluster. Table 2.6 gives a summary of its astrometric and photometric properties. Using the NextGen models for the primary and the DUSTY models for the fainter secondary and assuming an age of 120 Myr, we can estimate the masses of each component to be M_A=0.063 $M_\odot$ and M_B=0.039 $M_\odot$, corresponding to a mass ratio of $q = 0.62$. According to Kepler's laws (Kepler 1609), the corresponding period is ∼200 years.

2.4.4 Cl* Melotte 22 IPMBD 29

Cl* Melotte 22 IPMBD 29 was confirmed as a Pleiades member via proper motion measurements by Hambly et al. (1999). It was observed twice: the first time with WFPC2 (18th September 2000), and the second time with ACS (13th December 2003). Table 2.4 gives a summary of the astrometric and photometric properties measured at both epochs. Unfortunately a satellite crossed the field of our ACS image exactly on the target (see Figure 2.6). The flux of the satellite track is relatively low. Measuring the number of counts in an area of 11 pixels around the source and in another area centred on the satellite track away from the source, we can estimate that the flux of the satellite track corresponds to less than 5% of that of the source. The elongation and the duplicity are nevertheless real, since it appears clearly on the 3 individual exposures of the CR-SPLIT that have not been affected by the satellite track. It is moreover confirmed by the previous detection in the WFPC2 image 3 years earlier, with consistent relative astrometry of the two components. The difference of magnitude is different at the two epochs. They agree within 3-σ, but the WFPC2 value should be considered with more caution than the ACS value. The ACS image is indeed much better sampled (the pixel-scale of ACS is twice as good as that of WFPC2), and the separation is much below the sampling limit of WFPC2, while it is above that of ACS. We therefore consider that the ACS value is more reliable than the WFPC2 one. Cl* Melotte 22 IPMBD 29 is a binary with a separation of ∼0.″050 and P.A of ∼90°, corresponding to a physical separation of 6.75 A.U at 135 pc. Correcting for a statistical factor of 1.26 as explained in Fischer & Marcy (1992), it leads to a semi-major axis of 8.5 A.U. Its proper motion and the presence of Li absorption in its spectrum indicate that it is substellar and belongs to the Pleiades cluster. Using the NextGen models for the primary and the DUSTY models for the fainter secondary and assuming an age of 120 Myr, we can estimate the masses of each component to be M_A=0.045 $M_\odot$ and M_B=0.038 $M_\odot$, corresponding to a mass ratio of $q = 0.84$. According to Kepler's laws (Kepler 1609), the corresponding period is ∼86 years. Considering a face-on circular orbit, the small relative motion of 5°/yr corresponds to an orbital period of ∼75 years, thus consistent with the period derived from the Kepler's laws.

2.5 Confirmed photometric binary candidates

From its position in the H-R diagram, Moraux et al. (2003) suspected CFHT-Pl-12 to be a brown dwarf binary. Similarly, from their photometric analysis, Pinfield et al. (2003) suspected this object to be multiple. Using our WFPC2 and ACS images, we resolve CFHT-Pl-12, with a mass ratio consistent with the one they derive from the photometry.

Table 2.4. Relative Astrometry and photometry of Cl* Melotte 22 IPMBD 29

Date DD/MM/YYYY	Instrument	Sep. [mas]	P.A [°]	ΔMag	Filter
18/07/2000	WFPC2	58±3	103±4.5	1.25±0.15[a]	F814W
13/12/2003	ACS	50±3	85.6±0.75	0.22±0.30[a]	F814W

[a]The difference of magnitude is different at the two epochs. They agree within 3-σ, but the WFPC2 value should be considered with more caution than the ACS value. We consider the ACS image more reliable than the WFPC2 one.

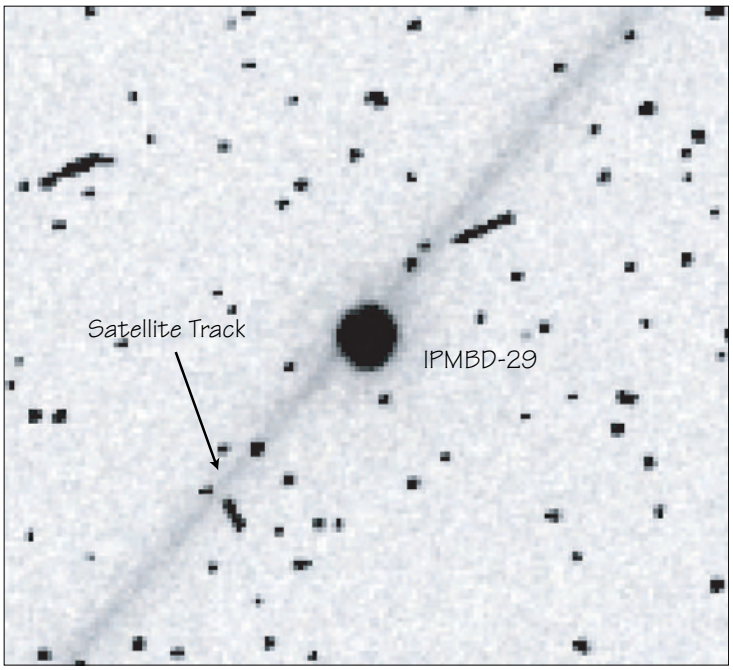

Figure 2.6 Satellite track on the ACS image of Cl* Melotte 22 IPMBD 29. Very unfortunately the way of a satellite crossed the field exactly on the position of the target. The corresponding flux is nevertheless relatively small, but might explain the difference between the ΔMag reported in Table 2.4

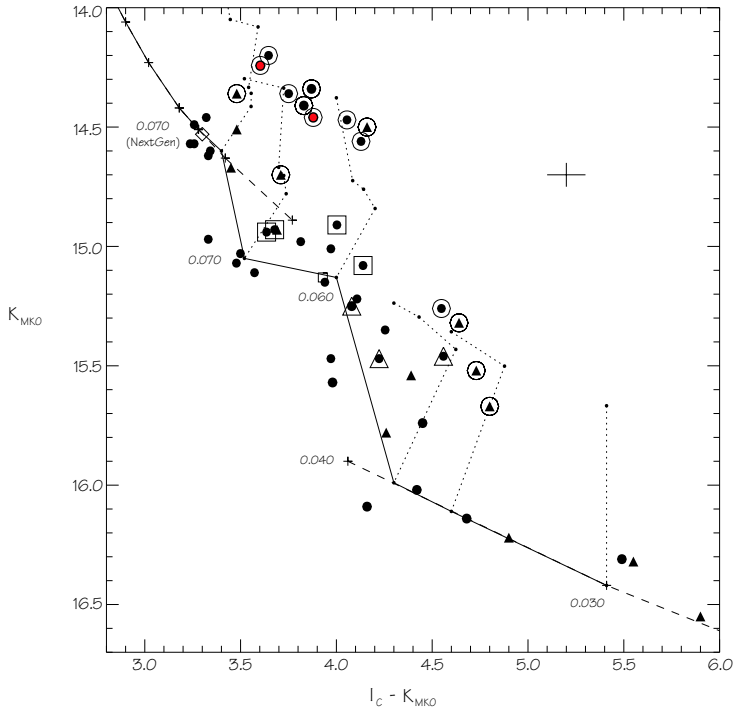

Figure 2.7 K vs $I_C - K$ from Pinfield et al. (2003) plus the two resolved binaries IPMBD-25 and IPMBD-29 (represented by circled filled red circles; values from Hambly et al. 1999). The symbols mean the same as in Pinfield et al. (2003) paper: circled objects are IK binary candidates, objects overplotted with an additional open square or triangle are respectively JK or JHK binary candidate. Dashed lines are the NextGen and DUSTY models. Solid and dotted lines are the cluster single and binary star sequences, respectively. Corresponding masses from the DUSTY models are indicated. The 0.070 $M_{\odot}$ point around K=14.5 is the NextGen model prediction for a 125 Myr isochrone.The two resolved binaries fall on the binary sequence.

It is interesting to note that the two resolved binaries IPMBD-25 and IPMBD-29, which have I_C and K photometric measurements available, fall just on the binary sequence of the K vs. $(I_C - K)$ CMD defined by Pinfield et al. (2003), as shown in Figure 2.7, although they were not included in their study. From this diagram we can predict a mass ratio of 0.6–0.9 for IPMBD-25, very similar to that of CFHT-Pl-12 since the two objects are very close in the diagram, and consistent with the mass ratio we derive from the relative photometry of the two components. Similarly, the CMD predict a mass ratio of 0.7–1.0 for IPMBD-29, in good agreement with the one we derive from the relative photometry of the two components.

2.6 Unresolved photometric binary candidates

From their positions in the H-R diagram, Moraux et al. (2003) suspected CFHT-Pl-16 to be a brown dwarf binary. It is not resolved in our ACS images. From their photometric study, Pinfield et al. (2003) also classify this object as binary, and derive a mass ratio of about 0.75–1. According to the DUSTY models, this mass ratio corresponds to a difference of magnitude between 0.0$\leq \Delta$mag$\leq$6 mag in the I band, thus just at/above the limit of sensitivity of our study.

Table 2.5. Properties of the unresolved photometric binary candidates

object	$q_{phot.}$	I_C [mag]	Δmag [mag]	Limit on Sep. [A.U]
CFHT-Pl-16	0.75–1.0	18.7	0.0–6.0	<5.4–34
CFHT-Pl-21	0.5–0.7	19.0	3.5–8.8	<13.0–34
CFHT-Pl-23	∼1	19.3	∼0.0	<5.4
CFHT-Pl-25	<0.75–1.0	19.7	>0.0–3.5	<5.4–13.0

[a] $q_{phot.}$ is the mass ratio reported by Pinfield et al. (2003) from their photometric study. I_C from Moraux et al. (2003). Δmag is obtained using I_C, $q_{phot.}$, and the DUSTY evolutionary models. The limit on the separation is then derived using Figure 2.4

This indicates that, if multiple, this system should have a separation less than 5.4–34 A.U (the sensitivity depending on the separation, see Figure 2.4 and Table 2.5).

Due to its peculiar proper motion, Moraux et al. (2001) suggested that CFHT-Pl-15 might be a multiple system. Martín et al. (2000a) found evidence for high residuals after PSF subtraction on their NICMOS image, and suspected the presence of a companion at a separation less than 0.″22. Using ACS, we do not resolve any companion at separation larger than 0.″040. If multiple, this object should have a separation smaller than 5.4 A.U, and/or a difference in magnitude larger than 5.9 mag in the F814W band.

From their photometric analysis, Pinfield et al. (2003) suspected CFHT-Pl-25, CFHT-Pl-23 and CFHT-Pl-21 to be binaries. Using our ACS images, we do not find any evidence of companions around these three objects. Pinfield et al. (2003) also predict mass ratios of q ∼1 for CFHT-Pl-23, q <0.75∼1 for CFHT-Pl-25, and 0.5< q <0.7 for CFHT-Pl-21, corresponding to differences of magnitude of respectively 0 mag, >0–3 mag, and 3.3–8.8 mag. Together with our ACS study, this constrains the separations of CFHT-Pl-23 to be smaller than 5.4 A.U and that of CFHT-Pl-25 to be smaller than ∼5.4–13 A.U, while that of CFHT-Pl-21 should be less than 13–34 A.U (see Figure 2.4). Spectroscopic studies would be currently the only way to confirm these results. Table 2.5 summarizes this analysis.

Table 2.6. Results for Pleiades Binary Systems (WFPC2 sample)

Name	Mag. F814W		Mag. F875LP		Sep.	Sep.	P.A.	M_p	q	P[a]
	A	B	A	B	[″]	[A.U]	[°]	[$M_\odot$]		[yr]
CFHT-Pl 12	18.34±0.11	19.32±0.11	17.57±0.11	18.48±0.11	0.062±0.002	8.4	266.7±1.7	0.054	0.70	112
CFHT-Pl 19	19.40±0.11	20.38±0.11	18.79±0.11	19.57±0.11	0.066±0.003	...	262.7±1.8	...	...	...
IPMBD 25	17.93±0.09	19.38±0.09	17.22±0.09	18.74±0.09	0.094±0.003	16.0	340.5±2.1	0.063	0.62	200
IPMBD 29	18.70±0.15	19.95±0.15	17.81±0.11	19.06±0.11	0.058±0.004	6.75	103.0±4.5	0.045	0.84	86

[a]Orbital periods are estimated for circular orbits using Kepler's third law and are given in years. No masses and periods are estimated for CFHT-Pl-19 because it is thought to be a nonmember.

2.7 Analysis: binary frequency

The WFPC2 study found 2 binaries among 15 objects, leading to a *visual* binary frequency[5] of $f_{v.b}$=13^{+14}_{-4}%. No binary was found in the ACS sample of 13 new objects, leading to an upper limit on the *visual* binary fraction of $f_{v.b} \leq$1/13=7.7%. The two results thus agree within slightly more than 1-σ uncertainty. Considering the combination of the two studies, we found 2 binaries over a sample of 27 objects, leading to a binary fraction of $f_{v.b}$=$7.4^{+8.6}_{-2.4}$% for separations greater than 8.1 A.U and mass ratios between 0.45–0.9< q <1.

In order to estimate the overall[6] binary frequency, one has to estimate the number of spectroscopic binaries we missed. If we assume that the ratio of spectroscopic binaries is similar to that observed for M-dwarfs in the field and G–K dwarfs in the Pleiades, where ∼30% of the multiple systems have separations less than our limit of resolution of 5.4 A.U (see Marchal et al. 2003; Bouvier et al. 1997, for respectively the field M-dwarf and Pleiades G–K dwarfs binary statistics), then we would have missed 0.8 spectroscopic binaries in our sample of 27 objects, and the frequency of *spectroscopic* binaries would be $f_{s.b}$ ∼3%. In that case, the overall binary frequency is therefore $f_b \simeq$10%. This value is in fact an upper limit on the real binary frequency, since we were not sensitive to companions with difference in magnitude larger than ΔMag(F814W)=5.9 mag, corresponding to mass ratio of $q \leq$0.4 (see Figure 2.4).

2.8 Discussion

2.8.1 Binary properties and the environment

The observed upper limit on the binary frequency among the Pleiades brown dwarfs (≥10%) is similar to the values reported in the field: 1) for slightly more massive objects (see Chapter 1 of this Part, 10∼15% of late-M and L-dwarfs); 2) for field brown dwarfs, as reported by Burgasser et al. (2003, 9^{+15}_{-4}% for T5 to T8 field brown dwarfs).

This indicates that the statistical properties, and therefore the formation and evolution processes, of field and Pleiades binary brown dwarfs are probably similar. This would imply that the evolution processes of binaries do not depend much on the environment and the age after 125 Myrs. The formation, the evolution and disruption of binaries responsible for the low

[5]Because of the small-number statistic, the uncertainties are not Poisson uncertainties, but statistical uncertainties derived constructing a probability distribution given the total sample size and the number of binaries. Refer to Burgasser et al. (2003) for a detailed discussion on that matter.

[6]"overall" means here over the whole range of separation

rate of binaries and the cut-off in the separation range would thus have to occur during the early stages of the cluster, when its density and the probability of gravitational encounters are higher. N-body simulations performed by Kroupa (1995a,b) have shown that in dense stellar clusters, such as the Pleiades during its early stages, the binary fraction could drop from 100% to ∼50% in less than 1 Myr, which is consistent with the preliminary conclusion we draw here.

In their numerical simulations of the dynamical interactions in stellar clusters, Sterzik & Durisen (2003) show that the different properties cited above (binary fraction and distribution of separation) can be nicely reproduced when considering a model cluster where stars and brown dwarfs form from progenitor clumps. Choosing specific clump and stellar mass spectra, they were able to generate a cluster with an IMF consistent with that observed. Using Monte-Carlo simulations they could then study the stellar cluster decay dynamics and compute the properties of brown dwarfs and brown dwarf binaries. Their study shows that a simple gravitational point-mass dynamics, with weighting factors for the pairing probabilities as a function of the mass evaluated in the first of a two step process, gives results consistent with the observations over the entire range of mass. In particular, they obtain a binary fraction for brown dwarfs of 8–18%, consistent we the ≥10% upper limit we report here. They also model a distribution of separation in remarkable agreement with that reported for the field brown dwarfs and for the three Pleiades binaries of our study, with a peak around 4 A.U and most (∼85%) objects with separations less than 20 A.U. On the other hand, they produce a flat distribution of mass ratio in the range $0.2< q <1.0$, which is apparently not observed in the field and in the Pleiades. In Chapter 1 of this Part, we showed that our observations in the field, although statistically inconclusive, suggest that there is a preference for equal mass systems. Halbwachs et al. (2003) showed also that the mass ratio distribution of spectroscopic binaries among field and Pleiades F–G dwarfs is not flat but bimodal and decreasing toward small mass ratios.

2.8.2 Photometric binary frequency

Our work allows to measure the binary frequency among brown dwarfs in the Pleiades Open Cluster for separations greater than 8.1 A.U and mass ratios in the range $0.45–0.9< q <1$, with $f_b \simeq 10\%$. We will compare this result to that obtained by Pinfield et al. (2003) via the study of binary sequences in colour-magnitude diagrams.

The results of Pinfield et al. (2003) do not agree with the observations we report here. From their study of IK, JK and JHK colour-magnitude diagrams, they measure a binary frequency of $50^{+11}_{-10}\%$ for brown dwarfs in the Pleiades in the mass ratio range $0.5< q <1.0$, thus comparable to the range covered by our study. This result is much higher than any of the two values reported in our WFPC2 and ACS studies. If correct, these results together would mean that most (∼85%) of the Pleiades brown dwarf binaries in the range $0.5< q <1.0$ have separations less than 5.4–8.1 A.U. Although we cannot rule out this possibility, it would contrast with the results obtained for late type G–K dwarfs in the Pleiades and for early-M dwarfs in the field. Bouvier et al. (1997) found indeed that only ∼30% of the G–K Pleiades binaries have separations smaller than 5 A.U. Similarly, Marchal et al. (2003) found that only ∼30% of the early-M field binaries have separations smaller than 5 A.U. These two values are much smaller than the above mentioned 85%. Assuming that the properties of brown dwarf binaries are similar to that of field or Pleiades late type stars is of course a strong assumption, although we showed in Section 2.8.1 that the current results tend to confirm it.

The discrepancy cannot be due to the companions we missed because of their too small mass ratios, since the study of Pinfield et al. (2003) is sensitive to a similar range of mass ratio than our study. Moreover Halbwachs et al. (2003) found that ∼60% of the F–G Pleiades spectroscopic

Table 2.7. Visual Binary Frequency measured in successive studies.

Ref.	$N_{Objects}$	$N_{Binaries}$	Sep. Range [A.U]	Mass range[a] [$M_\odot$]	Sensitivity (q_{min})[c]	Binary Freq.[b]
Martín et al. (2000a)	34	0	>24	>0.090	0.6	<3%
Martín et al. (2003)[d]	15	2	>8.1	0.035–0.065	0.45–0.9	13^{+14}_{-4}%
ACS study	13	0	>5.4	0.027–0.055	0.45–0.9	<7.7%
ACS+WFPC2 study	28	2	>8.1	0.035–0.065	0.45–0.9	$7.1^{+7.8}_{-2.1}$%

[a] for the primary

[b] Binary frequency defined as $N_{binaries}/N_{Objects}$

[c] Sensitivity to lower mass companions, expressed as the minimum mass ratio $q = M_2/M_1$ to which the observations were sensitive.

[d] The results of Martín et al. (2003) correspond to the WFPC2 study

binaries have a mass ratio larger than 0.5, and Marchal et al. (2003) that ∼75% of the field early M-dwarfs have a mass ratio larger than 0.5. If once again we make the assumption that field and Pleiades late type binaries have similar properties to Pleiades brown dwarfs binaries, we should have missed between 25–40% of the multiple systems "only", leading to a corrected binary fraction of 13–16%, still far from the 50% reported by Pinfield et al. (2003)

We suspect the discrepancy between the observations we report and the photometric binary frequency of Pinfield et al. (2003) to be due to a combination of the following reasons:

- underestimations of the photometric uncertainties, and of possible intrinsic photometric variability due, for example, to weather effects or magnetically driven surface features. Weather effects are known to be producing variability in the luminosity, up to 0.05 mag in I as observed by Bailer-Jones & Mundt (2001), and magnetically driven surface features modulation of up to 0.1 mag in J (for young Cha-1 brown dwarfs, Joergens et al. 2003a).

- spread in the age of the objects

- contamination by field objects. Only 14 over 39 brown dwarfs of their sample have been confirmed as cluster members by proper motion and/or Li detection, while all the objects of our sample have been confirmed by one or both tests. The remaining 25 objects (64% of the sample) have been classified as brown dwarfs on the only basis of their photometric properties. From their photometric (I vs I-Z) and proper motion surveys, Moraux et al. (2003, 2001) estimated that the contamination by foreground M-dwarfs in their sample of Pleiades brown dwarfs can be as high as 30%. Although they use three colour criteria to determine the membership of the objects in their sample instead of one, a non-negligible level of contamination could be expected and explain some of the red objects identified as binaries. Since the contaminating objects would be foreground (i.e closer) M-dwarfs, most of them would indeed appear close to the binary sequence.

- effect of rotation: brown dwarfs are known to be fast rotators (Bailer-Jones 2004), and a correlation between the rotation and the luminosity, by up to 0.1 mag, could affect the

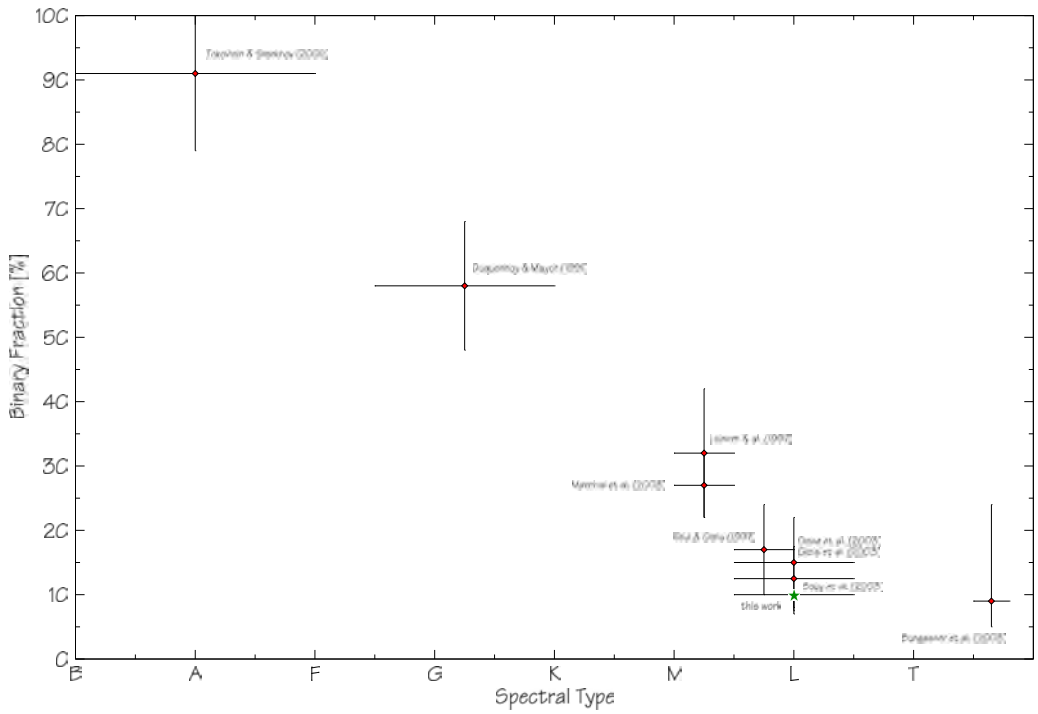

Figure 2.8 Binary frequency as function of the spectral type in the field and in the Pleiades. Values from Duquennoy & Mayor (1991); Reid & Gizis (1997b); Leinert et al. (1997); Shatsky & Tokovinin (2002); Close et al. (2003); Bouy et al. (2003); Gizis et al. (2003); Marchal et al. (2003). The value reported in the present work is indicated with a green star. The values for spectral types later than M5 are upper limits and do not cover the same ranges of mass ratio and separation than the studies for earlier spectral types.

colours of some objects, as measured by van Leeuwen & Alphenaar (1982). Deformation of the objects due to their fast rotation can produce variable light curves. A rapidly rotating brown dwarf seen pole-on may be reddened enough to perhaps be identified as a binary by the photometric technique.

It is also interesting to note that the limit on the binary frequency we report here for brown dwarfs in the Pleiades is consistent with that observed for similar objects in the field, as shown in Figure 2.8. It is comparable to that of slightly more massive field late-M/early-L dwarfs (see Chapter 1), and close to the frequency observed for field T-dwarfs, which have masses comparable to the brown dwarfs of our Pleiades sample.

A spectroscopic survey, if possible[7], should allow us to answer these important open questions, and to know whether we underestimated the spectroscopic binary frequency.

2.8.3 Separations and mass ratios

The three binaries observed in the WFPC2 study all have separations less than 12 A.U. The mass ratios are all larger than 0.62. PPL 15, the spectroscopic binary brown dwarfs discovered by Basri & Martín (1999), has a semi-major axis of 0.03 A.U and a mass ratio of 0.87. Although

[7] the high rotational velocity of brown dwarfs might blend the Doppler shift due to the binarity

this sample is too small for allowing any meaningful statistical study, these results are consistent with that obtained in the field for slightly more massive objects, as described in Chapter 1 of this Part, for which we found a cut-off in the separation range at 20∼30 A.U, and a possible lack of small mass ratios ($q \leq 0.5$).

In his statistical analysis of the photometric binary properties in the Pleiades, Kähler (1999) shows that the distribution of mass ratios for late type stars should be similar to that in the field. The distribution is expected to be bimodal, with a major peak at q=0.4 and a minor one at ∼1. In a more recent observational study of unbiased samples of spectroscopic binaries of F to K dwarfs in the field and in the Pleiades cluster, Halbwachs et al. (2003) refine the results of Kähler (1999) in the range of periods shorter than 10 yrs. They report a mass ratio distribution with a primary peak at q=1, decreasing towards smaller mass ratios, with a broad secondary peak around q=0.4. They observe no difference between the distributions of mass ratio of F–G and K stars, and find that these are identical in the field and in the Pleiades.

If confirmed, the lack of multiple systems with small mass ratios would then imply a major difference between the distributions of mass ratios (and therefore the formation and evolution processes) of late type stars and brown dwarfs. The current studies are inconclusive regarding that question since the observed lack might well be due to a combination of the following reasons:

- the bias toward bright magnitudes in favor of binaries with large mass ratios (Öpik 1924)
- the current limit of sensitivity: $q > 0.4$ for separation larger than 30 A.U, and only $q > 0.7$ for separations larger than 10 A.U (see Figure 2.4)

Deep spectroscopic surveys on unbiased samples should allow to answer these questions, and see how many binaries of small mass ratios and small separations we missed.

Chapter 3

A binary brown dwarf in the R-CrA star forming region

3.1 Introduction

Although we did not have the opportunity to perform a search for multiple systems and a statistical analysis in a star forming region, we were able to resolved a peculiar binary brown dwarf with a disk[8]. The object had been detected by the ISO infrared satellite, and shows a near-infrared excess, indicating the presence of a disk.

3.2 Observations

3.2.1 DENIS-P J185950.9-370632

The DENIS observations are carried out on the ESO 1 m telescope at La Silla. Dichroic beam splitters separate three channels, and a focal reducing optics provide scales of $3\farcs0$ per pixel on the 256×256 NICMOS3 arrays used for the two infrared channels, and $1\farcs0$ per pixel on the 1024×1024 Tektronix CCD detector of the I channel. The image data were processed with the standard DENIS software pipeline (Borsenberger 1997) at the Paris Data Analysis Center (PDAC). Source extraction and photometry are performed at PDAC, using a space-varying kernel algorithm (Alard 2000). When searching very rare objects in a large data base, the first challenge is artefact rejection. We use a set of morphological parameters, based on the correlation between PSF model and the object profile and on the consistency between several aperture magnitudes (Delfosse et al. in prep.).

DENIS-P J185950.9-370632, was selected as a candidate very low mass star or and brown dwarf due to its red colors ($I - J = 3.0 \pm 0.1$ mag). It is located in the R-CrA complex between the TY-CrA and ϵ-CrA stars (see Figure 3.2), and very close to the core of the very dense molecular cloud ($A_V \sim 45$ mag; Wilking et al. 1992). Locally the absorption is low, however (see Section 3.3.1). Figure 3.1 shows finding charts in I and J.

The apparent magnitude of DENIS-P J185950.9-370632 is consistent with a ∼5 Myr late-M dwarf at the distance of the CrA complex (see section 3.3.2), which makes it an excellent brown dwarf candidate.

[8] Although one object is clearly not enough to perform a statistical analysis, we present this object in this Part as a complementary study of field and Pleiades objects

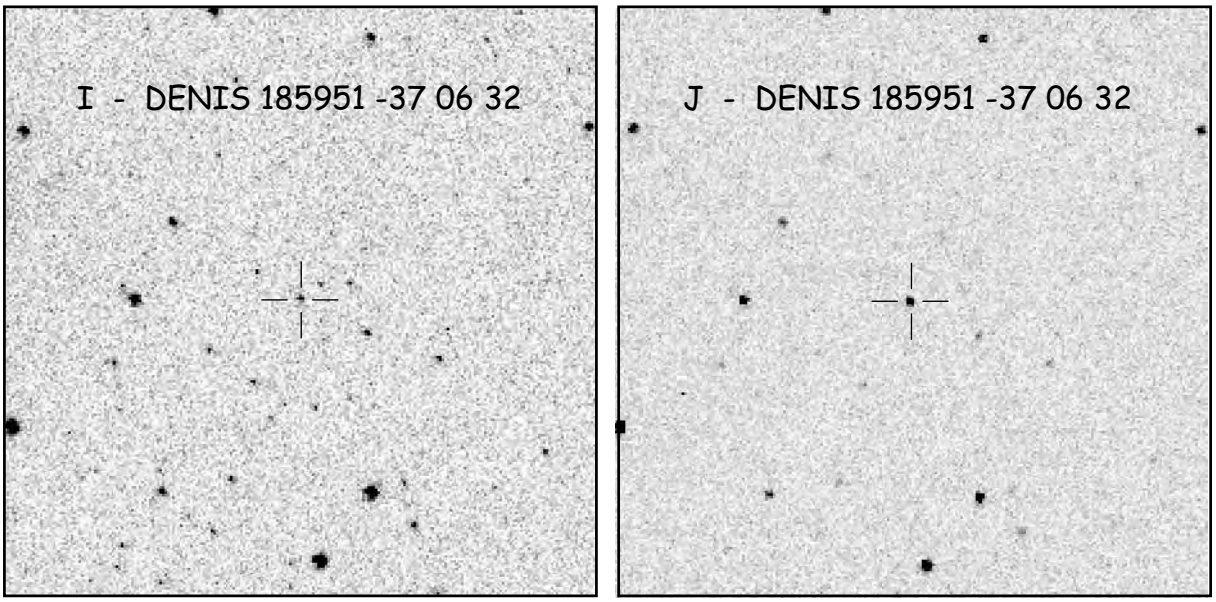

Figure 3.1 Finding charts of DENIS-P J185950.9-370632 in the I and J filters (DENIS images). The field of view is $3.5' \times 3.5'$, North is up and East is left.

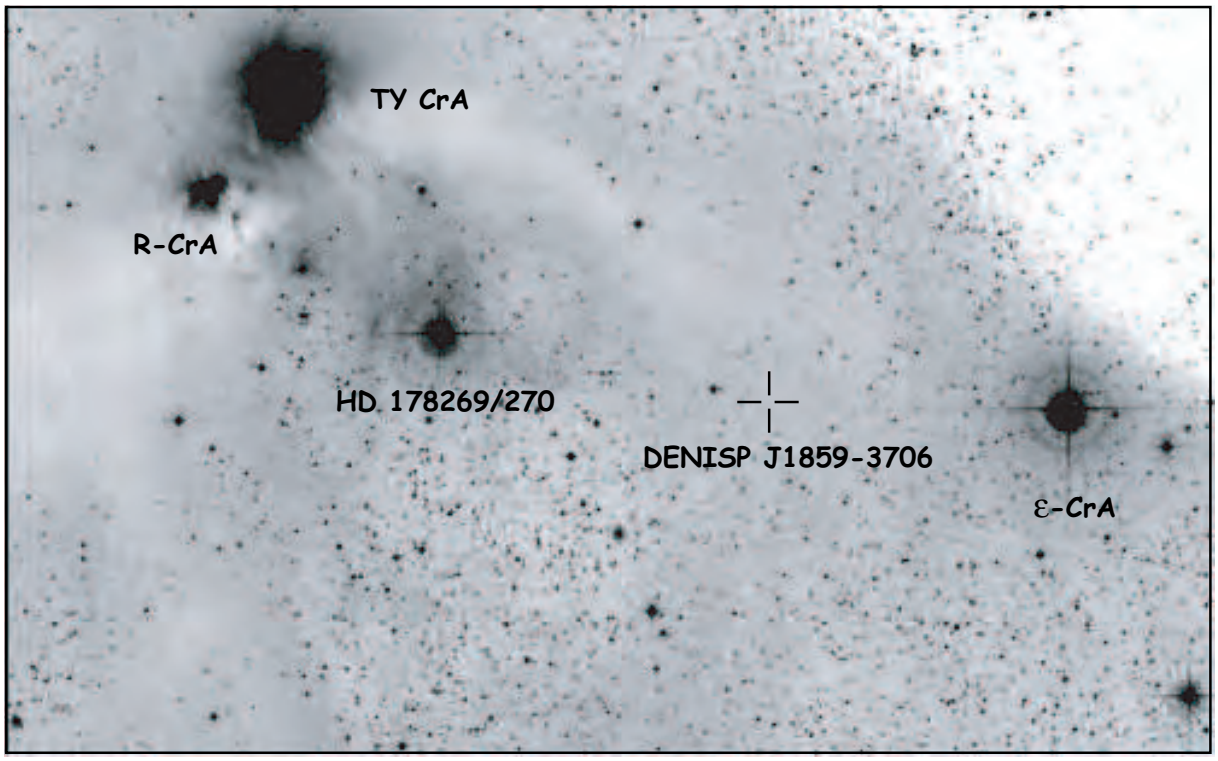

Figure 3.2 The environment of DENIS-P J185950.9-370632 in the CrA molecular cloud complex. The cross marks the position of the DENIS objects on this DSS1/STSci J plate. The field of view is $50' \times 35'$. North is up and East is left.

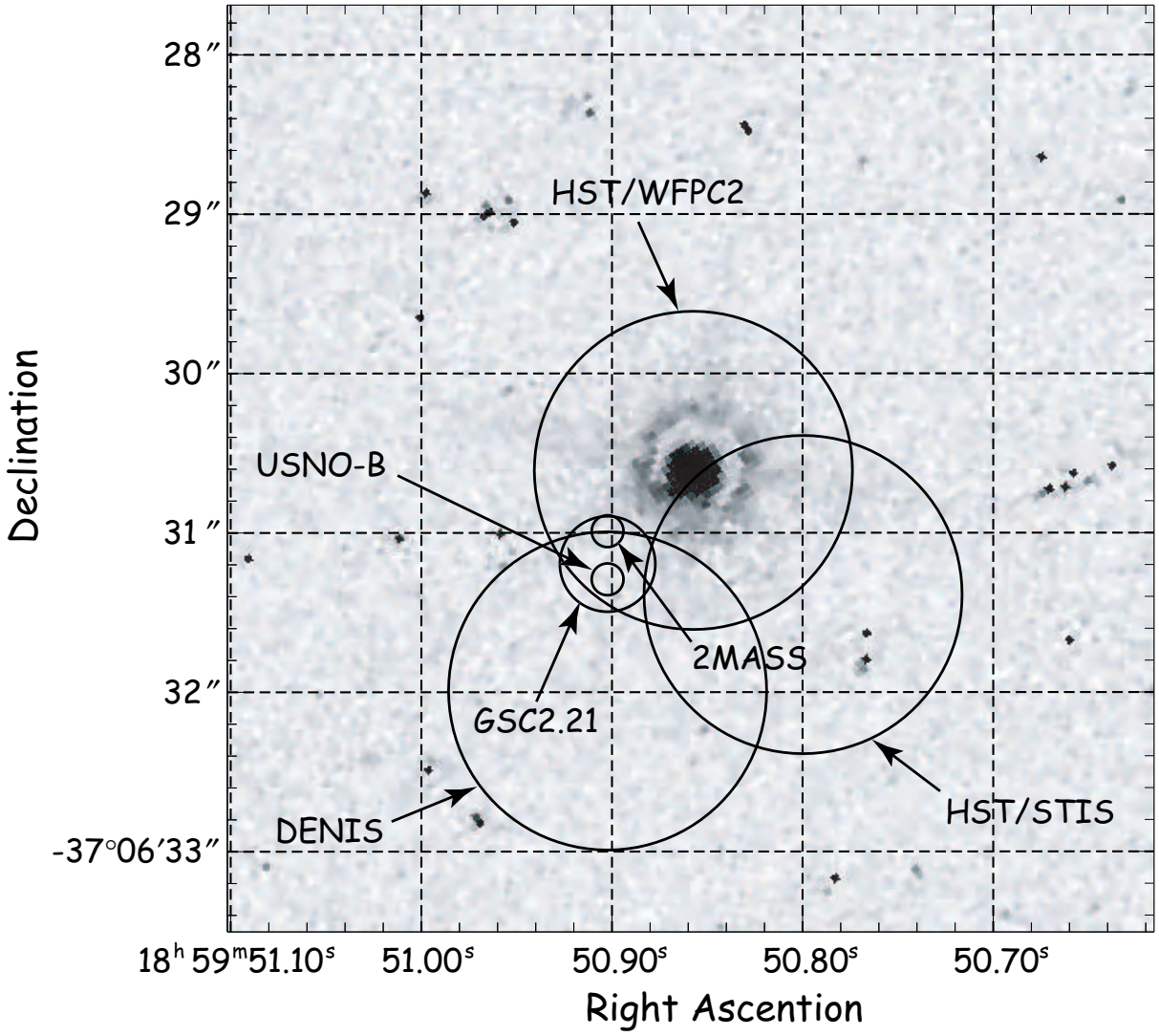

Figure 3.3 HST-WFPC2/PC image obtained in the F675W and F814W filters (composite image) on 2000 September 12th. The over-plotted circles represent the position of DENIS-P J185950.9-370632 at different epochs and with different instruments. The radius of each circle corresponds to the uncertainty of that measurement. Although the different measurements are not fully consistent, no other source than DENIS-P J185950.9-370632 can be associated in the image.

Table 3.1. Astrometry and photometry of DENIS-P J185950.9-370632.

Epoch	R.A	Dec.	Uncert.	Fiilter	Mag.	Source
01/01/1985	18 59 50.9	-37 06 31.0	±0.″1	R1	18.9	USNO-B1.0
				B2	21.7	
				R2	19.9	
				I	17.3	
06/07/1989	18 59 50.9	-37 06 31.2	±0.″3	F	20.2	GSC2.21
20/04/1996	18:59:50.7	-37:06:28.0	±6.″0	LW2	11.6	ISO
				LW3	>10.7	
28/04/1999	18:59:50.9	-37:06:32.0	±1.″0	I	17.01	DENIS
				J	13.99	
				K	12.60	
25/06/1999	18:59:50.9	-37:06:31.3	±0.″1	J	13.98	2MASS
				H	13.10	
				K	12.56	
12/09/2000	18:59:50.9	-37:06:30.6	±1.″0	F675W	19.33	HST/WFPC2
				F814W	16.88	
24/09/2002	18:59:50.8	-37:06:27.6	±1.″0	F625W		HST/ACS
				F775W		
				F850LP		
26/06/2003	18:59:50.8	-37:06:31.4	±1.″0	Long pass	19.6	HST/STIS

In addition to the DENIS survey, DENIS-P J185950.9-370632 has been detected in several sky surveys, such as the USNO-B1.0 catalogue (Monet et al. 2003, , where it is reported as USNO-B1.0 0528-0926219), the GSC2.21 catalog (reported as GSC2 S33202002902), and the 2MASS survey, where it is reported as 2MASSW J18595094-3706313. Table 3.1 and Figure 3.3 summarize these astrometric and photometric measurements.

3.2.2 Observation Summary

Table 3.2 gives an overview of all the observations we have been conducting or retrieved from the archives. We obtained high angular resolution imaging using the *Hubble Space Telescope* (HST). Spectroscopy was obtained at both high (Keck-HIRES) and low (VLT-FORS2 and HST-STIS) spectral resolution. Finally, we retrieved ISO archival data in which DENIS-P J185950.9-370632 was detected.

Table 3.2 Observation log.

Imaging				
Instrument	Filter	Exp. Time [s]	Date Obs.	Pixel Scale ["]
WFPC2-PC	F675W	600	19/09/2000	0.″045
WFPC2-PC	F814W	300	19/09/2000	0.″045
ACS-HRC	F625W	1 000	24/09/2002	0.″027
ACS-HRC	F775W	460	24/09/2002	0.″027
ACS-HRC	F850LP	340	24/09/2002	0.″027
ISO-CAM1	LW2	4 328	20/04/1996	6.″0
ISO-CAM1	LW3	4 326	20/04/1996	6.″0
Spectroscopy				
Instrument	Wavelength Range [μm]	Exp. Time [s]	Date Obs.	Dispersion [Å/pixel]
VLT-FORS2	0.590-0.715	600	06/05/2002	0.60
VLT-FORS2	0.690-0.910	200	06/05/2002	1.06
HST-STIS	0.525-1.300	4140	16/06/2003	4.92
Keck-HIRES	0.667-0.895	1200	30/05/2000	1.1

Imaging

We observed DENIS-P J185950.9-370632 twice at high angular resolution using the HST, first with the Planetary Camera (PC) of WFPC2 (Baggett et al. 2002) and second with the High Resolution Channel (HRC) of ACS (Mack et al. 2002). The WFPC2 data were taken in SNAPSHOT mode (program GO8720, P.I Brandner). We took single exposure for each filter (F675W and F814W), to minimise overheads and increase exposure times. This prevent automatic removal of cosmic ray hits, but we were fortunate enough that no cosmic ray fell close enough to the target that it would affect the analysis. The ACS data (program GO9451, P.I Brandner) were obtained on 2002 September 24th in CR-SPLIT mode and with a four points dithering pattern in each of the F625W, F775W, and F850LP filters. This allows correction for cosmic ray events and bad pixels. The WFPC2 and ACS data together provide accurate photometry in five different optical filters and positions at two epochs. The target-acquisition frame for the STIS spectroscopy gives a third-epoch position.

DENIS-P J185950.9-370632 is obviously elongated on the WFPC2, ACS and STIS images (Figure 3.4). PSF subtraction brings up the companion more clearly on the WFPC2 and ACS images (Figure 3.5).

We retrieved ISO archival data of the R-CrA region obtained on 1996 April 20th (TDT 15500328, CAM01, Olofsson et al. 1999) with ISOCAM1 which include DENIS-P J185950.9-370632. Olofsson et al. (1999) report a 2.1 mJy ± 0.4 mJy detection in the LW2 filter (5.0-8.5μm), at a position that is 4.″0 away from our coordinates for DENIS-P J185950.9-370632. This is well within the pointing uncertainties of ISO (∼6.″0, Blommaert et al. 2001), and we identify the infrared source, ISO-CrA 63, with DENIS-P J185950.9-370632. The source is not detected in the LW3 filter (12-18μm), and we measured a 3 σ upper limit of 1.1 mJy. No other optical/near-IR source is present in the ∼6″ ISO error box.

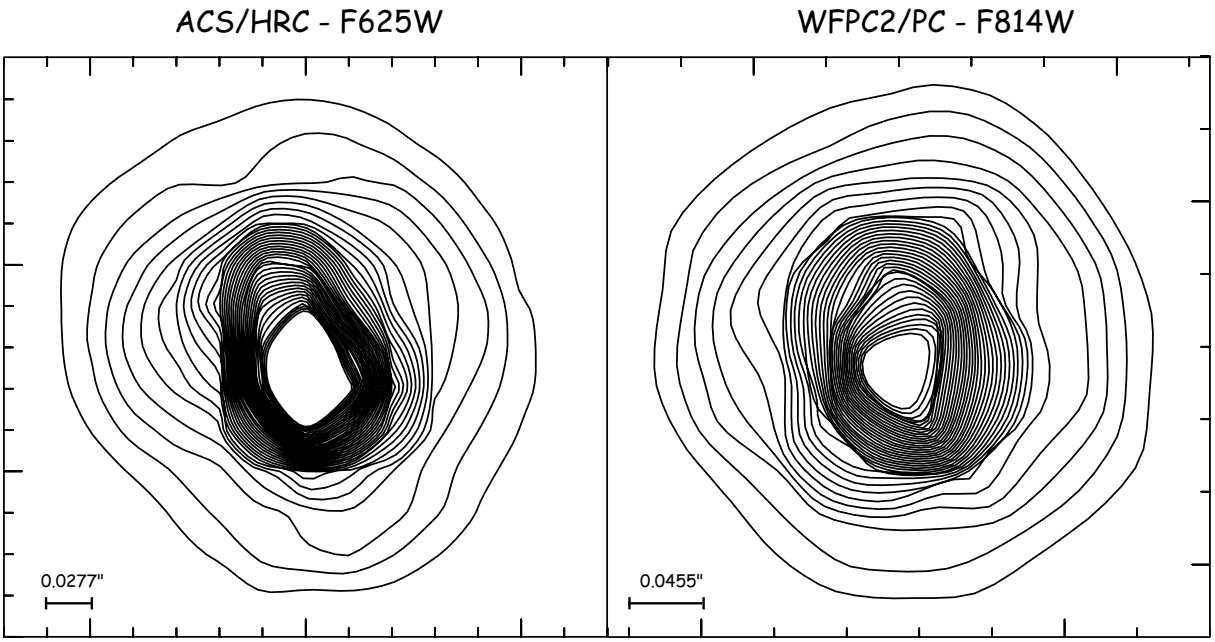

Figure 3.4 Contour plots of the ACS/HRC (F625W) and WFPC2/PC (F814W) images. The WFPC2/PC and ACS/HRC image have identical scales for easier comparison. The object is clearly elongated on both images, but is better resolved on the higher resolution and better sampled ACS image.

High Resolution Spectroscopy

DENIS-P J185950.9-370632 was observed on 30 May 2000 with the High Resolution Echelle Spectrometer (HIRES; Vogt et al. 1994) on the Keck I telescope. A slit width of $1\farcs15$ and two-pixel binning in the spectral direction gave a resolving power of R=33 000. The exposure time was 1 200 s and the airmass 1.83. Fifteen echelle orders were recorded on the detector, covering the wavelength range from 667.1 nm to 895.0 nm, with gaps between the orders. The data were reduced following a standard procedure in the IRAF[9] environment, including bias subtraction, flat-field correction, aperture extraction and wavelength calibration using a Th-Ar lamp spectrum.

Low Resolution Spectroscopy

We obtained long slit low resolution spectra with FORS2 at VLT on Paranal on 2002 March 25th. The VLT uses an active optics platform to achieve high quality image. The seeing conditions were excellent ($\sim 0\farcs64$) and we obtained high quality spectra. We used a $0\farcs7$ slit and the GR600I+25 and GR1200R+93 grisms, therefore covering a large wavelength range in the red part of the optical spectrum (Table 3.2). The spectra were processed using a custom pipeline based on standard procedures in IRAF. First, the two-dimensional images for the two separate CCDs which make up the FORS2 detector were independently overscan-, bias- and flat field-corrected. The lower chip image was then normalised to the median value of the upper one, and the images for the two chips could then be merged using the *fsmosaic* tool of the FIMS software

[9]IRAF is distributed by National Optical Astronomy Observatories, which is operated by the Association of Universities for Research in Astronomy, Inc., under contract with the National Science Foundation.

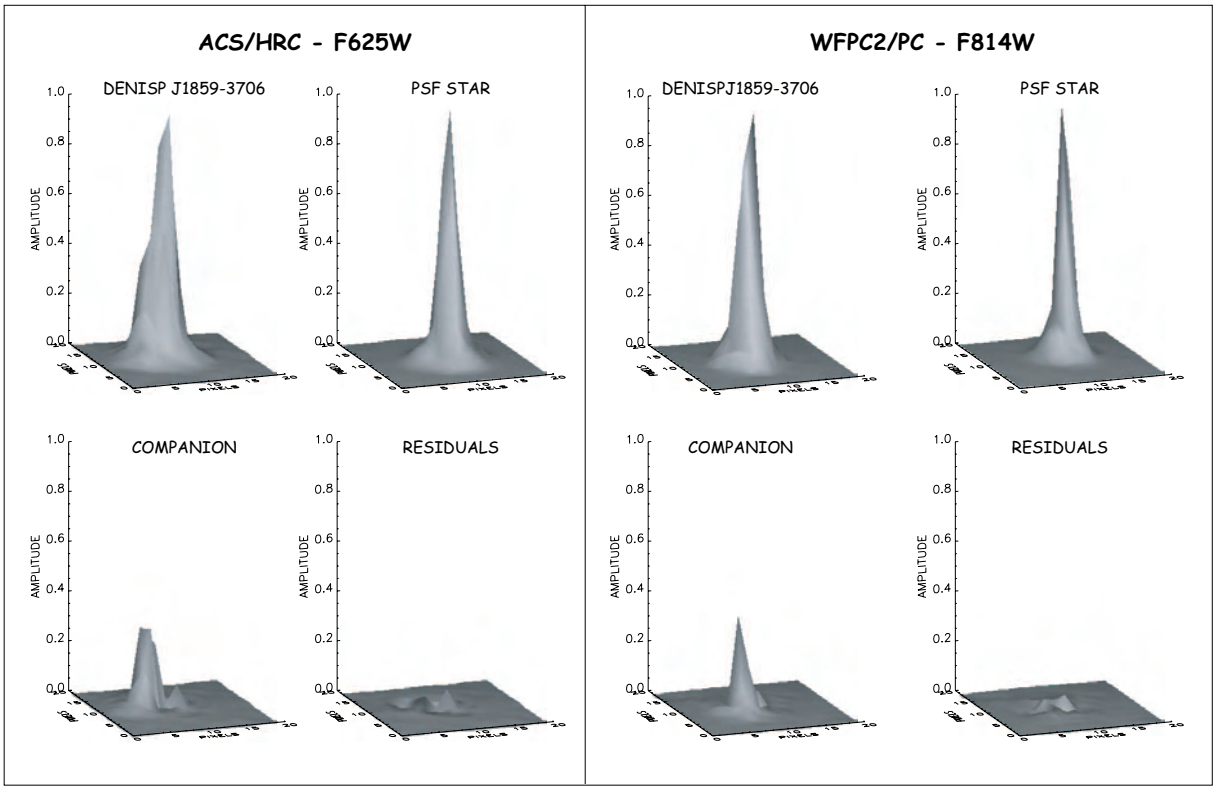

Figure 3.5 Surface plots showing the results of the non-linear PSF fitting on the ACS/HRC (F625W filter) and WFPC2/PC (F814W) images. Amplitudes are normalised. The sky background has been subtracted. The figure shows the images obtained with HST/HRC and WFPC2/PC, one of the PSF stars, the companion appearing after PSF subtraction, and the residuals after subtracting the modelled binary system. The pixel scale of the ACS/HRC is almost twice finer than that of the WFPC2/PC.

(FORS1+2 FIMS manual, issue 2.6). The 1-D spectra were then extracted, and wavelength and flux calibrated in a standard manner, using the best calibration files provided by the VLT team.

We obtained a HST-STIS low spectral resolution observation, aiming for spatially resolved spectra of the two components. Observations occurred on 2003 June 26th. We used the G750L grating (0.525μm-1.300μm, 4.92Å/pixel) with the 0.″2 slit oriented along the axis of the binary. Unfortunately, the small separation ($\sim$0.″060), the relatively small flux ratio ($\sim$0.3 in R and I, Section 3.3.3), and the relatively low S/N prevent us from properly resolving the two components (the pixel scale of STIS spectra is $\sim$0.″050). We processed the integrated spectrum using the recommended STSDAS tools in IRAF and the best calibration files provided by the STScI archive.

3.3 Analysis

3.3.1 Spectral Type and extinction

In order to estimate the spectral type of DENIS-P J185950.9-370632, we compare its optical spectrum to that of brown dwarfs from the field, and from the Upper Scorpius OB association (hereafter USco, Delfosse et al. 2003; Martín et al. 2004). The age and distance of USco, respectively estimated at 5 Myr (Preibisch & Zinnecker 1999) and 145 pc (de Zeeuw et al. 1999), are very close to those of R–CrA, and A_V is close to zero, with local maxima reaching $\sim$1.0 mag (see Cambrésy 1999). Each reference spectrum was artificially reddened with different values of extinction (using the *redden* task of IRAF) and then compared to DENIS-P J185950.9-370632 spectrum. Figures 3.6 and 3.7 shows the best match obtained with the USco M8 brown dwarf DENIS-P J161916.5-234722.9, and the M8 field ultracool dwarf VB 10, both for an extinction of A_V=0.5 mag. The correlation is very good and the two results agree perfectly. One can note that the K I and Na I doublets are stronger in VB 10, as expected because of its higher gravity, while they are very similar in the case of DENIS-P J161916.5-234722.9. This is another hint that DENIS-P J185950.9-370632 is young and is likely to belong to the R–CrA association, which age is very close to that of the Usco OB association. The next best match was with DENIS-P J1556-2106 (USco, M7) for a reddening of Av=1.0. We thus adopt a spectral type of M8$\pm$0.5 for DENIS-P J185950.9-370632 and an extinction of A_V=0.5$\pm$0.3 mag.

We applied the *NICER* (Near Infrared Colour Excess Revisited) technique (Lombardi & Alves 2001) on the 2MASS catalog photometry to produce an extinction map of the R–CrA region, with a 2′ resolution (Figure 3.8). DENIS-P J185950.9-370632 lies next to a region of strong absorption. The mean V band extinction in the 2′ pixel that contains DENIS-P J185950.9-370632 is A_V=3.7$\pm$0.4 mag [10]. As explained above, the observed optical spectrum implies instead that DENIS-P J185950.9-370632 is reddened by A_V $\sim$0.5 mag. This suggests that DENIS-P J185950.9-370632 probably lies somewhat on the near side of the cloud, or in a relative gap of the patchy extinction.

3.3.2 R-CrA membership

Photometric distance

After correcting for A_V=0.5 mag, the magnitude and colour of DENIS-P J185950.9-370632 are $I \sim 16.8$ mag and $I - J$ =2.9 mag. The DUSTY theoretical isochrones (Chabrier et al. 2000)

[10] The 0.4 mag uncertainty quoted here is the measurement uncertainty on the mean extinction; the standard deviation of the extinction inside the 2′ pixel is 1.8 mag

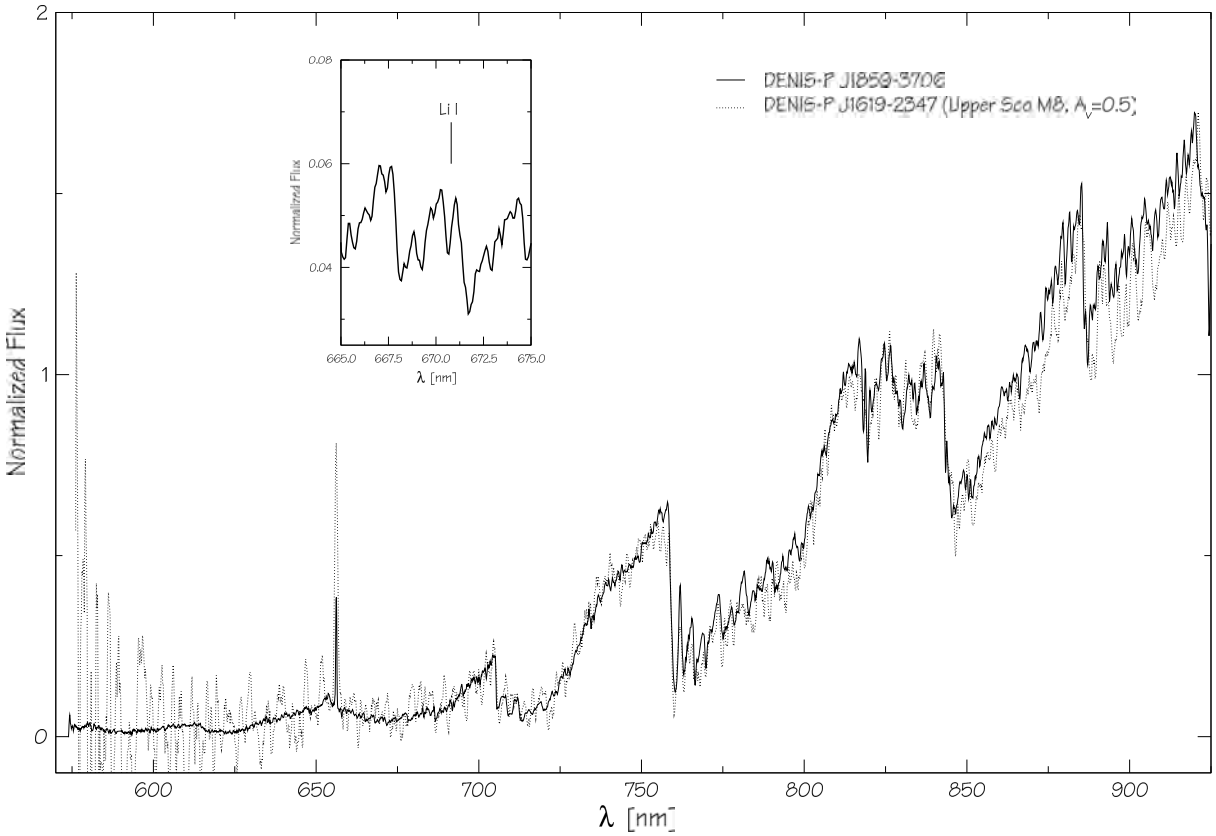

Figure 3.6 Comparison of DENIS-P J185950.9-370632 FORS2 spectrum (smoothed via a boxcar with a width of 5 pixels) with the spectrum of the Upper Scorpius member M8 dwarf DENIS-P J161916.5-234722.9 artificially reddened with A_V=0.5 mag. The match is very good. The inset box shows a zoom of DENIS-P J185950.9-370632 spectrum around the Li I absorption. Spectrum of DENIS-P J161916.5-234722.9 from Martín et al. (2004). Fluxes have been normalized at the pseudocontinuum level at 840.0 nm.

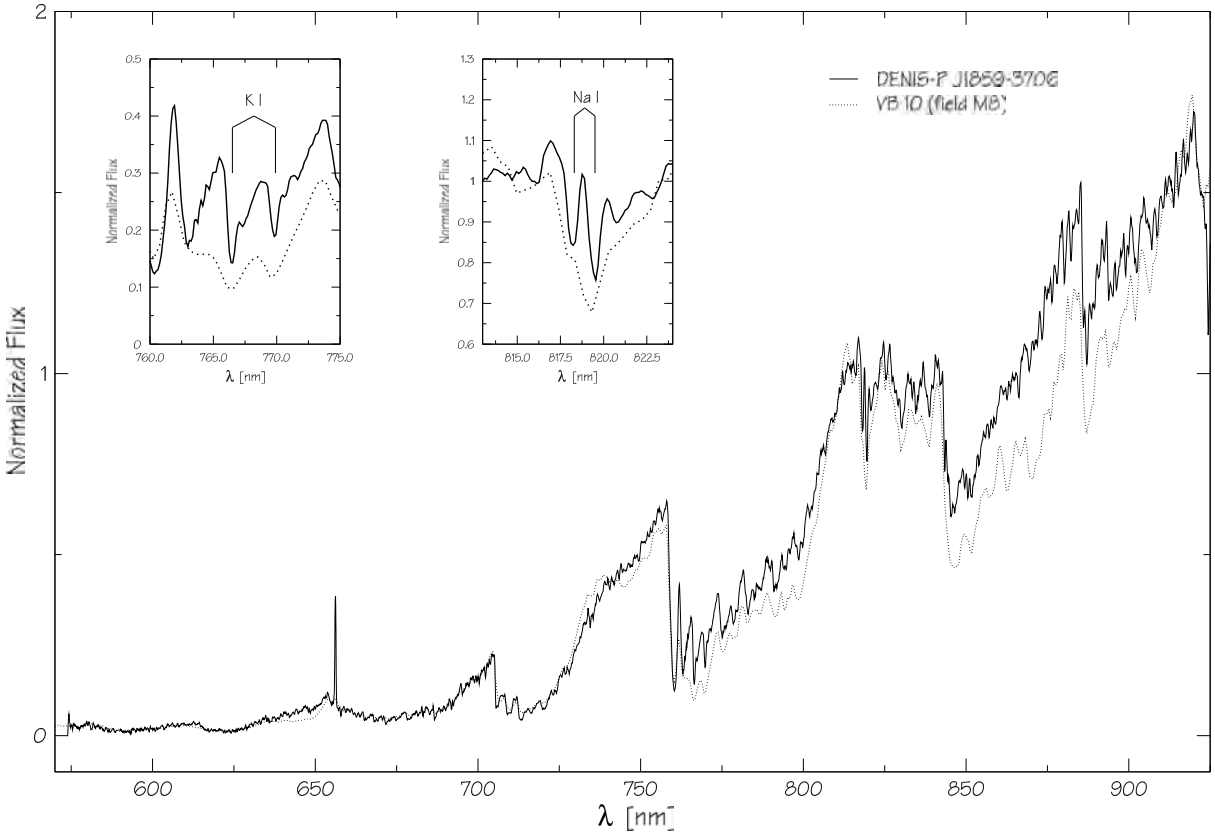

Figure 3.7 Comparison of DENIS-P J185950.9-370632 spectrum (smoothed via a boxcar with a width of 5 pixels) with the spectrum of the field M8 dwarf VB 10, artificially reddened with A_V=0.5 mag. The match is very good. The inset boxes show zooms of the two spectra around the K I and Na I doublet. It shows clearly that these two doublets are stronger in VB 10, as expected because of its higher gravity. Spectrum of VB 10 from Martín et al. (1999b). Fluxes have been normalized at the pseudocontinuum level at 840.0 nm.

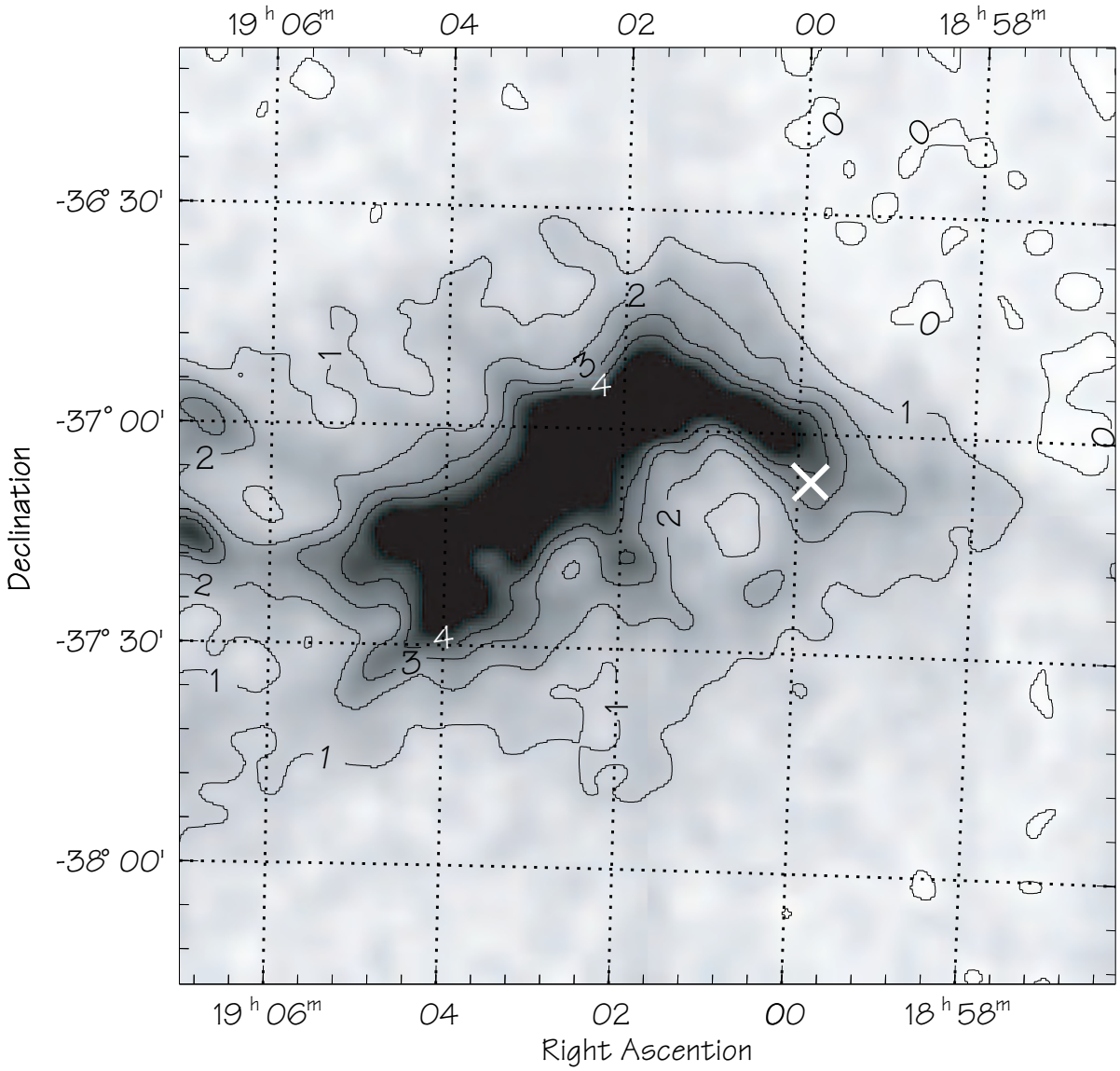

Figure 3.8 Extinction map of the R–CrA Region around DENIS-P J185950.9-370632 (indicated by white cross). Isocontours of A_V=0.0, 1.0, 2.0, 3.0 and 4.0 mag indicate the scale.

associate to those parameters a distance of ∼150 pc at 5 Myr and 110 pc at 10 Myr. Corrected for binarity (assuming a flux ratio f_2/f_1 =0.3 as measured in the F814W filter, see Table 3.3 and Section 3.3.3), it corresponds to distances of ∼170 pc and 125 pc. The corresponding masses are respectively ∼0.025 $M_\odot$ and ∼0.035 $M_\odot$.

The late-M dwarfs sequence in Upper Scorpius (Delfosse et al. 2003; Martín et al. 2004) provides a sanity check: M7.5 dwarfs in USco have I between 16.0 and 17.5 mag for M6.5 to M7.5 dwarfs, indicating for DENIS-P J185950.9-370632 a photometric distance similar to that of Upper Scorpius, whose distance is close to that of the CrA complex.

Proper motion

As discussed in section 3.2.1, DENIS-P J185950.9-370632 has been detected at many epochs. Figure 3.3 shows that HST/ACS position is clearly discrepant, which we suspect is due to underestimated uncertainties on the position obtained with HST/ACS, which lies over 3-σ away from any other. Direct comparison with the HST/WFPC2 images confirms that the pointing is correct, and we suspect that the problem arises in the astrometric processing of the ACS data by the STSDAS pipeline. The DENIS, 2MASS, HST/WFPC2, HST/STIS, GSC 2.21 and USNO-B1.0 observations all agree to within less than 1-σ for epochs spread over 18 years, confirming that the HST/ACS measurement is most suspicious. There are unfortunately not enough other stars in the field of the HRC to perform meaningful and precise astrometric recalibration. We derive an approximate motion for DENIS-P J185950.9-370632 by comparing the most precise of recent measurements, from 2MASS, with the earliest position reported in the USNO-B1.0 (with similar uncertainties, ∼14 years earlier). This rough estimate of the proper motion, $\mu_\alpha \cos\delta = 0\farcs0\ \mathrm{yr}^{-1} \pm 0\farcs013\ \mathrm{yr}^{-1}$ and $\mu_\delta = -0\farcs021\ \mathrm{yr}^{-1} \pm 0\farcs013\ \mathrm{yr}^{-1}$, agrees within the (large) uncertainties with the Neuhäuser et al. (2000) value for the R-CrA region, $\mu_\alpha \cos\delta = 0\farcs005\ \mathrm{yr}^{-1}$ and $\mu_\delta = -0\farcs027\ \mathrm{yr}^{-1}$. This is consistent with membership of DENIS-P J185950.9-370632 in the star forming region, though the significance of the result is obviously not very high.

3.3.3 Imaging: a close companion

As shown in Figures 3.4 and 3.5, DENIS-P J185950.9-370632 is clearly elongated in the high resolution HST images, at 2 epochs and in 6 different filters. We analysed the HST images for precise separations, position angles and flux ratios of the possible multiple system, using a custom-made program described in Bouy et al. (2003) and adapted here for ACS/HRC. Briefly, the PSF fitting routine builds a model binary using ten different PSF stars from several ACS/HRC images, and then perform a non-linear PSF fit of the observed image to determine the best-fit values for the 3 free parameters: separation, position angle and flux ratio. Bouy et al. (2003) discuss the uncertainties and limitations of the algorithm in detail, but slight improvements since then have led to a much better understanding of the uncertainties and systematic errors (Bouy 2004, , in prep.).

Table 3.3 summarises the resulting best-fit binary parameters. For the three filters where the source is best resolved (F625W, F675W, F775W; see Figures 3.4 and 3.5) they are fully consistent, demonstrating that a binary star is an excellent model of the observations. The nominally discrepant parameters in the other filters are from marginally resolved images, either due to diffraction broadening at redder wavelength (WFPC2/PC F814W, ACS/HRC F850LP) or because of wider pixels (STIS/F28X50LP). They should therefore not be given much weight. Given the proper motion derived in section 3.3.2.0, two independent objects should have moved

Table 3.3. PSF fitting results for DENIS-P J185950.9-370632

Date Obs.	Instr.	Filter	Sep.[1][″]	P.A[1][°]	ΔMag[1][mag]
23/06/2003	STIS/CCD	F28X50LP	elongated[2]	elongated[2]	elongated[2]
24/09/2002	ACS/HRC	F625W	0.″065±0.″001	279.2±0.1	1.74±0.06
24/09/2002	ACS/HRC	F775W	0.″057±0.″0005	279.1±0.1	0.66±0.05
24/09/2002	ACS/HRC	F850LP	elongated[2]	elongated[2]	elongated[2]
12/09/2000	WFPC2/PC	F675W	0.″066±0.″003	283.8±1.2	1.30±0.11
12/09/2000	WFPC2/PC	F814W	0.″059±0.″003	271.8±1.2	1.10±0.11

[1]The uncertainties reported here are 1-σ uncertainties as explained in Annex A.

[2]As explained in the text, the PSF fitting program did not give good enough results, although the object is clearly elongated.

apart by ∼0.″042 between the two observations. The lack of any apparent change is thus a strong indication that they form a common proper motion pair.

3.3.4 Spectral Analysis

Spectral Features

Table 3.4 lists the equivalent width (EW) of several spectral features measured in the different data sets. The only emission line in the HIRES spectrum is Hα. Other common emission lines such as He I at 667.8 nm, O I at 844.6 nm, and Ca II at 866.2 nm are not detected, with upper limits on their equivalent width (EW) below 0.5 Å. By direct integration of the line profile (using the *splot* IRAF task) we measure an Hα equivalent width of 18±3 Å in the HIRES spectrum, 18±3 Å from the low-resolution STIS spectrum, and 17±2 Å from the FORS2 spectrum. According to Barrado y Navascues & Martín (2003) EW(Hα)=47.5 Å for an M7.5 spectral type implies that the Hα emission is caused by accretion, while weaker lines can be due to either accretion or chromospheric activity. The Hα line strength by itself is thus here insufficient to distinguish between an accretor and a chromospherically active star. The Hα line however is relatively broad (Figure 3.9), with a full width at 10% of peak intensity of 205±10 km s^{-1}. Hα line widths above 200 km s^{-1} in brown dwarfs are due to accretion (Jayawardhana et al. 2003a), and by this measure DENIS-P J185950.9-370632 is slighty above the limit and is likely an accretor. If accreting, the mass accretion rate is probably rather low, given the modest Hα strength and the lack of optical veiling. Accretion rates below 10^{-9} M$_\odot$ yr^{-1} produce no measurable veiling (Muzerolle et al. 2000). The consistency of the EW measured at the three epochs suggests that we are measuring quiescent emission rather than variable activity. This is more consistent with steady accretion than with chromospheric activity, where strong and broad Hα lines are only observed during outbursts. Further observations should be made in order to confirm that DENIS-P J185950.9-370632 is accreting or not.

In the region of the Li I resonance line (670.8 nm) the HIRES spectrum is rather noisy,

Table 3.4. Spectral Features.

Feature	Instrument	λ [nm]	EW [Å]
Hα	HST/STIS	656.3	-18 ± 3
Hα	VLT/FORS2	656.3	-17 ± 2
Hα	Keck/HIRES	656.3	-18 ± 3
Na I	VLT/FORS2	818.3	3.7 ± 0.3
Li I	VLT/FORS2	670.8	0.9 ± 0.4
Li I	Keck/HIRES	670.8	0.41± 0.08

but the line is well detected with EW(Li I)=0.41±0.08 Å. This line also appears clearly in the FORS2 spectrum, as shown in Figure 3.6, with EW(Li I)=0.9±0.4 Å. The resolution of the STIS spectrum is insufficient to isolate the Li I line. The K I line at 769.9 nm is also present in the HIRES and FORS2 spectra. As already mentioned in section 3.3.1, Figure 3.7 shows that the K I and Na I lines of DENIS-P J185950.9-370632 are much narrower and weaker than in the spectrum of a field M8 dwarf (VB 10), indicating a young age.

Comparison with model spectra

In order to estimate of the photospheric effective temperature, we compare the observed spectra with the DUSTY (Allard et al. 2001) and NextGen (Hauschildt et al. 1999) atmospheric models. The synthetic spectra were smoothed with a gaussian kernel matched to the slit size and resampled to the same grid as the observed spectra. The best fit model was determined by maximizing the cross-correlation with the dereddened observed spectrum (a minimum χ^2 adjustment, performed as a cross-check, gives identitical results).

The free parameters for the fit are the effective temperature and the surface gravity (the metallicity was fixed to solar metallicity; models for higher metallicities are not yet available, and lower metallicities gave significantly degraded agreement). The latest NextGen and DUSTY models give very similar surface gravities. For an age of 5 Myr and I-J$\sim$3.0, they respectively give log g $\sim$3.8 and log g $\sim$4.0, and for 10 Myr respectively log g $\sim$4.1 and log g $\sim$4.0. The available DUSTY models have a 100 K grid step, and cover surface gravities log g ranging from 3.5 to 6.0 with a 0.5 interval. We only considered models with effective temperature between 1500 K and 3000 K, and surface gravities between 3.5 and 4.5. The observed and synthetic spectra were both normalized to an integrated flux of unity prior to the analysis.

Figure 3.10 shows the best-fit DUSTY synthetic spectrum, over-plotted on the observed spectra. For both sets of models (DUSTY and NextGen), the best fits are obtained for T_{eff}=2600 K and log g=3.5 (STIS spectrum), and T_{eff}=2700 K and log g=3.5 (FORS2 spectrum). Attempts to account for the multiplicity by using two synthetic spectra at different effective temperatures did not produce a significantly improved fit. This is actually expected, since according to the DUSTY models the observed magnitude differences (from 0.60 mag in the HST F775W filter to 1.74 mag in the HST F625W filter) correspond to effective temperatures that differ by $\leq$200 K.

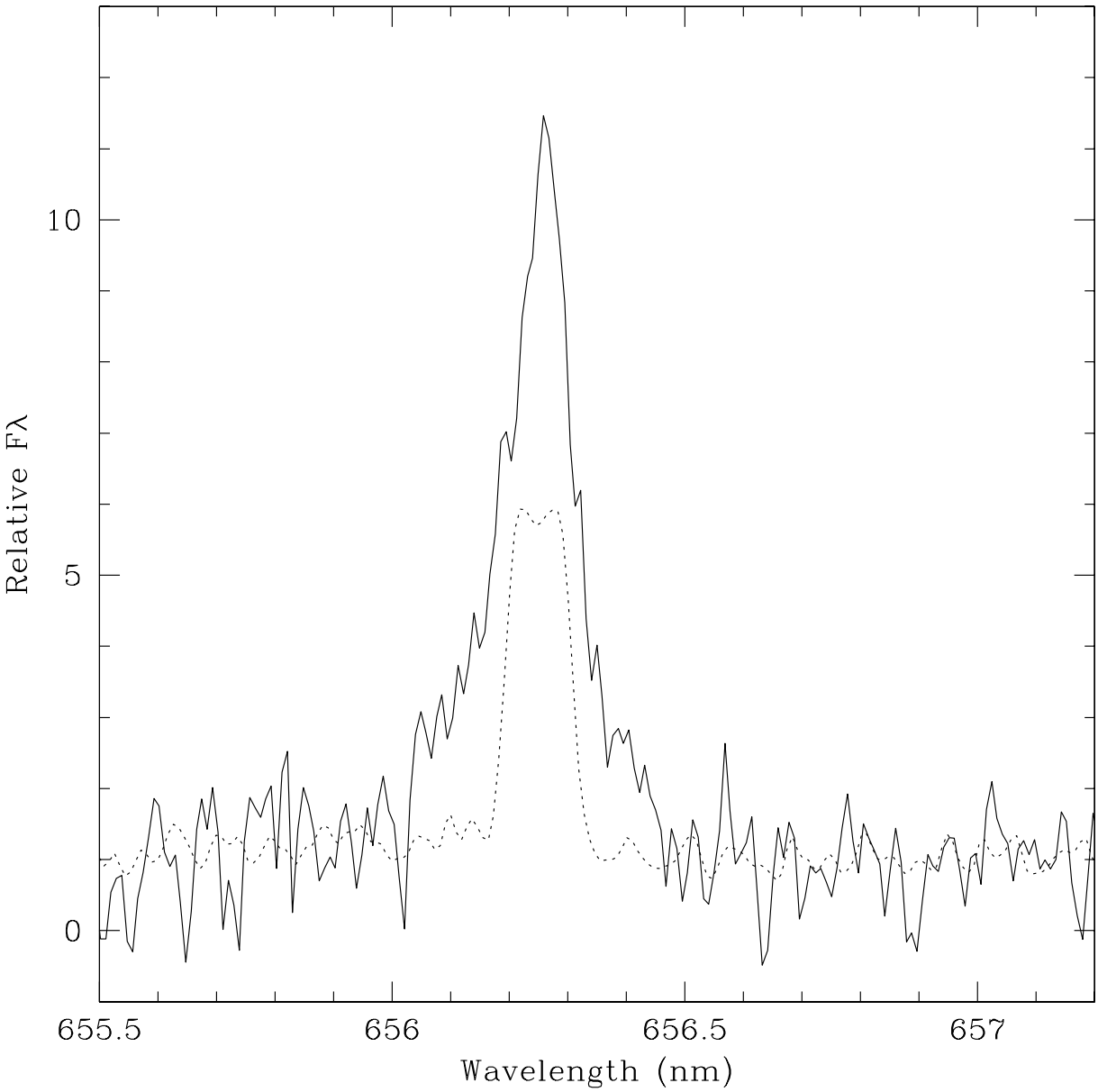

Figure 3.9 HIRES spectra of DENIS-P J185950.9-370632 (solid line) and Gl 406 (dotted line) in the H_α region. Gl 406 is a typical chromospherically active M6 dwarf. DENIS-P J185950.9-370632 has a much broader and asymmetric emission line, indicating that it is probably an accretor.

This is close to the effective temperature resolution of our adjustment, and a dual temperature fit is therefore not warranted. The obtained effective temperature should on the other hand represent a reasonable estimate for both components.

It is important to note that the model spectra do not match the observed ones very well over the present spectral range, perhaps because of their simplistic handling of the gravitational settling of dust. They probably underestimate the strength of molecular absorption bands like TiO, VO, but of also atomic lines like K I and Na I D. Since these features dominate the energy distribution in optical spectra of late M dwarfs, the parameters that we obtain most likely suffer from systematic errors. They should on the other hand be much more reliable when used in a relative sense, and compared with other analyses based on the same atmospheric models. The low surface gravity of DENIS-P J185950.9-370632 ($\log g = 3.5$) relative to field M8 dwarfs ($\log g \sim 4.5$), in particular, is a robust result.

3.4 Discussion

3.4.1 Infrared excess

Figure 3.11 compares the spectral energy distribution (SED) of DENIS-P J185950.9-370632 to the DUSTY and NextGen models (for 5 Myr), as well as to observed field late-M dwarfs. The fluxes have been normalized to have an integrated luminosity between 0 and 1.65 μm (H band) equal to one. The choice of the H band as limit instead of, for example, the overall SED, was made for the following reasons: first because the SED of late-M dwarfs peaks around this value (see the DUSTY, NextGen and field M dwarfs SED in the figure), and second because in this wavelength range, the SED should be less affected by accretion-related continuum emission and infrared emission from the disk than at redder colours. The infrared excess is already very strong in the K band, which is relatively unusual in comparison with the SED of other know brown dwarf with disks. If the presence of a disk is confirmed, this would mean that the disk emission is dominating in this part of the SED, or at least gives an important contribution. This would imply that the disk is composed of hot dust only, relatively hotter than for most brown dwarfs. Near-infrared K band spectroscopy as well as mid-infrared photometry should allow us to understand better the properties of this peculiar object. The CO bands should indeed look different from purely photospheric ones, or even may not be there, or even may be in emission, which would certify the origin of the infrared excess. A proposal for VLT/ISAAC K band spectroscopy will be submitted for period 75.

DENIS-P J185950.9-370632 shows a strong excess over the models and the field dwarfs at wavelength greater than the H band. This wavelength range ($\lambda \geq 1.6$ μm) is on the Raleigh-Jeans tail of the spectrum, and models are expected to be very reliable. We did not find any published observations of field late-M dwarfs in the 5.0 μm–8.5 μm range, but the available photometric measurements in the R to L' bands already demonstrate that the field M dwarfs have a much lower flux between K and L' than DENIS-P J185950.9-370632, independently demonstrating the infrared excess. Since DENIS-P J185950.9-370632 is a binary we checked that its SED cannot be fitted by any meaningful combination of two synthetic SED, and the infrared excess is robust.

3.4.2 An accreting close Binary

As discussed in Section 3.3.3, DENIS-P J185950.9-370632 is very likely to be a binary, with a separation of $\sim 0\farcs060$, or 7.8 A.U at its 130 pc distance. This separation is well within the 0–20 A.U range observed for field brown dwarf systems (Bouy et al. 2003; Burgasser et al. 2003;

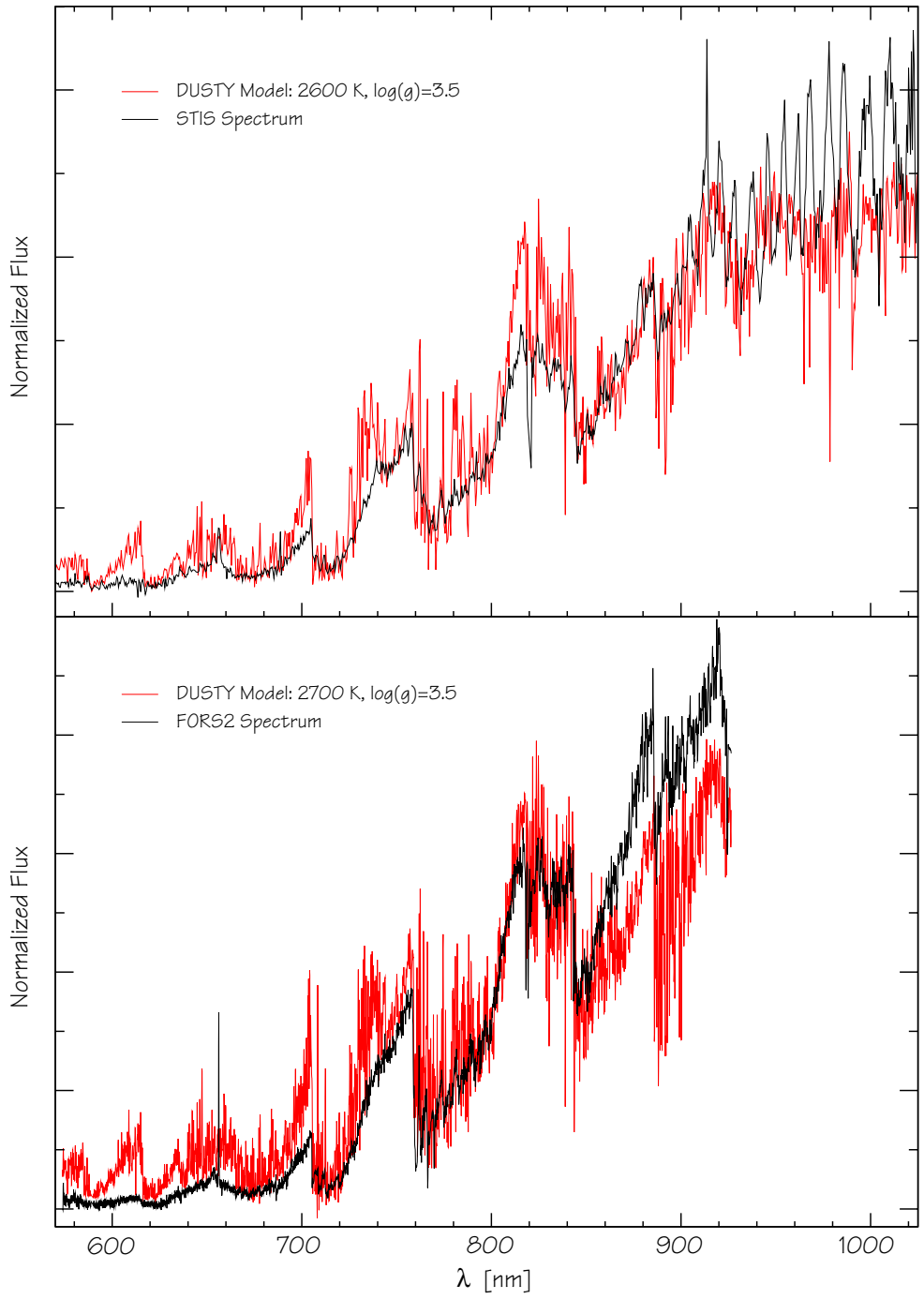

Figure 3.10 STIS and FORS2 spectra compared with models. Top panel: STIS spectrum of DENIS-P J185950.9-370632 compared with a synthetic spectrum. Bottom panel: FORS2 spectrum of DENIS-P J185950.9-370632 compared with a synthetic spectrum. The best fit is obtained for the same surface gravity (log g=3.5) but slightly different effective temperatures (2600 K and 2700 K). The two results therefore agree within the 100 K temperature step of the model atmosphere grid.

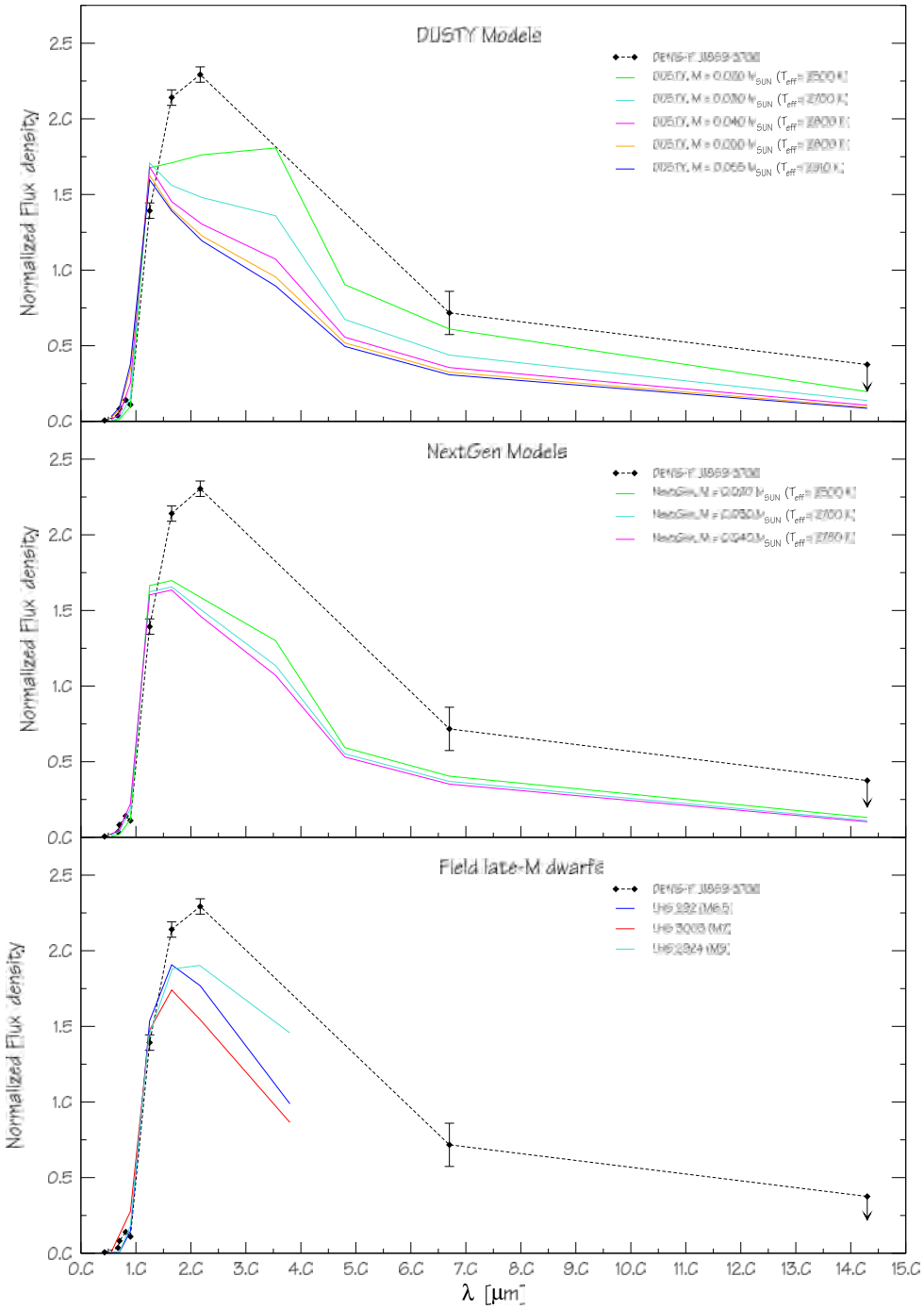

Figure 3.11 Spectral energy distribution of DENIS-P J185950.9-370632 compared with DUSTY and NextGen models (5 Myr) and field late M-dwarfs distributions: LHS 3003(M7), LHS 292 (M6.5), and LHS 2924 (M9). The values for DENIS-P J185950.9-370632 have been corrected for an extinction of A_V=0.5 mag. All fluxes have been normalized to their integrated luminosity between 0 and 1.65 μm. (values for the field dwarfs from Leggett 1992; Leggett et al. 2002).

Close et al. 2003; Gizis et al. 2003). The statistical correction factor of 1.26 from Fischer & Marcy (1992), leads to a semi-major axis of a =9.8 A.U. As discussed in section 3.3, the photometry, the spectral distribution, and the optical low resolution spectra all indicate an age of 5∼10 Myr for a distance of 130 pc, and an effective temperature of ∼2 600 K. The small magnitude difference (Table 3.3) indicates that the two components of the system must have fairly similar masses. According to the DUSTY models, magnitude differences of 1.74 mag in the $F675W$ filter and 1.1 mag in the $F814W$ filter correspond to a mass ratio of M_B/M_A ∼75%. Considering a total mass of between 0.025 $M_\odot$ <M_{tot} <0.035 $M_\odot$ and an orbit with a semi-major axis of 9.8 A.U, this leads to an orbital period of 165–195 yrs

3.5 Conclusions

The results presented in this work demonstrate that DENIS-P J185950.9-370632 is a young multiple system in the R–Cra star forming region. On the optical images, we find a clear elongation. After PSF subtraction on 3 epochs data we conclude that DENIS-P J185950.9-370632 is very likely to be a common proper motion pair with a separation of ∼0.″060, close to the resolution limit of the instruments we used. The spectroscopy constrains the effective temperature to 2600∼2700 K for a low surface gravity (log g=3.5), consistent with a young age. This temperature corresponds to a total mass of ∼0.030±0.010 $M_\odot$ for an age ranging between 5 and 10 Myr. This mass is consistent with the photometry, and DENIS-P J185950.9-370632 is therefore clearly substellar. Infrared excess observed with the ISOCAM in the 5.0-8.5μm band and the presence of a strong Hα emission as well as lithium absorption at 670.8 nm suggest a young age, the presence of circumstellar material, and a sub-stellar mass object. Added to a consistent preliminary estimate of the proper motion and consistent colours, these observations suggest that DENIS-P J185950.9-370632 belongs to the R–CrA star forming region. From the magnitude difference between the two components we estimate a mass ratio of ∼75%. The estimated orbital period is about 170 yrs. The mid-infrared excess observed by ISO and the width of the Hα emission suggest that it might be surrounded by a disk and slowly accreting.

Part II

Physical properties of binary ultracool dwarfs

Chapter 1

High angular resolution imaging and spectroscopy

1.1 Follow-up Imaging with HST/ACS and VLT/NACO

In order to follow-up the multiple systems on their orbits and to have updated measurements of their position angle for the spectroscopy (required to align properly the slit along the axis of the binary), we obtained high angular resolution images using both HST/STIS (program GO9451, P.I. Brandner) and VLT/NACO (programs 070.D-0773, P.I. Bouy). Table 1.1 shows the results of these observations as well as a reminder of any previous observations of these multiple systems. Most of these objects show only little motion.

1.2 Optical Spectroscopy with HST-STIS

1.2.1 Analysis of the data

In order to get the spatially resolved spectra of each component of the multiple systems, we tried to align the slit along the axis of the binary. Scheduling constraints of HST made it difficult to get long slit STIS observations at a particular roll angle of HST. In order to ease scheduling, a range of admitable roll angle was defined, and in general the misalignment was small and not more that $\sim$5 degrees.

In order to extract the spectrum of each component, we used a custom made program able to perform a fit of the two blended spectra. On each cross-dispersion column, a minimum χ^2 fit was performed to the data using the cross-dispersion profile of a reference spectrum at the same wavelength. The latter spectrum was obtained with the same instrument settings on a K7 dwarf (TWA6, program 8176, P.I. Schneider). The free parameters for the fit are the amplitude of the primary, the amplitude of the secondary, the position of the primary and the position of the secondary. Since the cross dispersion profile is barely sampled, we also performed a linear re-sampling of the data by a factor of four prior to the fit, in order to avoid problems due to spectral aliasing. To ensure more robustness and increase reliability, the program was used in 2 passes. A polynomial fit of the results on the positions of the two individual spectra was made after the first pass, in order to identify and remove outliers (due to bad pixels or cosmic rays). The results of these fits were then used as first guess inputs for the second pass. The results obtained with the second pass are very close to that obtained with the first pass but cleaner (without the more obvious bad pixels, cosmic rays and outliers), ensuring that the whole

Table 1.1. Results of the PSF fitting

Date of Obs.	Instrument	Sep. [mas]	P.A [°]	Δmag	Filter	Source[a]
			2MASSW J0850359+105715			
01-02-2000	HST/WFPC2	157.2±2.8	114.7±0.3	1.47±0.09	F814W	(2) & (3)
21-10-2002	HST/ACS	139.0±0.5	125.4±0.15	1.45±0.02	F625W	(1)
	HST/ACS	142.9±0.5	125.2±0.15	1.18±0.02	F775W	(1)
	HST/ACS	144.7±0.5	124.1±0.15	0.87±0.08	F850LP	(1)
			2MASSW J1426316+1557013			
20-06-2001	Gemini/Hokupa'a	152±6	344.1±0.7	0.78±0.05	J	(4)
	Gemini/Hokupa'a			0.70±0.05	H	(4)
	Gemini/Hokupa'a			0.65±0.10	K_S	(4)
	Gemini/Hokupa'a			0.57±0.14	K	(4)
19-07-2001	HST/WFPC2	157.1±2.8	339.9±0.3	1.40±0.09	F814W	(3) & (5)
	HST/WFPC2	154.2±2.8	327.5±1.2	0.76±0.11	F1042M	(3) & (5)
10-03-2003	HST/ACS	194.8±0.5	342.2±0.15	1.11±0.08	F625W	(1)
	HST/ACS	194.8±0.5	341.7±0.15	1.48±0.08	F775W	(1)
	HST/ACS	193.4±0.5	342.0±0.15	1.31±0.08	F850LP	(1)
28-04-2003	HST/STIS	194.1±2.8	341.6±1.2	···	Longpass	(1)
			2MASSW J1311391+803222			
30-07-2000	HST/WFPC2	300.8±2.8	167.2±0.3	0.39±0.07	F814W	(3) & (5)
	HST/WFPC2	300.0±2.8	167.3±0.3	0.45±0.09	F1042M	(3) & (5)
21-10-2002	HST/STIS	263.2±2.8	170.4±0.3	···	Longpass	(1)
			DENIS-P J035726.9-441730			
21-04-2001	HST/WFPC2	97.0±2.8	174.0±1.2	1.23±0.11	F675W	(3)
	HST/WFPC2	98.1±2.8	174.7±1.2	1.50±0.11	F814W	(3)
21-08-2002	HST/ACS	105.3±0.5	176.0±0.15	1.12±0.02	F625W	(1)
	HST/ACS	103.4±0.5	175.3±0.15	1.24±0.02	F775W	(1)
	HST/ACS	98.3±0.5	176.2±0.15	1.25±0.02	F850LP	(1)
03-01-2003	HST/STIS	103.8±2.8	176.6±1.2	···	Longpass	(1)
			DENIS-P J100428.3-114648			
27-10-2000	HST/WFPC2	146.0±2.8	306.1±1.2	0.25±0.07	F675W	(3)
	HST/WFPC2	146.0±2.8	304.5±1.2	0.66±0.11	F814W	(3)
14-02-2003	HST/STIS	103.8±2.8	315.2±1.2	···	Longpass	(1)

[a](1) This work; (2) Reid et al. (2000); (3) Chapter 1 of Part I; (4) Close et al. (2002b); (5) Gizis et al. (2003)

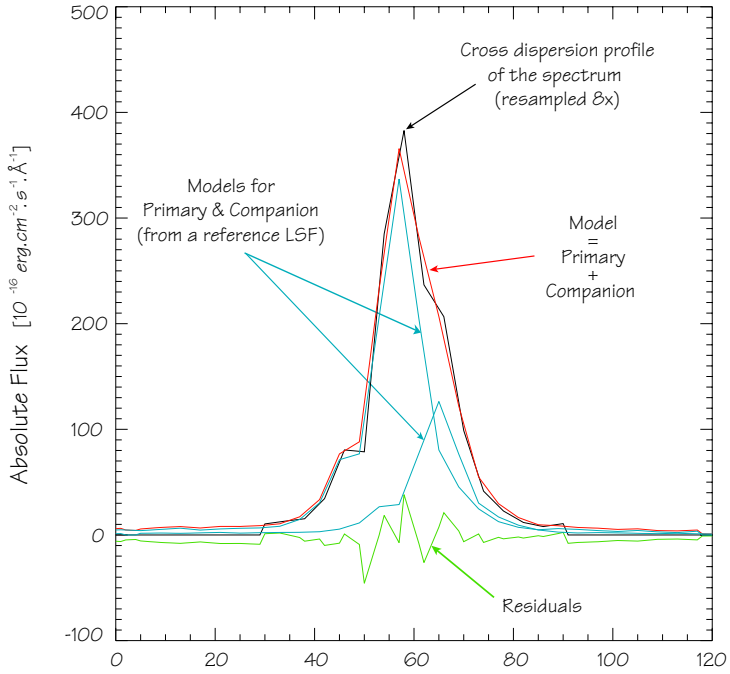

Figure 1.1 Extraction of the individual spectra. This figure shows the cross dispersion profile of the 2-D spectrum around 850 nm, and the best fits of the primary and the secondary (light blue). The sum of the primary and secondary (red) is also indicated for comparison with the raw data (black). In that case the intensity of the residuals (green) is less than ∼2% of the intensity of the raw data.

algorithm is robust enough and converging properly. Figure 1.1 gives an overview of the results at a particular wavelength. The residuals after the fit represent between 1.5% and 9% of the total intensity of the original spectrum depending on the wavelength, thus of the same order than the signal to noise ratio, ensuring that the quality of the fit is good.

1.2.2 2MASSW J1311391+803222

2MASSW J1311391+803222 is one of the widest binaries of this sample (see Table 1.1). The alignment of the slit along the axis was very good. Figure 1.2 shows that it was easily resolved with STIS and that we could extract nicely the spectrum of each component. 2MASSW-J1311391+803222 B shows a little motion between the two epochs separated by two years: about 27 mas and 3°. In order to estimate the spectral type of 2MASSW J1311391+803222, we compare its optical spectrum to that of ultracool dwarfs from the field available in the literature. The best match is obtained for a spectral type of M7 for both components (see Figure 1.3). We thus attribute a spectral of M7±0.5 for the two component. As one could expect, the two components have very similar masses and effective temperatures, the secondary being only slightly fainter than its primary. The flux ratio in the optical spectrum has a median value of ∼0.8, slightly larger but consistent with that measured in the F814W and F1042M filters (∼0.7), and confirming that the two components must have very similar masses.

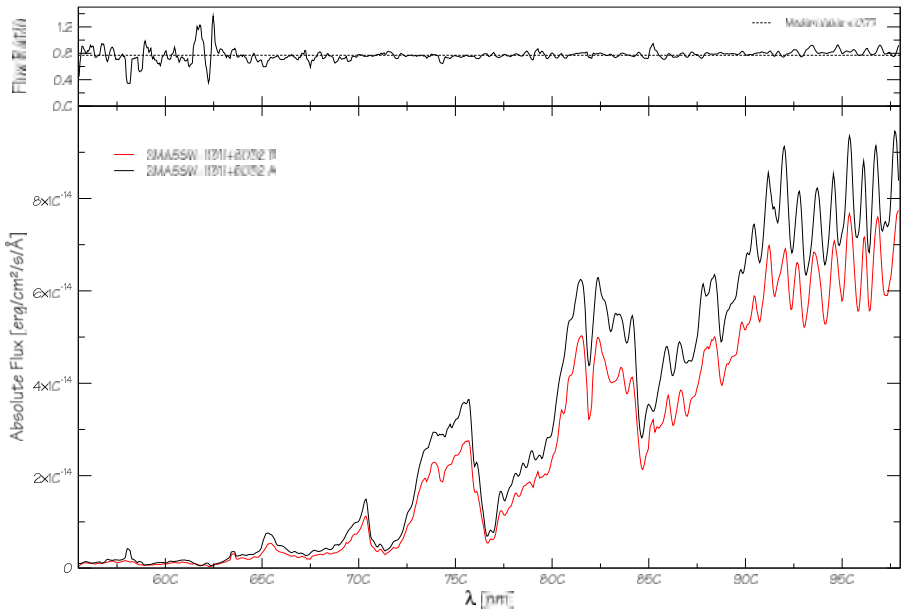

Figure 1.2 Optical Spectra of 2MASSW J1311391+803222 A (black) & B (red) obtained with HST/STIS (smoothed via a boxcar with a width of 5 pixels) . The upper plot shows the flux ratio as a function of the wavelength and its median value.

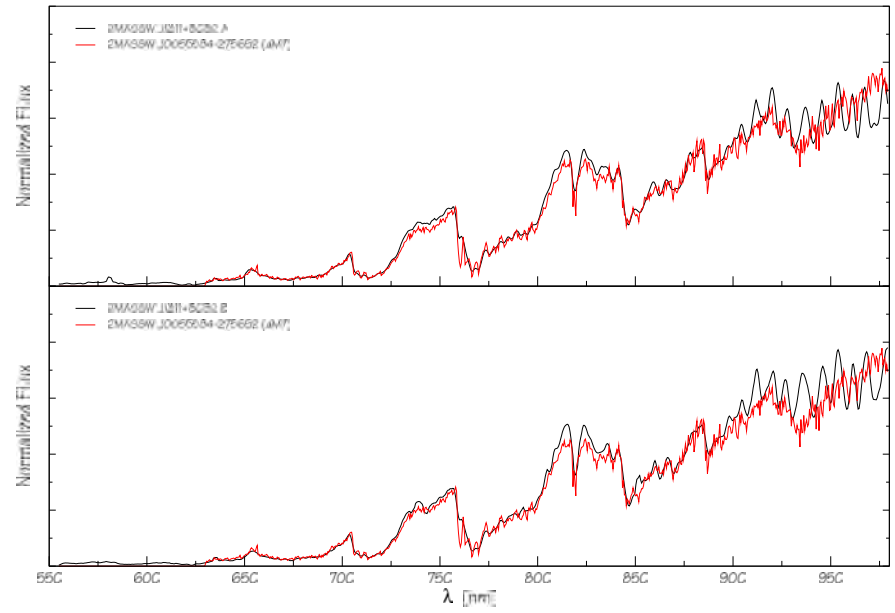

Figure 1.3 Spectral types of 2MASSW J1311391+803222 A (upper panel) & B (lower panel). The spectra of A and B (black) are compared to that of field very low stars (red). The best match indicates a spectral type of M7±0.5 for both A and B.

1.2.3 2MASSW J1426316+155701

2MASSW J1426316+155701 is one of most observed binaries of this sample, as shown by the many measurements reported in Table 1.1. Unfortunately, the motion of this object, ∼42 mas in separation but almost 0° in position angle shows that we see the system edge-on. We will therefore not be able to compute a precise orbit despite the relatively large number of observations, the uncertainty on the eccentricity beeing the main limitation.

The alignment of the slit along the axis was very good. Figure 1.4 shows that we could extract nicely the spectrum of each component. Comparing the spectra of the individual components to that of ultracool dwarfs from the field, we obtain measure a spectral type of M7±0.5 for the primary and L0±0.5 for the secondary (see Figure 1.5, page 112). The two components must have slightly different effective temperatures and masses. The median flux ratio measured in the spectra is equal to 0.34∼0.37, therefore in good agreement with the flux ratios we measure in the three ACS optical filters. It corresponds to a mass ratio of 0.75∼0.95 depending on the age (see Table 1.8 on page 62). The three spectral classes between the two components indicate that they must have effective temperatures differing by ∼500 K (Basri et al. 2000).

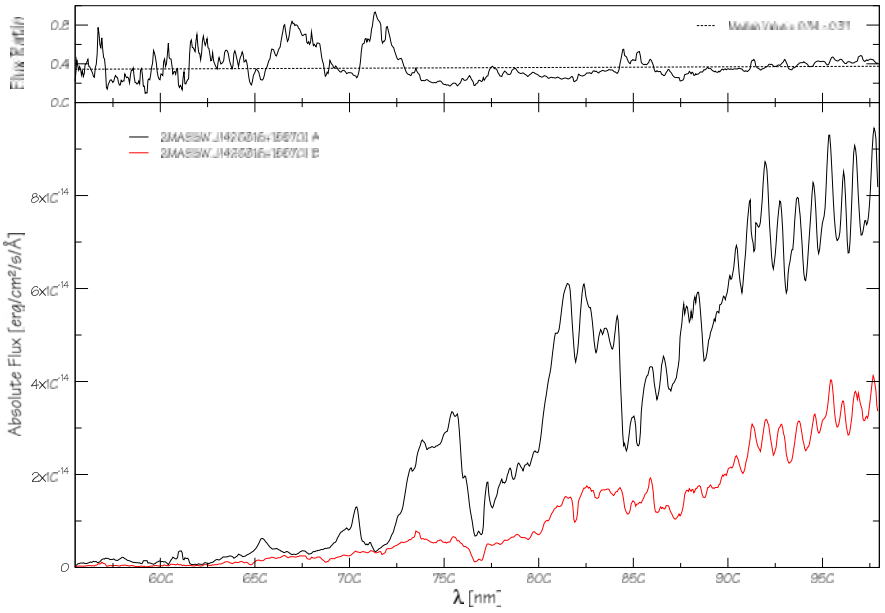

Figure 1.4 Optical Spectra of 2MASSW J1426316+155701 A (black) & B (red) obtained with HST/STIS (smoothed via a boxcar with a width of 5 pixels). The upper plot shows the flux ratio as a function of the wavelength and its median value.

1.2.4 DENIS-P J035726.9-44173

With a separation of only ∼0.″100, and a flux ratio of only 0.37, and an F814W magnitude of only 17.94 mag, DENIS-P J035726.9-44173 was the most difficult object we had in our sample, and the extracted individual spectra are more noisy than the other, as shown in Figure 1.6. The secondary shows almost no motion during the 2 years of follow-up. The difference of magnitude (1.08 mag) measured in the optical spectrum is consistent with that measured with the three ACS and two WFPC2 optical filters (see Table 1.1).

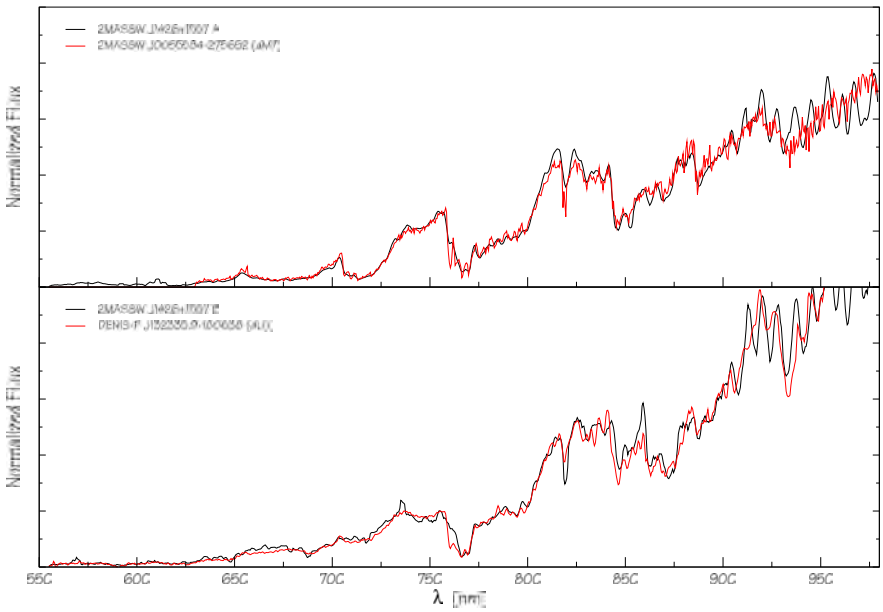

Figure 1.5 Spectral types of 2MASSW J1426316+155701 A (upper panel) & B (lower panel). The spectra of A and B (black) are compared to that of field very low stars (red). The best match indicates a spectral type of M7±0.5 for A and L0±0.5 for B.

In Figure 1.7 we compare the spectra of the individual components to that of ultracool dwarfs from the field. The best match is obtained with a L8 for the primary and a L2 for the secondary. We thus attribute a spectral type of M8±1 for the primary and L2±1 for the secondary. Because the individual spectra are relatively noisy, the correlation between the field dwarfs and the component spectra is not as good as for the other objects, explaning why we give larger uncertainties to the inferred spectral types. The four spectral classes of difference between the primary and the secondary indicate that the two components must have effective temperatures different by 500∼600 K (Basri et al. 2000). Their masses must nevertheless be similar, since a difference of magnitude of ∼1.1 mag in I corresponds to a mass ratio between $0.80 < q < 0.95$ depending on the age (see Table 1.8, page 62).

1.2.5 DENIS-P J100428.3-114648

DENIS-P J100428.3-114648 was also a difficult object: it is relatively faint and the individual spectra are just resolved (its separation is ∼0.″100, for a pixel-scale of 0.″055 for the STIS/CCD). The extracted individual spectra are noisy, as shown in Figure 1.8, but still better than that of DENIS-P J035726.9-441730 because the flux ratio is almost twice as large (0.60). The secondary shows a little motion: 43 mas and ∼10°between the two epochs separated by 2.5 years. The difference of magnitude (0.55 mag) measured in the optical spectrum is consistent with that measured with the two WFPC2 optical filters (see Table 1.1).

Figure 1.9 shows the best match between the spectra of the individual components and that of ultracool dwarfs from the field. it is obtained with a M8 for both the primary and the secondary. We thus attribute a spectral type of M8±0.5 for the primary and the secondary. Although the individual spectra are somewhat noisy, the correlation between the field dwarfs and the component spectra is relatively good. The identical spectral classes indicate that the two components

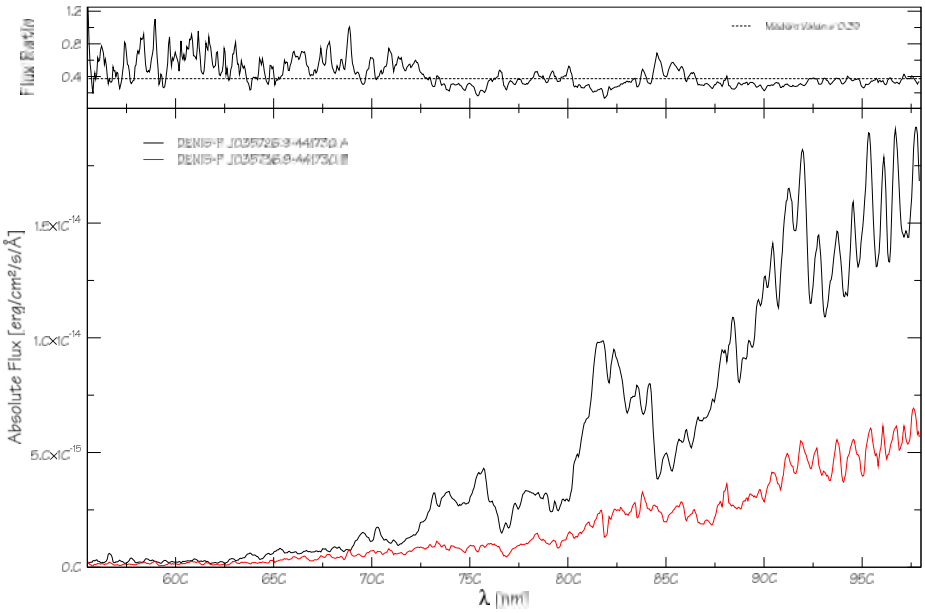

Figure 1.6 Optical Spectra of DENIS-P J035726.9-441730 A (black) & B (red) obtained with HST/STIS (smoothed via a boxcar with a width of 5 pixels). The upper plot shows the flux ratio as a function of the wavelength and its median value.

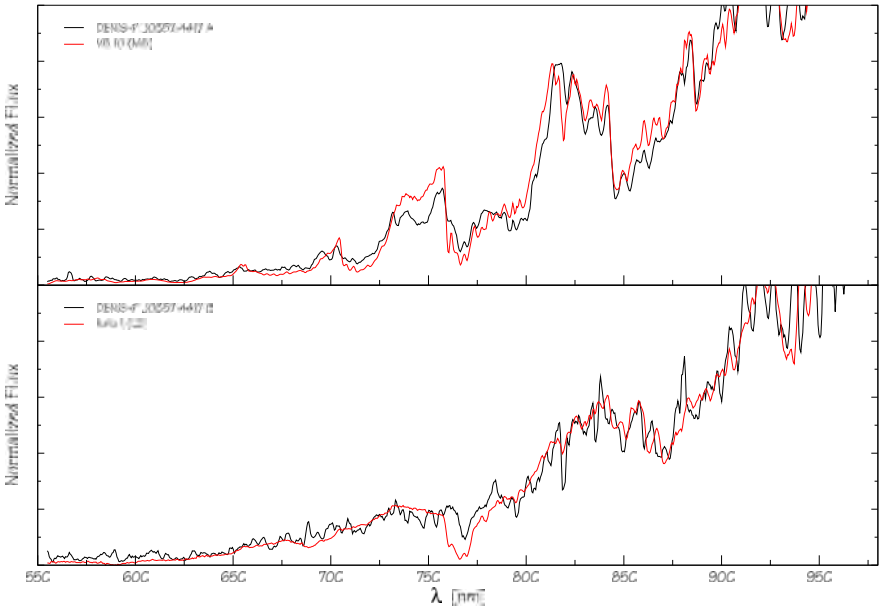

Figure 1.7 Spectral types of DENIS-P J035726.9-441730 A (upper panel) & B (lower panel). The spectra of A and B (black) are compared to that of field very low stars (red). The best match indicates a spectral type of M8±0.5 for A and L2±1 for B.

must have similar effective temperatures of about 2500–2600 K according to Basri et al. (2000). Their masses must be very similar, since a difference of magnitude of ∼0.6 mag in I corresponds

to a mass ratio between q >0.90.

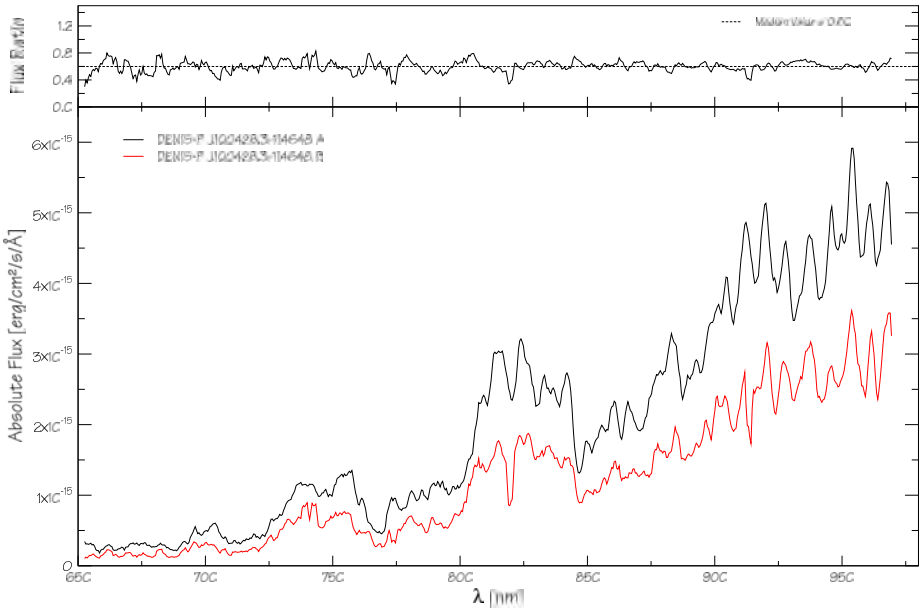

Figure 1.8 Optical Spectra of DENIS-P J100428.3-114648 A (black) & B (red) obtained with HST/STIS (smoothed via a boxcar with a width of 5 pixels). The upper plot shows the flux ratio as a function of the wavelength and its median value.

1.3 Analysis

The K I absorption lines at 766.5 and 769.9 nm are known to be sensitive to the surface gravity of the objects: their strength decreasing with increasing surface gravity. Figure 1.11 shows that the ratios of the EW(K I) of the primaries to that of the secondaries are very close to 1.0. This result indicates that the components of these multiple systems must have very similar surface gravities, as one could expect from the mass ratios obtained from the relative photometry.

2MASSW J1426316+155701 is noticeably further away from this line in comparison with the other objects, possibly[11] indicating that the surface gravity of the secondary is slightly lower than that of the primary. Close et al. (2002a) estimated the masses of the individual components of this object to be 0.066 and 0.074 $M_{\odot}$. Assuming these masses, Figure 1.10 shows that in order for the secondary to have a surface gravity lower than that of its primary, the system must be younger than 1∼1.5 Gyr. Although the uncertainties are large and the significance of this comparison not so strong, it is interesting to note that this value is consistent with the age of $0.8^{+6.7}_{-0.2}$ Gyr reported by Close et al. (2002a) from the luminosity. DENIS-P J035726.9-44173 is also noticeably further away, but as shown in the Figure, the two lines of the doublet are barely resolved in the spectrum of the secondary and the value reported are not reliable enough to enable further analysis.

[11] the deviation of this point to the line is well within the uncertainties

Table 1.2. K I atomic lines EW of binary ultracool dwarfs components

Object	K I line 7665	7699
2MASSW J1311391+803222 A	8.2	3.8
2MASSW J1311391+803222 B	7.2	4.2
2MASSW J1426316+155701 A	6.4	4.6
2MASSW J1426316+155701 B	10.7	6.7
DENIS-P J035726.9-44173 A	···	3.4[1]
DENIS-P J035726.9-44173 B	···	2.1[1]
DENIS-P J100428.3-114648 A	2.5	2.4
DENIS-P J100428.3-114648 B	1.9	2.8

Note. — All units are in angströms. 1-σ uncertainties are ∼0.5 Å.

[1]The S/N is poor and the uncertainties are large.

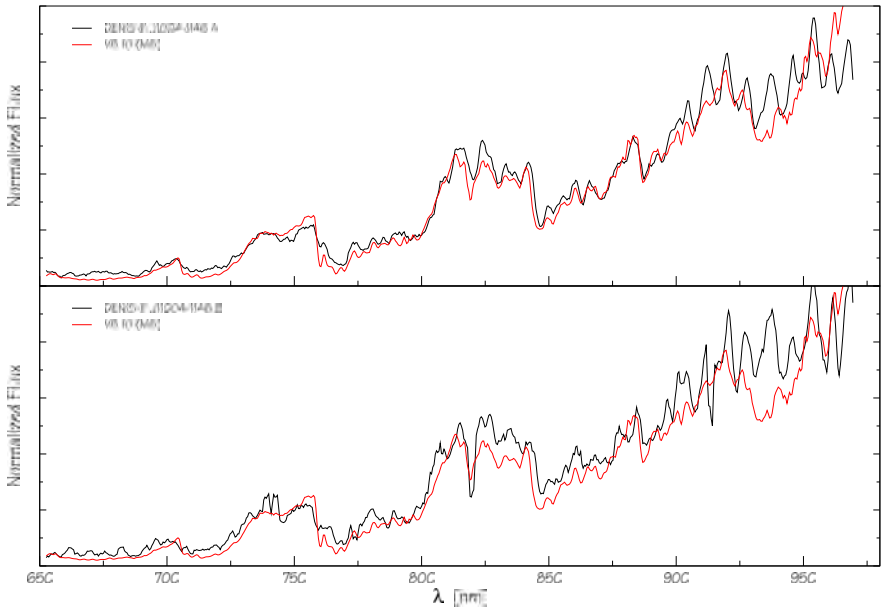

Figure 1.9 Spectral types of DENIS-P J100428.3-114648 A (upper panel) & B (lower panel). The spectra of A and B (black) are compared to that of field very low stars (red). The best match indicates a spectral type of M8±1 for both A and B.

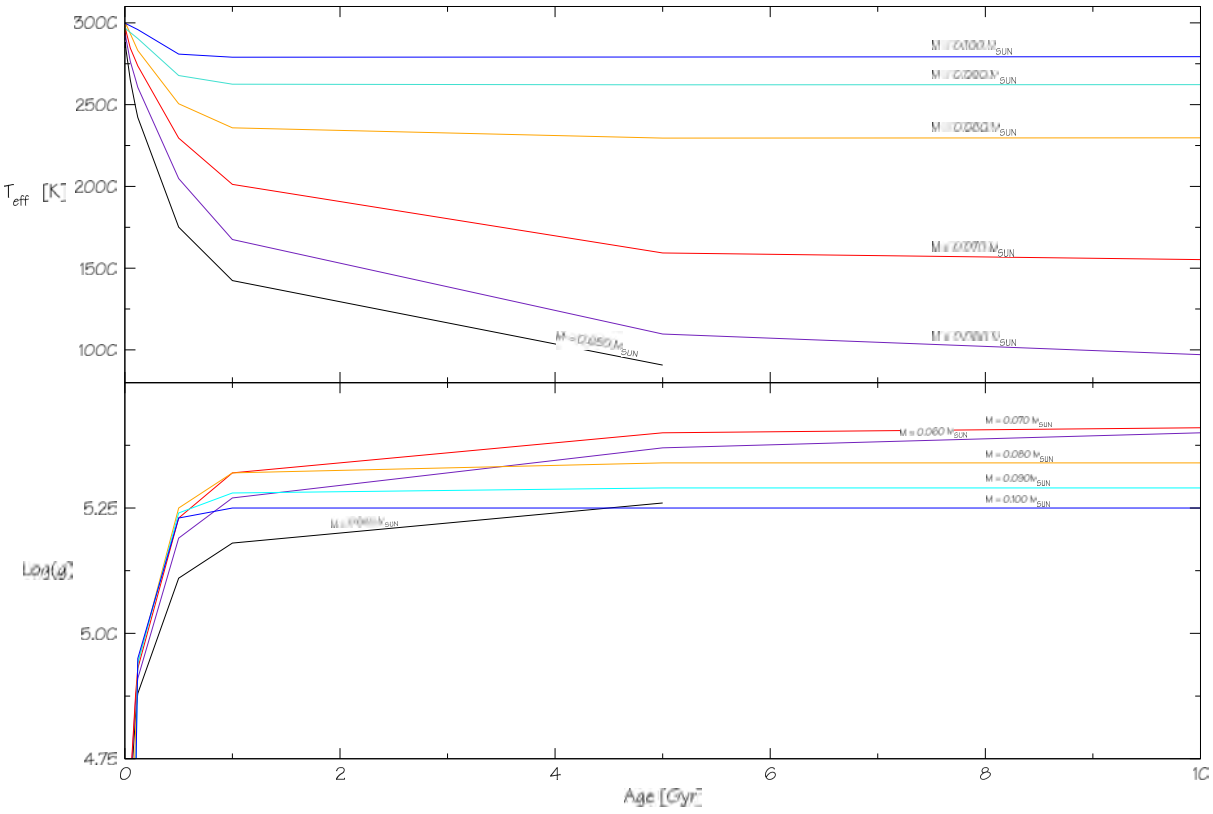

Figure 1.10 T_{eff} vs Age (top panel) & $Log(g)$ vs Age (bottom panel) relation from the DUSTY models, represented for different masses ranging from 0.050 to 0.1 M$\odot$.

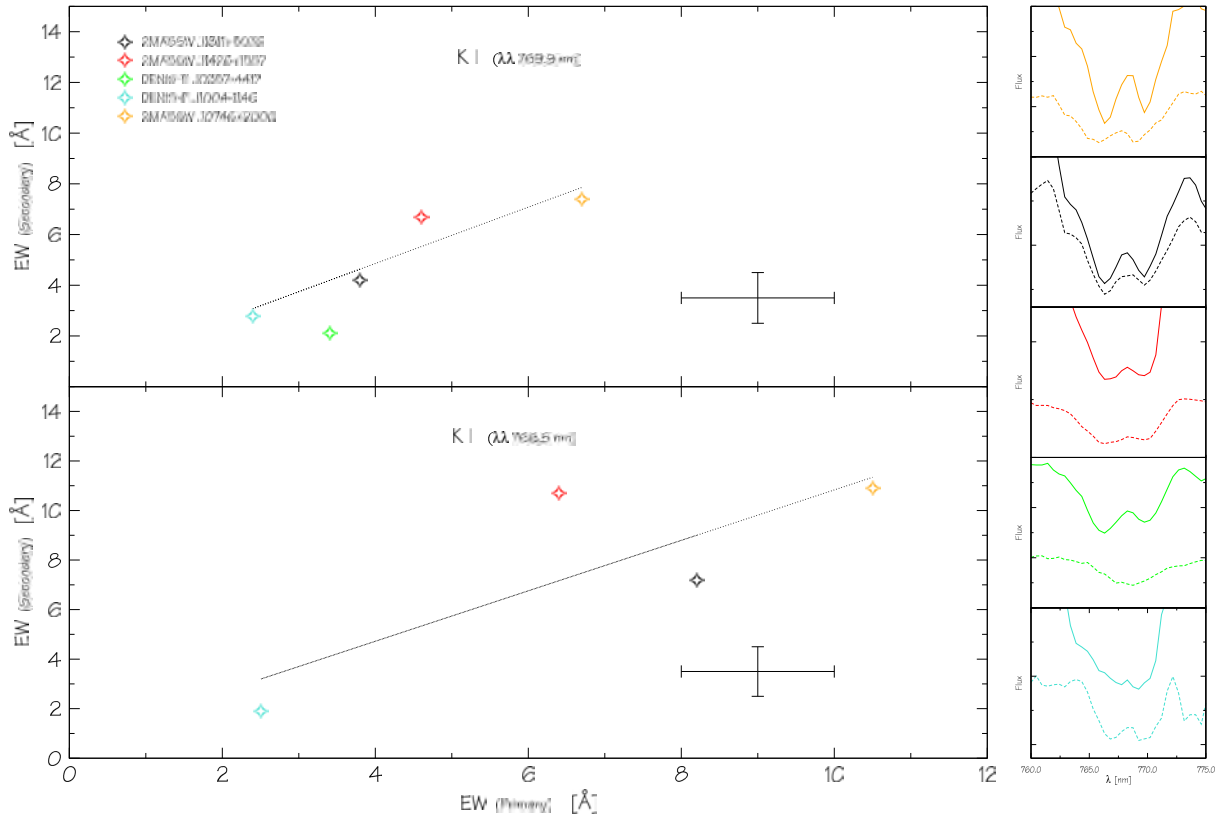

Figure 1.11 EW(K I) of the primary vs that of the secondary for the 4 field brown dwarfs. The K I doublet is known to be a gravity sensitive feature of the optical spectrum of ultracool dwarfs. This figure shows the correlation for the equivalent widths of these lines for the secondary and the primary of the co-eval binaries of our sample. The slopes are equal to 1.0 and 1.1, and therefore indicates that the primaries and secondaries have almost equal surface gravities. The individual lines of the doublet only barely appear in DENIS-P J0357-4417 spectrum (in green), and the corresponding values are not very reliable. 2MASSW J0746+2000 is presented in detailed in Chapter 2 of this Part.

Chapter 2

Determination of the dynamical mass of a binary L dwarf

2.1 2MASSW J0746425+2000321

2MASSW J0746425+2000321 has been observed and reported in several catalogues and articles. It has been identified as a L0.5 dwarf by Kirkpatrick et al. (2000), and suggested to be a binary by Reid et al. (2000) based on its position in a colour-magnitude diagram. It has been resolved as a multiple system by Reid et al. (2001) with a separation of $0\farcs22$ and a position angle (P.A) of 15°, a measurement later corrected by Bouy et al. (2003) to $0\farcs219\pm0\farcs003$ and P.A=$168\fdg8\pm0\fdg3$. 2MASSW J0746425+2000321 has been reported in several surveys, such as USNO-B (Monet et al. 2003), GSC2.2, and 2MASS (Cutri et al. 2003). Table 2.1 gives an overview of the astrometric and photometric properties of 2MASSW J0746425+2000321 as reported in these catalogues. Dahn et al. (2002) and the USNO-B.1 catalogue both report a measurement of the proper motion of this objects, with μ_α=-370±4 mas yr^{-1} and μ_δ=-42±4 mas yr^{-1} (USNO-B.1) and μ_α=-374±0.3 mas yr^{-1} and μ_δ=-58±0.3 mas yr^{-1} (Dahn et al. 2002). These measurements confirm that 2MASSW J0746425+2000321 is a common proper motion pair. Such a proper motion indeed implies a motion of $\sim1\farcs5$ during the 4 years we made the follow up observations, whereas the separation between the two components varied only of $\sim0\farcs1$. Using high resolution spectra obtained at Keck, Reid et al. (2002) measured a rotational velocity of 24 km/s. Using VLT/UVES high resolution spectra, Bailer-Jones (2004) measured a rotational velocity ranging between $25.6\leq v\sin i \leq30.6$ km/s, corresponding to a period between $1.73\leq T\leq3.71$ hours. Both Clarke et al. (2002) and Gelino et al. (2002) report photometric variability, which they attribute mainly to the formation of clouds in the upper layers of the atmospheres. Dahn et al. (2002) measured its distance using trigonometric parallax at 12.21±0.05 pc.

2.2 Observation and data processing

Table 2.2 gives a log of all the observations we use in this study.

Table 2.1. 2MASSW J0746425+200032 in different catalogues

Date DD/MM/YYYY	R.A (J2000)	Dec. (J2000)	Uncert.	Filter	mag. [mag]	Source	Ident.
01/01/1984[1]	07 46 42.5	+20 00 32.6	±0.″1	R1	18.28	USNO-B1.0	USNO-B1.0 1100-0150847
				B2	21.7		
				R2	17.87		
01/01/1998	07 46 42.55	+20 00 32.14	±0.″3	R	17.6	GSC2.21	GSC 2W 22110125398
05/12/1997	07 46 42.56	+20 00 32.2	±0.″1	J	11.759	2MASS	2MASSW J07464256+2000321
				H	11.007		
				K	10.468		
06/12/2002				L'	11.19	Leggett et al. (2002)	

[1]Mean epoch of observation

2.2.1 High Angular Resolution imaging with HST/ACS and STIS

High angular resolution images have been obtained with the HST Advanced Camera for Survey (ACS, Pavlovsky et al. 2003) and Space Telescope Imaging Spectrograph (STIS, Kim Quijano et al. 2003). We observed 2MASSW J0746425+2000321 using the ACS and its High Resolution Channel (HRC) in three different optical filters (F625W, F775W and F850LP), and STIS in the long-pass filter. 2MASSW J0746425+2000321 is clearly resolved on both sets of data (see Figure 2.1), and we were able to get precise astrometric and photometric measurements. The data have been analyzed using the custom-made program performing PSF fitting describe in Section 1.2.2 of Chapter 1 in Part I, and in Annex B.

2.2.2 High Angular Resolution imaging with VLT/NACO

We also obtained high angular resolution images using the ground based facilities offered by ESO on Cerro Paranal on 2003 February 18th and 2003 March 22nd. The VLT on *Yepun* uses NACO, an adaptive optics platform (Rousset et al. 2003; Lenzen et al. 2003; Brandner et al. 2002) to achieve diffraction limited images. NACO offers the possibility to use an infrared wavefront sensor, and is therefore ideally suited for the study of ultra-cool and red objects. Its CONICA array offers a 0.″01326±0.″001 pixel-scale that provides critical Nyquist sampling of the diffraction limited images of the telescope at these wavelengths. Its absolute orientation is known to within ∼1°.

The atmospheric conditions during the observations were good (respectively λ/r_0=0.″62 and airmass=1.5, and λ/r_0=0.″67 and airmass=1.4), and very sharp images in K_S (first observation) and J, H and K_S (second observation) were obtained with strehl ratios of $S_r(K_S)$ ∼30% (first obs.) and $S_r(J)$ ∼13% ,$S_r(H)$ ∼27%, and $S_r(K_S)$ ∼46% (last obs.). Figure 2.1 shows the two K_S images obtained during these two nights.

During the last observation, a PSF star was also acquired in order to perform accurate photometry of the adaptive optics data of the corresponding night. The object, DENIS-P J131500.9-251302 (spectral type ∼M8, J=15.2, H=14.54 and K_S=14.02 mag), was observed under better conditions (λ/r_0=0.″43 and airmass=1.03) with a strehl ratio of $S_r(H)$ ∼10%, and $S_r(K_S)$ ∼40%. Unfortunately it was not observed in J. We performed the photometry using standard DAOPHOT PSF fitting photometry. The results are summarized in Table 2.3. Although the PSF star has a spectral type earlier than 2MASSW J0746425+2000321 and was observed at much better airmass and better seeing, the relative photometry we obtain in H and K_S is in very good agree-

Table 2.2. Observation log. for 2MASSW J0746425+2000321

Imaging				
Instrument	Filter	Exp. Time [s]	Date Obs. DD/MM/YYYY	Pixel Scale [″]
HST/WFPC2-PC	F814W	50	25/04/2000	0.″0455
Gemini North/Hokupa	J	120	07/02/2002	0.″0199
Gemini North/Hokupa	H	720	07/02/2002	0.″0199
Gemini North/Hokupa	K	120	07/02/2002	0.″0199
HST/ACS-HRC	F625W	960	21/10/2002	0.″0250[1]
HST/ACS-HRC	F775W	440	21/10/2002	0.″0250[1]
HST/ACS-HRC	F850LP	340	21/10/2002	0.″0250[1]
VLT/NACO	K_S	0.4	18/02/2003	0.″0148[2]
VLT/NACO	J	10	22/03/2003	0.″0148[2]
VLT/NACO	H	5	22/03/2003	0.″0148[2]
VLT/NACO	K_S	5	22/03/2003	0.″0148[2]
Keck I/NIRC	K_S	20	04/12/2003	0.″0203
HST/STIS	longpass	10	09/01/2004	0.″0508
Spectroscopy				
Instrument	Wavelength Range [nm]	Exp. Time [s]	Date Obs. DD/MM/YYYY	Dispersion [Å/pixel]
HST/STIS	525–1300	1980	09/01/2004	4.92

[1]Effective value on the processed images, slightly different from the 0.″028×0.″025 given in the manual.

[2]Effective value on the processed images, slightly different from the 0.″01326 given in the manual.

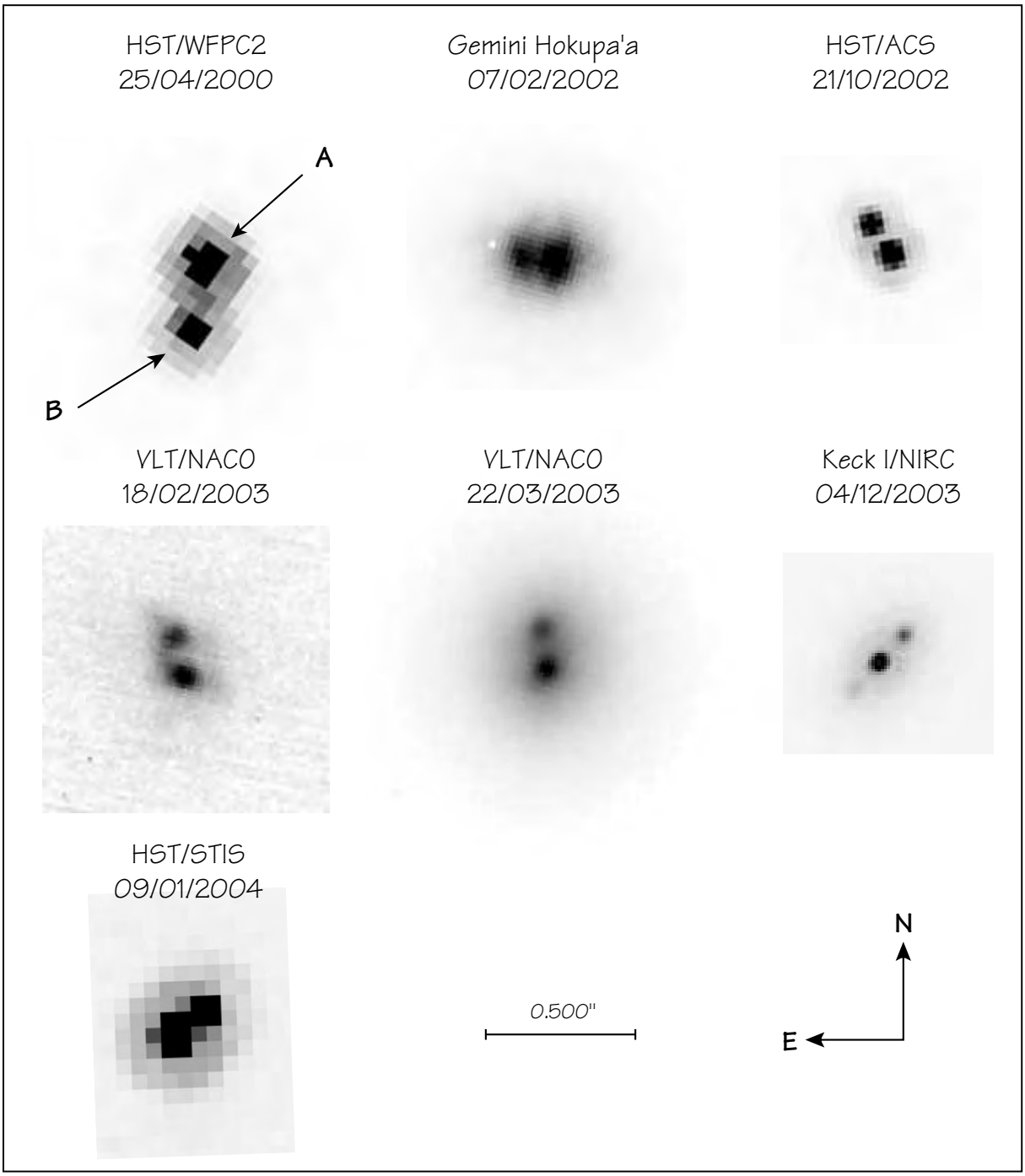

Figure 2.1 Images of 2MASSW J0746425+2000321A and B obtained at different epochs with HST, Gemini, NACO and Keck I. The scale and the orientation are the same for all images, and indicated on the figure.

Table 2.3. Relative Photometry of 2MASSW J0746425+2000321AB

Date DD/MM/YYYY	Instrument	Filter	Mag. Prim. [mag]	ΔMag. [mag]	Source
25/04/2000	HST/WFPC2	F814W	15.41±0.15	1.00±0.09	(1)
07/02/2002	Gemini North/Hokupa'a	J	12.19±0.07	0.60±0.20	(2)
07/02/2002	Gemini North/Hokupa'a	H	11.54±0.11	0.48±0.15	(2)
07/02/2002	Gemini North/Hokupa'a	K'	11.05±0.09	0.44±0.15	(2)
21/10/2002	HST/ACS	F625W	18.81±0.05	0.48±0.03	(3)
21/10/2002	HST/ACS	F775W	15.98±0.05	0.68±0.04	(3)
21/10/2002	HST/ACS	F850LP	14.24±0.05	0.76±0.04	(3)
22/03/2003	VLT/NACO	H	11.55±0.08	0.46±0.15	(3)
22/03/2003	VLT/NACO	K_S	11.06±0.09	0.42±0.15	(3)
04/12/2003	Keck I/NIRC	K_S	11.03±0.03	0.52±0.03	(3)

Note. — Source: (1) Chapter 1 of Part I; (2) Close et al. (2003); (3) this work

ment with the one reported by Close et al. (2003) with Gemini North/Hokupa'a and the one we measure with Keck I/NIRC (K_S band).

2.2.3 Speckle Observations with Keck

On 2003 December 04, we obtained K band speckle observations of our target at the 10 m Keck I telescope with the facility instrument NIRC (Kleinmann et al. 1994). With its re-imaging optics (Matthews et al. 1996), this 256×256 near-infrared array offers a $0\farcs0203 \pm 0\farcs0003$ pixel scale that provides Nyquist sampling of the diffraction limit of the telescope at this wavelength (about $0\farcs05$); its absolute orientation is known to within 1°. Several stacks of 200 short-integration exposures were obtained ($t \sim 0.1$ s, i.e., fast enough to effectively "freeze" the atmospheric turbulence and retain the high-angular resolution information in the image), and similar stacks on two calibration point sources were obtained immediately before and after our target. Standard speckle data reduction routines were applied to the data; we refer the reader to Ghez (1993) and Patience et al. (1998) for more details and only summarize briefly the various stages involved in the data reduction process. Each individual exposure is first sky subtracted, flat-fielded and bad pixel-corrected; its power spectrum is then calculated. The power spectra are median-averaged over each stack and divided by that of the calibrator. A 2-D sinusoidal function is then fitted to the power spectrum to determine the binary properties: separation, position angle and flux ratios. Uncertainties are estimated from the standard deviation of the parameters extracted

Table 2.4. Relative Astrometry of 2MASSW J0746425+2000321AB

Date	Time[1]	Sep.[2]	P.A[2]	Instrument	Source[3]
DD/MM/YYYY	HH/MM/SS	[mas]	[°]		
25/04/2000	08:14:14	219±3	168.8±0.8	HST/WFPC2	(1)
07/02/2002	09:48:55	121±8	85.7±3.5	Gemini North/Hokupa'a	(2)
21/10/2002	23:10:43	119.5±1	33.9±0.5	HST/ACS	(3)
18/02/2003	01:40:45	131.3±3.9	13.8±1.9	VLT/NACO	(3)
22/03/2003	01:22:00	123.5±2.1	4.6±1.0	VLT/NACO	(3)
04/12/2003	15:15	126.5±1.8	317.9±0.7	Keck I/NIRC	(3)
09/01/2004	18:51:45	134.5±3	311.1±1.2	HST/STIS	(3)

[1]The uncertainty corresponds to the exposure time (see Table 3.1)

[2]1-σ uncertainties (combined instrumental and measurement)

[3]Source: (1) Chapter 1 of Part I; (2) Close et al. (2003); (3) this work

from all stacks. There is a 180° ambiguity in the position angle of the binary as derived through power spectrum analysis, but this can be resolved by shift-and-adding all individual exposures using the brightest speckle as a reference. The resulting image shows the companion to be roughly to the Northeast of the primary and the astrometric accuracy of the power spectrum analysis is much higher. The results obtained are reported in Tables 2.3 and 2.4 and Figure 2.1 shows the final image. As mentioned above, the difference of magnitude is in very good agreement with the previous measurements within the uncertainties.

2.2.4 High Angular Resolution/Low Spectral Resolution Spectroscopy

We obtained the spatially resolved spectra of each component of the multiple system by aligning the slit of STIS along the axis of the binary. Scheduling constraints of HST made it difficult to get long slit STIS observations of 2MASSW J0746425+2000321 at a particular roll angle of HST. In order to ease scheduling, a range of admitable roll angle was defined. This combined with the relatively rapid orbital motion of 2MASSW J0746425+2000321 meant that the entrance slit of STIS was not optimally aligned with the position angle of 2MASSW J0746425+2000321 at the time of the observations. Since the size of the slit we used ($0\farcs2$) is larger than the separation of the binary ($\sim 0\farcs125$), we could nevertheless obtain a resolved 2-D spectrum and perform an extraction of the two spectra. The effects on the spectral analysis can be the following: since the red and the blue photocentres of each component are not symmetrically centred in the slit,

the dispersion of the red and blue parts of the spectrum suffers differently from obstruction by the slit. Since the position of the photocentres and the dispersion of the light depends on the wavelength, the loss in flux also varies with the wavelength. This effect produces a "bluer" spectrum for the secondary.

The separation between the two spectra is about 2 pixels, whereas the full width at half maximum (FWHM) of the line spread function (LSF) varies between 1.0 and 1.2 pixel, so that the two spectra are barely resolved. We used the same technique as described in Section 1.2.1 on page 107 to extract the individual spectra.

2.3 Orbital parameters and determination of the total mass

We used three different and independent custom-made programs to determine the best fitting orbital solution for 2MASSW J0746425+2000321 and the uncertainties on each of the fitted parameters. The orbit can be entirely described by seven independent parameters: semi-major axis (a), orbital period (P), inclination (i), eccentricity (e), position angle of the ascending node (Ω), angle between the ascending node and periastron (ω) and time of periastron passage (T_0). With seven two-dimension astrometric data-points, this fully-constrained problem has seven free parameters. The total mass of the system can be derived from the orbital period and semi-major axis through Kepler's Third Law.

2.3.1 "*Amoeba*" method

The first method minimizes in the nonlinear 7-dimensions function by downhill simplex method, using the *amoeba* algorithm (see e.g Press et al. 1992, for a description of the method and algorithm.). It fits all seven orbital parameters simultaneously, taking into account non-equal errors of the measurements. The *reduced*-χ^2 of 1.41 ensures that the fit is satisfactory (see section 2.3.4 below). The results are shown in Figure 2.3 and Table 2.5. No uncertainties on the derived parameters are available with this method.

2.3.2 Iterative method

This method uses 50 000 independent starting points that consist of a set of the 7 parameters being randomly chosen from their entire range of possible values. For each starting point, a Powell convergence algorithm minimizing the total χ^2 (Press et al. 1992) modifies simultaneously all 7 parameters until it converges to a local minimum. Once convergence for all 50 000 sets of initial guesses has been achieved, we read through the output file to find the absolute minimum of the χ^2 function, which reveals the best-fitting orbital solution. Our best-fitting solution, illustrated in Figure 2.3 has a satisfying *reduced*-χ^2 value of 1.38.

Uncertainties for each parameters are defined by the range of possible values indicated by all solutions with *total* χ^2 between χ^2_{min} and $\chi^2_{min} + 4$. These represent the 95.4% confidence level for each parameters. Due to the highly non-linear behavior of the equations of orbital motion, the uncertainties do not follow a Gaussian statistics and nor even symmetric about the best fit. Note that the uncertainties are derived under the assumption that all parameters are independent, which is not correct. For instance, the uncertainties derived for P and a would yield an uncertainty on the system mass on order of $\pm 0.055\,M_\odot$, $\sim$4 to 9 times larger than we actually derived here. Therefore, the uncertainties quoted here are only valid if they are used for one parameter at a time. Figure 2.2 shows that this is because the fitted values of P and a are tightly correlated and correspond to a very narrow range of possible masses. Although the orbit is not

perfectly known yet, the total mass is relatively precisely determined: $M_{tot}=0.146^{+0.016}_{-0.006}$ $M_\odot$, corresponding to 4∼11% uncertainty.

The uncertainty on the distance to the system translates into a separate 2.4% uncertainty (2-σ), or 0.035 $M_\odot$, on the system mass. The uncertainty on the orbital fitting is therefore the major source of uncertainty for this binary system since both sources of uncertainty (fit and distance) should be added in quadrature.

2.3.3 *ORBIT*

We also used the *ORBIT* program of Forveille et al. (1999), fully described in this article. Briefly, "*the program performs a least square adjustment to all available observations, with weights inversely proportional to the square of their standard errors [. . .] The program uses a Levenberg-Marquardt minimization algorithm (Marquardt 1963) [...] Standard errors for derived parameters are computed from the full covariance matrix of the linearized least square adjustment.*"

2.3.4 Reduced-χ^2 and uncertainties

The reduced-χ^2 values of ∼1.4 indicate that some of the uncertainties on the astrometric measurements may be slightly underestimated, although with only seven measurements for seven free parameters, such a value is statistically acceptable. Although rescaling the astrometric uncertainties to reach a reduced-χ^2 of 1.0 could be argued for, the diversity of the instruments used for this orbital analysis suggests that such a treatment would be at least as erroneous as it could be helpful. For the time being, we decided to stick to the quoted astrometric uncertainties to derive the uncertainties on the orbital parameters of the binary.

2.4 Discussion

2.4.1 Spectral Types, Effective Temperatures

The composite spectrum of 2MASSW J0746425+2000321 AB in the optical has been previously studied by Kirkpatrick et al. (2000), who derived a spectral type of L0.5.

In order to derive the spectral types of each component, we compared their STIS spectra, extracted with the procedure described in Section 2.2.4, with the spectra of field L dwarfs published by Martín et al. (1999b). As explained in this latter article, the relative strength of the TiO bands between 840–860 nm and the CrH and FeH bands between 860–880 nm are good indicators for the effective temperature changes. In later L dwarfs the TiO bands get weaker with respect to the CrH and FeH bands. Figures 2.4 and 2.5 shows the comparison. 2MASSW-J0746425+2000321 A is clearly very similar to the L0 field dwarf DENIS-P J090957.1-065806, while 2MASSW J0746425+2000321 B is between the L1 (DENIS-P J144137.3-094559) and L2 (Kelu 1) field dwarfs. We thus derive a spectral type of L0±0.5 and L1.5±0.5 for A and B, respectively. This is consistent with the spectral type obtained by Kirkpatrick et al. (2000), which is a blend of A and B. It is also consistent with the modest difference in brightness (see Table 2.3), which implies a difference in temperature of only 100 K according to the models of Chabrier et al. (2000).

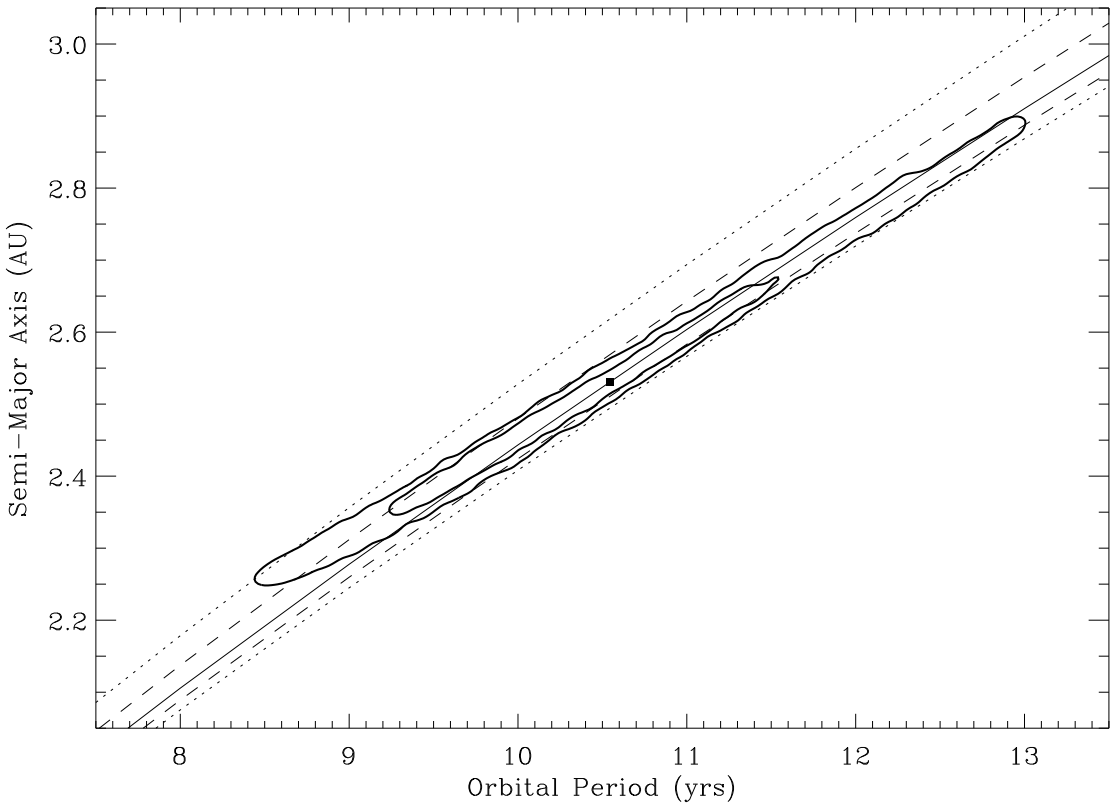

Figure 2.2 Ambiguity in the orbital parameters: the contours represent the solutions at 1- and 2-σ ($\Delta\chi^2$=1.0 and 4.0 respectively) in the semi-major axis vs period space. The lines corresponding to different masses indicate the levels of confidence at 68.7% and 95.4% (1- and 2-σ respectively). The filled square in the centre corresponds to the best fit. Although relatively large ranges are possible for the period and the semi-major axis, the range of corresponding acceptable masses is very narrow: between 0.143 and 0.153 $M_\odot$ at 1-σ (represented by dashed lines) and between 0.141 and 0.160 $M_\odot$ at 2-σ (dotted lines). Although the orbit is not perfectly known yet, the mass is relatively precisely determined, with a best value at $0.146^{+0.016}_{-0.006}$ $M_\odot$ (2-σ uncertainties, solid line).

Table 2.5. Orbital Parameters of 2MASSW J0746425+2000321AB

Parameter	Iterative Method[1]	*Amoeba* Method	*ORBIT*[2]
Total Mass [$M_\odot$]	$0.146^{+0.016}_{-0.006}$	0.1511	0.148
Period, P [days]	3850.9^{+904}_{-767}	3718	3863±609
Eccentricity, e	$0.41^{+0.08}_{-0.09}$	0.3999	0.417±0.062
Semi-major axis, a, [A.U]	$2.53^{+0.37}_{-0.28}$	2.50	2.55±0.25
Inclination, i [°]	$141.6^{+2.5}_{-3.4}$	141.65	140.65±2.29
Argument of Periapsis, ω [°]	$350.6^{+5.2}_{-5.9}$	350.15	350.65±3.58
Longitude of ascending node, Ω [°]	$20.7^{+9.9}_{-14.2}$	18.97	20.84±7.68
Periastron Passage, T_0 (year)	$2002.89^{+0.14}_{-0.09}$	2002.91	2002.84±0.07
reduced-χ^2 of the fit	1.38	1.41	1.46

[1]2-σ uncertainties, corresponding to a 95.4% level of confidence. These uncertainties do not include the uncertainty on the distance (∼2.4%, 2-σ). This latter one should be added in quadrature.

[2]2-σ uncertainties. These uncertainties do include the uncertainty on the distance, but assume that the uncertainty are linear, which is not the case here.

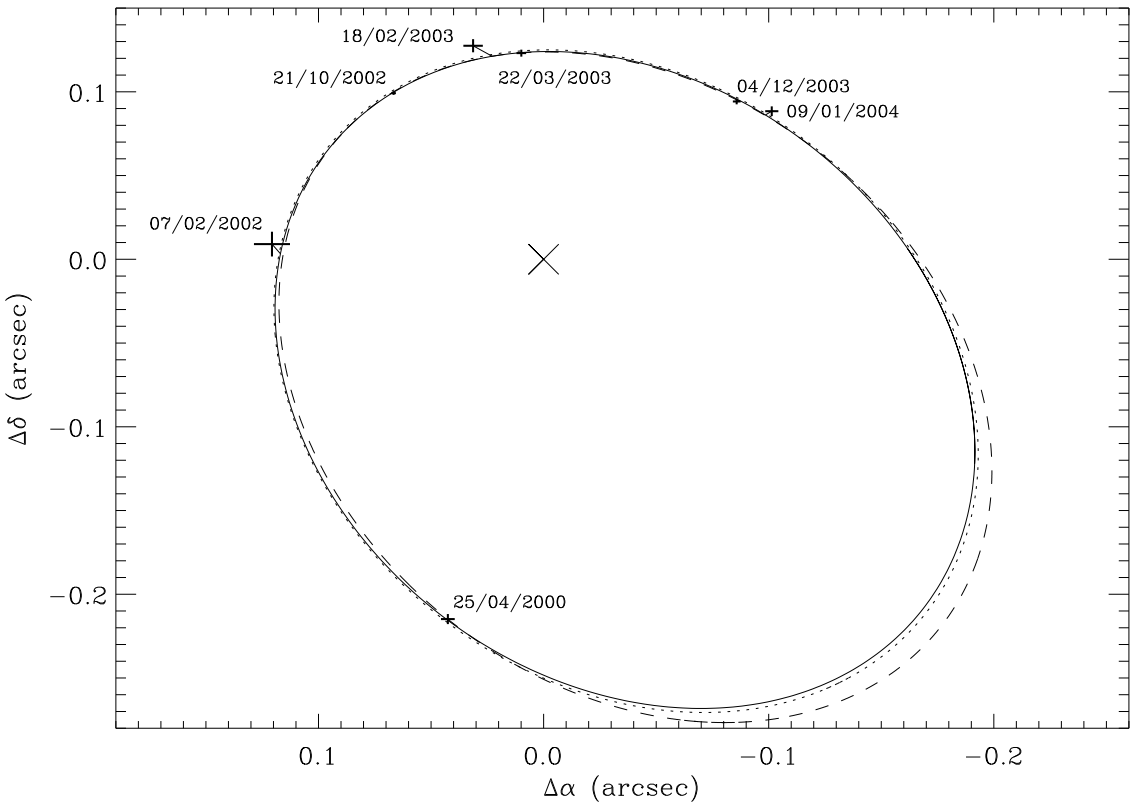

Figure 2.3 Positions of 2MASSW J0746425+2000321A and B and best fit of the orbit . The dotted curve represents the best bit orbit obtained with the *amoeba* method, and the solid curve the result obtained with the iterative method, and the dashed curve the solution given by *ORBIT*. It appears clearly that the three methods give close results, well within the uncertainties. The plus indicate the observations and their uncertainties, and the corresponding epoch is indicated. The central cross shows the position of the primary.

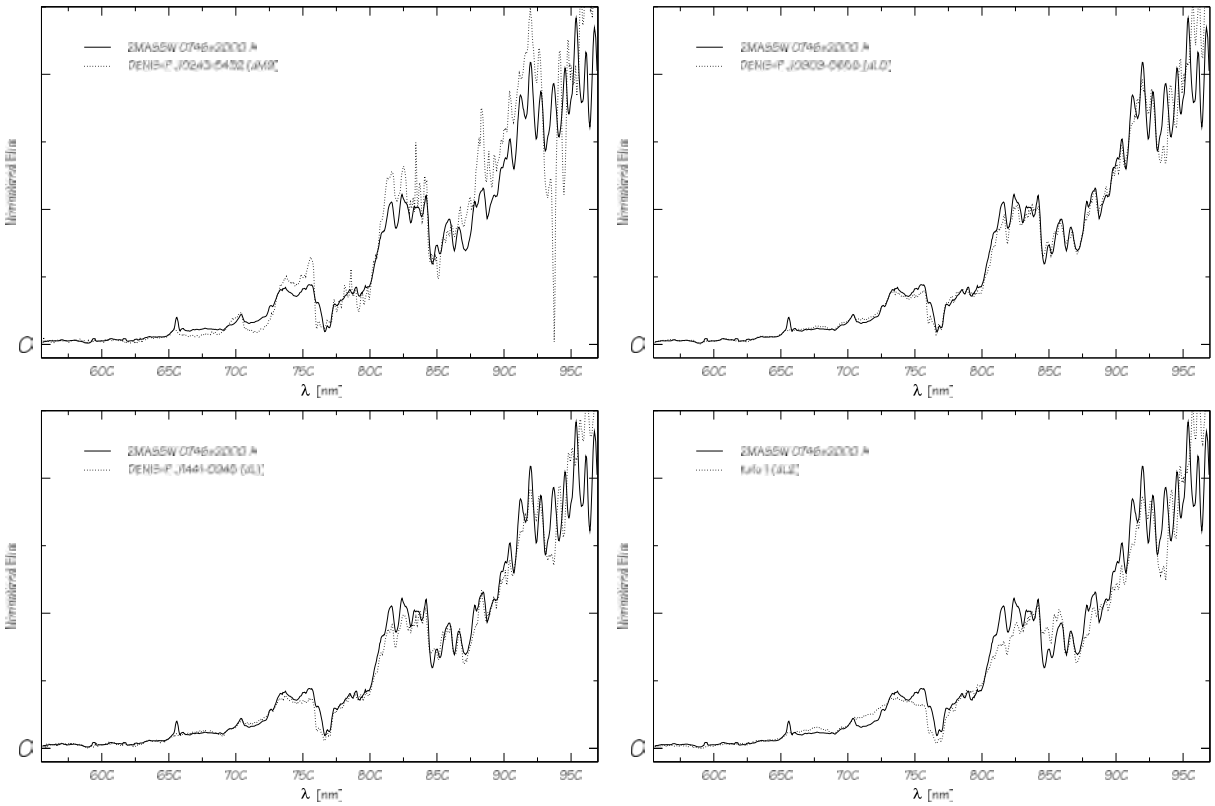

Figure 2.4 STIS optical low resolution spectrum of 2MASSW J0746425+2000321A compared to spectra of field ultra-cool dwarfs. The four plots show the STIS spectrum of 2MASSW J0746425+2000321A, smoothed via a boxcar (width = 5 pixels), and compared to: a) DENIS-P J024351.0-543219 (dM9); b) DENIS-P J090957.1-065806 (dL0); c) DENIS-P J144137.3-094559 (dL1); d) Kelu 1 (dL2). All spectra have been normalized at 840 nm. Spectra for the field dwarfs from Martín et al. (1999b).

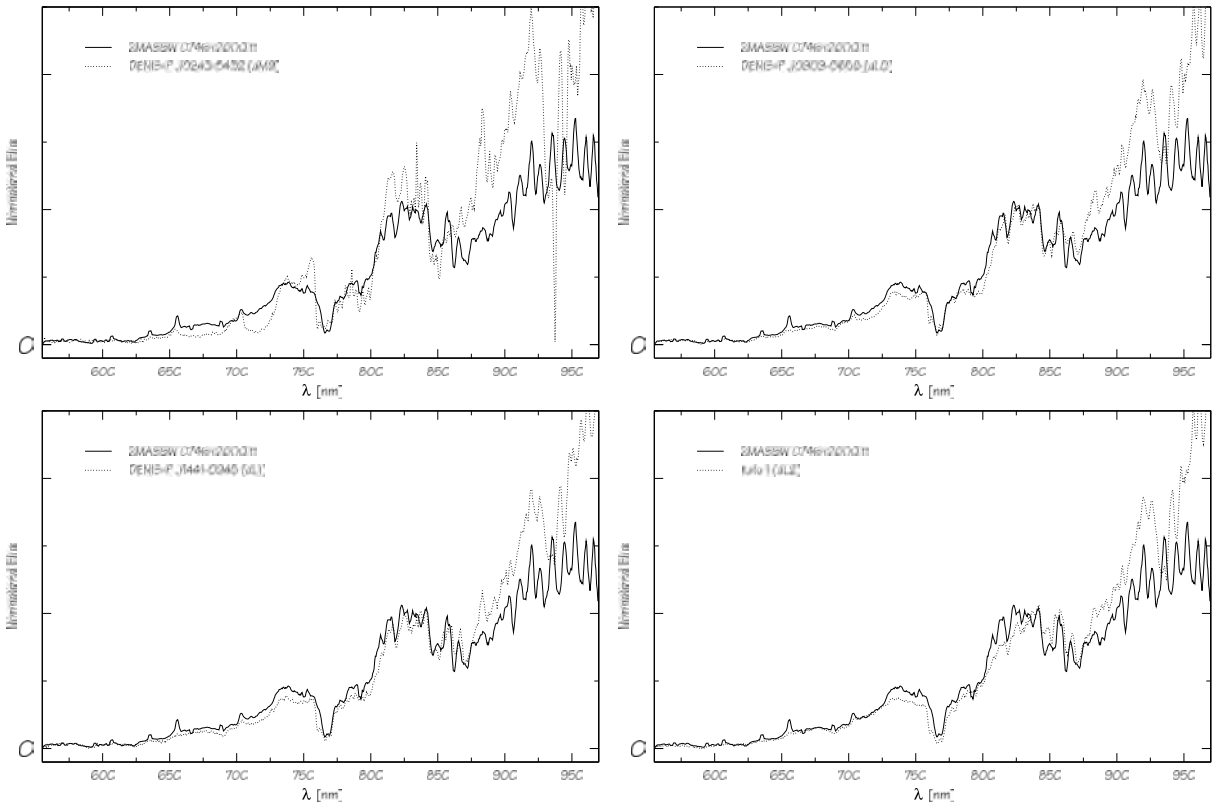

Figure 2.5 Same as Figure 2.4 but for 2MASSW J0746425+2000321B

Table 2.6. Atomic lines in the spectra of 2MASSW J0746425+2000321A and B

	K I Wavelength		Cs I Wavelength		Na I D Wavelength[1]
Object	7665	7699	8521	8943	8183-8195
2MASSW J0746425+2000321A	22.6	17.4	2.1	0.99	8
2MASSW J0746425+2000321B	19.0	16.4	...	...	5

Note. — All units are in angströms. 1-σ uncertainties are $\sim$0.5 Å.

[1]Corresponds to the blend of the 8183 and 8195 Å doublet.

2.4.2 Spectral Features

The main emission lines present in the primary's spectrum is Hα (EW=-25.0$\pm$0.5 Å, 1-σ). The spectrum of the secondary is more noisy but the Hα emission line appears clearly, with an equivalent width of EW=-18.0$\pm$0.5 Å. From their high-resolution spectra, Reid et al. (2002) reported a Hα emission of -1.2 Å for the unresolved system. The difference between the two measurements indicates that 2MASSW J0746425+2000321 A and B display some chromospheric and/or magnetic activity. Li I absorption is not detected in any of the two components with an upper limit of $\sim$1.5 Å. Reid et al. (2002) did not detect any Li I absorption with an upper limit of detection at $\leq$0.5 Å. The presence of strong resonance doublets of alkali elements (K I at 766.5 and 769,9 nm; Na I at 818.4 and 819.5 nm; and Cs I at 852.1 and 894.3 nm) as well as strong metallic molecular band-heads (CrH at 861.1 nm and FeH at 869.2 nm) is characteristic for L-dwarfs (Martín et al. 1997). The measurements of equivalent widths of the main atomic lines are reported in Table 2.6. It is interesting to note that the equivalent width we measure for Cs I at 852.1 nm for the primary corresponds to an effective temperature of $\sim$1900–2000 K in the effective temperature scale of Basri et al. (2000), therefore in good agreement with the effective temperature derived by Schweitzer et al. (2001) from their comparison of low and high resolution Keck spectra with the DUSTY models.

2.4.3 Colour-Magnitude Diagrams

Figure 2.6 shows a colour-magnitude diagram of 2MASSW J0746425+2000321 AB, 2MASSW-J0746425+2000321 A and 2MASSW J0746425+2000321 B, and compares with the isochrones of the most recent DUSTY models for solar metallicity. To convert the observed magnitudes to absolute magnitudes we used the trigonometric parallax reported by Dahn et al. (2002).

The position of 2MASSW J0746425+2000321A shows that the age ranges between 150 and 500 Myr, thus relatively young. This is not consistent with the very high surface gravity obtained by Schweitzer et al. (2001). They used high and low resolution unresolved spectra and compared it with the DUSTY atmospheric models of Allard et al. (2001). Using a χ^2-fitting algorithm, they obtain an effective temperature of 2000 K and a surface gravity log g=6.0 from their low

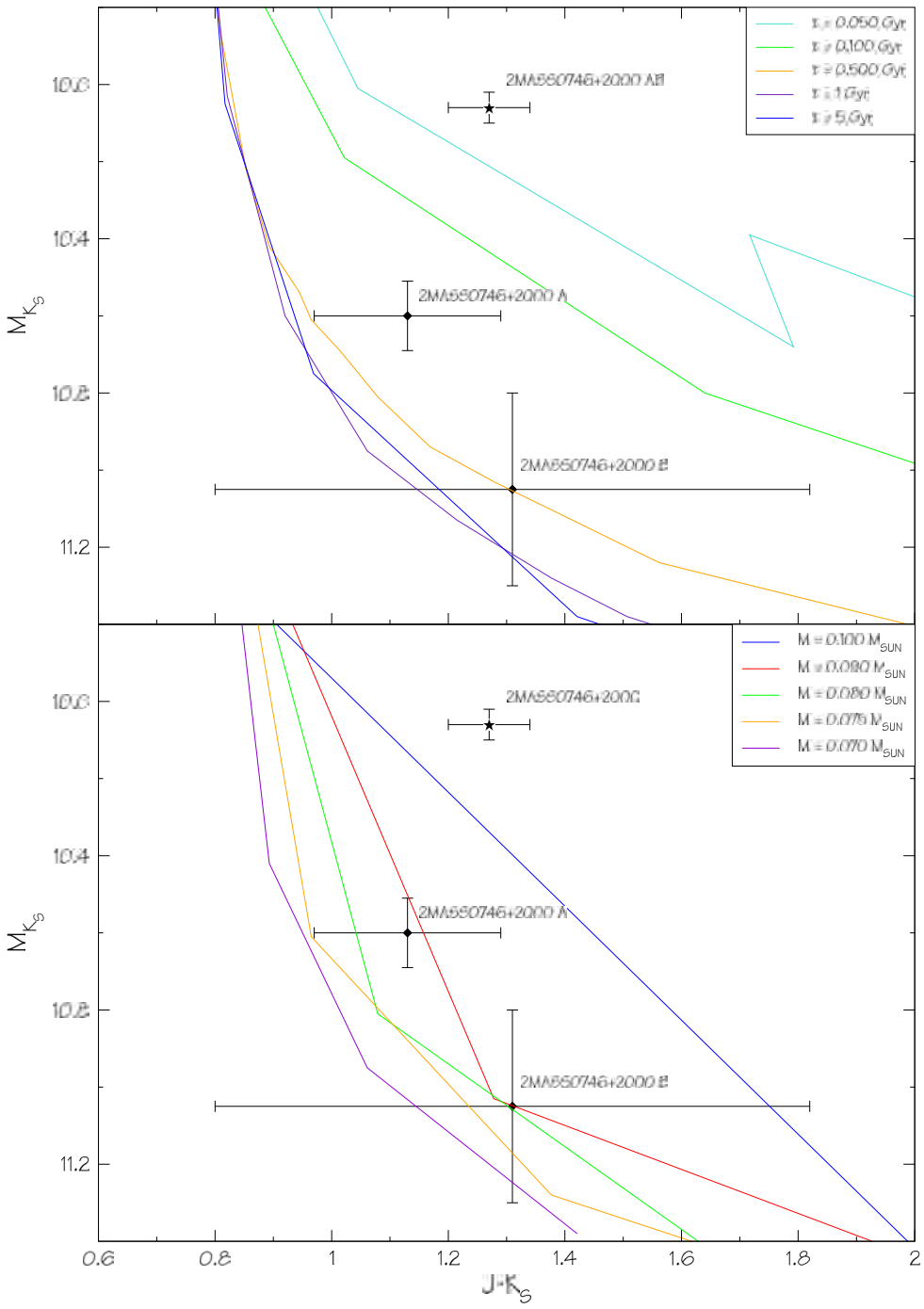

Figure 2.6 Colour-Magnitude diagrams M_{K_S} vs $(J - K_S)$ displaying the location of 2MASSW J0746425+2000321A, B and AB (combined light). The 1–σ combined uncertainties include the uncertainty on the distance. Isochrones of the DUSTY models (Chabrier et al. 2000) are over-plotted for different ages (upper panel) and different masses (lower panel).

resolution spectra. From their high resolution spectra, they obtain an effective temperature of 1900∼2000 K and a surface gravity log g=5.0∼5.5. The temperatures are in good agreement with the spectral types and colours we report here, but the surface gravity is too high for the young age. This is probably because the DUSTY models overestimate the dust effects. As a consequence, the strength of the alkali lines in the optical decreases, and the surface gravity is biased toward higher values.

The mass of the primary ranges between 0.075 and 0.095 $M_{\odot}$, while the mass of the secondary has large error bars and ranges between 0.055 and 0.100 $M_{\odot}$. The total mass of the system therefore ranges between ∼0.130 and ∼0.190 $M_{\odot}$, which is consistent with the dynamical mass considering the large uncertainties in the H-R diagram.

For the secondary's mass it appears more appropriated to use the mass of the primary from the H-R diagram, which has reasonable uncertainties, together with the very precise dynamical total mass. This yields to a mass between 0.052 and 0.072 $M_{\odot}$, therefore clearly substellar. The absence of lithium absorption in the spectra gives also a constraint on the lower limit of the mass. According to the DUSTY evolutionary models, Lithium should be depleted for masses greater than 0.075 $M_{\odot}$ at 150 Myr and masses greater than 0.060 $M_{\odot}$ at 500 Myr. The mass of the secondary must therefore be greater than 0.060, and ranges between $0.060 \leq M_B \leq 0.072$ $M_{\odot}$.

The system is thus very likely made of a brown dwarf orbiting a slightly more massive very low mass star. Both objects are very close to the stellar-substellar boundary.

Chapter 3

A possible triple system: DENIS-P J020529.0-115925

In this chapter we present results showing that the multiple system DENIS-P J020529.0-115925 is likely to be a triple system of very low mass stars and brown dwarfs. The secondary of this previously known binary system shows a clear elongation on six images obtained at six different epochs. Significant residuals remain after PSF subtraction on these images, characteristic of multiplicity, and indicating that the secondary is probably a double itself. Dual-PSF fitting shows that the shape of the secondary is consistent with that of a binary system. These measurements show that the probability that DENIS-P J020529.0-115925 is a triple system is very high. The photometric and spectroscopic properties of the system are consistent with the presence of three components with spectral types L5, L8 and T0.

3.1 Introduction

Multiple systems are important tests for the models of formation and evolution of very low mass stars and brown dwarfs. The binary fraction reported recently by Bouy et al. (2003); Burgasser et al. (2003); Close et al. (2003); Gizis et al. (2003); Martín et al. (2003) for very low mass stars and brown dwarfs (between 10–15%) cannot be well reproduced by the so-called "photo-evaporation" and "embryo-ejection models", which generally predict a much lower binary frequency (<5%; see Part III, and e.g Kroupa & Bouvier 2003, for a discussion on the different scenarios of formation mentioned here). On the other hand the "star-like" model cannot explain the observed distribution of separation (all less than 20 A.U, with a peak around 4–8 A.U), and of mass ratios (with a strong lack of multiple systems with large mass ratios). The overall process of formation of brown dwarfs is still not well understood., and further improvements of the current simulations are required in order to fit the observations. The existence itself of an old triple system made of brown dwarfs gives already extremely important and new constraints on these models, since no such object had been observed until now.

In section 3.2, we will present a summary of the known properties of DENIS-P J020529.0-115925. In section 3.3 we will describe the observations. In section 3.4, we will present the analysis of the data leading to the discovery of a possible third component, and in section 3.5 we will discuss about the triple system and its properties.

3.2 DENIS-P J020529.0-115925

DENIS-P J020529.0-115925 is L5 field very low mass star (Martín et al. 1999b). It was discovered by Delfosse et al. (1997) and first resolved as a binary by Koerner et al. (1999) using Keck images. This object has been well studied and observed, and is reported in several surveys (DENIS, and 2MASS, as)2MASSW J0205293-115930. Several authors (Delfosse et al. 1997; McLean et al. 2001; Burgasser et al. 2003) report methane absorption in their spectra, which implies a mass below the sub-stellar limit and an effective temperature less than 1800 K, as stated by Schweitzer et al. (2002). Tokunaga & Kobayashi (1999) report similar absorption features in their spectra but attribute it to H_2 rather than CH_4. Martín et al. (1997) reported a non-detection of lithium absorption from high resolution optical spectra, and inferred a lower limit on the mass of DENIS-P J020529.0-115925 A of 60 Jupiter masses. Its distance (19.76±0.57 pc) and proper motion (437.8±0.8 mas/yr with P.A=82.8±0.1°) have been measured via trigonometric parallax (Dahn et al. 2002). Basri et al. (2000) also measured its rotational velocity (22±5 km/s), and from the Cs I and Rb I absorption, they estimated its temperature to be T_{eff}=1700–1800 K.

3.3 Observations

We observed DENIS-P J020529.0-115925 using the Hubble Space Telescope (HST) at six different epochs. The observations occurred between October 2000 and December 2003 during HST Cycles 8, 9, 10, 11 and 12 (program GO8720, P.I. Brandner, and programs GO9157, GO9345 and GO9968, P.I. Martín). DENIS-P J020529.0-115925 was observed with the Planetary Camera of WFPC2 (Biretta 2002), in the F675W and F814W filters (GO8720) and F606W and F814W filters (GO9157, GO9345 and GO9968). Table 3.1 gives a log of all the observations we used for this study. The target is very red, and the observations in the F814W filter were more sensitive than the one in the F675W or F606W filters, despite the shorter exposure times and the lower quantum efficiency of WFPC2 at longer wavelengths. The possible third component does not appear clearly on the F675W and F606W images. For these reasons, the following analysis is made essentially in the F814W filter. The high angular resolution of the WFPC2-PC (0.″0455 pixel scale) allowed us to resolve easily the 0.″3 secondary, and to discover that it is elongated.

3.4 Data analysis

We processed the data in two steps: a point spread function (PSF) subtraction on each component of the binary to look for residuals indicating the presence of a third companion, and a dual-PSF fitting of the secondary for confirmation.

3.4.1 PSF Subtraction and Residuals

Using the relative intensity of the residuals as defined in Section 1.2.1 of Chapter 1 of Part I, we compare the relative intensity of the residuals after PSF subtraction on the secondary of DENIS-P J020529.0-115925, using the same library of PSF stars. Figure 3.2 shows the results. The residuals at six different epochs are all clearly much higher than that of unresolved objects and unresolved companions of known binaries of the same sample, but very similar to that of other multiple systems. This figure shows clearly that DENIS-P J020529.0-115925B is very

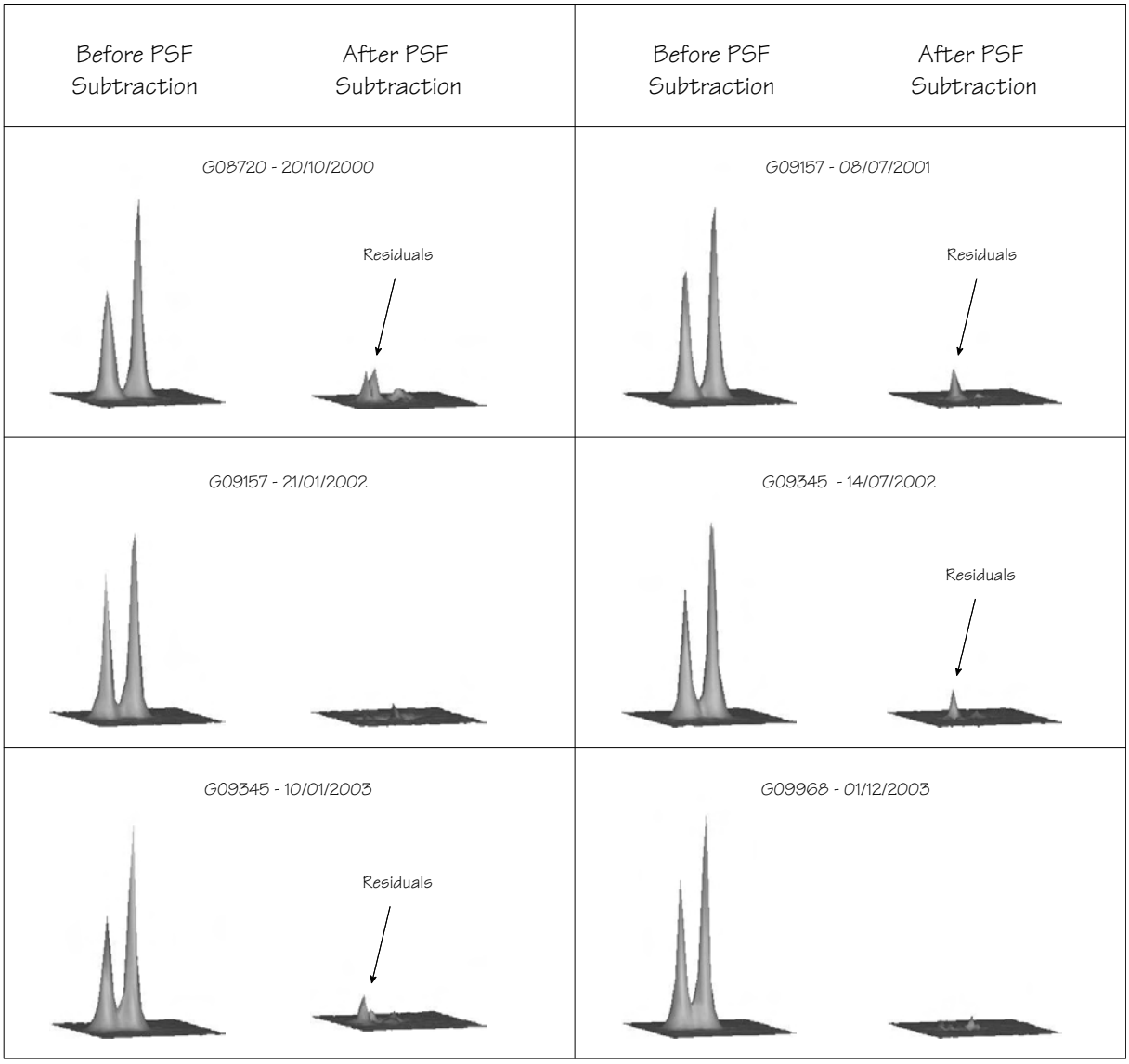

Figure 3.1 Results of the PSF subtraction at different epochs. This figure shows surface plots of the results of the PSF subtraction with one of the 10 reference PSF used. The primary is well subtracted whereas much stronger residuals remain for the secondary (clearly noticeable in 4 of the 6 epochs, indicated by arrows), indicating the presence of a third component. Similar results are obtained with the 9 other reference PSF stars.

Table 3.1. Observation log.

Filter	Exp. Time [s]	Date Obs. DD/MM/YYYY	Program
F814W	600	28/10/2000	GO8720
F675W	300	28/10/2000	GO8720
F814W	1700	08/07/2001	GO9157
F814W	1800	21/01/2002	GO9157
F814W	400	14/07/2002	GO9345
F606W	1600	14/07/2002	GO9345
F814W	400	10/01/2003	GO9345
F814W	800	01/12/2003	GO9968
F606W	1000	01/12/2003	GO9968

likely to be a binary system itself. Figure 3.2 shows also that even for the two images where the residuals do not appear clearly by eyes (see Figure 3.1), the $\mathcal{R}.\mathcal{I}$ is always much higher than in any unresolved system.

3.4.2 PSF fitting

In order to confirm that these residuals are consistent with the presence of a third component, we performed a dual-PSF fitting, on the secondary only, using the custom-made program described in Section 1.2.2 of Chapter 1 in Part I and in Annex A. Figure 3.3 shows that the residuals after this dual-fit are much better than after the single-PSF subtraction described in the previous section and in Figure 3.1. Moreover, the stability of the results for the ten different PSF stars at each of the six epochs shows that the results are reliable and robust, and that the third component hypothesis is consistent with the shape of the elongated PSF and highly probable.

Table 3.2 gives the flux ratios between the three components of the multiple system estimated with this method, as well as the corresponding differences of magnitude. According to the most recent DUSTY models of Chabrier et al. (2000), these differences of magnitudes indicate that the three components must have similar masses. A difference of magnitude of 1.5 mag in the F814W corresponds indeed to a mass ratio of 75, 85 and 95% at respectively 0.5, 1.0, and 5 Gyr.

The dual-PSF fitting indicates that over the six epochs the separation between B and C is bounded between $0\farcs053$–$0\farcs074$, while the position angle is bounded between 63° and 109°. Although the motion of C around B observed with this method can not be orbital in nature (P.A does not vary monotonously), we consider that the dual-PSF fitting is a valuable sanity check showing that the elongation of the secondary is consistent with a binary, and gives a very rough estimate of the photometric and astrometric properties of the possible third component. It is important to remember that the third component is barely resolved (the pixelscale of the Planetary Camera is $0\farcs0455$). These astrometric results have large uncertainties hardly assessable, and should be considered with caution. Moreover, the separation is so small that there is a ±180° ambiguity on the P.A of C with respect to B. For all these reasons, it would be hazardous to try to deduce any estimate of some orbital motion from these results. It is therefore

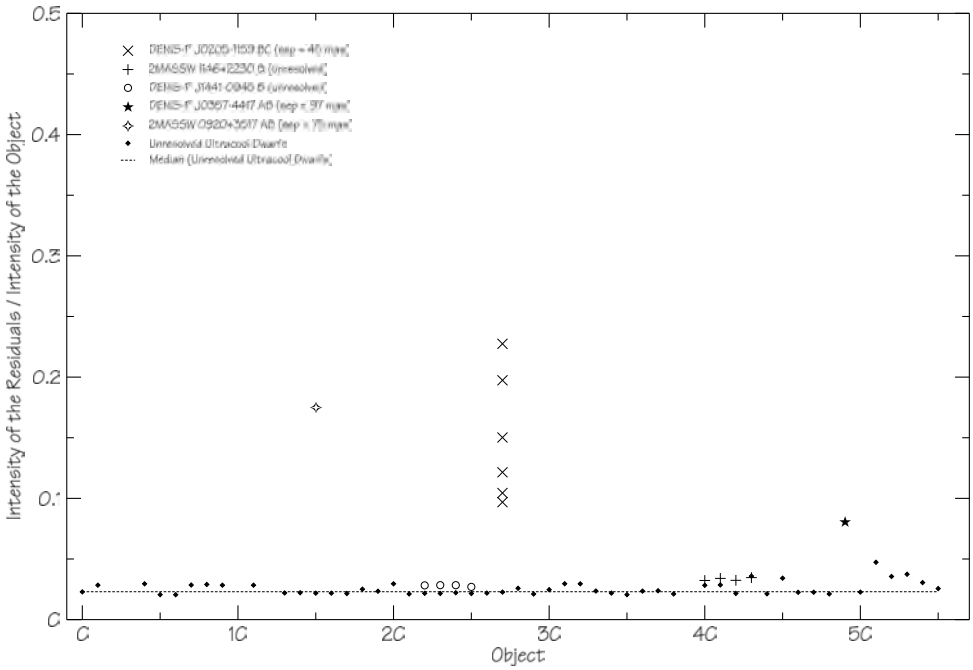

Figure 3.2 Residuals after PSF subtraction on HST/WFPC2 images of DENIS-P J020529.0-115925B, compared to unresolved objects (diamonds), resolved multiple systems (DENIS0357-4417AB, and 2MASSW J0920+3517AB), and unresolved companions of known multiple systems (2MASSW J1146+2230B and DENIS-P J1441-0945B) from programs GO8720 and GO8146. DENIS-P J020529.0-115925B appears clearly different from the unresolved objects and from the unresolved companions of known multiple systems, while its residuals are comparable to that of known close multiple systems. See also Fig. 1.1.

Table 3.2. Flux ratios and difference of magnitudes in the F814W filter

Components	Flux Ratio	ΔMag
B/A	0.37	1.08
C/A	0.25	1.50
C/B	0.66	0.45

Note. — Mag(A)=17.3 mag
The measurements reported here have large uncertainties, and should be considered with caution. The relative error from one image to the other is about 0.15 mag, but the real uncertainties can be higher. Measurements obtained on the GO8720 image.

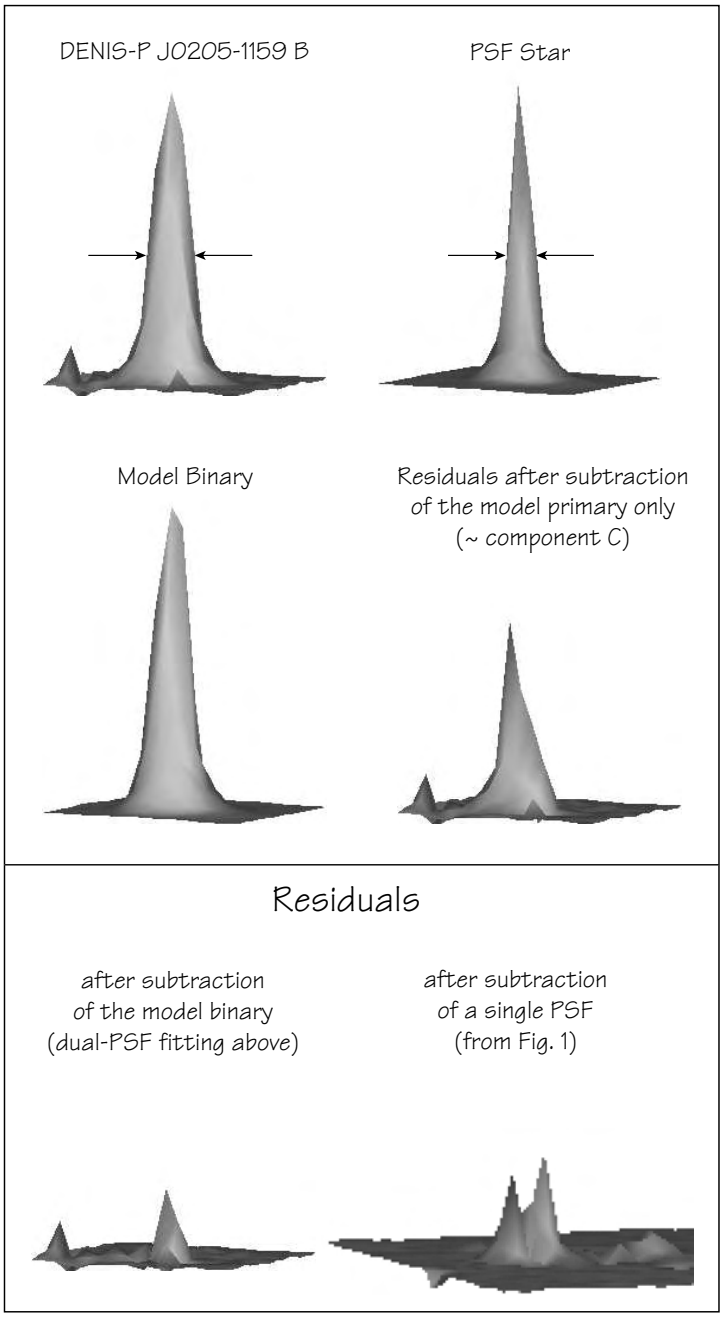

Figure 3.3 Results of the dual-PSF fitting on DENIS-P J020529.0-115925B for the GO8720 image. As shown with arrows, DENIS-P J020529.0-115925B has a FWHM much wider than the reference PSF star. The companion appears clearly after subtraction of the model primary. The residuals are small (lower panel, on the left), indicating that the quality of the fit is good. They are especially smaller than that obtained with a single PSF subtraction (lower panel, on the right). Similar results have been obtained with the 9 other reference PSF stars, showing that the result of the fit is robust and reliable.

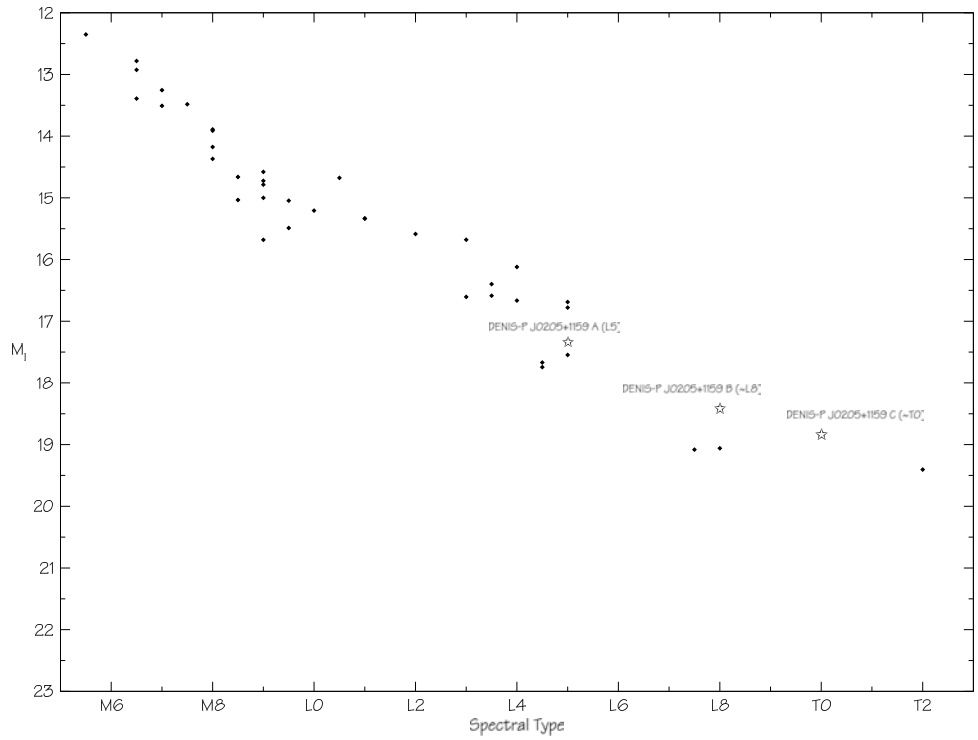

Figure 3.4 M_{I_C} vs Spectral Type relation. All measurements from Dahn et al. (2002) except for DENIS-P J020529.0-115925A, B and C. The absolute magnitudes of DENIS-P J020529.0-115925A, B and C have been estimated using the differences of magnitude reported in Table 3.2, and the DENIS I magnitude of the unresolved system.

not so surprising that the relative astrometry obtained with this method is not consistent with an Keplerian motion.

3.5 Discussion

3.5.1 Properties of the triple system

The present analysis of the high angular resolution images indicates that DENIS-P J020529.0-115925 is very likely to be a triple system.

Figure 3.4 shows the M_{I_C} vs Spectral Type relation for all the objects reported in Dahn et al. (2002). Assuming differences of magnitude in I_C equal to that reported in Table 3.2 for the F814W filter (F814W filter is close to I_C, Biretta 2002), and the DENIS I magnitude[12] of the unresolved object, one can estimate the spectral types of the three components. DENIS-P J020529.0-115925 A is consistent with a L5 dwarf, in good agreement with the measurement reported by Martín et al. (1999b), and showing that the primary would be dominating the optical spectrum. B and C would be consistent with ∼L8 and ∼T0 dwarfs respectively.

Several authors report the detection of methane absorption in the infrared spectrum of DENIS-P J020529.0-115925 (Delfosse et al. 1997; McLean et al. 2001; Burgasser et al. 2003). Tokunaga & Kobayashi (1999) also observed this absorption feature in the spectrum but attribute it to H_2 rather than methane. Burgasser et al. (2002) note that this feature is weak and

[12] I_{DENIS} is very close to the $I_{Cousins}$ (Delfosse 1997)

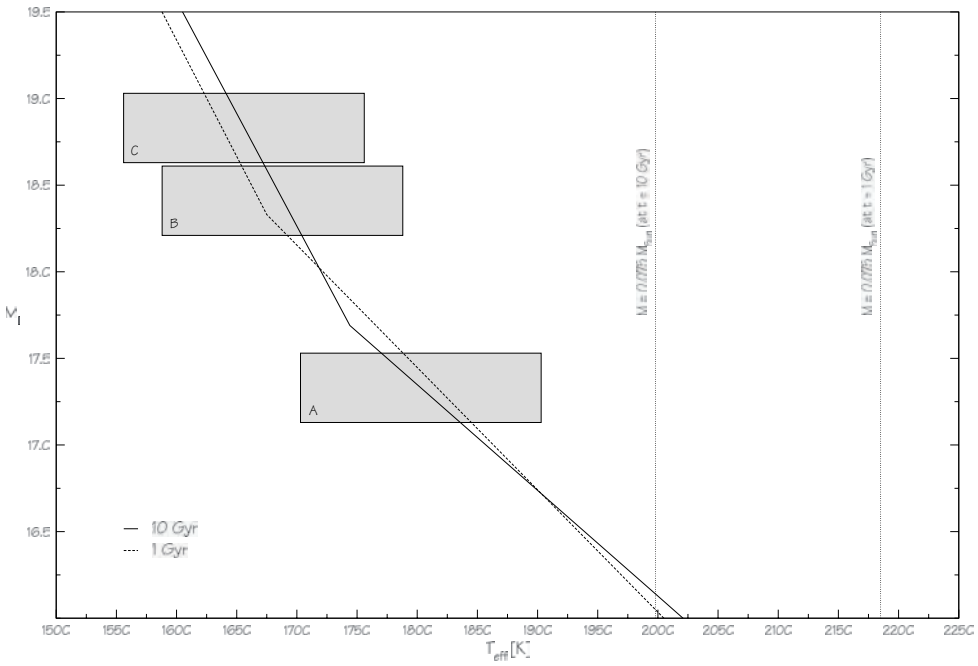

Figure 3.5 M_{I_C} vs Effective temperature. This figure shows the M_{I_C} as a function of the effective temperature, as given by the DUSTY models. Two isochrones (1 and 10 Gyr) are shown, together with the corresponding limits for sustained hydrogen burning. The position of the three components is represented by grey boxes, assuming ±100 K uncertainty on the effective temperatures of the three components of DENIS-P J020529.0-115925, and including the uncertainty on the distance for the M_{I_C}. This figure shows that all three components must be substellar.

variable, and consider that it does not constitute a clear detection of methane. We note that if real, this feature could be related to the presence of L8 and T0 companions, and its variability to some weather effects, as already observed in other late L and T dwarfs by Enoch et al. (2003). Dahn et al. (2002) showed that the absolute J and K-band magnitudes of early T-dwarfs are similar to that of late-L dwarfs, so that the contribution of B and C in the near-infrared can be larger than in the optical.

According to the DUSTY models (Chabrier et al. 2000), and assuming an age between 1 and 10 Gyr, Figure 3.5 shows that the absolute M_{I_C} magnitude of DENIS-P J020529.0-115925 A corresponds to an effective temperature between 1 700–1 900 K, while B and C range between 1 550–1 800 K. These temperatures are consistent with the value reported by Basri et al. (2000) for the unresolved system (1700–1800 K), and show that all components appear to be clearly substellar. According to the DUSTY models, the stellar/substellar limit is indeed around 2000 K at 10 Gyr and 2180 K at 1 Gyr, therefore warmer than any of the components of DENIS-P J020529.0-115925.

Finally, the proper motion of the object (∼438 mas yr^{-1}, Dahn et al. 2002) and the presence of these strong residuals at six different epochs spread over three years allow us to rule out definitively the eventuality of a coincidence with some background object.

3.5.2 Dynamical Stability

The separation between the primary and the secondary changed from $\sim$0.″390 to 0.″270 between October 2000 and December 2003, while the separation between the second and the third component is contained between $\sim$0.″075$\leq \delta_{BC} \leq$0.″055. As stated by Harrington (1968) and then Szebehely & Zare (1977) in their analytical study, triple systems with moderate eccentricity and equal mass components are stable for ratios between the semi-major axes of the outer (a_2) and the inner orbits (a_1) greater than $a_2/a_1 \geq$3.2. Assuming that the orbits of DENIS-P J020529.0-115925 components have moderate eccentricities, and considering that the 3 components must have similar masses as explained above, DENIS-P J020529.0-115925 would fit above the stability criterium, with a ratio between $3.6 \leq a_2/a_1 \leq 7.1$. The presence of a third component at the positions reported here is therefore dynamically possible.

The estimate of the separation corresponds to a semi-major axis of $\sim$1.2 A.U ($\sim$0.″075 at 19.7 pc). Corrected for a statistical factor of 1.26 as explained in Fischer & Marcy (1992), it leads to a semi-major axis of 1.9 A.U. According to Kepler's Third Law (Kepler 1609) and assuming a total mass of $\sim$0.1 $M_\odot$, the corresponding period, is $\sim$8 years.

3.6 Conclusions

We present here results of high angular resolution observations with HST/WFPC2 that allow us to conclude that DENIS-P J020529.0-115925 is very likely to be a triple system of brown dwarfs. PSF subtraction on the secondary at six different epochs show unusual residuals in comparison with unresolved objects. Dual-PSF fitting shows that the shape of the secondary is consistent with that of a binary. The configuration is consistent with a dynamically stable multiple system. The observed relative motion is not consistent with a Keplerian motion but we attribute this to the limitation of the PSF fitting method.

Observations at higher angular resolution, using for example the HST/ACS, ground based adaptive optics or speckle imaging, should allow to confirm if DENIS-P J020529.0-115925 is a triple system or not.

Part III

Discussion

In this last part, we will give an outlook of the results presented in this work in comparison with that of other teams. We will then compare these results to the predictions of the models of formation and evolution, and see what constraints we can infer, and what questions remain open. Finally, we will present the research already on-going on some of the remaining questions, as well as suggestions of research projects to be done in order to supplement our current knowledge and understanding of ultracool objects.

Chapter 1

Comparison with other studies

Several teams have been doing similar research on the same topic, almost at the same time we obtained our results. These complementary and independent measurements are important to validate the ones we report.

1.1 Ultracool dwarf binary statistics in the field

1.1.1 Binary frequency

As for the field ultracool dwarfs, four major studies have been conducted, one two years earlier than ours by Reid et al. (2001) using HST/WFPC2 on a sample of 20 L-dwarfs, and the three others in parallel to ours, by Gizis et al. (2003) using HST/WFPC2 on a sample of 82 late-M and L dwarfs, by Close et al. (2003) using the adaptive optics instrument Hokupa'a on Gemini North on a sample of 39 of late-M and L dwarfs, and Burgasser et al. (2003) using HST/WFPC2 on a sample of 10 T-dwarfs. The first three samples are smaller and included in our own study of 133 late-M and L dwarf binaries, and therefore do not provide independent checks of our own statistical results. They nevertheless independently confirm the detection of the multiple systems that we resolved.

Table 1.1 gives a summary of the major results of these four studies, as well as the results we report in this work. This table shows that all results agree well, which is not surprising since the corresponding samples overlap.

The binary frequency thus derived is much less than the one observed on a similar range of separation for M2–M4.5 dwarfs in the field (Fischer & Marcy 1992), where 32±9% of the objects are found to be binaries. It is also much less than the corresponding ∼30% binary frequency[13] among G dwarfs reported by Duquennoy & Mayor (1991). These studies cover a larger range of mass ratio, and the direct comparison with our results should therefore be made with caution. It would nevertheless be unlikely that the distribution of mass ratio among ultracool dwarf binaries shows a peak at small values large enough to cover the difference between these numbers. This brings us to the distribution of mass ratios.

1.1.2 Distribution of mass ratio

All four studies of visual ultracool dwarfs binaries cited above report a possible preference for equal mass systems. The systems with large differences of mass are indeed rare. This latter

[13] Duquennoy & Mayor (1991) report 57% of binaries for the overall range of separations, corresponding to 30% in the same range of separation as in our study

Table 1.1. Visual Binary Frequency for field ultracool dwarfs measured in successive studies.

Ref.	$N_{Objects}$	$N_{Binaries}$	Sep. Range [A.U]	SpT[a]	Sensitivity (q_{min})[c]	Binary Freq.[b]
Reid et al. (2001)	20	4	>1.2	L0.5–L8	>0.6	20%[d]
Close et al. (2003)	39	9	>2.6	M8–L0.5	>0.6	15±7%
Gizis et al. (2003)	82	13	1.6–16	M8–L8	>0.6	15±5%
Burgasser et al. (2003)	10	2	>1	T5–T8	>0.4	9^{+15}_{-4}%
this work	133	25	>1.2	M8–L8	>0.6	12±3%

[a] for the overall system

[b] Binary frequency defined as $N_{binaries}/N_{Objects}$, corrected for biases in the range of separation and mass ratio indicated

[c] Sensitivity to lower mass companions, expressed as the minimum mass ratio $q = M_2/M_1$ to which the observations were sensitive.

[d] raw observed binary fraction, not corrected for biases

conclusion is only tentative because of the limits of sensitivity of these surveys, and of the magnitude biased samples considered which favour the detection of equal-mass systems (see Öpik 1924). If confirmed, this result would be in contrast to the distribution of mass ratio of G binaries, as reported by Duquennoy & Mayor (1991). On the same range of mass ratio than our study ($0.5< q <1.0$), they observe a distribution rising toward low mass ratios, as shown in Figure 1.1, while we observe a (possible) rise toward high mass ratios for ultracool dwarfs. On the other hand, it would be consistent with the deficiency of multiple systems having mass ratios of 0.4–0.6 among M-dwarfs, as observed by Fischer & Marcy (1992) in their complete sample of early M-dwarfs. If confirmed, the lack of ultracool dwarfs binaries could mean that there is a trend for the distribution of mass ratio to have less and less small mass ratios with decreasing masses of the primary. Figure 1.1 shows that the slope of the distribution of mass ratios might even eventually show an inversion when passing from G to L dwarfs.

1.1.3 Distribution of separation

The shape of the distributions of separation of ultracool dwarfs over the range of separation of our study is similar to that of field G and early-M dwarfs (Gaussian for the G and M dwarfs Fischer & Marcy 1992), as shown in Figure 1.9 (page 54). On the other hand, while G and early-M dwarfs seem to have similar median semimajor axis (around 30 A.U), ultracool binaries seem to have a peak at much smaller separations, and a deficiency of systems with large separations. All four studies indeed report a peak in the distribution around 4–8 A.U, and a deficiency of multiple systems at separations larger than ∼20 A.U. This latter result cannot be an artifact since the wider binaries are easier to resolve.

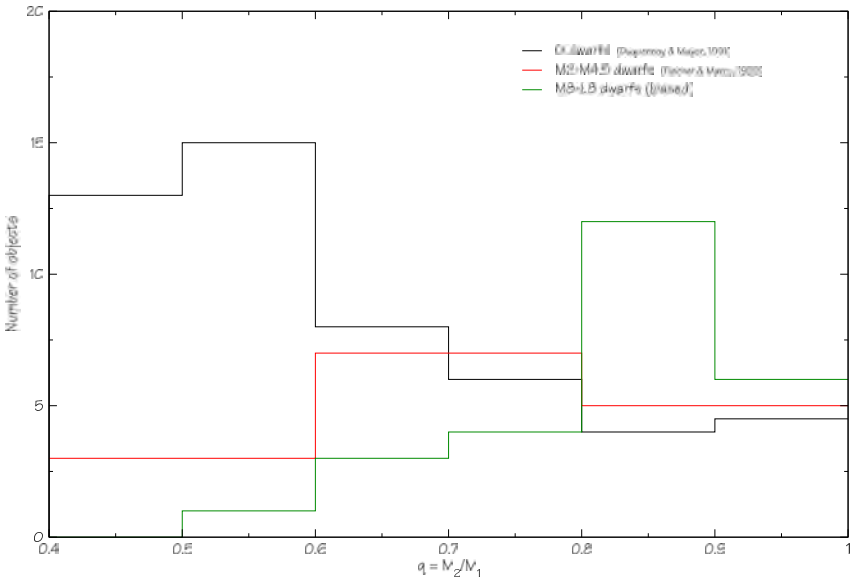

Figure 1.1 Distributions of mass ratio for G, early-M and late-M-L dwarfs in the field. Values for G-dwarfs from Duquennoy & Mayor (1991) and Fischer & Marcy (1992) for early-M dwarfs. The histogram corresponding to our study is biased toward smaller mass ratio. The comparison should thus be done cautiously, until a better statistical study confirms it. There seems to be a trend for an increasing deficiency of systems with small mass ratio from G to L dwarfs, and eventually an inversion of the slope when passing from G to L dwarfs.

1.2 Ultracool dwarf binary statistics in the Pleiades

A direct comparison with the results obtained for other types of stars is not easy in the case of the Pleiades since the several studies reported in the literature have been performed under very different conditions, spanning different ranges of mass ratios, separations and sensitivity.

In their studies of F–G dwarfs and early-M dwarfs, Bouvier et al. (1997) and Stauffer (1984) respectively observe corrected binary fractions similar to that of field G dwarfs (∼60%, but ∼30% over the range of separation of our study). They obtained this result assuming a mass ratio distribution similar to that of field late type stars. Under the same assumption, and correction for the spectroscopic binaries, we obtain a binary frequency of 13∼14% for brown dwarfs (see Section 2.8.2, page 81), which is much lower than the one they estimate. If confirmed, this would mean that the decrease of the rate of binaries between G + K + early-M dwarfs and brown dwarfs is common to field and Pleiades objects. Any evolution process responsible for that difference would have occurred before the age of the Pleiades, i.e 120 Myr. On the other hand, the photometric study of Pinfield et al. (2003) indicates a binary frequency of ∼50% among Pleiades ultracool dwarfs, which would be consistent with that of G and early-M dwarfs. Further investigations are required in order to refine the measurement of the binary fraction among Pleiades brown dwarfs.

Finally, the current small sample of multiple systems in the Pleiades (4 binaries) does not allow to perform any meaningful statistical analysis of the distributions of separation and mass ratio. We can nevertheless note that all four binaries have separations less than 20 A.U, and mass ratios greater than 0.6, which tentatively indicates that these distributions do not differ from that in the field, and again contrast with the one reported for G and early-M dwarfs.

1.3 Comparison of field/clusters/SFR binary ultracool dwarfs

The only search for multiple ultracool binaries reported in another cluster was performed in the 80 Myr old α-Persei cluster by Martín et al. (2003), who did not detect any binary among the eight objects observed with HST/WFPC2, leading to a lower limit of the binary frequency of 9% for separations greater than 10.5 A.U. This value is similar to the one we report for the Pleiades. No search for ultracool binaries is available in other clusters at the date of this work, so that the properties we have measured cannot be directly compared to that in other clusters. One can nevertheless compare the properties of the Pleiades brown dwarf binaries to that of late type stars of other clusters, and see if the comparison is similar to that discussed in Section 1.2.

Fortunately, several clusters have been scanned to look for multiple systems among late type stars. These are the 700 Myr old Praesepe cluster (Mermilliod & Mayor 1999; Bouvier et al. 2001), the 600 Myr old Hyades (Reid & Gizis 1997b), and the young 2 Myr old IC 348 (Duchêne et al. 1999). All these studies confirm that the binary fractions, distributions of separations and of mass ratios of low mass stars are indistinguishable from that measured in the field for the same types of objects, showing that the binary properties of low mass stars are well established before 2 Myr and remain stable after that.

Only few observations are available in even younger associations. A proposal in which I was involved and aiming at looking for binaries among a sample of bona-fide brown dwarfs in the Upper Scorpius and Chameleon associations with HST/ACS has been rejected during the 13th call for proposal (P.I Martín). Using HST/WFPC2, Neuhäuser et al. (2002) observed 11 M6–M8 brown dwarfs in the 1∼5 Myrs old Chameleon I dark cloud. They resolved two possible candidate companions. The first one has later been classified as a reddened background K star (Neuhäuser et al. 2003), while the remaining one, at a separation of 28 A.U, still needs to be confirmed by second epoch observations. A search for spectroscopic binaries among a sample of 9 objects (all in common with the sample of Neuhäuser et al. 2002) by Joergens et al. (2003b) lead to the discovery of only one binary candidate, which also needs to be confirmed. These two studies therefore indicate that binaries are rather rare, with an upper limit on the binary frequency at about ∼10%. This value is very similar to the one we obtained in the field and in the Pleiades.

The previous analysis (Sections 1.1 & 1.2) and the corresponding conclusions can therefore be extended to the four open clusters and the one star forming region mentioned above.

1.4 Physical properties of binary ultracool dwarfs

1.4.1 Spectroscopy of the individual components of multiple systems

Goto et al. (2002) present near-infrared spatially resolved spectra of the components of the binary ultracool dwarfs HD130948B and C. HD130948 is a common proper motion triple system discovered by Potter et al. (2002), consisting of a primary G2 dwarf and a binary companion at 2.″63 from the primary. The binary companion has a separation of ∼0.″134, corresponding to a physical separation of 2.4 A.U at a distance of 17.9 pc as measured with Hipparcos (Perryman et al. 1997). Using the adaptive optics of the Subaru telescope, Goto et al. (2002) were able to resolve the binary companion and obtain spectra of the individual components. Correcting for the non-linear effects of the adaptive optics, they could then measure the spectral types of each components. They found the two objects to have similar spectral properties and attribute to both of them a spectral type of L4±1. This is consistent with the measurement of Potter et al. (2002) who report a spectral type of L2±2 for the unresolved system. The presence

of the G2 primary offers the great advantage to be able to constrain the age of the triple system. Gaidos et al. (2000) and Chen et al. (1997) estimated its age to range between 0.3–0.8 Gyr. Considering that the three components must be coeval, and using the evolutionary tracks of Chabrier et al. (2000), it leads to a mass 0.040–0.065 $M_{\odot}$ for both objects, therefore well below the hydrogen-burning limit

1.4.2 Orbit of ultracool binaries

Only one binary brown dwarf orbit has been reported to date. GJ 569B was discovered as a binary by Martín et al. (2000b) using the Keck adaptive optics. It is orbiting the GJ 569A M2.5 dwarf, which distance was measured by Hipparcos (9.81±0.16 pc Perryman et al. 1997). The first determination of its orbital parameters was obtained by Kenworthy et al. (2001) thanks to speckle interferometry at the MMT. They constrained the total to 0.115–0.210 $M_{\odot}$. This measurement was refined the same year by Lane et al. (2001) using Keck adaptive optics images. They were able to obtained an improved orbital fit and a total mass of $0.123^{+0.027}_{-0.022}$ $M_{\odot}$. They determine the spectral types of the objects to be M8.5±0.5 (GJ 569Ba) and M9±0.5 (GJ 569Bb). Using theoretical evolutionary tracks, they were able to derive the mass ratio and the following individual masses: 0.065 $M_{\odot}$ for GJ 569Ba and 0.058 $M_{\odot}$ for GJ 569Bb. Complementary observations obtained by Zapatero-Osorio et al. (2004, in press) cover the whole orbit and allow to constrain even better the total mass of the objects[14].

[14]The corresponding measurements were not published at the time of this manuscript

Chapter 2

Consequences on the models

2.1 The different models of formation and their predictions

2.1.1 Star like models

The "Jeans" model

Assuming that ultracool dwarfs might form just like stars, the scaled Jeans[15] model predicts naturally binary properties similar to that of other stars, scaled down to the smaller masses. We should thus expect to observe a similar binary fraction, and distributions of separation and mass ratio with similar shapes to that observed for stars.

The "photo-evaporation" model

Although the evaporation process is thought to be very efficient (Kroupa & Bouvier 2003), it is not expected to be representative of the formation of the majority of the ultracool dwarfs, since it can occur only under specific conditions in specific places. In this case, the ultracool dwarf formation should indeed happen in a dense molecular cloud, close enough to a nearby massive star, and the ionization and evaporation process should be efficient early enough to prevent the forming object to reach the hydrogen burning limit. One can reasonably assume that although frequent, it is not the case for a large number of objects. The binary properties resulting of this formation process can hardly be predicted, but up to now only one "binary-proplyds" over more than 150 in total has been observed in Orion (Graham et al. 2002). For these reasons, and although this formation is likely to be at work in dense associations (see Figure 4 in page 8 in the introduction), we will not discuss it further.

The "embryo-ejection" model

This model is currently one of the most debated ones. Depending on the initial conditions and the level of the numerical analysis chosen, the resulting properties of the formed brown dwarfs can vary a lot. In this section, we will review four complementary treatments of that scenario, starting with the most complex one.

[15] Refer to the Section 3.1 of the introduction (page 5)

a) Hydrodynamical simulations of the fragmentation of a cloud

Bate et al. (2002) study the formation of ultracool and brown dwarfs via hydrodynamical simulations of the fragmentation and collapse of a molecular cloud. They generate an IMF from the turbulent cloud and then study the dynamical interactions of the protostars between themselves and with the gaseous environment. An overview of these simulations is shown in Figure 3 on page 7. They result in the formation of brown dwarfs mainly through instabilities in the massive circumstellar disk, but also in a lower rate as ejected stellar embryos from unstable multiple protostellar systems. Among the formed brown dwarfs, only less than 5% are binary systems. This study has the merit to do a full treatment of both the effects of the remaining gas and of the gravitational interactions between the protostars, but requires extremely heavy and CPU-time consuming calculations. Consequently it does not allow to study the statistical properties of the formed objects because of the CPU-power required and because of the small number of objects produced ($\sim$50 objects). Given these considerations, it is not possible to make a direct comparison of their results with the observations. Several authors therefore tried to perform complementary analysis in order to investigate the statistical properties of the brown dwarfs formed via this process, using different approaches.

b) Hydrodynamical simulations of the decay of a 5-body accreting system

In order to investigate the regions close to the stars, Delgado-Donate et al. (2003) chose to perform similar simulations as the ones of Bate et al. (2002) but at a different scale. Instead of following the fragmentation of the whole molecular cloud, they focused on the evolution and dynamical decay of small 5-body systems, taking into account both the dynamical interactions of the protostars between themselves, the interactions with the gaseous environment and accretion. Although still sophisticated, this treatment allowed them to study the outcomes over 100 different cases and to start deriving statistical properties of the formed objects. They come to the conclusion that the number of binary brown dwarfs formed strongly depends on the parent core mass function of the cloud: a core mass function with a lower cut off at 0.25 $M_{\odot}$ (as observed in ρ-Ophiuchi by Motte et al. 1998) results in only very few binaries, while a parent core mass function extended to the substellar regime results in a higher binary frequency, possibly consistent with the observational results. Once again they formed too few binaries to perform an analysis of the properties of the multiple systems formed.

c) Neglecting accretion and interactions with the gas

In their simulations, Sterzik & Durisen (1998, 2003) study the dynamical decay of small constant-mass N-body clusters reproducing the observed IMF, neglecting the hydrodynamical interactions with the surrounding gas. By using this approach, they are able to perform the computations over a much larger number of cases, and to derive statistical properties of the outcoming objects. They obtain a remarkable agreement with the results we report for the binary fraction (around 10%) and the distribution of separations (with a peak around 4 A.U and a lack of wide systems with separations larger than 20 A.U).

d) Neglecting only the interactions with the gas

In a more recent study, Umbreit et al. (2004) present the results of N-body calculations of the dynamical decay of accreting triple systems, therefore neglecting only the effects of the

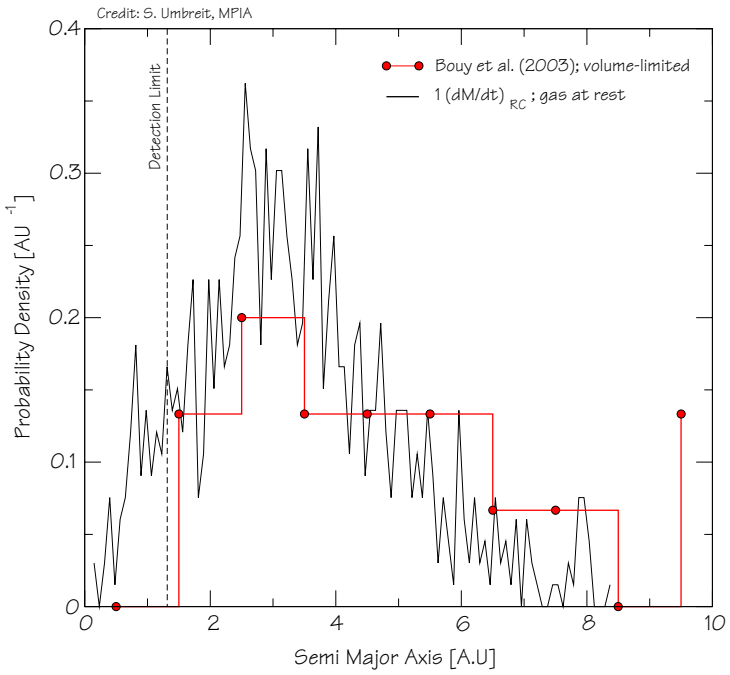

Figure 2.1 Distribution of mass ratio in Umbreit et al. (2004) simulations based on the Reipurth & Clarke (2001) model of formation. it shows a remarkably good agreement with the distribution of semimajor axis we observe for field ultracool dwarfs (from Chapter 1 of Part I).

surrounding gas. Although slightly more sophisticated than the simulations of Sterzik & Durisen (2003), they were also able to perform the computations over a statistically meaningful number of cases. Assuming equal initial masses for the components of the protostellar systems and a certain accretion rate, they were also able to reproduce remarkably well the observed binary fraction and distribution of separation, as shown in Figure 2.1. They also conclude that depending on the rate of accretion and the kinematic properties of the accreted gas, the embryo-ejection model can be become very efficient at producing brown dwarfs.

2.1.2 Planetary models

As already mentioned above, Bate et al. (2002) show that the formation of brown dwarfs can occur mainly through instabilities in the massive circumstellar disk, forming only few multiple systems. The complementary models of Mayer et al. (2002) describing the formation and collapse of gravitational instabilities in thin disks (see Figure 5 on page 9 and the corresponding section) have not reach a level that allow the comparison with our observational results. Two majors constraints should nevertheless be considered for the future development of these simulations:

- the observed small number of brown dwarfs orbiting more massive stars (between 1 and 3% around G to early-M stars, Gizis 2003; McCarthy et al. 2003)

- the observed large number of free floating ultracool dwarfs, which need to somehow leave the disk

2.2 Impact of our observational results on the models of formations

As discussed in the previous section, the observational results we obtained give tight constraints on the models of formations. The observed properties of multiple systems among very low mass objects will have to be better reproduced by the different models, and should help the authors of the simulations to define the way they should carry on with their investigations.

For the moment, our results nevertheless do not allow us to rule out any of these models or decide which one might dominate the formation process. The current impact of our results is therefore limited for the two following reasons: first because our results still need to be confirmed by further studies (as will be discussed in the next Chapter), and second because the models have not reach yet a level of sophistication that would allow a direct comparison with the observations. It is still too early to draw firm conclusion, but the observed properties that seem to be intermediate between the several scenarios proposed, the observations we report and the simulations that have been performed suggest that ultracool dwarfs are likely to form via several competing and/or parallel processes. The developments on both the theoretical and observational sides will be a great challenge in the field of ultracool dwarfs in the coming years.

Chapter 3

Future prospects and on-going research

Following the conclusions of the study we present in this work, we can suggest new research projects to be done in order to complete and improve the results obtained to date. These future prospects can be split in two categories:

- improvements of the currently available measurements
- extension to other environments and ages, but also to new ranges of mass, of separation, and of wavelength

3.1 Improvements of the currently available measurements

3.1.1 Direct continuation of our work

As mentioned in the previous chapter, the conclusions we draw regarding the multiplicity of ultracool dwarfs in the field and their consequences on the models of formation and evolution are only tentative because of the limitations of the samples we used (magnitude limited sample). New investigations over a statistically well defined sample should be done in order to confirm the results we obtained. Such a study is already on-going with HST on a volume-limited complete sample of L dwarfs (K. Cruz, private communication) from the 2MASS survey, and a similar survey is planned with VLT/NACO on an even larger volume-limited complete sample of DENIS L-dwarfs (X. Delfosse, private communication).

As for the physical properties, an effort should be made in order to carry on with the study of individual properties via their spatially resolved spectra. In order to be able to derive statistical properties, this work should be extended to even more objects over a larger range of spectral types. A complementary study is on-going in the near-infrared: using VLT-NACO, we obtained K band resolved spectra of two of the four binaries presented in Chapter 1 of Part II. These spectra cover the spectral region where the following major spectral features can be identified: the CO bands (2.295 μm) which are dominating through L8, the CH_4 bands for late L and T dwarfs (2.2 μm), and the Na I doublet (2.206/2.209 μm) which becomes more pronounced in later spectral types.

Ultimately, it would be very important to follow more very low mass binaries on their orbits, with the aim of measuring dynamical masses. Only two such orbits have been covered nowadays (Lane et al. 2001, , and Chapter 2 of Part II). A "good candidate" for such a study should have the following properties:

- it should rotate fast enough to allow the determination of its orbital parameters in a reasonable time-scale (of let say 3 to 5 years). The uncertainties on the derived orbital parameters indeed depend strongly on the fraction of the orbit covered by the observations. Objects with periods larger than 15 years are unlikely to be followed on more than 50% of their orbit, depending on the eccentricity.

- its distance should be known with a high precision. The distance indeed appears to the cube in Kepler's law (through the semi-major axis), and a small uncertainty on the distance can translate into large uncertainties on the derived orbital parameters.

- its age should be known or at least sufficiently constrained. We have indeed mentioned that the impacts of the current orbital measurements on the models are relatively small, because the age of the two corresponding systems are unknown. A calibration of the models requires to know the age of the object, or at least constraints on its age.

- its separation should make it easily observable. If the separation is too close to the limit of resolution of the currently available instruments, the uncertainties on the relative astrometry will be relatively high, translating again into large uncertainties on the inferred dynamical masses.

- its inclination should not be close to edge-on: in such case, the orbital solutions cover a much broader range of eccentricities, translating also into large uncertainties on the dynamical mass of the system.

- the system should be bright enough to enable the use of ground-based adaptive optics instruments. HST is approaching the end of its "career", and the only high angular resolution instruments remaining for the near future will be ground based telescopes with adaptive optics. The imminent installation of laser guide stars should soften this condition. In the long term, NASA/ESA/CSA James Webb Space Telescope should allow to reach the required resolution in the near-infrared, thus down to even smaller mass ratios and separations.

- astrometric or spectroscopic orbits should be measurable as well. The visual orbit is indeed not enough to derive the dynamical masses of the individual components since it yields only the angular separation between the stars, while Kepler's Third law requires the linear separation. In order to derive the dynamical masses of the individual components, one thus needs to measure the linear separation either by observing the spectroscopic or *absolute* visual orbit[16]

Fortunately half a dozen of candidates meeting most of these conditions can be distinguished from the sample of currently known binaries. Most of them are binary brown dwarfs orbiting a G, K or M dwarf, which age and distance can therefore relatively easily well constrained. Moreover, the presence of this bright primary offers two major advantages: 1) it provides a good and bright reference star close to the object of interest, which is of first importance for adaptive optics observations; 2) it enables precise measurements of the absolute motion of each components of the binary, leading to the determination of the centre of mass and consequently to

[16]The absolute visual orbit refers to the motion of each components with respect to one or more other stars in the field, leading to the determination of the centre of mass, and therefore to the individual masses.

the individual masses of the system, exempting us of performing high resolution spectroscopy[17]. Proposals will be submitted to the relevant observatories in order to start this study.

In collaboration with Dr. W. Brandner, we are currently working on the orbital fit of DENIS-P J122813.8-154711. Seven observations spread over 6 years already allow us to constrain the orbital period to 42.7 yr for a total mass of 0.110±0.013 $M_{\odot}$ (Brandner et al., in prep.). A longer time will thus be needed before we can improve significantly these values.

As explained above, astrometric binaries provides a very straightforward method to measure the masses of the individual components. In a collaboration with prof. E. L. Martín and Dr. W. Brandner, I will work on the determination of the absolute astrometric orbits of a sample of 4 ultracool and brown dwarfs from the field. Six epochs images spread over 4 years have been obtained with HST/WFPC2 for each object, and the presence in the field of one (more in some cases) object will allow us to measure precisely the motion of the centre of mass and the individual masses.

3.1.2 Improvement of the quality of the samples

In order to be meaningful, a statistical study should be done over samples as large as possible. The "technical" limitations (limited number of known objects, limited telescope time, but also duration of the data processing) do not allow to observe very large samples. One should thus be careful to define samples large enough to obtain reasonable uncertainties on the derived statistics, but small enough to be reasonably feasible.

The size of the sample is of course not the only important criterium: the objects in the sample should be representative of a complete population, and not biased toward specific objects. For example, the sample of 134 objects we used in the field was large enough to perform statistics, but the way the objects had been chosen (limitation in magnitude rather than in volume) was introducing strong biases. On the other hand, our sample of 13 objects[18] was relatively too small to perform a precise statistical analysis, but well defined in terms of completeness. Finally, the only four objects for which we obtained spatially resolved spectra, the one orbit we could measure, and the one triple system we found are clearly not enough to perform any statistical analysis. We should thus aim at refining these studies over better defined and larger samples.

3.2 Extensions of the studies

Although they were among the largest presented at the date of this work, the samples we have been studying have several limitations.

3.2.1 Extension of the coverage of the studies

Our studies were limited to a certain range of separation. The coverage should thus be extended to larger ranges, using for example high angular resolution spectroscopy to search for spectroscopic binaries, and scan the range of small separations. Such a study would allow us to know whether we missed most of the binaries or if the proportion of spectroscopic binaries is similar to that for other types of objects. The other side of the distribution (large separations) could be investigated using the data coming from the all-sky surveys (2MASS, DENIS, SDSS) and/or

[17] As already mentioned, the measurement of spectroscopic orbits of binary ultracool dwarfs is complicated by their fast rotational velocity, the Doppler shift due to the rotation blending the shift of the companion's spectrum.

[18] The initial sample was made of 33 objects, but only 15 could be observed in the HST SNAPSHOT program. SNAPSHOT programs are indeed not guaranteed to be fully completed.

wide field imaging. This last issue is very important in order to confirm or not the deficiency of systems with large separations.

The same applies for the distribution of mass ratio: our limit of sensitivity did not allow us to find objects with mass ratios smaller than ∼0.5. Whether the distribution shows a deficiency of systems with small mass ratio or not is an important issue, which consequences on the models of formation and evolution have been discussed in this thesis work. Deeper search for companions should thus be performed.

The extension of the coverage in sensitivity and angular resolution of the present studies is also important from a more general point of view: in order to be able to compare the results regarding the multiplicity of ultracool dwarfs to that for other types of stars, we need to cover the same ranges of separation and mass ratio. The current studies of F, G and K dwarfs have been obtained on complete sample over larger ranges of separations than the one that have been reported for ultracool dwarfs.

Finally, in order to start deriving statistics of the physical properties of the individual components of ultracool binaries, we would need to extend the study of their spatially resolved spectra to a larger range of spectral types and ages.

3.2.2 Extension to other environments and ages

In order to check if the properties of ultracool dwarfs depend on the environment or evolve with time, it is necessary to perform similar studies in different regions of interests. Observing brown dwarfs in star forming regions and young clusters of increasing ages allows to follow their evolution over several megayears, up to several gigayears with the field objects, and to have in one shot a general overview of the evolution of these objects. It is therefore very important for our understanding of ultracool dwarfs to perform detailed analysis of their properties in star forming regions, open clusters and the field. As explain in the introduction, this was our motivation for the study of binary ultracool dwarfs in both the field and the Pleiades. In order to complete our present study, and in collaboration with other scientists, we now aim at studying the statistical and physical properties of brown dwarfs in star forming regions, looking for both binaries and disks in large and well defined samples. Proposals have been sent to several observatories.

3.2.3 Extension to other wavelength ranges

As shown by the history of science and in particular of astrophysics and astronomy, the numbers of discoveries and results literally explode each time a new spectral window is investigated. The recent/future launch of space observatories such as NASA/SPITZER (infrared), ESA/HERSCHEL (far infrared) or NASA/ESA/CSA JWST (near-infrared) or ground-based observatories such as VLTI in the optical/near infrared or ALMA in the radio, will open new perspectives with their unprecedented sensitivities and spatial resolutions. They will provide the unique opportunity to extend our present work to a new wavelength range, increased sensitivities and resolutions. Some of the above mentioned infrared instruments are particularly well studied (sometimes designed) for the study of ultracool objects, which emission peaks in the infrared. A huge number of important results is thus expected to come out of these missions.

Appendix A

Calibrations of the PSF fitting method for WFPC2-PC data

To evaluate the accuracy of the PSF fitting program, and look for systematic errors, we used the program on 4950 simulated binaries, covering a range of 11 various input flux ratios (varying from 0.05 to 1.0, expressed as f_{sec}/f_{prim}), 135 various separations (varying from $0\farcs060$ to $0\farcs600$, by steps of $0\farcs004$, thus oversampling the pixel scale) and 3 position angles (0°, 22.5°and 45°, measured in the detector's referential). It is important to note that these 3 angles, modulo 45 degrees, are sufficient to characterise 16 different position angles by symmetry in the detector. The simulated binaries were built using unresolved objects from the sample (different than the PSF stars used to make the PSF fitting). All these calibration have been made in the F814W filter and are expected to be the same in the other filters. The S/N does not influence significantly the conclusions of the calibrations since the library of PSF stars used to make the PSF fitting spans a large range of S/N in each filters.

A.1 Relative Astrometry: Separation and Position Angle

Figure A.1 gives an overview of these calibrations for the separation and the position angle. Both plots show a periodic pattern which period is correlated to the pixel scale ($p \propto 2\times$pixel scale, with a trigonometric scaling factor depending on the position angle). This effect is mostly due to the changes in the PSF shape and the location of the object's centroid within a pixel.

It appears that the program gives excellent astrometric results. For our study, we will consider that the systematic errors on the separation are equal to the average of the errors, and that the 1-σ uncertainties are equal to the standard deviation of the errors. The systematic errors are negligible (less than $0\farcs0005$ on the separation and almost zero on the position angle). The 1-σ uncertainty on the separation is $0\farcs0028$. For the position angle it appears more appropriated to distinguish two cases: before and after $0\farcs150$. The spreading of the values is indeed much larger in the first case than in the other (see Figure A.1). This value of $0\farcs150$ is certainly related to the size of the FWHM at these wavelengths ($\sim$2.4 pixels = $0\farcs110$). The 1-σ uncertainty on the position angle before $0\farcs150$ is 1.2°, and becomes only 0.3°after $0\farcs150$. As we could expect it (for symmetry reasons), there is no perceptible dependency on the position angle (except a slight change in the amplitude and period of the periodic pattern). The main variations are related to the difference of magnitude and of course to the separation.

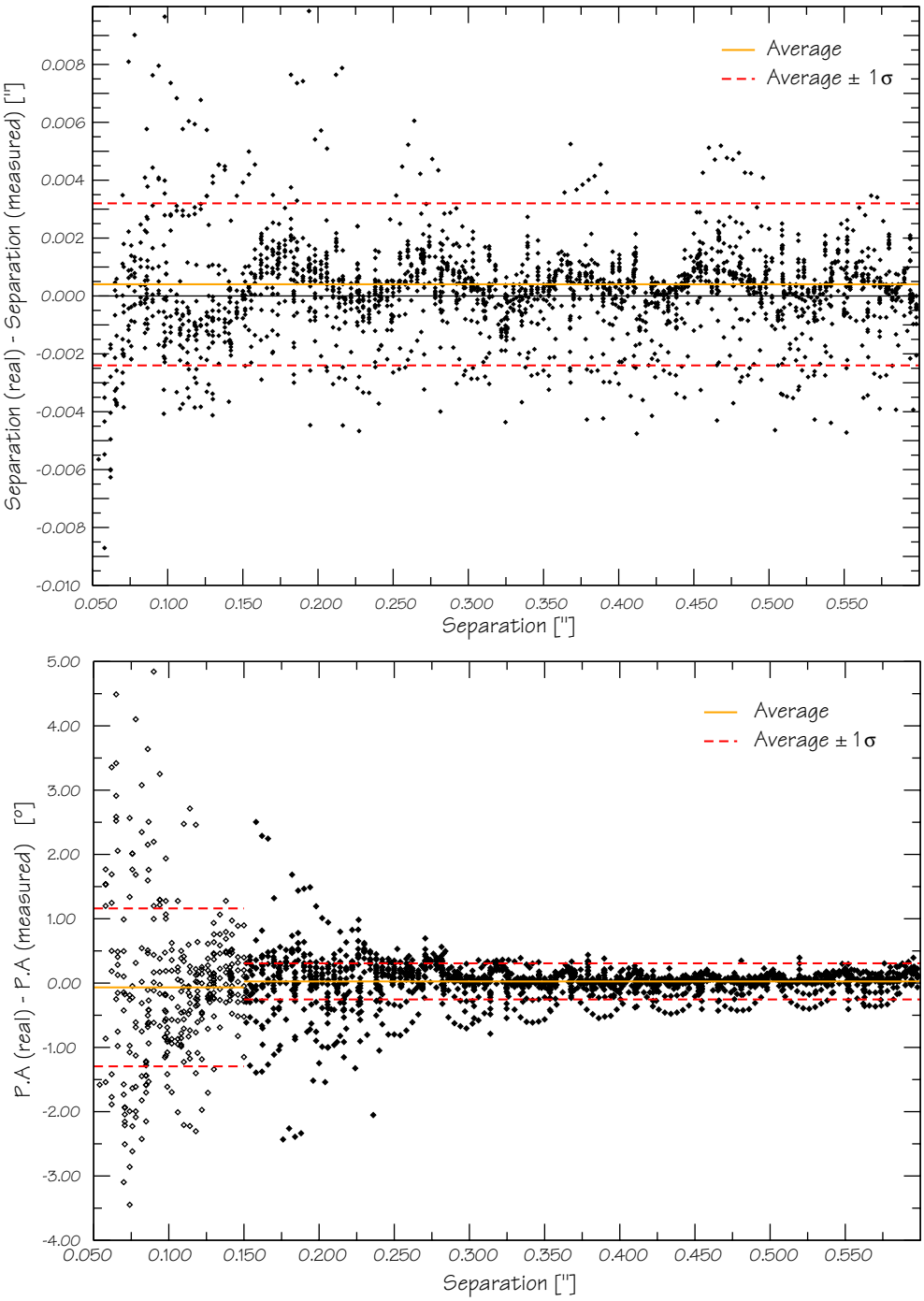

Figure A.1 Calibration of the systematic errors and uncertainties of the PSF fitting method. These figures shows the results obtained using the PSF fitting method on simulated binaries with various flux ratios, separations and position angles. Top Panel: error on the separation (i.e difference between the real separation and the separation measured) vs the real separation. Bottom Panel: same as top panel but for the error on the position angle. In both case the average and the standard deviation are represented. The systematic errors (corresponding to the average values) are almost null in both cases and I consider them negligible. The 1σ uncertainty on the separation is $0\farcs0028$. For the position angle, we can divide the plot in two parts: before and after $0\farcs150$. Before $0\farcs150$, the 1σ uncertainty is 1.2 °. After $0\farcs150$ it becomes only 0.3 °. The periodic pattern has a period almost equal to the pixel scale.

Table A.1. Systematic errors and 1-σ uncertainties on the photometric results

	$\delta < 0''.150$		$\delta > 0''.150$	
Δm_{F814W}	Systematic error[a]	1σ	Systematic error	1σ
0.00	$-6.9 + 171.4 \times \delta - 1425.3 \times \delta^2 + 3948.7 \times \delta^3$	$\pm$0.05	-0.01	$\pm$0.01
0.11	$-5.6 + 132.4 \times \delta - 1033.8 \times \delta^2 + 2674.5 \times \delta^3$	$\pm$0.05	0.09	$\pm$0.02
0.11 $\rightarrow$ 0.24	$-5.3 + 130.5 \times \delta - 1036.8 \times \delta^2 + 2713.5 \times \delta^3$	$\pm$0.07	0.17	$\pm$0.07
0.24 $\rightarrow$ 2.50	$-3.5 + 103.3 \times \delta - 925.4 \times \delta^2 + 2687.6 \times \delta^3$	$\pm$0.11	0.20	$\pm$0.09

[a]The systematic errors (in mag) are obtained using the given relation, with δ corresponding to the separation in arcseconds.

Note. — The systematic errors given in this table had to be added to the value we measured. See also Figure A.1.

A.2 Relative Photometry: difference of magnitude

The systematic errors and uncertainties on the difference of magnitudes require a more detailed analysis and description. Figure A.2 gives an overview of these results. The errors are very dependent on the difference of magnitude itself and of course on the separation, but are almost independent on the position angle (only the period and amplitude of the periodic pattern depends slightly on the position angle, see above).

Again it is more appropriate to distinguish two different parts in the range of separation: before and after $0''.150$. The plots drawn in Figure A.2 show also clearly that it is necessary to distinguish four different cases in the range of differences of magnitudes: ΔMag=0.00 mag (hereafter case 1), ΔMag=0.11 mag (case 2), 0.11$<\Delta$Mag$\leq$0.24 mag (case 3) and 0.24$<\Delta$Mag$\leq$2.50 mag (case 4).

Cases 1 and 2 are the easiest to describe. The results are excellent after $0''.150$: the systematic errors and 1σ uncertainties are -0.01$\pm$0.01 mag for case 1 and 0.09$\pm$0.02 mag for case 2. Before $0''.150$ the errors can be precisely described by a 3^{rd} order law with dispersions of only 0.05 mag in both cases. We will not linger over a more detailed description of these two cases since they do not describe any of the objects of our sample.

The third and fourth cases are more difficult to analyse.

In the range of separation before $0''.150$, the systematic errors in the third case can be relatively precisely described by a 3^{rd} order law with a dispersion of 0.07 mag. On the same range of separation, the fourth case is not reproduced as well as the other cases by a 3^{rd} order law. Nevertheless, the dispersion is 0.11 mag which is still reasonable. For the rest of our study, we will assimilate the systematic errors on these ranges of separation and differences of magnitude to the values given by the corresponding third order laws, and the 1-σ uncertainties to the corresponding dispersions (see Table A.1).

In the range of separation after $0''.150$, the third case shows also an obvious periodic pattern. Although it is obvious, this pattern cannot be easily fitted by a sinusoidal function without

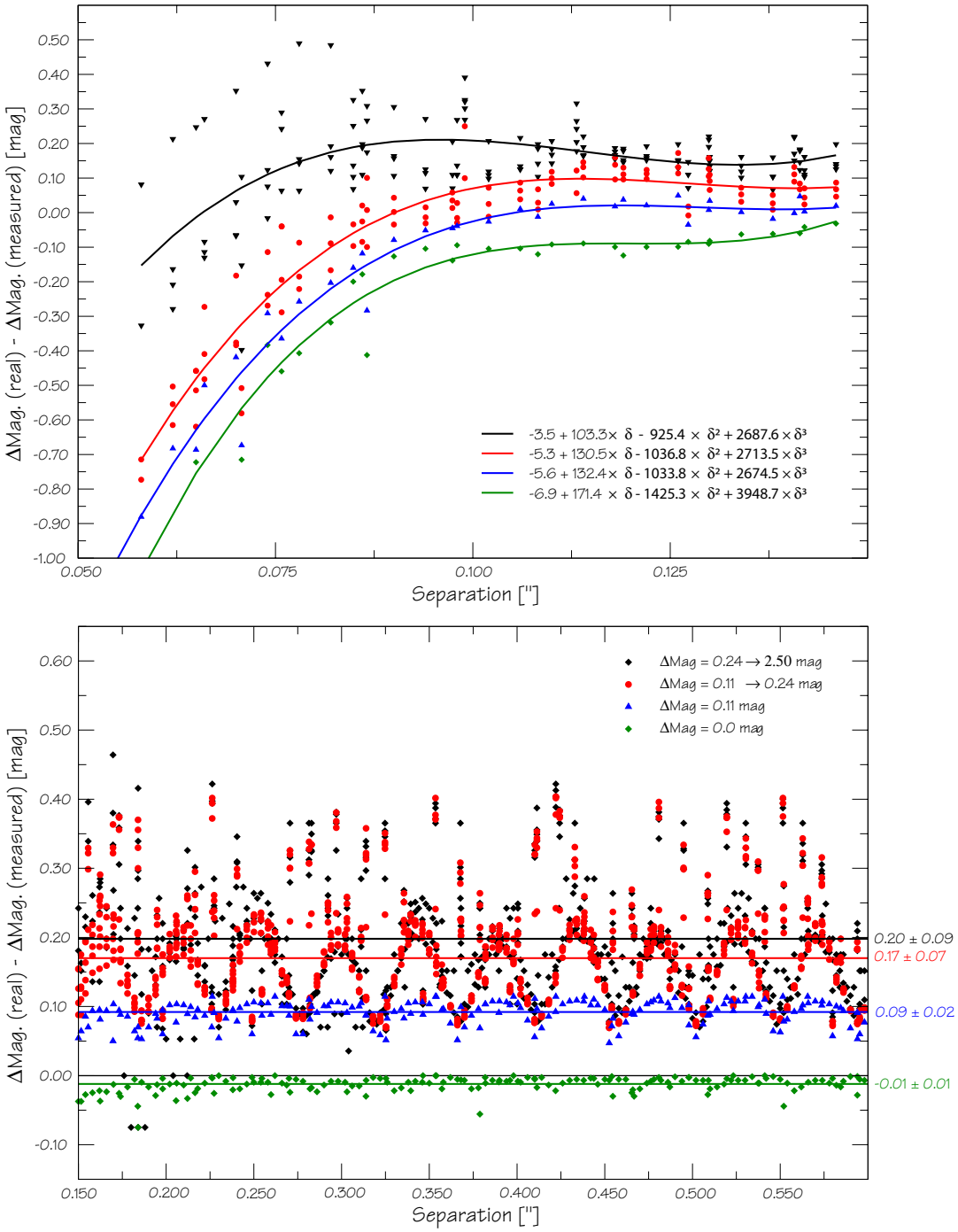

Figure A.2 Calibration of the systematic errors and uncertainties of the PSF fitting method. These figures shows the results obtained using the PSF fitting method on simulated binaries with various flux ratios, separations and position angles. Top Panel: error on the difference of magnitude (i.e difference between the real difference of magnitude and the one measured) as a function of separation between 0.″060 and 0.″150. Bottom panel: same as top panel for the separation range between 0.″150 and 0.″600.

Table A.2. Systematic errors and 1-σ uncertainties on the astrometric results

	$\delta < 0\farcs150$	$\delta > 0\farcs150$
P.A	$\approx 0.0^\circ \pm 1.2^\circ$	$\approx 0.0^\circ \pm 0.3^\circ$
Separation	$\approx 0\farcs0 \pm 0\farcs0028$	$\approx 0\farcs0 \pm 0\farcs0028$

Note. — see also Figure A.2 and Table A.1. δ represents the separation.

underestimating the systematic error, mainly because of the many points that are far away from the pattern. The systematic error on these values are thus assimilated to the average (0.17 mag) and the 1-σ uncertainties to the standard deviation ($\pm$0.07 mag).

The pattern still appears but less obviously in the fourth case where the spreading of the errors is much larger. Here also we assimilate the systematic error to the average of these values (0.20 mag) and the 1-σ uncertainties to their standard deviation ($\pm$0.09 mag).

Table A.1 and A.2 gives an overview of the conclusions of these calibrations. All the values given in the text and in the tables have been corrected for the systematic errors and the given uncertainties correspond to the 1-σ uncertainties calculated as explained in this section, unless specified explicitly.

Appendix B

Calibrations of the PSF fitting method for ACS-HRC data

In order to evaluate the accuracy of the PSF fitting program with ACS-hRC data, and look for systematic errors, we used the program on 3240 simulated binaries, covering a range of 11 various input flux ratios (varying from 0.05 to 1.0, expressed as f_{sec}/f_{prim}), by steps of 0.05), 135 various separations (varying from 0.″060 to 0.″600, by steps of 0.″010, thus oversampling the pixel scale) and 3 position angles (0°, 22.5°and 45°, measured in the detector's referential). As mentioned in the case of WFPC2, these 3 angles, modulo 45 degrees, are sufficient to characterise 16 different position angles by symmetry in the detector. The simulated binaries were built using unresolved objects from the sample (different than the PSF stars used to make the PSF fitting). All these calibrations have been made in the F814W filter and are expected to be the same in the other filters. As for WFPC2, the S/N does not influence significantly the conclusions of the calibrations since the library of PSF stars used to make the PSF fitting spans a large range of S/N in each filters.

B.1 Relative Astrometry: Separation and Position Angle

Figure B.1 gives an overview of these calibrations for the separation and the position angle. As one could expect, the results are much better than in the case of WFPC2, since the PSF is well sampled by the better pixel scale (0.″0277 instead of 0.″0455), and the sensitivity (and therefore the S/N) is better.

B.1.1 Separation

It appears that the program gives excellent astrometric results. We will consider that the systematic errors on the separation are equal to the average of the errors, and that the 1-σ uncertainties are equal to the standard deviation of the errors. As shown in Figure B.1, it appears to be more appropriated to distinguish two cases: separations less than 0.″090 and separations greater than 0.″090. In the first case, the systematic error is equal to 0.″001, and the corresponding 1-σ uncertainty is 0.″003, while in the second case the systematic error is negligible, and the 1-σ uncertainty is 0.″0005.

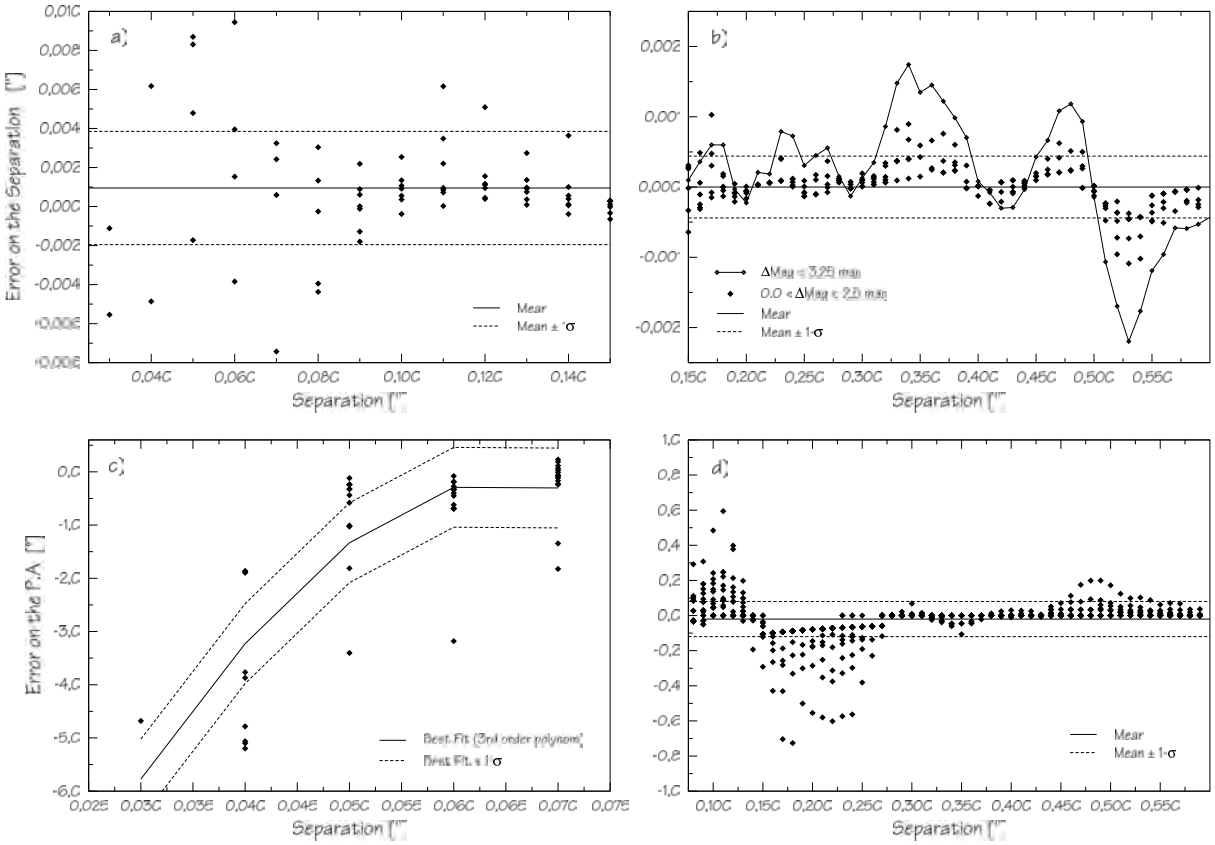

Figure B.1 Calibration of the systematic errors and uncertainties of the PSF fitting method with ACS-HRC. These figures shows the results obtained using the PSF fitting method on simulated binaries with various flux ratios, separations and position angles. a) error on the separation (i.e difference between the real separation and the separation measured) vs the real separation for separations ranging between 0.″040 and 0.″150; b) same as a) but for separations greater 0.″150. The "worst" case (ΔMag=3.25 mag) is indicated with a line; c) error on the position angle for separations ranging between 0.″040 and 0.″085; d) same as c) but for separations greater than 0.″085. The mean values and the standard deviations, or the polynomial fit (panel c), are represented.

Table B.1. Systematic errors and 1-σ uncertainties on the separation and P.A for ACS

Separation		
Sep. Range	Systematic error	1-σ
$\delta < 0\farcs090$	$0\farcs001$	$0\farcs003$
$\delta > 0\farcs090$	$0\farcs000$	$0\farcs0005$
Position Angle		
Sep. Range	Systematic error	1-σ
$\delta < 0\farcs075$[a]	-15.3 + 323.8×δ + 790×δ^2 - 33676×δ^3	0.75°
$0\farcs075 < \delta < 0\farcs275$	0.3°	0.15°
$\delta > 0\farcs275$	0.0 °	0.1 °

[a]The systematic errors (in mag) is obtained using the given relation, with δ corresponding to the separation in arcseconds.

Note. — The systematic errors given in this table had to be added to the value we measured. See also Figure B.1.

B.1.2 Position Angle

As shown in Figure B.1, it is more appropriated to distinguish three cases: separations less than $0\farcs075$, separations between $0\farcs075$ and $0\farcs275$, and separations greater than $0\farcs275$.

In the last case, we will consider that the systematic errors on the position angle are equal to the average of the errors, and that the 1-σ uncertainties are equal to the standard deviation of the errors. The systematic error appears to be negligible, and the 1-σ uncertainty of the order of 0.1°. Between $0\farcs075$ and $0\farcs275$, the mean value (systematic error) is equal to 0.3°and the standard deviation (1-σ uncertainty) is equal to 0.15°. We dont have any explanation for this peculira structure of the error on the P.A. In the first case, the error on the position angle seems to follow a trend and it therefore appears more appropriated to perform a polynomial fit of the values. We then consider that the systematic error on the position angle at a certain separation is equal to the corresponding value of the 3rd order polynomial fit, and that the 1-σ uncertainties are equal to the dispersion around the fit. Table B.1 gives a summary of the systematic errors and uncertainties on the P.A and on the separation depending on the separation.

B.2 Relative Photometry: difference of magnitude

The systematic errors and uncertainties on the difference of magnitudes require a more detailed analysis and description. Figure B.2 and B.3 give an overview of these results. The errors are

very dependent on the difference of magnitude itself and of course on the separation, but are almost independent on the position angle.

It is more appropriate to distinguish two different parts in the range of difference of magnitude: $0.00 \leq \Delta\text{Mag} \leq 0.87$ mag (hereafter case 1) and $0.99 \leq \Delta\text{Mag} \leq 3.25$ mag (case 2).

It appears also that we should distinguish two cases in the range of separation. For case 1, we should split in two parts, between $0\farcs000 \leq \delta \leq 0\farcs100$ (case 1a), and for $\delta \geq 0\farcs100$ (case 1b) (see Figure B.3). Similarly, case 2 should be split in two parts: between $0\farcs000 \leq \delta \leq 0\farcs150$ (case 2a), and for $\delta \geq 0\farcs150$ (case 2b) (see Figure B.2).

Cases 1b and 2b are the easiest to describe. The systematic errors and 1-σ uncertainties can be described by a 2^{nd} order polynom fit and its dispersion respectively. The results are given in Table B.2.

Case 1a is also easy. The dispersion of the values is relatively large, but we chose to assimilate the systemattic error to the mean value, and the 1-σ uncertainty to the standard deviation. As shown in Figure B.3, this encloses most of the cases. At short wavelength and larger difference of magnitude, it can be nevertheless more appropriated to consider 2-σ uncertainty instead of one. The detailed results are given in Table B.2

Case 2a requires a more case by case approach. Figure B.2 shows indeed that the systematic errors can be nicely described by 3_{rd} order polynom fits. The corresponding dispersion is relatively loweven in the worst cases. Table B.2 gives all the details concerning the individual fits and their corresponding dispersion.

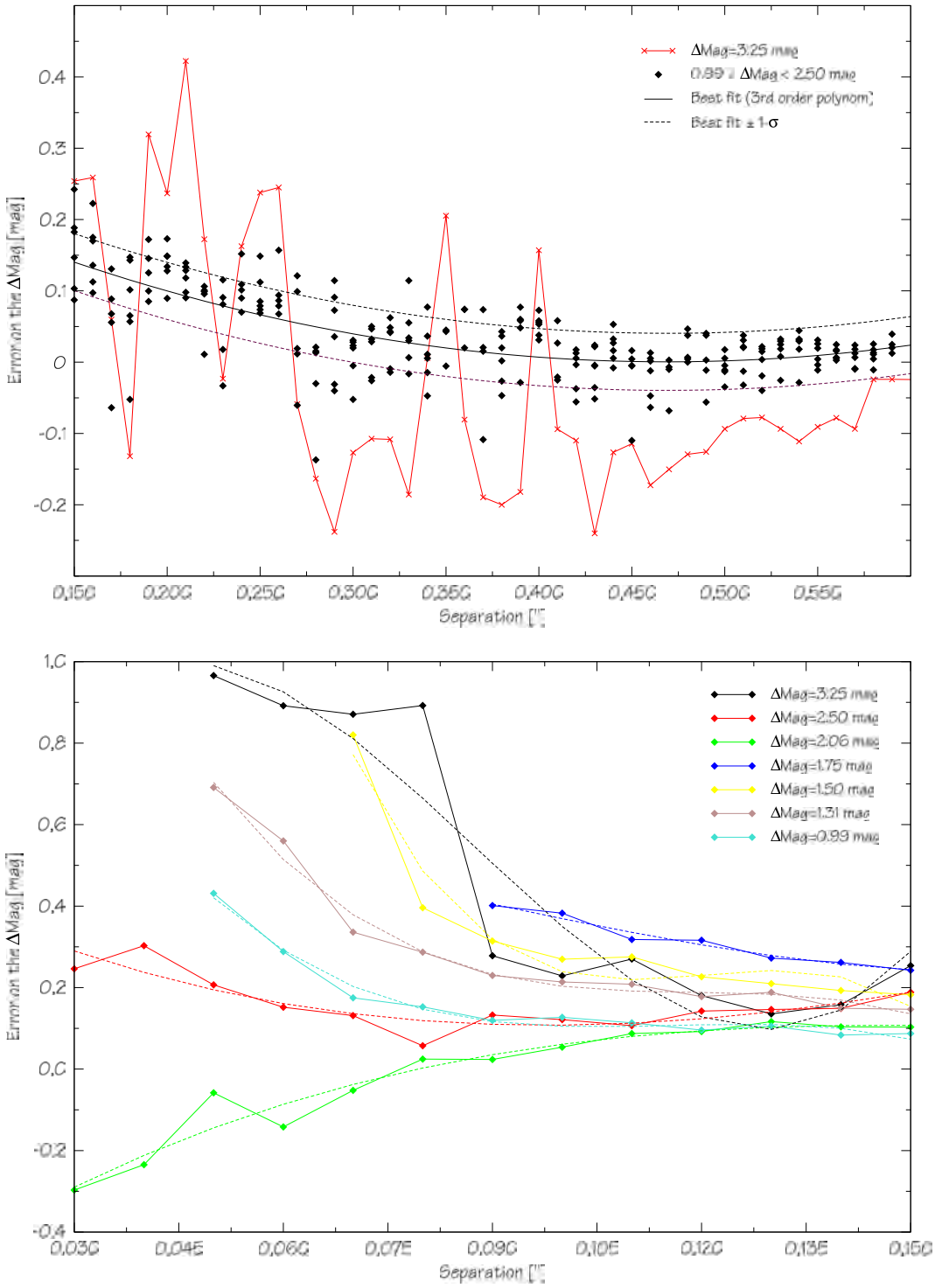

Figure B.2 Calibration of the systematic errors and uncertainties of the PSF fitting method. These figures shows the results obtained using the PSF fitting method on simulated binaries with various flux ratios, separations and position angles. Bottom Panel: error on the difference of magnitude (i.e difference between the real difference of magnitude and the one measured) as a function of separation between 0″.030 and 0″.150. Top panel: same as bottom panel for the separation range between 0″.150 and 0″.600.

Table B.2. Systematic errors and 1-σ uncertainties on the ΔMag for ACS

Domain of validity			Value	
Case	Range of ΔMag	Range of δ	Syst. Error[a]	1-σ
1a	0.00→0.87 mag	0.″030→0.″100	-0.05 mag	0.15 mag
1b	0.00→0.87 mag	≥0.″100	$0.027\text{-}0.105\times\delta+0.120\times\delta^2$	0.12 mag
2a	0.99→3.25 mag	≥0.″150	$0.303\text{-}1.288\times\delta+1.372\times\delta^2$	0.12 mag
2b	3.25 mag	0.″030→0.″150	$-0.080 + 53.753\times\delta - 799.69\times\delta^2+3051.4\times\delta^3$	0.05 mag
2b	2.50 mag	0.″030→0.″150	$0.510 - 9.010\times\delta + 57.99\times\delta^2- 81.4\times\delta^3$	0.02 mag
2b	2.06 mag	0.″030→0.″150	$-0.593 + 11.960\times\delta - 65.43\times\delta^2+ 112.2\times\delta^3$	0.02 mag
2b	1.75 mag	0.″030→0.″150	$0.610 + 0.719\times\delta - 51.62\times\delta^2+ 203.7\times\delta^3$	0.02 mag
2b	1.50 mag	0.″030→0.″150	$8.508 - 209.390\times\delta+ 1751.6\times\delta^2- 4846.8\times\delta^3$	0.02 mag
2b	1.31 mag	0.″030→0.″150	$2.776 - 64.740\times\delta + 541.94\times\delta^2- 1517.8\times\delta^3$	0.02 mag
2b	0.99 mag	0.″030→0.″150	$1.919 - 47.797\times\delta + 416.45\times\delta^2- 1198.9\times\delta^3$	0.02 mag

[a]The systematic errors (in mag) is obtained using the given relation, with δ corresponding to the separation in arcseconds.

Note. — The systematic errors given in this table had to be added to the value we measured. See also Figure B.1.

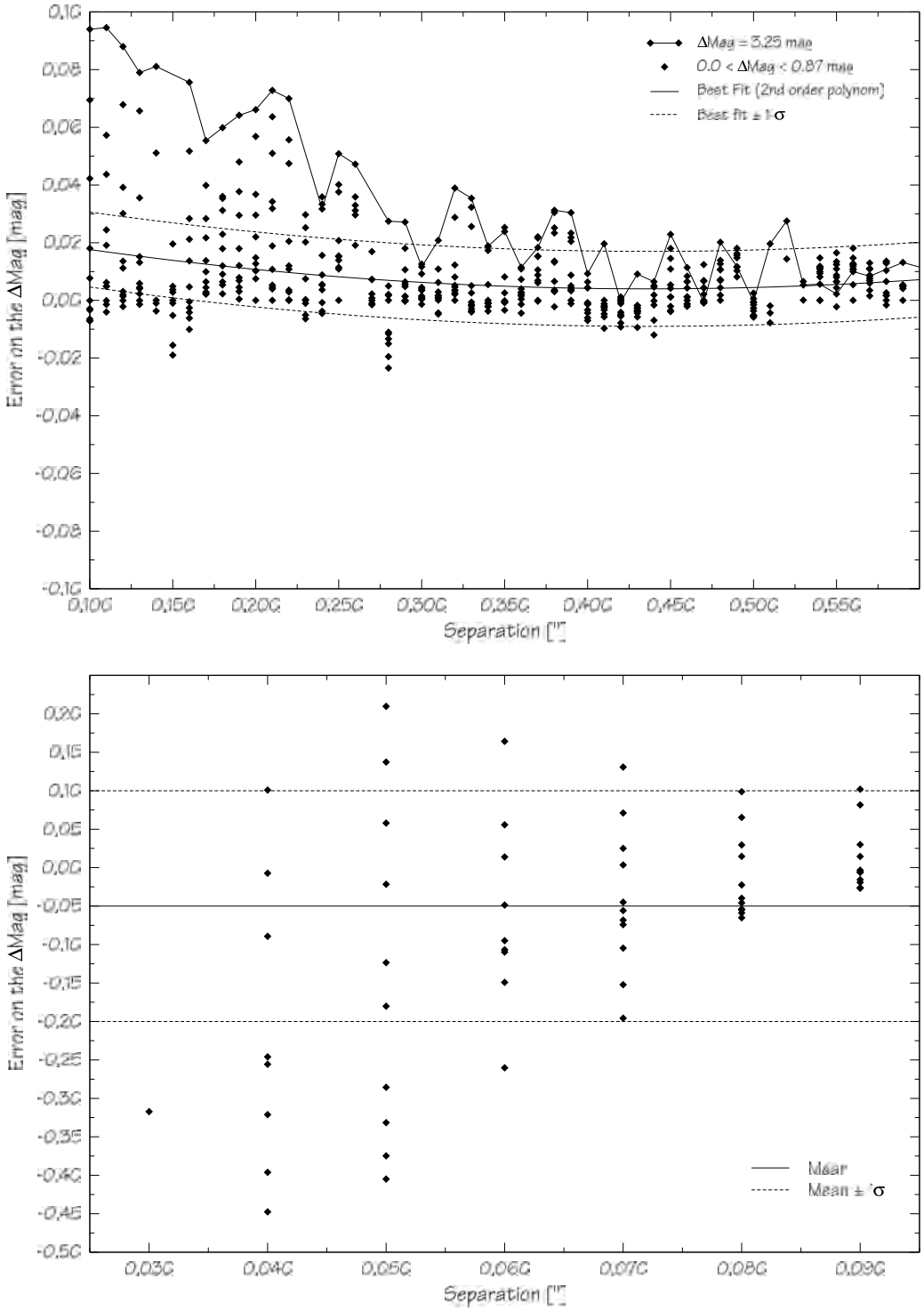

Figure B.3 Calibration of the systematic errors and uncertainties of the PSF fitting method. These figures shows the results obtained using the PSF fitting method on simulated binaries with various flux ratios, separations and position angles. Top Panel: error on the difference of magnitude (i.e difference between the real difference of magnitude and the one measured) as a function of separation between 0.″060 and 0.″150. Bottom panel: same as top panel for the separation range between 0.″150 and 0.″600.

Appendix C

Other studies: X-ray emission of brown dwarfs

Beside my PhD project, I was able to conduct or be involved in several other projects concerning X-ray emission of brown dwarfs. These works have lead to the publication of two articles in refereed journals. They are reported here.

ELSEVIER

New Astronomy 7 (2002) 595–602

New Astronomy

www.elsevier.com/locate/newast

XMM-Newton observations of the nearby brown dwarf LP 944-20

Eduardo L. Martín[a,*], Hervé Bouy[b]

[a]Institute for Astronomy, 2680 Woodlawn Drive, Honolulu, Hawaii 96822, USA
[b]E.S.O, Karl Schwarzschildstraße 2, D-85748 Garching, Germany

Received 2 July 2002; received in revised form 14 August 2002; accepted 16 August 2002
Communicated by W. Soon

Abstract

The nearby ($d = 5.0$ pc) brown dwarf LP 944-20 was observed with the *XMM-Newton* satellite on 07 January 2001. The target was detected with the Optical Monitor ($V = 16.736 \pm 0.081$), but it was not detected during the ≈ 48 ks observation with the X-ray telescopes. We determine a 3σ upper limit for the X-ray emission from this object of $L_X < 3.1 \times 10^{23}$ ergs·s^{-1}, equivalent to a luminosity ratio upper limit of $\log(L_X/L_{bol}) \leq -6.28$. This measurement improves by a factor of three the previous *Chandra* limit on the quiescent X-ray flux. This is the most sensitive limit ever obtained on the quiescent X-ray emission of a brown dwarf. Combining the *XMM-Newton* data with previous *ROSAT* and *Chandra* data, we derive flare duty cycles as a function of their luminosities. We find that very strong flares [$\mathrm{Log}(L_X/L_{bol}) > -2.5$] are very rare (less than 0.7% of the time). Flares like the one detected by Chandra [$\mathrm{Log}(L_X/L_{bol}) = -4.1$] have a duty cycle of about 6%, which is lower than the radio flare duty cycle ($\sim 13\%$). When compared with other M dwarfs, LP 944-20 appears to be rather inactive in X-rays despite of its relative youth, fast rotation and its moderately strong activity at radio wavelengths.

PACS: 97.20.Vs; 98.70.Qy
Keywords: Stars: individual: LP 944-20; Stars: low-mass, brown dwarfs; X-rays: stars

1. Introduction

LP 944-20 (=BRI 0337-3535) is an isolated nearby brown dwarf (mass < 0.075 $M_\odot$) first identified by Luyten and Kowal (1975). Spectroscopic observations reported by Tinney (1998) give a spectral type of dM9, an age of about 500 Myr and a mass of about 0.065 $M_\odot$ using the lithium test proposed by Magazzù et al. (1993). Because of its substellar mass and its proximity to the Sun, this object is a benchmark in the study of very low-mass objects. LP 944-20 was observed in the X-ray regime for the first time with the *ROSAT* satellite by Neuhäuser et al. (1999), but was not detected. It has been detected with the *Chandra* satellite (Rutledge et al., 2000) in december 1999 during an X-ray flare of duration 1 ~ 2 h. Outside the flare, LP 944-20 was not detected with a 3σ upper limit on the emission at $L_X < 1.0 \times 10^{24}$ ergs·s^{-1}. Both quiescent and flaring

*Corresponding author.
E-mail addresses: ege@teide.ifa.hawaii.edu (E.L. Martín), hbouy@eso.org (H. Bouy).

1384-1076/02/$ – see front matter
PII: S1384-1076(02)00178-1

radio emission have been observed with the VLA (Berger et al., 2001).

X-ray emission is widespread among fully-convective M dwarfs (spectral type M3 and later), and it is frequently variable (Fleming et al., 1993; Marino et al., 2000; Feigelson et al., 2002). X-ray observations of ultracool dwarfs (spectral type M7 and later) are still very scarce. Strong variability has been observed in a few objects (Rutledge et al., 2000; Fleming et al., 2000; Schmitt and Liefke, 2002). It is thought that the X-ray photons are emitted from a hot corona. The properties of coronae (permanent or transient) in ultracool dwarfs are not well understood.

LP 944-20 was targeted for observations with *XMM-Newton* for two reasons mainly, first to try to catch it during a flare, which would have allowed to obtain spectroscopy if a flare had occurred, and second to search for quiescent X-ray emission. Unfortunately, we did not detect LP 944-20 at all. Nevertheless, we improve the value of the upper limit on the quiescent X-ray emission from LP 944-20, and we derive X-ray flare rates as a function of X-ray luminosity that may be useful for planning future observations of this brown dwarf.

2. Observations

XMM-Newton observed LP 944-20 on 2001 January 07–08, between 14:21:05 and 04:43:52 UTC for 51 767 s. The pointing position was *R.A.* = 03 h 39 min 34.60 s and *Dec* = −35°25″51.0′ Epoch 2000, according to the Simbad database.[1]

2.1. Optical data and source identification

Besides its three X-ray telescopes, *XMM-Newton* also has a 30-cm optical-UV telescope, providing the possibility to observe simultaneously in the X-ray and optical-UV regimes. The Optical Monitor (*OM*) was used with the *V* filter for four exposures of 5000 s each in imaging mode. The OM detector has a format of 2048 × 2048 pixels, each 0.5″ × 0.5″. The field of view is therefore 17′ × 17′.

We used the data given by the OM to confirm the presence of the source in the field of view. The coordinates we used to identify LP 944-20 are different from the pointing coordinates. We used the more recent coordinates given by the astrometry of Rutledge et al. (2000) after their observation of LP 944-20 with *Chandra* during a X-ray flare in 1999 December. These coordinates are: *R.A.* = 03 h 39 min 35.16 s±0.1″ and *Dec* = −35°25′44.0′±0.1″, epoch 1999.95.

We identified LP 944-20 in the field of view by plotting these coordinates on the four images given by the OM. The result is shown in Fig. 1. We found a point-source at a distance of 0.4″±0.1″ from the expected coordinates of LP 944-20. This offset is small in comparison with the <2″ known systematic uncertainties in the *XMM-Newton* preprocessing analysis astrometry (XMM-Newton User's Handbook, 2000). Moreover a small offset was also expected because of the proper motion of LP 944-20 since it was observed by Rutledge et al. (2000) more than 1 year ago. The offset in the optical position is consistent with the known proper motion of LP 944-20. We were also able to identify the three other sources in the field of view simply by direct comparison with the image obtained by Rutledge et al. (2000). We therefore identify this optical source with the brown dwarf LP 944-20 on the basis of positional coincidence with the expected coordinates.

We also used the four exposures given by the OM to look for optical variability. The magnitudes of the source identified as LP 944-20 and of two other stars in the field of view were calculated using the *IRAF* `phot` task. This allowed us to plot the evolution of the magnitude during the whole observation. The result is shown in Fig. 2. The behavior of LP 944-20's magnitude is different than that of the two other stars. We notice that whereas the magnitudes of the two reference stars are roughly correlated, LP 944-20's magnitudes are not. We measure a mean magnitude of $V = 16.736$ and a standard deviation of 0.081 for LP 944-20. For reference star 1 we measure a mean magnitude of $V = 16.681$ and a standard deviation of 0.028. For reference star 2 we measure a mean magnitude of $V = 16.770$ and a standard deviation of 0.067. We conclude that LP 944-20 may be variable in the OM data. The variability of LP 944-20, however, is only slightly higher than that of reference star 2. We cannot make

[1] Simbad database, operated at CDS, Strasbourg, France.

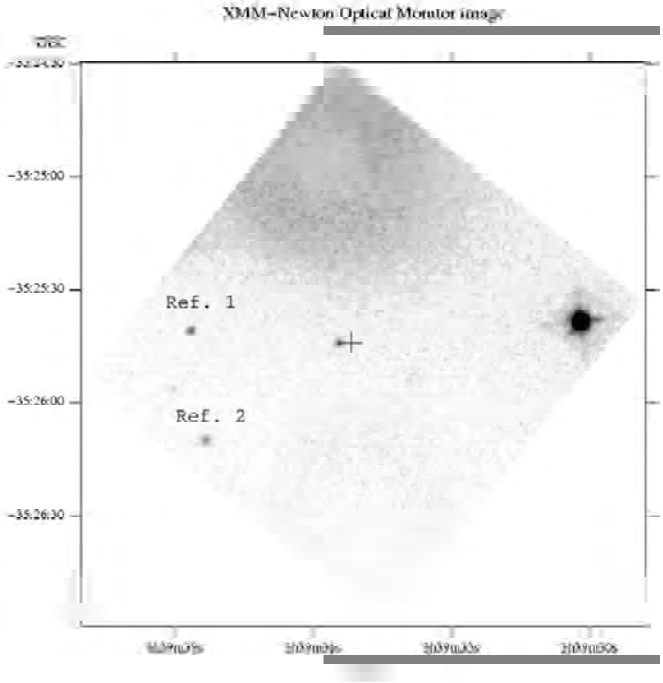

Fig. 1. Indentification of LP 944-20 in the field of view of the Optical Monitor Data. The plus indicate the expected coordinates of LP 944-20. The diffuse bright area on the top of the image is an artifact.

a definitive claim that LP 944-20 is variable in our data because of the lack of enough reference stars in the field of view.

2.2. X-ray data and analysis

The European Photon Imaging Camera (*EPIC*) MOS1 & MOS2 were used. The total ontarget exposure time in each camera was 48 724 s in prime full window mode with 2.5 s time resolution. The EPIC PN was used in prime full window mode with 73.4 ms time resolution and ontarget exposure 46 618 s. Each EPIC instrument was used with the thin filter, which suppresses the optical contamination up to m_V of 18 (MOS) or m_V of 17 (PN). Both MOS & PN detectors have a circular field of view of 30′ diameter. For more details on *XMM-Newton* and its instruments, we refer to XMM-Newton User's Handbook (2000).

The first step was to search for LP 944-20 in the field of view of each EPIC MOS & PN detector. We plotted the coordinates of LP 944-20 on each image obtained by each detector, but we did not detect any source. To be sure that we were using the most sensitive exposure, we used the image given by the pipeline which combines data from all EPIC's MOS & PN in the entire energy range (0.1 − 12.0 keV), as shown in Fig. 3.

On these figures, the X-ray source closest to the expected position is offset by $\delta(R.A.) = 2.5'' \pm 0.1''$ and $\delta(Dec) = -28.37'' \pm 0.1''$. This offset is large in comparison with the $0.4'' \pm 0.1''$ offset observed with the optical data. So at this point we already knew that LP 944-20 was not detected.

We performed differential astrometry between the *XMM-Newton* and *Chandra* images. This allowed us to identify all the X-ray sources in our field of view in an area of $20'' \times 10''$ centered on the expected

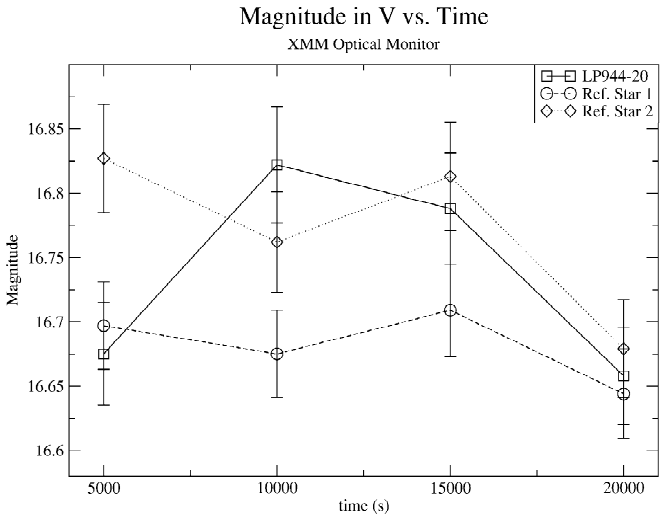

Fig. 2. Optical magnitude of LP 944-20 and of two reference stars in the field of view of the Optical Monitor.

coordinates of LP 944-20. We were then able to conclude that LP 944-20 was not detected during the *XMM-Newton* observation.

Since the target was not detected, the first conclusion is that there was no significant X-ray flare during this 48 ks observation. Nevertheless, it is interesting to calculate the upper limit on the time average quiescent X-ray luminosity. We did the calculation of the upper limit of X-ray flux with each of the three images of the preprocessing products, corresponding to the three exposures obtained with the EPIC MOS1, MOS2 & PN detectors on the entire energy range (0.1 − 12.0 keV). To calculate a 3σ flux upper limit, we considered an area of twice the FWHM (= 2 pixels) around the expected position of LP 944-20. In this area we calculated the mean value of $counts \cdot pixel^{-1}$ and the corresponding standard deviation σ using the IRAF[2] `phot` task, which gives count rates corrected for background. The results are listed in Table 1. As the EPIC PN camera is the most sensitive detector, we therefore only consider its result to calculate the flux upper limit.

To convert this count rate to flux, we followed XMM-Newton User's Handbook (2000) instructions, by using the PIMMS[3] software. As LP 944-20 was not detected during the observation, we were not able to fit its spectrum in order to know its spectral type. We adopted the results of Rutledge et al. (2000) summarized in Table 2. The HI column density was calculated using the *nH* software: $n_H = 1.31 \times 10^{20}$ cm^{-2}.

The results for the upper limit of flux and X-ray luminosity (3σ, assuming Gaussian statistics) are listed in Table 3. The uncertainties on these values are Poisson (counting statistics) plus ~10% spectral uncertainty, according to Rutledge et al. (2000). As their best fit on the spectrum was obtained with the Raymond–Smith thermal plasma model, we finally kept the corresponding 3σ flux as the upper limit on the time average quiescent X-ray luminosity for LP

[2] *IRAF* is distributed by the National Optical Astronomy Observatory, which is operated by the Association of Universities for Research in Astronomy, Inc., under contract with the National Science Foundation.

[3] *nH* and *PIMMS* (Portable, Interactive, Multi-Mission Simulator) are distributed by the NASA's HEARSAC.

Table 1
Count rates

Instrument	Counts·pixel^{-1} (average)	Standard deviation σ (counts·pixel^{-1})	3σ (counts·pixel^{-1}·s^{-1})
EPIC PN	4.53	2.00	1.3×10^{-4}
EPIC MOS1	1.59	1.18	7.3×10^{-5}
EPIC MOS2	1.73	1.24	7.6×10^{-5}

Table 2
Spectral parameters of LP 944-20

Model	Associated feature
Black body	$k_B\times T=0.17$ keV
Power law	$\alpha_{photon}=2.6$
Thermal plasma	$k_B\times T=0.26$ keV

Rutledge et al. (2000).

944-20: $L_X<3.1\times10^{23}$ ergs·s^{-1}, equivalent to a luminosity ratio upper limit of $\log(L_X/L_{bol})\leq -6.28$.

3. Discussion

The first observation of LP 944-20 in the X-ray regime by Neuhäuser et al. (1999) with the *ROSAT* satellite placed an upper limit of $\log(L_X/L_{bol})\leq -4.17$ after a 220 ks *ROSAT-HRI* observation. The second X-ray observation (Rutledge et al., 2000) placed a better upper limit of $\log(L_X/L_{bol})\leq -5.70$ after the 44 ks *Chandra-ACIS-S* observation before the flare. Our new value improves this upper limit of quiescent X-ray emission at $\log(L_X/L_{bol})\leq -6.3$. The corresponding upper limit of X-ray luminosity ($L_X\leq3.1\times10^{23}$ ergs·s^{-1}) is thus improved by a factor of three. This value is close to the solar X-ray emission level during its maxima of activity.

In Fig. 4 we display the dependence of X-ray activity versus spectral type for M dwarfs. The upper envelope of X-ray activity is remarkably independent of M subclass. There is no obvious connection between age and X-rays. The M dwarfs in the ChaI, ρOph and Taurus star-forming regions show X-ray emission comparable to much older field dwarfs (Neuhäuser et al., 1999; Mokler and Stelzer, 2002). We conclude that there is no evidence for a decline in coronal emission with increasing age in fully convective M dwarfs.

We have estimated the rate of X-ray flare occurrence in LP 944-20 by adding 287.5 ks of *ROSAT* data analyzed by Neuhäuser et al. (1999), 43.8 ks of *Chandra* data analyzed by Rutledge et al. (2000) and 51.7 ks of *XMM-Newton* data (this paper). The duration of the only flare so far observed was 2.76 ks Rutledge et al. (2000). Thus, we get an X-ray flare frequency of 0.72% for flares with luminosity $\mathrm{Log}(L_X/L_{bol})>-2.5$. Weaker flares could not have been detected by *ROSAT*. Thus, we derive the duty cycle of flares with luminosity comparable with the flare detected by *Chandra* [$\mathrm{Log}(L_X/L_{bol})=-4.1$] to be about 6%.

The published VLA radio data have a duration of 79.9 ks (Berger et al., 2001). Three flares were detected with a total duration of ~10.4 ks. Hence, we estimate a radio flare frequency of about 13%. It is not known to what X-ray luminosity the radio flares correspond, but we can set an upper limit using the *XMM-Newton* data. If we assume a flare duty cycle of 13%, the flare X-ray luminosity has to be $\mathrm{Log}(L_X/L_{bol})<-5.39$ to be consistent with our non detection.

LP 944-20 is a relatively inactive object. Tinney

Table 3
X-ray luminosity upper limit

Model	Flux (10^{-17} erg·cm^{-2}·s^{-1})	log L_X (ergs·s^{-1})	$\log\left(\frac{L_X}{L_{bol}}\right)$
Black body	≤1.1	≤23.50	≤-6.27
Power law	≤1.3	≤23.59	≤-6.19
Thermal plasma	≤1.0	≤23.49	≤-6.28

Tinney (1996) for $L_{bol}\sim6\times10^{29}$ ergs·s^{-1}.

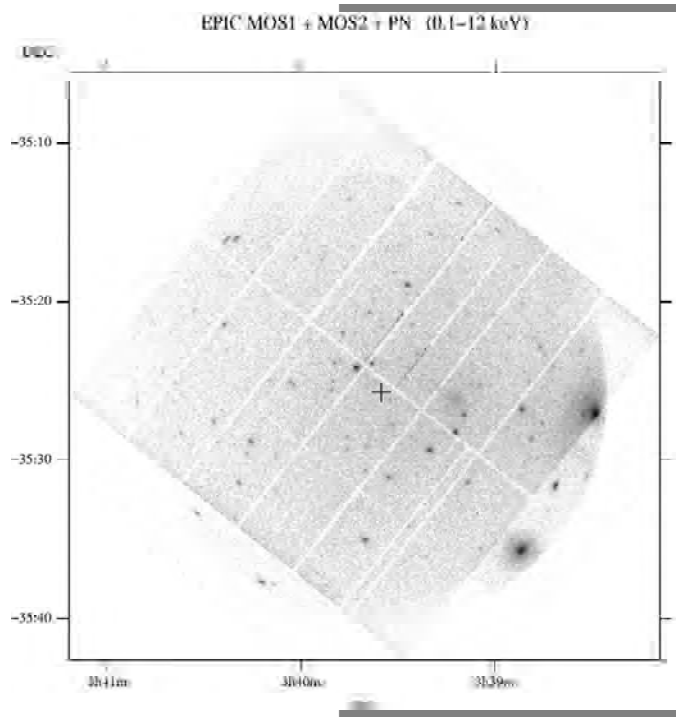

Fig. 3. Combined image from all EPICs MOS & PN instruments in the energy range (0.1 – 12.0 keV). The figure shows the entire field of view. The square chips of the EPIC PN and the circular field of view of MOS1 & 2 appear on this figure. A plus indicates the expected position of LP 944-20.

(1998) reported H_α weakly in emission. Berger et al. (2001) estimated a surface magnetic field strength of $B \sim 5$ G assuming synchrotron emission during the radio flares. For comparison, active dM stars have magnetic field strengths of a few kG, solar flares have $B \sim 100$ G, and Jupiter has an average $B \sim 10$ G (Hide and Stannard, 1976). Our low upper limit on the quiescent X-ray emission of LP 944-20 is consistent with a weak magnetic field. The detection of low-amplitude photometric variability in LP 944-20, and the low-level of X-ray emission in this object, suggests the presence of surface thermal inhomogeneities due to non-magnetic clouds, as discussed by Tinney and Tolley (1999) for LP 944-20 and by Martín et al. (2001) for the M9.5 dwarf BRI0021-0214. Recent theoretical works (Gelino et al., 2002; Mohanty et al., 2002) show that in ultracool dwarfs there should not be much interaction between the gas and the magnetic field because the Reynolds number is very low throughout the photosphere.

LP 944-20 appears to be an object with substellar mass, weak magnetic field, fast rotation and cloudy atmosphere. We speculate that the radio activity may be enhanced by the presence of a close planetary-mass companion (Io-type), which provides a continuous supply of ionized particles to the ionosphere of LP 944-20. Radial velocity variability has been detected by Guenther and Wuchterl (2003) which could be due to a planetary-mass close companion, but they did not have enough data to derive an orbital period.

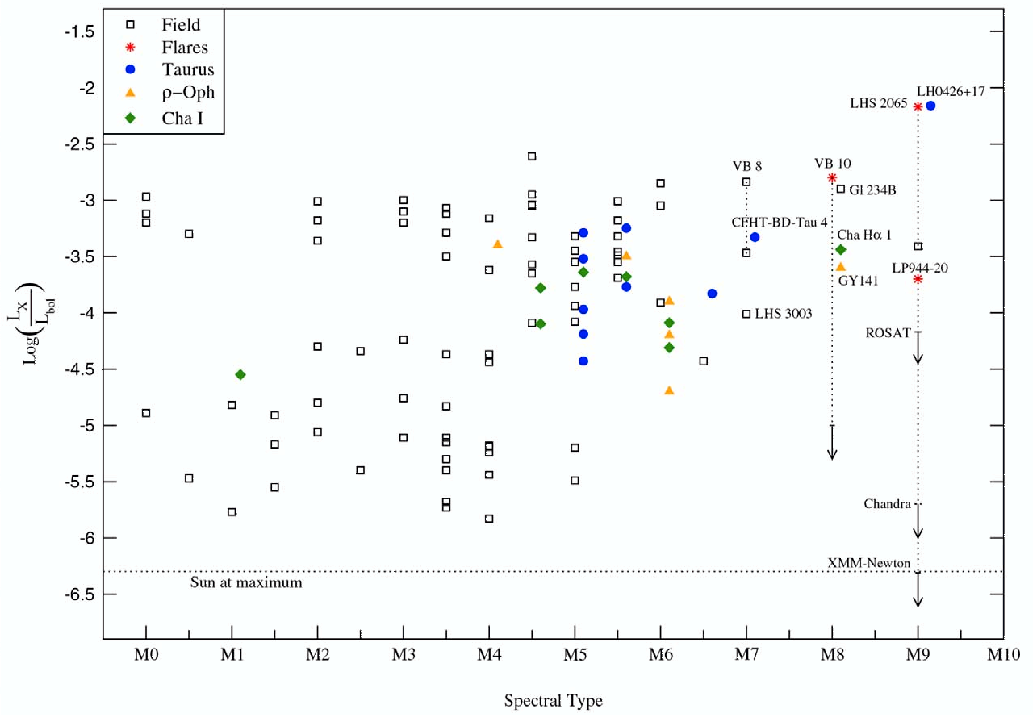

Fig. 4. Distribution of X-ray luminosity of dM dwarfs as a function of spectral type. The squares represent values obtained for field dwarfs (Fleming et al., 1993, 1995, 2000; Giampapa et al., 1996; Rutledge et al., 2000). The circles, diamonds and triangles denote young objects in star-forming regions. The stars represent the flaring objects at their maximum with the corresponding value or upper limit on the quiescent emission linked by a dotted line. To avoid confusion, the Taurus object's spectral types have been shifted by 0.1 subclass.

Acknowledgements

This research has made use of the Simbad [4] database, operated at CDS, Strasbourg, France. Support for this project has been provided by NASA grant NAG5-9992. We thank our collaborators Gibor Basri, Lars Bildsten and Bob Rutledge, and an anonymous referee for helpful discussions.

[4] http://simbad.u-strasbg.fr/.

References

Berger, E., Ball, S., Becker, K.M., Clarkes, M. et al., 2001. Nature 410, 338.
Feigelson, E.D., Broos, P., Gaffney, J.A., Garmier, G., Hillenbrand, L.A., Pravdo, S.H., Townsley, L., Tsuboi, Y., 2002. ApJ 574, 258.
Fleming, T.A., Giampapa, M.S., Schmitt, J.H.M.M., Bookbinder, J.A., 1993. ApJ 410, 387.
Fleming, T.A., Schmitt, J.H.M.M., Giampapa, M.S., 1995. ApJ 450, 401.
Fleming, T.A., Giampapa, M.S., Schmitt, J.H.M.M., 2000. ApJ 533, 372.
Gelino, C.R., Marley, M.S., Holtzman, J.A., Ackerman, A.S., Lodders, K., 2002. astroph-005305.

Giampapa, M.S., Rosner, R., Kashyaf, V., Fleming, T.A., Schmitt, J.H.M.M., Bookbinder, J.A., 1996. ApJ 463, 707.
Guenther, E., Wuchterl, G., 2003. In: Martín, E.L. (ed.), IAU Symposium 211: Brown Dwarfs, in press.
Hide, R., Stannard, D., 1976. In: Gehrels, T. (Ed.), Jupiter. The University of Arizona Press, Tucson, AZ.
Luyten, W. J., Kowal, C.T., 1975. Proper Motion Survey with the 48 inch Schmidt Telescope. XLIII. One Hundred and Six Faint Stars with Large Proper Motion. University of Minnesota, Minneapolis, MN.
Magazzù, A., Martín, E.L., Rebolo, R., 1993. ApJ 404, L17.
Marino, A., Micela, G., Peres, G., 2000. A&A 353, 177.
Martín, E.L., Zapatero Osorio, M.R., Lehto, H., 2001. ApJ 557, 822.
Mohanty, S., Basri, G., Shu, F., Allard, F., Chabrier, G., 2002. ApJ 571, 469.
Mokler, F., Stelzer, B., 2002. A&A, in press.
Neuhäuser, R. et al., 1999. A&A 343, 883.
Rutledge, R.E., Basri, G., Martín, L E., Bildsten, L., 2000. ApJ 538L, 141.
Schmitt, J.H.M.M., Liefke, C., 2002. A&A 382, L9.
Tinney, C.G., 1996. MNRAS 281, 644.
Tinney, C.G., 1998. MNRAS 296, L42.
Tinney, C.G., Tolley, 1999. MNRAS 304, 119.
XMM-Newton SOC Team, 2000. XMM-Newton User's Handbook Issue 2, 03.31.2000.

Astronomy & Astrophysics manuscript no. 0016 June 4, 2004
(DOI: will be inserted by hand later)

X-ray Detections of Two Young Bona-Fide Brown Dwarfs ⋆

H. Bouy[1,2,3]

[1] Max Planck für Extraterrestrische Phyisk, Giessenbachstraße, D-85748 Garching bei München, Germany
e-mail: hbouy@mpe.mpg.de
[2] Laboratoire d'Astrophysique de l'Observatoire de Grenoble, 414 rue de la piscine, F-38400 Saint Martin d'Hère, France

[3] European Southern Observatory, Karl Schwarzschildtstraße 2, D-85748 Garching bei München, Germany

Received 06/01/2004 ; accepted 04/05/2004

Abstract. I report the detection of two bona-fide brown dwarfs by *XMM-Newton*: [GY92] 141 in the ρ-Ophiuchus star-forming region and DENIS J155601-233809 in the Upper Scorpius OB association. The two objects have been detected with luminosities of L_X=8.35±2.86×10^{28} erg s^{-1} and L_X=6.54±1.35×10^{28} erg s^{-1} respectively, corresponding to luminosity ratios of $\log(L_X/L_{bol})$= -2.07 and $\log(L_X/L_{bol})$= -2.69. The two sources were close to the limit of detection of the instruments at only 2∼3-σ above the background level, and no significant flare or variation could be detected during the 48.3 ks and 33.9 ks observations. [GY92] 141 had already been observed 10 months earlier with *Chandra* by Imanishi et al. (2001) with a luminosity ∼14 times fainter than the one reported here, indicating that the X-ray emission of this object is strongly variable.

Key words. - Stars: low-mass, brown dwarfs - Stars: coronae - X-rays: Individuals: [GY92] 141, DENIS J155601-233809

1. Introduction

Brown dwarfs are very low mass objects unable to sustain stable nuclear reactions. Although these objects are extremely cool and their atmospheres fully convective, they appear to be able to display some X-ray coronal activity. Several surveys in the field or in star forming regions using *ROSAT* (Mokler & Stelzer 2002; Neuhäuser et al. 1999; Neuhauser & Comeron 1998; Fleming 1998), *XMM-Newton* (Imanishi et al. 2003; Stelzer & Neuhäuser 2003; Martín & Bouy 2002) or *Chandra* (Wolk 2003; Tsuboi et al. 2003; Preibisch & Zinnecker 2002; Adams et al. 2002; Imanishi et al. 2001; Rutledge et al. 2000; Fleming et al. 2000) lead to the identification of several ultracool and brown dwarfs as faint X-ray emitters, with typical luminosities of L_X ∼$10^{27\sim28}$erg s^{-1}, and some of them displaying strong variability. These observations suggest that there is apparently no drop in the X-ray luminosity at the substellar boundary. Although these X-ray features are likely to have a magnetic origin, the standard (α–ω) dynamo cannot be at work because of the absence of a radiative core and the fully convective nature of these objects. Küker & Rüdiger (1999) suggested that the magnetic field could be generated by a so-called α^2–dynamo effect, where the magnetic field is produced by the action of the Coriolis force on the convective zones of the atmosphere. The X-ray emission might then be correlated to the rotation, and therefore the age, of the object, which is still not clear as shown by the X-ray detection of old late-M dwarfs in the field (Martín & Bouy 2002; Rutledge et al. 2000; Fleming et al. 2000; Fleming 1998). Finally, since no abrupt changes are observed at the convective transition, the α^2–dynamo would probably be present in the convective zones of more massive stars. The study of the X-ray activity of ultracool and brown dwarfs will therefore bring extremely important results not only on their own characteristics but also on the properties of more massive objects.

In this paper, I present the detection of two young brown dwarfs with the ESA *XMM Newton* satellite. In the first section, the two objects and their optical and infrared properties are presented; in Sect. 3 the observations are described, then in Sect. 4 a description is given of the data processing and analysis and finally in Sect. 5 the results are analyzed.

Send offprint requests to: H. Bouy
⋆ Based on observations obtained with the ESA *XMM-Newton* Satellite, reported in the The First XMM-Newton Serendipitous Source Catalogue, XMM-Newton Survey Science Centre (SSC), 2003

2. Two Young Brown Dwarfs

The two objects have been confirmed as brown dwarfs and as members of the Upper Scorpius and ρ-Oph star forming regions by spectroscopic measurements. In this section, I will summarize the properties of these objects as reported in the literature.

2.1. DENIS J155601-233809

DENIS J155601-233809 has been reported as an M6.5 dwarf and as a member of the Upper Scorpius OB association by Martín et al. (2004) on the basis of spectroscopic measurements. Proper motion measurements confirm that the object belongs to the association (Bouy et al., in prep.). Martín et al. (2004) report a clear Hα emission with an equivalent width of EW(Hα)=-20±3 Å, not strong enough to indicate significant accretion, but indicating that DENIS-P J155601-233809 is chromosphericaly active (see e.g Barrado y Navascues & Martín (2003) or Jayawardhana et al. (2003) for a discussion on Hα emission as an indicator of accretion and activity).

DENIS J155601-233809 was also reported in the 2MASS catalogue as 2MASS J155601-233808. Table 1 gives an overview of the photometric and astrometric properties of DENIS J155601-233809. DENIS and 2MASS photometry (see Table 1) indicate an $I-J$ colour of 2.46±0.10 mag. If we assume an intrinsic colour for M6.5 dwarfs of $I-J$=2.5–2.7 mag as reported by Dahn et al. (2002), the measured $I-J$ colour corresponds to almost zero extinction $A_V \sim 0$ mag. Using the bolometric correction B_K=2.95±0.15 mag evaluated for M6.5 dwarfs by Leggett et al. (2002), the 2MASS apparent magnitude m_K=12.81±0.03 mag, and assuming a distance of 145±2 pc as measured with *Hipparcos* by de Zeeuw et al. (1999), I arrive at $\log L/L_\odot$=-2.08±0.05.

2.2. [GY92] 141

[GY92] 141 (hereafter GY 141) was reported by Luhman et al. (1997) as a M8.0 dwarf and as member of the ρ-Oph star forming region (ρ–Oph 162349.8-242601) using spectroscopic measurements. On 1997 April 14-15th they report relatively strong Hα emission with an equivalent width of EW(Hα)$\sim$-60 Å. On 2002 October 31 Jayawardhana et al. (2002) report Hα emission with an equivalent width of EW(Hα)=-13.4±0.2 Å. The variability and the strength of this emission suggest chromospheric activity, but part of it could be due to accretion. The detection of mid-infrared excess emission by Comeron et al. (1998) with a magnitude of 12.25±0.3 mag at 4.5 μm in the LW1 filter of ISOCAM indeed indicates the presence of circumstellar material. Luhman et al. (1997) estimated a mass of 0.01–0.06 $M_\odot$ using the evolutionary tracks of Burrows et al. (1997) and Baraffe et al. (1997), and Gorlova et al. (2003) estimated a mass of 0.024±0.015 $M_\odot$. GY 141 is therefore clearly substellar.

GY 141 has already been observed twice in X-rays, first in September 1994 with *ROSAT* by Neuhäuser et al. (1999) who did not detect it with an upper limit on the luminosity of $\log L_X \leq 27.86$, and second by Imanishi et al. (2001) with *Chandra* in May 2000, who detected it with a luminosity $L_X = 0.25\times10^{28}$ erg/s and $\log (L_X/L_{bol})$=-3.6. The source was too faint to allow them to do spectroscopy. They also estimated the chance of a background source falling within their 9″ beam to be 0.6%–1%.

GY 141 was also reported in the DENIS catalogue as DENIS J162651.3-243242.9 and in the 2MASS catalogue as 2MASS J16265113-243242. Table 1 gives an overview of the photometric and astrometric properties of this object as reported in these two catalogues.

3. Observations

The two sources were reported in the XMM-Newton Serendipitous Source Catalogue (XMM-Newton Survey Science Centre 2003). By doing a cross-matching between a list of currently know brown dwarfs and brown dwarf candidates with the catalogue, two X-ray sources were found to have been reported at the position of these two objects. The corresponding data have been retrieved from the XMM-Newton Public Archive (program 0112380101, P.I. Turner, and program 0111120201, P.I. Watson) for further analysis.

3.1. DENIS J155601-233809

DENIS J155601-233809 was observed on 2000 August 26th for 48309 s. The pointing was made at R.A= 15°56′25.00″ and Dec=-23h37′47.02″, which is 331″ away from DENIS J155601-233809. The observation was done in prime full window mode with the medium filter, which prevents optical contamination from point sources as bright as m_v=8$\sim$10 mag. Both MOS and PN detectors have a 27′ diameter field of view. DENIS J155601-233809 appears only on the EPIC PN and MOS2 images. It is reported in the XMM-Newton Serendipitous Source Catalogue as 1XMM J155601.1-233809. Figure 1 shows the combination of the EPIC PN, MOS1 and MOS2 images and the position of DENIS J155601-233809. For more details on *XMM-Newton* and its instruments, please refer to the XMM-Newton Users' Handbook (Ehle et al. 2003).

The X-Ray source lies 1″.0 away from the DENIS and the 2MASS coordinates, therefore well within the absolute astrometric uncertainties of the pointing (4″ on average, according to the XMM-Newton Users' Handbook). No other optical/near infrared counterpart can be found in the DENIS or 2MASS catalogues within an area of $\sim$20″ around this position, which makes it very likely that the faint X-ray source is associated with the DENIS object. Moreover, and as will be discussed in Section 4, the associated flux is consistent with that of a brown dwarf. The corrected detection likelihood value reported in the cata-

logue is 44.8, with a quality flag of 4, ensuring that the probability that the detection is real is very high. [1]

3.2. GY 141

GY 141 was observed on 2001 February 19th for 33908 s. The pointing was made on the core of the ρ–Oph star forming region, 722″ away from GY 141. This observation was also made in prime full window mode with the medium filter. Figure 1 shows the EPIC PN image and the position of GY 141 in the field. GY 141 was not detected in the EPIC MOS2 camera. This source is reported in the XMM-Newton Serendipitous Source Catalogue as 1XMM J162651.3-243242. The catalogue does not report any detection in the EPIC PN camera, although the source appears clearly in it (see Fig. 1). In both EPIC PN and MOS1 the source is very faint, which might explain why the pipeline used to build the catalogue missed it in the EPIC PN image. The corrected detection likelihood value reported in the catalogue for the MOS1 detection is 9.0, with a quality flag of 4. According to the User Guide to the Catalogue, sources with likelihood greater than ∼8 and quality flag of 4 are reliable. GY 141 is just above this limit, which probably explains why it was not detected by the pipeline in the other EPIC detectors. Using an aperture of 320 pixels, 92.6 counts are measured in the EPIC PN image (corrected for background using a standard *phot* sky algorithm). The corresponding rate is 0.00273±00092 count/s, which is consistent with the value reported in the catalogue for the EPIC MOS1 camera (see Table 2). The detection in two of the three detectors increases the likelihood that the detection is real, and the chances of coincidence are very low. On the basis of all these considerations, I will consider for the rest of this paper that the detection is real, although the possibility that it is spurious cannot be ruled out.

The X-ray source lies less than 0.″5 away from the DENIS and 2MASS coordinates, and once again no optical/near infrared counterpart can be found in the DENIS and 2MASS catalogues in an area of ∼25″ around this position, which makes it very likely that the faint X-ray source is associated with the brown dwarf. As will be discussed in Section 4, the associated flux is also consistent with that of a brown dwarf, but higher than the one reported by Imanishi et al. (2001) with *Chandra*.

4. Data Processing

Since the source was not centered in the field of view, a correction for vignetting had to be applied using the recommended *evigweight* task of the XMM-Newton Science Analysis System software (Loiseau 2003). Once this correction was applied, the light curve of each object was extracted in a circular area of 400 pixels around the source, and the light-curve of their respective background in an empty annulus region between 450 and 602 pixels around the source, therefore with the same surface to allow direct comparison. Figure 2 shows the light curves obtained. It is clearly seen that the sources are very faint, i.e not much brighter than the background. Neither timing nor spectral analysis can therefore reasonably be performed on these data, and I was only able to get flux measurements.

The fluxes reported in the XMM-Newton Serendipitous Source Catalogue were computed for N_H=3.0×10^{20} cm^2, and assuming as a spectral model a power law with a slope of 1.7. For more details about the construction of the catalogue, please refer to the corresponding User Guide [2]. As this spectral model is not the best adapted to this kind of source, the fluxes were recomputed using the count rates reported in the catalogue (see Table 2, except for the PN values of GY 141, measured as explained in section 3.2) and the recommended *PIMMS* and *nH* softwares[3].

Table 3 gives the results obtained assuming a thin thermal plasma with a temperature kT varying from 0.5 to 2.5, a distance of 145 pc for both objects as measured by de Zeeuw et al. (1999), and bolometric luminosities estimated as explained in Section 2.

Table 1. Astrometric and photometric measurements available for the two objects

R.A.[1]	Dec.[1]	Filter	Mag.	Source
DENIS J155601-233809				
15 56 01.04	-23 38 08.1	J	13.86±0.03	2MASS
		H	13.24±0.02	2MASS
		K	12.81±0.03	2MASS
15 56 01.04	-23 38 08.1	I	16.32±0.07	DENIS
		J	13.96±0.11	DENIS
		K	12.85±0.14	DENIS
GY 141				
16 26 51.28	-24 32 42	J	15.30±0.04	2MASS
		H	14.47±0.05	2MASS
		K	13.89±0.06	2MASS
16 26 51.31	-24 32 42.9	I	18.42±0.18	DENIS
		J	15.33±0.15	DENIS
		K	13.47±0.18	DENIS

[1] J2000

5. Data analysis

Since no spectral analysis could be performed to determine which spectral model best describes the sources, the analysis was done using the results obtained for a thermal plasma with kT=2.0 keV as shown in Table 3.

[1] According to the User Guide to the Catalogue, *"the likelihood value stands for the detection likelihood of the source, $L = -ln(p)$, where p is the probability of the detection occurring by chance. A value of ∼7 corresponds roughly to one false detection per exposure. A summary quality flag of 4 indicates that the detection is good (0=bad; 1-3=suspect, 4=good)". For more details please refer to the User Guide to the Catalogue.*

[2] XMM-Newton Survey Science Centre Consortium (http://xmmssc-www.star.le.ac.uk/)

[3] *PIMMS* and *nH* are distributed by the NASA's HEARSAC (http://heasarc.gsfc.nasa.gov/)

Table 3. X-ray flux and luminosities (in the energy range 0.2–12 keV)

Detector	kT^1 [keV]	Flux [10^{-15}ergs·cm^{-2}·s^{-1}]	L_X [10^{28}ergs·s^{-1}]	log L_X/L_{bol}
DENIS J155601-233809				
MOS1	1.0	7.87±2.67	1.98±0.67	-3.21
	1.5	12.48±4.24	3.14±1.06	-3.00
	2.0	17.57±5.96	4.42±1.50	-2.86
	2.5	22.32±7.58	5.61±1.91	-2.75
PN	1.0	15.26±2.32	3.84±0.58	-2.92
	1.5	23.37±3.55	5.88±0.89	-2.73
	2.0	31.28±4.75	7.87±1.19	-2.61
	2.5	38.06±5.77	9.57±1.45	-2.52
MOS1+PN[2]	1.0	12.08±2.49	3.04±0.62	-3.02
	1.5	18.88±3.89	4.75±0.97	-2.83
	2.0	25.95±5.36	6.54±1.35	-2.69
	2.5	32.28±6.67	8.12±1.68	-2.59
GY 141				
MOS1	1.0	22.30±6.22	5.61±1.56	-2.25
	1.5	35.23±9.82	8.86±2.47	-2.05
	2.0	49.49±13.80	12.44±3.47	-1.90
	2.5	62.82±17.52	15.80±4.41	-1.80
PN	1.0	13.01±4.38	3.27±1.10	-2.49
	1.5	19.81±6.67	4.98±1.68	-2.30
	2.0	26.44±8.91	6.65±2.24	-2.18
	2.5	32.12±10.83	8.08±2.72	-2.09
MOS1+PN[2]	1.0	16.09±5.30	4.05±1.33	-2.39
	1.5	24.67±8.24	6.21±2.08	-2.20
	2.0	33.22±11.35	8.35±2.86	-2.07
	2.5	40.61±14.17	10.21±3.57	-1.99

[1] temperature of the thermal plasma spectral model used to convert from count rate to flux
[2] mean total flux/luminosity of the detections weighted by the errors

Table 2. X-ray Count Rates[1]

Detector	Count Rates [10^{-3}·counts·s^{-1}]
DENIS J155601-233809	
MOS1	0.59±0.20
MOS2	not detected
PN	3.25±0.49
MOS1+PN[2]	2.48±0.40
GY 141	
MOS1	1.66±0.46
MOS2	not detected
PN	2.73±0.92
MOS1+PN[2]	2.37±0.77

[1] Source: XMM-Newton Serendipitous Source Catalogue, except EPIC PN value for GY 141
[2] mean total count rate of the detections weighted by the errors

5.1. DENIS J155601-233809

As shown in Figure 3, DENIS J155601-233809 has an X-ray luminosity very similar to that of other late type M-dwarfs in star forming regions and the field. It belongs to the strongest X-ray emitters among that class of objects. It is important to note that no detailed timing analysis can be done because of the very low flux (see Figure 2), and that more sensitive observations are required to know if the observed emission is quiescent or related to some flare events.

5.2. GY 141

The X-ray activity of GY 141 shows that this object has a strong coronal activity. In order to compare the different measurements available, I used the *PIMMS* software to convert the *Chandra* luminosity (measured in the energy range 0.5–9.0 keV) and the *ROSAT* upper limit (measured in the energy range 0.1–2.4 keV) to the energy range of the *XMM-Newton* observations (0.2–12.0 keV). The results are summarized in Table 4, and show that the flux of GY 141 increased by a factor of ∼14 between the *Chandra* and the *XMM-Newton* observations. The X-ray emission is therefore highly variable, and GY 141 would not have been detected in the 33.9 ks *XMM-Newton* frame if its emission had been at the same level as in the 100.6 ks *Chandra* observation. The present *XMM-Newton* measurement is close to the limit of detection of the *ROSAT* observation.

As shown in Figure 3, GY 141 has a very high X-ray luminosity for a late-type object, and displays strong variability between two observations separated by a period of

Table 4. X-ray Luminosities (0.2–12 keV) of GY 141 at different epochs

Instrument	Date Obs.	L_X $[10^{28}\mathrm{ergs\cdot s^{-1}}]$	log L_X/L_{bol}
ROSAT[1]	09/1994	$\leq$13.00	$\leq$-1.9
Chandra	05/2000	0.60	-3.22
XMM-Newton	02/2001	8.35	-2.07

[1] GY 141 was not detected. The corresponding value is an upper limit.
Remarks: Values computed assuming a thermal plasma spectral model with kT=2 keV.

$\sim$10 months. Neuhäuser et al. (1999) did not detect it with *ROSAT* in 1994, but their limit of detection was higher than the two values obtained with *XMM-Newton* and *Chandra*. Its X-ray luminosity increased by a factor of $\sim$14 between the *Chandra* and the *XMM-Newton* observations. Although the light curve of the emission detected with *XMM-Newton* suggests that there was no significant variation during the 34 ks *XMM-Newton* observation (see Figure 2), the shortness of the observation (34 ks) and the faintness of the detection make it possible to conclude that it was not a flare-like event. Further observations should be made to verify if the observed variability occurs on long ($\sim$months) or short ($\sim$10 ks) time-scales. This issue is very important since the only few sources known to show variability are flaring objects with periods of 10$\sim$50 ks and, except for the old field brown dwarfs LP944-20 and VB 10, with amplitudes less than a factor of 10 (Imanishi et al. 2003). If confirmed by further observations, a strong variability over a long time-scale would probably mean that two types of activity, governed by different mechanisms, can occur in the corona of late type objects. Recently, Schmitt & Liefke (2002) reported a significant variation of the quiescent X-ray emission of the M9 dwarf LHS 2065 after a flare. Such a phenomenon might also be at work and explain the variation observed for GY 141 between the *Chandra* and *XMM-Newton* observations. Finally, since it has been shown that the object is surrounded by a disk, part of its emission could also come from the circumstellar material interacting with the magnetic field, following a emission scenario as suggested by Montmerle et al. (2000).

6. Conclusions

I report here the detection with *XMM-Newton* of two young bona-fide brown dwarfs. DENIS J155601-233809 displays an X-ray emission similar to other young objects of the same age and spectral class, with log(L_X/L_{bol})= -2.69. No significant variability was observed during the 48.3 ks observation, but the faintness of the source did not allow me to perform precise timing analysis. More sensitive observations are required to know if this emission is quiescent or associated to a flare-like event. GY 141 has the highest X-ray luminosity reported up to date for that class of object, with log(L_X/L_{bol})= -2.07. Its luminosity has increased by a factor of 14 since the previous *Chandra* observation. No significant flare-like event could be detected in the 33.9 ks *XMM-Newton* observation. In this case again the faintness of the source did not allow me to perform precise timing analysis, and more sensitive observations are also required to know if this emission is due to a flare or if it is quiescent. Follow-up observations of this object should allow us to know if this variability occurs on long ($\sim$months) or short ($\sim$10 ks) time-scales.

Acknowledgements. I would like to thank Elisa Constantini for her precious and generous help regarding the processing of XMM-Newton data. I would like to thank Eduardo Martín and Xavier Delfosse for providing me with the list of Upper Scorpius brown dwarfs prior to publication, and Jérôme Bouvier and Wolfgang Brandner for their kind support.

This research has made use of the XMM-Newton Public Archive and of the XMM-Newton Serendipitous Source Catalogue (XMM-Newton Survey Science Centre 2003). This research has also made use of the VizieR on-line Service at Centre de Donnés astronomiques de Strasbourg, France (Ochsenbein et al. 2000). This publication makes use of data products from the Two Micron All Sky Survey (2MASS) and DEep Near Infrared Survey (DENIS). The Two Mass Survey is a joint project of the University of Massachusetts and the Infrared Processing and Analysis Center/California Institute of Technology, funded by the National Aeronautics and Space Administration and the National Science Foundation. The DENIS project has been partly funded by the SCIENCE and the HCM plans of the European Commission under grants CT920791 and CT940627. It is supported by INSU, MEN and CNRS in France, by the State of Baden-Wrttemberg in Germany, by DGICYT in Spain, by CNR in Italy, by FFwFBWF in Austria, by FAPESP in Brazil, by OTKA grants F-4239 and F-013990 in Hungary, and by the ESO C&EE grant A-04-046.

References

Adams, N., Wolk, S., Walter, F. M., Jeffries, R., & Naylor, T. 2002, Bulletin of the American Astronomical Society, 34, 1176
Baraffe, I., Chabrier, G., Allard, F., & Hauschildt, P. H. 1997, A&A, 327, 1054
Barrado y Navascues, D. & Martín, E. L. 2003, AJ, in press
Burrows, A., Marley, M., Hubbard, W. B., et al. 1997, ApJ, 491, 856
Comeron, F., Rieke, G. H., Claes, P., Torra, J., & Laureijs, R. J. 1998, A&A, 335, 522
Dahn, C. C., Harris, H. C., Vrba, F. J., et al. 2002, AJ, 124, 1170
de Zeeuw, P. T., Hoogerwerf, R., de Bruijne, J. H. J., Brown, A. G. A., & Blaauw, A. 1999, AJ, 117, 354
Ehle, M., Pollock, A. M. T., Talavera, A., et al. 2003, XMM-Newton Users' Handbook, V2.1
Fleming, T. A. 1998, ApJ, 504, 461
Fleming, T. A., Giampapa, M. S., & Garza, D. 2003, ApJ, 594, 982
Fleming, T. A., Giampapa, M. S., & Schmitt, J. H. M. M. 2000, ApJ, 533, 372

Gorlova, N. I., Meyer, M. R., Rieke, G. H., & Liebert, J. 2003, ApJ, 593, 1074
Imanishi, K., Nakajima, H., Tsujimoto, M., Koyama, K., & Tsuboi, Y. 2003, PASJ, 55, 653
Imanishi, K., Tsujimoto, M., & Koyama, K. 2001, ApJ, 563, 361
Jayawardhana, R., Mohanty, S., & Basri, G. 2002, ApJ, 578, L141
Jayawardhana, R., Mohanty, S., & Basri, G. 2003, ApJ, 592, 282
Küker, M. & Rüdiger, G. 1999, A&A, 346, 922
Leggett, S. K., Golimowski, D. A., Fan, X., et al. 2002, ApJ, 564, 452
Loiseau, N. 2003, XMM-Newton Science Analysis System Users' Guide, V2.1
Luhman, K. L., Liebert, J., & Rieke, G. H. 1997, ApJ, 489, L165+
Martín, E. L. & Bouy, H. 2002, New Astronomy, 7, 595
Martín, E. L., Delfosse, X., & Guieu, S. 2004, Accepted for Publication in AJ
Mokler, F. & Stelzer, B. 2002, A&A, 391, 1025
Montmerle, T., Grosso, N., Tsuboi, Y., & Koyama, K. 2000, ApJ, 532, 1097
Neuhäuser, R., Briceño, C., Comerón, F., et al. 1999, A&A, 343, 883
Neuhauser, R. & Comeron, F. 1998, Science, 282, 83
Ochsenbein, F., Bauer, P., & Marcout, J. 2000, A&AS, 143, 23
Preibisch, T. & Zinnecker, H. 2002, AJ, 123, 1613
Rutledge, R. E., Basri, G., Martín, E. L., & Bildsten, L. 2000, ApJ, 538, L141
Schmitt, J. H. M. M. & Liefke, C. 2002, A&A, 382, L9
Stelzer, B. & Neuhäuser, R. 2003, in Brown Dwarfs, Proceedings of IAU Symposium 211, held 20-24 May 2002 at University of Hawai'i, Honolulu, Hawai'i. Edited by Eduardo Martín., 443–+
Tsuboi, Y., Maeda, Y., Feigelson, E. D., et al. 2003, ApJ, 587, L51
Wolk, S. J. 2003, in Brown Dwarfs, Proceedings of IAU Symposium 211, held 20-24 May 2002 at University of Hawai'i, Honolulu, Hawai'i. Edited by Eduardo Martín., 447–+
XMM-Newton Survey Science Centre. 2003, The First XMM-Newton Serendipitous Source Catalogue

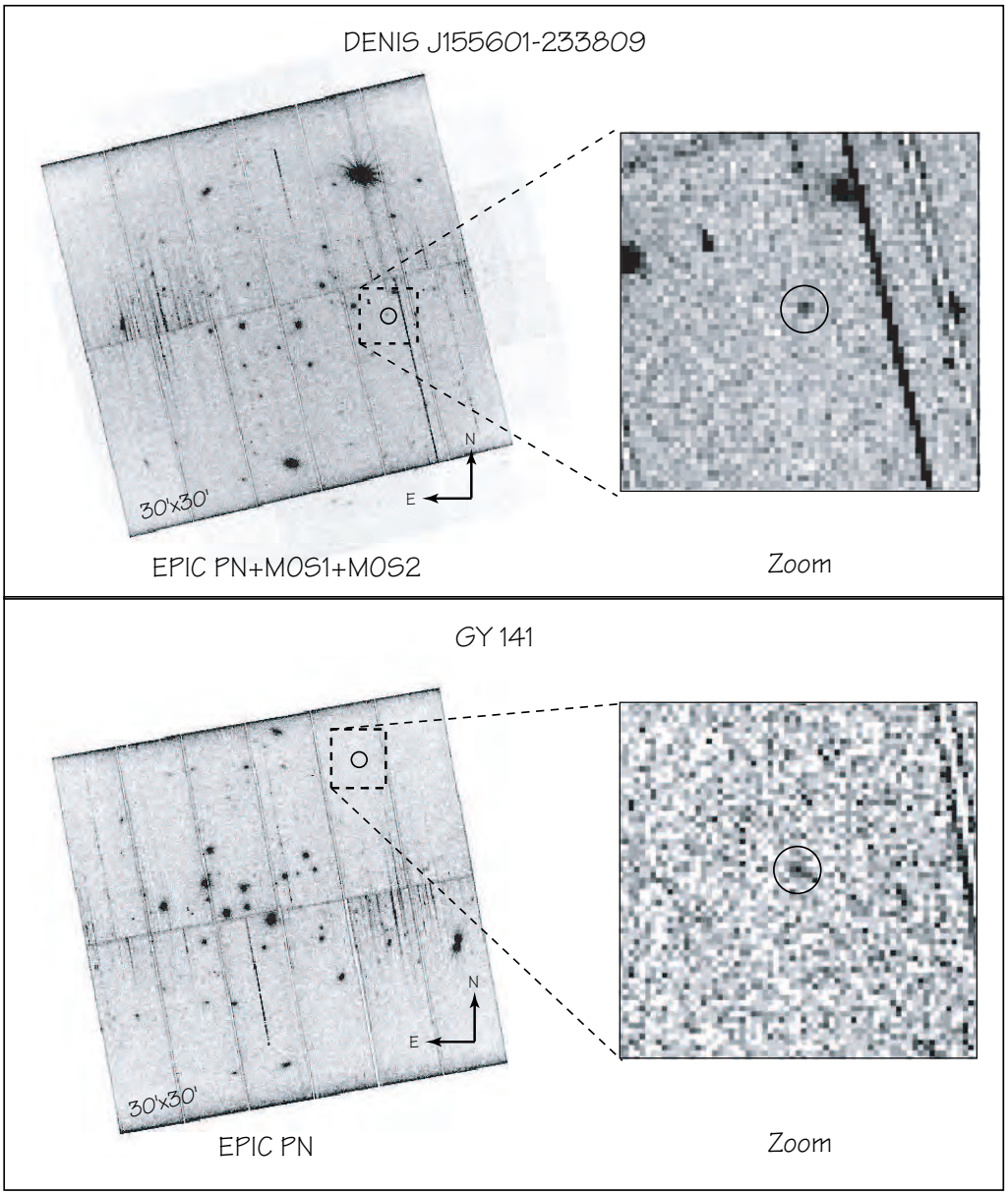

Fig. 1. This figure shows the *XMM-Newton* images where the two objects have been detected. For DENIS J155601-233809 it shows the combination of the images obtained with the 3 instruments (EPIC MOS1, MOS2 and PN cameras) and for GY 141 only the EPIC PN image.

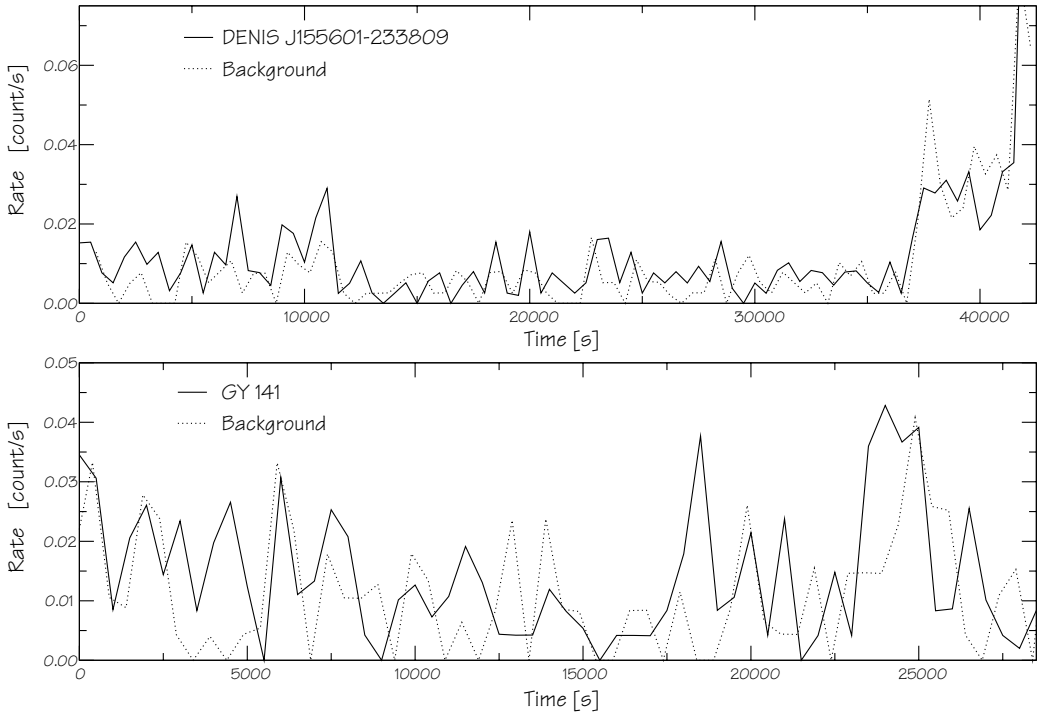

Fig. 2. Light curves of DENIS J155601-233809, GY 141, and the background around their positions. The size of the time bins is 500 s. In both cases the source and the background have very similar amplitudes and variations, indicating that the sources are at the limit of detection. Figure 1 also shows that the two sources are very faint.

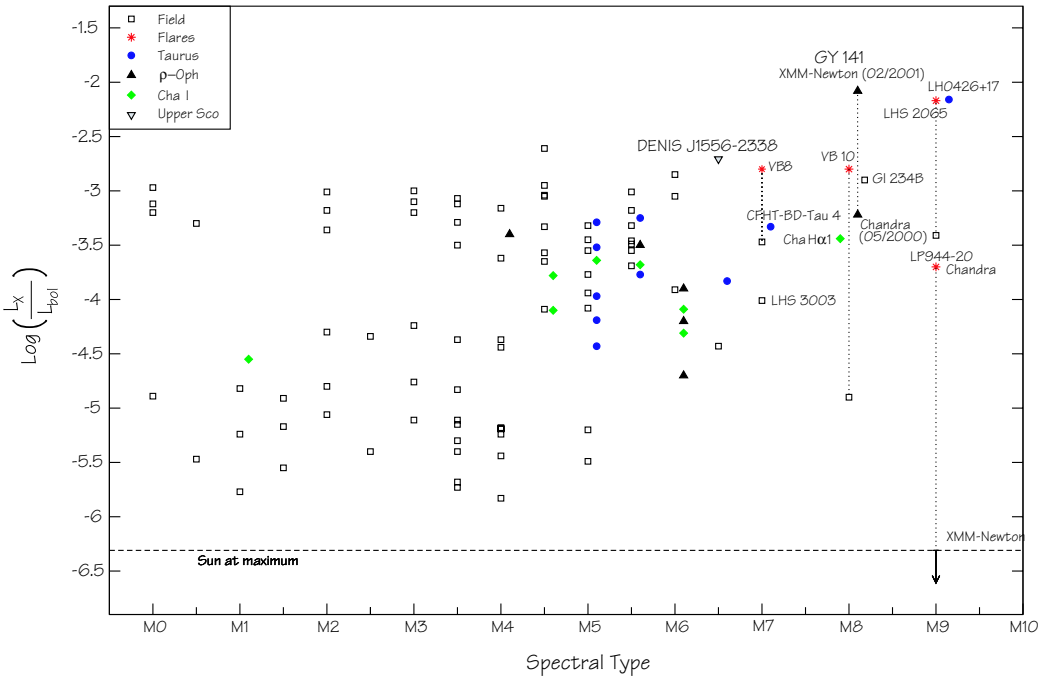

Fig. 3. Distribution of X-ray luminosity of M dwarfs as a function of spectral type. The open squares represent the values obtained for field M-dwarfs. The circles, diamonds, triangles up and down denote young objects in star-forming regions. The stars represent the flaring objects at their maximum with the corresponding value or upper limit on the quiescent emission. While DENIS J155601-233809 seems to have a normal X-ray luminosity in comparison with other M6∼M7 dwarfs, GY 141 shows a strong variability between the *Chandra* and *XMM-Newton* observations. To avoid confusion, the spectral types of some objects have been shifted by 0.1 subclass. Values are from Martín & Bouy (2002) and references therein, except the quiescent value for VB 10, which is from Fleming et al. (2003).

Appendix D

Curriculum Vitæ & List of Publications

Hervé Bouy

Curriculum Vitæ

Riemerfeldring 37
D-85748 Garching bei München
Germany
Phone : +49 (0)89 171 380 72 74
Mail : hbouy@mpe.mpg.de

Born 14th January 1977
in Angers (France)
French Nationality
Single, no child

EDUCATION

2004- Postdoc.
Postdoc position at the I.A.C in Tenerife, Spain.
▷ *3 years contract.*

2001-2004 PhD.
PhD thesis, « Fundamental Properties of Binary Ultracool Dwarfs », E.S.O & M.P.E (Garching, Germany), L.A.O.G (Grenoble, France)
▷ *« cotutelle »(=«* double PhD *») between Université de Grenoble and Ludwig Maximilian Universität in Munich.*

2000-2001 D.E.A « Astrophysics & Plasmas ».
5th year at University, L.A.O.G (Grenoble, France)
▷ *passed with distinction.*

1998-2000 C.A.P.E.S Physics and Chemical sciences.
Preparation to the competitive examination conducted by the French State for admission to posts on teaching staff of High Schools in physics and chemical sciences
▷ *passed.*

1997-1998 Maîtrise in Physical Sciences.
4th year at University (≈ Master), Université Paul Sabatier, Toulouse, France
▷ *passed with distinction.*

1996-1997 Licence in Physics and Chemical Sciences.
3rd year at University (≈ Bachelor Degree), Université d'Angers, France
▷ *passed with distinction.*

1994-1996 Diplôme d'Études Universitaires Générales.
1rst & 2nd years at University, Université d'Angers, France

1995 Diplôme Universitaire of Astrophysics & Astronomy.
Degree taken after 1 year at University, Université Paris XI

INTERNATIONAL ASTRONOMICAL MEETINGS AND CONFERENCES

2002 ▷ International Astronomical Union Symposium 211, "Brown Dwarfs", Hawai'i, U.S.A, May 20-14

2003 ▷ International Astronomical Union General Assembly, Sydney, Australia, July 16-25
▷ E.S.O Workshop : "Science with Adaptive Optics", Garching, Germany, 16-19 September, Member of the Local Organizing Committee

TRAINING COURSE & SCHOOLS

15-21 Dec. 2003	Extrasolar Planets and Brown Dwarfs, Santiago de Chile. First Advanced Chilean School in Astrophysics
9-21 Sept. 2002	3rd NEON Euro School, Asiago, Italy. Observing Summer School, Asiago Observatory (Network of European Observatories in the North), sponsored by the European Community
15 Mar 2001 to 25 Jun 2001	Institute for Astronomy, Hawai'i. Research Assistant at the Institute for Astronomy of University of Hawai'i, working on brown dwarfs and halo-binaries, using XMM- and IR-data, observing with UH88" on Mauna Kea Observatory

OBSERVATIONAL EXPERIENCE

High Angular Resolution	Hubble Space Telescope. Intensive use of HST high resolution cameras (WFPC2, ACS, STIS). Development of a PSF fitting program to analyse binary stars images, with a calibrated accuracy of 0.001" on the relative astrometry.
High Angular Resolution	Adaptive Optics at the ESO/VLT. Intensive use of VLT/NACO (P.I on 3 programs). Participation to the commissioning of the instrument in Paranal
Spectroscopy	Low Resolution Spectroscopy. Observation and Analysis of VLT/FORS2 and HST/STIS low resolution spectra
X-Ray	XMM-Newton. Experienced with the processing and analysis of XMM X-Ray data

COMPLEMENTARY INFORMATIONS

Computer Sciences	UNIX & Linux, C, IDL, LaTeX, Windows, Adobe Illustrator & Photoshop
Languages	French ▷ *Mother tongue.* English ▷ *Read : good, Written : good, Spoken : good.* German ▷ *Read : good, Written : good, Spoken : good.* Spanish ▷ *Read : beginner, Written : beginner, Spoken : beginner.*

GRANTS AND STUDENTSHIPS

2004	1 Year Studentship at M.P.E in Garching, Germany
2001–2003	2 Years Studentship at E.S.O headquarters in Garching, Germany
2001	5 Months Undergraduate Studentship at the IfA in Honolulu, U.S.A

REFEREED PUBLICATIONS

2004

▷ *Discovery of a triple system of brown dwarfs with the Hubble Space Telescope*, **Bouy H.**, Martín E. L., Brandner W., Bouvier J., in prep. for Astrophysical Journal, 2004

▷ *Astrometric monitoring of the binary brown dwarf DENIS-P J1228.2-1547*, Brandner W., Martín E. L., **Bouy** et al., accepted for publication in Astronomy & Astrophysics

▷ *First determination of the orbit and dynamical mass of a binary L1 dwarf*, **Bouy** et al., Astronomy & Astrophysics, 2004, 423, 341

▷ *A young binary Brown Dwarf in the R-CrA star formation region*, **Bouy, H.**, Brandner, W., Martín, E. L., Delfosse, X., Allard, F., Baraffe, I., Forveille, T., Demarco, R., Astronomy & Astrophysics, 424, 213

▷ *X-ray detection of two Young Bona fide Brown Dwarfs*, **H. Bouy**, Astronomy & Astrophysics, 2004, 424, 619

2003

▷ *Multiplicity of Nearby Free Floating Ultracool Dwarfs : a HST/WFPC2 search for companions*, **Bouy, H.**, Brandner, W., Martín, E. L., Delfosse, X., Allard, F., Basri, G., The Astronomical Journal , 2003, 126, 1526-1554

▷ *An HST/WFPC2 Survey for Brown Dwarf Binaries in the alpha Per and the Pleiades Open Clusters*, E. L. Martín, D. Barrado y Navascues, I. Baraffe, **H. Bouy**, S. Dahm, The Astrophysical Journal, 594, 525-532, 2003

▷ *First NACO observations of the Brown Dwarf LHS 2397aB*, E. Masciadri, W. Brandner, **H. Bouy**, R. Lenzen, A.M. Lagrange, F. Lacombe, Astronomy & Astrophysics, 2003, 411, 157

2002

▷ *XMM-Newton observation of the Nearby Brown Dwarf LP944-20*, Martín, E. L. & **Bouy, H.**, New Astronomy , 2002

NON REFEREED PUBLICATIONS AND PROCEEDINGS

2004

▷ *Statistical and Physical properties of binaries of low-mass stars and brown dwarfs*, **H. Bouy**, W. Brandner, E. L. Martín, *"SF2A-2004 : Semaine de l'Astrophysique Francaise, meeting held in Paris, France, June 14-18, 2004"*, Eds. : F. Combes, D. Barret, T. Contini, F. Meynadier and L. Pagani EdP-Sciences

2003

▷ *Substellar companions to Brown Dwarfs : First steps toward a direct detection of Exoplanets*, W. Brandner & **H. Bouy**, *"Towards Other Earths - Darwin/TPF and the Search for Extrasolar Terrestrial Planets"*, MPIA, Heidelberg, June 2003

▷ *Brown Dwarfs Companions to Solar-type Stars and other Brown dwarfs*, Martín, E.L, Connelley M., Potter, D., **Bouy, H.**, IAU Symposium Vol 213 , 2003, R. Norris

▷ *High Resolution Observations of Binary Brown Dwarfs*, **Hervé Bouy** & Wolfgang Brandner, *"Science with Adaptive Optics"*, E.S.O Garching , September 2003

2002

▷ *NAOS+CONICA at YEPUN : first VLT adaptive optics system sees first light*, Brandner **et al.**, E.S.O Messenger, 107, 2002

▷ *A census of Brown Dwarf Binaries*, Wolfgang Brandner & **Hervé Bouy**, IAU Symposium, Vol. 211 , 2002, E. L. Martín, p. 241

▷ *HST Observations of Candidates and Bona-fide Binary Brown Dwarfs*, **Bouy et al.**, IAU Symposium, Vol. 211 , 2002, E.L. Martín, p. 245

OTHER MERITS

2004	Member of the French Astronomical and Astrophysical Society (SF2A) and of the European Astronomical Society (EAS)
	Scientific Referee for the journals "*Astronomical Journal*" and "*Astronomy & Astrophysics*"
	Principal-Investigator of ESO/VLT program 74.C-0018A & B
	Principal-Investigator of ESO/VLT program 73.C-0557A & B
	co-Investigator of HST program GO10208
2003	Principal-Investigator of ESO/VLT program 71.C-0327A
2002	Principal-Investigator of HST program GO9831
	Principal-Investigator of ESO/VLT programs 70.D-0773A and 71.C-0327A
2001	co-Investigator (P.I Brandner) of HST program GO9451
	Principal-Investigator of ESO/VLT program 69.C-0588A

Glossary

2MASS : Two Micron All-Sky Survey

A.U : Astronomical unit
ACS : Advanced Camera for Surveys

BD : brown dwarf

CMD : Colour vs Magnitude Diagram
CSA : Canadian Space Agency

DENIS : DEep Near Infrared Survey

ESA : European Southern Agency
ESO : European Southern Observatory
EW : Equivalent Width

H-R diagram : Hertzsprung-Russel diagram
HIRES : High Resolution Spectrograph (Keck)

HRC : High Resolution Channel (ACS)
HST : Hubble Space Telescope

IAU : International Astronomical Union
IMF : Initial Mass Function.
IR : Infrared

JWST : James Webb Space Telescope

LSF : Line Spread Function

NASA : National Aeronautics and Space Administration

P.A : Position Angle
P.I. : Principal Investigator
PC : Planetary Camera (WFPC2)
PSF : Point Spread Function

RMS : Root Mean Square

S/N : signal to noise ratio
SDSS : Sloan Digital Sky Survey
SED : Spectral Energy Distribution
SFR : star forming region.

UV : ultra-violet

VLM : Very Low Mass
VLT : Very Large Telescope

WFPC2 : Wide Field Planetary Camera 2

Bibliography

Abt, H. A., Barnes, R. C., Biggs, E. S., & Osmer, P. S. 1965, ApJ, 142, 1604

Adams, F. C., Lada, C. J., & Shu, F. H. 1987, ApJ, 312, 788

Adams, N., Wolk, S., Walter, F. M., Jeffries, R., & Naylor, T. 2002, Bulletin of the American Astronomical Society, 34, 1176

Alard, C. 2000, A&AS, 144, 363

Allard, F. & Hauschildt, P. H. 1995, ApJ, 445, 433

Allard, F., Hauschildt, P. H., Alexander, D. R., Tamanai, A., & Schweitzer, A. 2001, ApJ, 556, 357

Allard, F., Hauschildt, P. H., & Schweitzer, A. 2000, ApJ, 539, 366

Alves, J. F., Lada, C. J., & Lada, E. A. 2001, Nature, 409, 159

Andre, P. & Montmerle, T. 1994, ApJ, 420, 837

Baggett, S., McMaster, M., Biretta, J., et al. 2002, HST WFPC2 Data Handbook, v. 4.0, ed. B. Mobasher, Baltimore, STScI

Bailer-Jones, C. A. L. 2004, A&A, 419, 703

Bailer-Jones, C. A. L. & Mundt, R. 2001, A&A, 367, 218

Baraffe, I., Chabrier, G., Allard, F., & Hauschildt, P. H. 1997, A&A, 327, 1054

Baraffe, I., Chabrier, G., Allard, F., & Hauschildt, P. H. 1998, A&A, 337, 403

Baraffe, I., Chabrier, G., Allard, F., & Hauschildt, P. H. 2002, A&A, 382, 563

Barrado y Navascues, D. & Martín, E. L. 2003, AJ, in press

Basri, G., Marcy, G. W., & Graham, J. R. 1996, ApJ, 458, 600

Basri, G. & Martín, E. L. 1999, AJ, 118, 2460

Basri, G., Mohanty, S., Allard, F., et al. 2000, ApJ, 538, 363

Bate, M. R., Bonnell, I. A., & Bromm, V. 2002, MNRAS, 332, L65

Bate, M. R., Bonnell, I. A., & Bromm, V. 2003, MNRAS, 339, 577

Biretta, J., e. a. 2002, Baltimore: STSci

Blommaert, J., Siebenmorgen, R., Coulais, A., et al. 2001, ISO Handbook, Volume III

Bodenheimer, e. a. 1999, Space Science Series: University of Arizona Press

Bodenheimer, P. 1998, in ASP Conf. Ser. 134: Brown Dwarfs and Extrasolar Planets, 115–+

Borsenberger, J., e. a. 1997, F. Garzon et al. (eds), Kluwer Dordrecht, 121

Boss, A. P. 2001, ApJ, 563, 367

Bouvier, J., Duchêne, G., Mermilliod, J.-C., & Simon, T. 2001, A&A, 375, 989

Bouvier, J., Rigaut, F., & Nadeau, D. 1997, A&A, 323, 139

Bouvier, J., Stauffer, J. R., Martin, E. L., et al. 1998, A&A, 336, 490

Bouy, H. 2004, in prep.

Bouy, H., Brandner, W., Martín, E. L., et al. 2003, AJ, 126, 1526

Bouy, H., Martín, E., Delfosse, X., & Brandner, W. 2004, in prep.

Brandner, W., Rousset, G., Lenzen, R., et al. 2002, The Messenger, 107

Burgasser, A. J., Kirkpatrick, J. D., Brown, M. E., et al. 2002, ApJ, 564, 421

Burgasser, A. J., Kirkpatrick, J. D., Brown, M. E., et al. 1999, ApJ, 522, L65

Burgasser, A. J., Kirkpatrick, J. D., Reid, I. N., et al. 2003, ApJ, 586, 512

Burrows, A., Marley, M., Hubbard, W. B., et al. 1997, ApJ, 491, 856

Burrows, A. & Sharp, C. M. 1999, ApJ, 512, 843

Cambrésy, L. 1999, A&A, 345, 965

Casey, B. W., Mathieu, R. D., Vaz, L. P. R., Andersen, J., & Suntzeff, N. B. 1998, AJ, 115, 1617

Cesarsky, C. J., Abergel, A., Agnese, P., et al. 1996, A&A, 315, L32

Chabrier, G., Baraffe, I., Allard, F., & Hauschildt, P. 2000, ApJ, 542, 464

Chen, B., Asiain, R., Figueras, F., & Torra, J. 1997, A&A, 318, 29

Chiang, E. I. & Goldreich, P. 1997, ApJ, 490, 368

Clarke, F. J., Oppenheimer, B. R., & Tinney, C. G. 2002, MNRAS, 335, 1158

Close, L. M., Potter, D., Brandner, W., et al. 2002a, ApJ, 566, 1095

Close, L. M., Siegler, N., Freed, M., & Biller, B. 2003, ApJ, 587, 407

Close, L. M., Siegler, N., Potter, D., Brandner, W., & Liebert, J. 2002b, ApJ, 567, L53

Comeron, F., Rieke, G. H., Claes, P., Torra, J., & Laureijs, R. J. 1998, A&A, 335, 522

Cutri, R. M., Skrutskie, M. F., van Dyk, S., et al. 2003, VizieR Online Data Catalog, 2246, 0

Dahn, C. C., Harris, H. C., Vrba, F. J., et al. 2002, AJ, 124, 1170

de Zeeuw, P. T., Hoogerwerf, R., de Bruijne, J. H. J., Brown, A. G. A., & Blaauw, A. 1999, AJ, 117, 354

Delfosse, X. 1997, PhD Thesis, Université de Grenoble

Delfosse, X., Martin, E. L., Forveille, T., et al. 2003, in SF2A-2003: Semaine de l'Astrophysique Francaise

Delfosse, X., Tinney, C. G., Forveille, T., et al. 1997, A&A, 327, L25

Delfosse, X., Tinney, C. G., Forveille, T., et al. 1999, A&AS, 135, 41

Delgado-Donate, E. J., Clarke, C. J., & Bate, M. R. 2003, MNRAS, 342, 926

Duchêne, G., Bouvier, J., & Simon, T. 1999, A&A, 343, 831

Duquennoy, A. & Mayor, M. 1991, A&A, 248, 485

Durisen, R. H., Sterzik, M. F., & Pickett, B. K. 2001, A&A, 371, 952

Ehle, M., Pollock, A. M. T., Talavera, A., et al. 2003, XMM-Newton Users' Handbook, V2.1

Enoch, M. L., Brown, M. E., & Burgasser, A. J. 2003, AJ, 126, 1006

Epchtein, N., de Batz, B., Capoani, L., et al. 1997, The Messenger, 87, 27

Fernández, M. & Comerón, F. 2001, A&A, 380, 264

Festin, L. 1998a, A&A, 333, 497

Festin, L. 1998b, MNRAS, 298, L34+

Fischer, D. A. & Marcy, G. W. 1992, ApJ, 396, 178

Fleming, T. A. 1998, ApJ, 504, 461

Fleming, T. A., Giampapa, M. S., & Garza, D. 2003, ApJ, 594, 982

Fleming, T. A., Giampapa, M. S., & Schmitt, J. H. M. M. 2000, ApJ, 533, 372

Forveille, T., Beuzit, J., Delfosse, X., et al. 1999, A&A, 351, 619

Freed, M., Close, L. M., & Siegler, N. 2003, ApJ, 584, 453

Gaidos, E. J., Henry, G. W., & Henry, S. M. 2000, AJ, 120, 1006

Geballe, T. R., Knapp, G. R., Leggett, S. K., et al. 2002, ApJ, 564, 466

Gelino, C. R., Marley, M. S., Holtzman, J. A., Ackerman, A. S., & Lodders, K. 2002, ApJ, 577, 433

Ghez, A. 1993, Ph.D. Thesis

Gizis, J. E. 2003, in IAU Symposium, 281–+

Gizis, J. E., Monet, D. G., Reid, I. N., et al. 2000, AJ, 120, 1085

Gizis, J. E., Reid, I. N., Knapp, G. R., et al. 2003, AJ, 125, 3302

Goldberg, D. & Mazeh, T. 1994, A&A, 282, 801

Golimowski, D. A., Burrows, C. J., Kulkarni, S. R., Oppenheimer, B. R., & Brukardt, R. A. 1998, AJ, 115, 2579

Gorlova, N. I., Meyer, M. R., Rieke, G. H., & Liebert, J. 2003, ApJ, 593, 1074

Goto, M., Kobayashi, N., Terada, H., et al. 2002, ApJ, 567, L59

Graham, M. F., Meaburn, J., Garrington, S. T., et al. 2002, ApJ, 570, 222

Guenther, E. W. & Wuchterl, G. 2003, A&A, 401, 677

Halbwachs, J. L., Mayor, M., Udry, S., & Arenou, F. 2003, A&A, 397, 159

Hambly, N. C., Hodgkin, S. T., Cossburn, M. R., & Jameson, R. F. 1999, MNRAS, 303, 835

Harrington, R. S. 1968, AJ, 73, 190

Hauschildt, P. H., Allard, F., & Baron, E. 1999, ApJ, 512, 377

Hawley, S. L., Covey, K. R., Knapp, G. R., et al. 2002, AJ, 123, 3409

Imanishi, K., Tsujimoto, M., & Koyama, K. 2001, ApJ, 563, 361

Jayawardhana, R., Ardila, D. R., Stelzer, B., & Haisch, K. E. 2003a, AJ, 126, 1515

Jayawardhana, R., Mohanty, S., & Basri, G. 2002, ApJ, 578, L141

Jayawardhana, R., Mohanty, S., & Basri, G. 2003b, ApJ, 592, 282

Joergens, V., Fernández, M., Carpenter, J. M., & Neuhäuser, R. 2003a, ApJ, 594, 971

Joergens, V., Neuhäuser, R., Guenther, E. W., Fernández, M., & Comerón, F. 2003b, in IAU Symposium, 233–+

Kähler, H. 1999, A&A, 346, 67

Küker, M. & Rüdiger, G. 1999, A&A, 346, 922

Kenworthy, M., Hofmann, K., Close, L., et al. 2001, ApJ, 554, L67

Kepler, J. 1609, Astronomia nova. (Pragae, 1609)

Kepler, J. 1619, Harmonices mvndi libri (Lincii Austriae, sumptibus G. Tampachii, excudebat I. Plancvs, 1619.)

Kim Quijano, J., Mobasher, B., Brown, B., et al. 2003, Baltimore: STScI

Kirkpatrick, J. D. 2003, in IAU Symposium, 497–+

Kirkpatrick, J. D., Beichman, C. A., & Skrutskie, M. F. 1997, ApJ, 476, 311

Kirkpatrick, J. D., Dahn, C. C., Monet, D. G., et al. 2001, AJ, 121, 3235

Kirkpatrick, J. D., Reid, I. N., Liebert, J., et al. 1999, ApJ, 519, 802

Kirkpatrick, J. D., Reid, I. N., Liebert, J., et al. 2000, AJ, 120, 447

Kleinmann, S. G., Lysaght, M. G., Pughe, W. L., et al. 1994, Experimental Astronomy, 3, 65

Knacke, R. F., Strom, K. M., Strom, S. E., Young, E., & Kunkel, W. 1973, ApJ, 179, 847

Koerner, D. W., Kirkpatrick, J. D., McElwain, M. W., & Bonaventura, N. R. 1999, ApJ, 526, L25

Krist, J. & Hook, R. 2003, The Tiny Tim's User Guide, v. 6.1, Baltimore, STScI

Kroupa, P. 1995a, MNRAS, 277, 1491

Kroupa, P. 1995b, MNRAS, 277, 1522

Kroupa, P. & Bouvier, J. 2003, MNRAS, 346, 369

Kumar, S. S. 1963, ApJ, 137, 1121

Lane, B. F., Zapatero Osorio, M. R., Britton, M. C., Martín, E. L., & Kulkarni, S. R. 2001, ApJ, 560, 390

Leggett, S. K. 1992, ApJS, 82, 351

Leggett, S. K., Allard, F., Geballe, T. R., Hauschildt, P. H., & Schweitzer, A. 2001, ApJ, 548, 908

Leggett, S. K., Golimowski, D. A., Fan, X., et al. 2002, ApJ, 564, 452

Leinert, C., Henry, T., Glindemann, A., & McCarthy, D. W. 1997, A&A, 325, 159

Lenzen, R., Hartung, M., Brandner, W., et al. 2003, in Instrument Design and Performance for Optical/Infrared Ground-based Telescopes. Edited by Iye, Masanori; Moorwood, Alan F. M. Proceedings of the SPIE, Volume 4841, pp. 944-952 (2003)., 944–952

Liu, M. C., Najita, J., & Tokunaga, A. T. 2003, ApJ, 585, 372

Loiseau, N. 2003, XMM-Newton Science Analysis System Users' Guide, V2.1

Lombardi, M. & Alves, J. 2001, A&A, 377, 1023

Lowrance, P. J., Becklin, E. E., Schneider, G., NICMOS IDT/EONS Team, & STIS/8176 Team. 2000, American Astronomical Society Meeting, 197, 0

Luhman, K. L., Liebert, J., & Rieke, G. H. 1997, ApJ, 489, L165+

Luhman, K. L. & Rieke, G. H. 1999, ApJ, 525, 440

Mack, J., Boffi, F., Bohlin, R., et al. 2002, HST ACS Data Handbook, version 1.0, ed. B. Mobasher, Baltimore, STScI

Marchal, L., Delfosse, X., Forveille, T., et al. 2003, in SF2A-2003: Semaine de l'Astrophysique Francaise

Marquardt, D. W. 1963, Journal of the Society for Industrial and Applied Mathematics, 11, 431

Marraco, H. G. & Rydgren, A. E. 1981, AJ, 86, 62

Martín, E. L., Rebolo, R., & Zapatero-Osorio, M. R. 1996, ApJ, 469, 706

Martín, E. 2000, in ASP Conf. Ser. 212: From Giant Planets to Cool Stars, 38–+

Martín, E. L., Barrado y Navascués, D., Baraffe, I., Bouy, H., & Dahm, S. 2003, ApJ, 594, 525

Martín, E. L., Basri, G., Brandner, W., et al. 1998, ApJ, 509, L113

Martín, E. L., Basri, G., Delfosse, X., & Forveille, T. 1997, A&A, 327, L29

Martín, E. L. & Bouy, H. 2002, New Astronomy, 7, 595

Martín, E. L., Brandner, W., & Basri, G. 1999a, Science, 283, 1718

Martín, E. L., Brandner, W., Bouvier, J., et al. 2000a, ApJ, 543, 299

Martín, E. L., Delfosse, X., Basri, G., et al. 1999b, AJ, 118, 2466

Martín, E. L., Delfosse, X., & Guieu, S. 2004, AJ, 127, 449

Martín, E. L., Koresko, C. D., Kulkarni, S. R., Lane, B. F., & Wizinowich, P. L. 2000b, ApJ, 529, L37

Matthews, K., Ghez, A. M., Weinberger, A. J., & Neugebauer, G. 1996, PASP, 108, 615

Mayer, L., Quinn, T., Wadsley, J., & Stadel, J. 2002, Science, 298, 1756

McCarthy, C., Zuckerman, B., & Becklin, E. E. 2003, in IAU Symposium, 279–+

McLean, I. S., Prato, L., Kim, S. S., et al. 2001, ApJ, 561, L115

Mermilliod, J.-C. & Mayor, M. 1999, A&A, 352, 479

Mermilliod, J.-C., Rosvick, J. M., Duquennoy, A., & Mayor, M. 1992, A&A, 265, 513

Mokler, F. & Stelzer, B. 2002, A&A, 391, 1025

Monet, D., Bird, A., Canzian, B., et al. 1996, U.S. Naval Observatory, Washington DC

Monet, D. G., Levine, S. E., Canzian, B., et al. 2003, AJ, 125, 984

Montmerle, T., Grosso, N., Tsuboi, Y., & Koyama, K. 2000, ApJ, 532, 1097

Moraux, E., Bouvier, J., & Stauffer, J. R. 2001, A&A, 367, 211

Moraux, E., Bouvier, J., Stauffer, J. R., & Cuillandre, J.-C. 2003, A&A, 400, 891

Motte, F., Andre, P., & Neri, R. 1998, A&A, 336, 150

Muench, A. A., Alves, J., Lada, C. J., & Lada, E. A. 2001, ApJ, 558, L51

Munari, U., Dallaporta, S., Siviero, A., et al. 2004, A&A, 418, L31

Muzerolle, J., Briceño, C., Calvet, N., et al. 2000, ApJ, 545, L141

Nakajima, T., Oppenheimer, B. R., Kulkarni, S. R., et al. 1995, Nature, 378, 463

Nakajima, T., Tsuji, T., & Yanagisawa, K. 2001, ApJ, 561, L119

Natta, A. & Testi, L. 2001, A&A, 376, L22

Neuhäuser, R., Brandner, W., Alves, J., Joergens, V., & Comerón, F. 2002, A&A, 384, 999

Neuhäuser, R., Briceño, C., Comerón, F., et al. 1999, A&A, 343, 883

Neuhäuser, R., Guenther, E., & Brandner, W. 2003, in IAU Symposium, 309–+

Neuhäuser, R., Walter, F. M., Covino, E., et al. 2000, A&AS, 146, 323

Ochsenbein, F., Bauer, P., & Marcout, J. 2000, A&AS, 143, 23

Olofsson, G., Huldtgren, M., Kaas, A. A., et al. 1999, A&A, 350, 883

Öpik, E. J. 1924, Pub. Obs. Astron. univ. Tartu XXV, No 6, 6

Padoan, P. & Nordlund, Å. 2002, ApJ, 576, 870

Pan, X., Shao, M., & Kulkarni, S. R. 2004, Nature, 427, 326

Papaloizou, J. C. B. & Lin, D. N. C. 1989, ApJ, 344, 645

Papaloizou, J. C. B. & Terquem, C. 2001, MNRAS, 325, 221

Pascucci, I., Apai, D., Henning, T., & Dullemond, C. P. 2003, ApJ, 590, L111

Patience, J., Ghez, A. M., Reid, I. N., Weinberger, A. J., & Matthews, K. 1998, AJ, 115, 1972

Pavlovsky, C., Biretta, J., Boffi, F., et al. 2003, Baltimore: STScI

Perryman, M. A. C., Lindegren, L., Kovalevsky, J., et al. 1997, A&A, 323, L49

Pinfield, D. J., Dobbie, P. D., Jameson, R. F., et al. 2003, MNRAS, 342, 1241

Potter, D., Martín, E. L., Cushing, M. C., et al. 2002, ApJ, 567, L133

Preibisch, T. & Zinnecker, H. 1999, AJ, 117, 2381

Preibisch, T. & Zinnecker, H. 2002, AJ, 123, 1613

Press, W. H., Teukolsky, S. A., Vetterling, W. T., & Flannery, B. P. 1992, Numerical recipes in C. The art of scientific computing (Cambridge: University Press, |c1992, 2nd ed.)

Raboud, D. & Mermilliod, J.-C. 1998, A&A, 329, 101

Rebolo, R., Magazzù, A., & Martín, E. L. 1995a, in The Bottom of the Main Sequence - and Beyond, Proceedings of the ESO Workshop Held in Garching, Germany, 10-12 August 1994, edited by Christopher G. Tinney. Springer-Verlag Berlin Heidelberg New York. Also ESO Astrophysics Symposia, 1995., p.159, 159–+

Rebolo, R., Martin, E. L., Basri, G., Marcy, G. W., & Zapatero-Osorio, M. R. 1996, ApJ, 469, L53+

Rebolo, R., Zapatero-Osorio, M. R., & Martin, E. L. 1995b, Nature, 377, 129

Reid, I. N. & Gizis, J. E. 1997a, AJ, 113, 2246

Reid, I. N. & Gizis, J. E. 1997b, AJ, 114, 1992

Reid, I. N., Gizis, J. E., Kirkpatrick, J. D., & Koerner, D. W. 2001, AJ, 121, 489

Reid, I. N., Kirkpatrick, J. D., Gizis, J. E., et al. 2000, AJ, 119, 369

Reid, I. N., Kirkpatrick, J. D., Liebert, J., et al. 2002, AJ, 124, 519

Reid, I. N. & Mahoney, S. 2000, MNRAS, 316, 827

Reipurth, B. & Clarke, C. 2001, AJ, 122, 432

Rieke, G. H. & Lebofsky, M. J. 1985, ApJ, 288, 618

Rousset, G., Lacombe, F., Puget, P., et al. 2003, in Adaptive Optical System Technologies II. Edited by Wizinowich, Peter L.; Bonaccini, Domenico. Proceedings of the SPIE, Volume 4839, pp. 140-149 (2003)., 140–149

Ruiz, M. T., Leggett, S. K., & Allard, F. 1997, ApJ, 491, L107+

Rutledge, R. E., Basri, G., Martín, E. L., & Bildsten, L. 2000, ApJ, 538, L141

Schweitzer, A., Gizis, J. E., Hauschildt, P. H., et al. 2002, ApJ, 566, 435

Schweitzer, A., Gizis, J. E., Hauschildt, P. H., Allard, F., & Reid, I. N. 2001, ApJ, 555, 368

Shatsky, N. & Tokovinin, A. 2002, A&A, 382, 92

Shu, F. H., Adams, F. C., & Lizano, S. 1987, ARA&A, 25, 23

Shu, F. H., Tremaine, S., Adams, F. C., & Ruden, S. P. 1990, ApJ, 358, 495

Stauffer, J. R. 1984, ApJ, 280, 189

Stauffer, J. R., Prosser, C. F., Hartmann, L., & McCaughrean, M. J. 1994, AJ, 108, 1375

Stauffer, J. R., Schultz, G., & Kirkpatrick, J. D. 1998, ApJ, 499, L199+

Stelzer, B. & Neuhäuser, R. 2003, in Brown Dwarfs, Proceedings of IAU Symposium 211, held 20-24 May 2002 at University of Hawai'i, Honolulu, Hawai'i. Edited by Eduardo Martín., 443–+

Stephens, D. C., Marley, M. S., Noll, K. S., & Chanover, N. 2001, ApJ, 556, L97

Sterzik, M. F. & Durisen, R. H. 1998, A&A, 339, 95

Sterzik, M. F. & Durisen, R. H. 2003, A&A, 400, 1031

Szebehely, V. & Zare, K. 1977, A&A, 58, 145

Testi, L., Natta, A., Oliva, E., et al. 2002, ApJ, 571, L155

Tinney, C. G., Burgasser, A. J., & Kirkpatrick, J. D. 2003, AJ, 126, 975

Tinney, C. G., Delfosse, X., & Forveille, T. 1997, ApJ, 490, L95+

Tokunaga, A. T. & Kobayashi, N. 1999, AJ, 117, 1010

Tsuboi, Y., Maeda, Y., Feigelson, E. D., et al. 2003, ApJ, 587, L51

Tsuji, T., Ohnaka, K., Aoki, W., & Nakajima, T. 1996, A&A, 308, L29

Tsvetanov, Z. I., Golimowski, D. A., Zheng, W., et al. 2000, ApJ, 531, L61

Umbreit, S., Burkert, A., Henning, T., Mikkola, S., & Spurzem, R. 2004, ApJ, submitted

van Leeuwen, F. & Alphenaar, P. 1982, The Messenger, 28, 15

Vogt, S. S., Allen, S. L., Bigelow, B. C., et al. 1994, in Proc. SPIE Instrumentation in Astronomy VIII, David L. Crawford; Eric R. Craine; Eds., Volume 2198, p. 362, 362–+

Wilking, B. A., Greene, T. P., Lada, C. J., Meyer, M. R., & Young, E. T. 1992, ApJ, 397, 520

Wilking, B. A., Greene, T. P., & Meyer, M. R. 1999, AJ, 117, 469

Wilking, B. A., McCaughrean, M. J., Burton, M. G., et al. 1997, AJ, 114, 2029

Wolk, S. J. 2003, in Brown Dwarfs, Proceedings of IAU Symposium 211, held 20-24 May 2002 at University of Hawai'i, Honolulu, Hawai'i. Edited by Eduardo Martín., 447–+

XMM-Newton Survey Science Centre. 2003, The First XMM-Newton Serendipitous Source Catalogue

York, D. G. e. a. 2000, AJ, 129, 1579

Zapatero Osorio, M. R., Rebolo, R., Martin, E. L., et al. 1997, ApJ, 491, L81+

Zapatero Osorio, M. R., Rebolo, R., Martín, E. L., et al. 1999, A&AS, 134, 537

Index